CIVIL ENGINEERING STUDIES
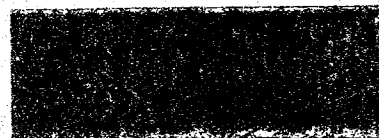
STATISTICAL ANALYSIS OF THE RESPONSE OF NONLINEAR SYSTEMS SUBJECTED TO EARTHQUAKES

by

R. RIDDELL

and

N. M. NEWMARK

DEPARTMENT OF CIVIL ENGINEERING
UNIVERSITY OF ILLINOIS AT URBANA-CHAMPAIGN
URBANA, ILLINOIS
AUGUST 1979

Intentionally Blank

DOCUMENTATION PAGE	1. REPORT NO. NSF/RA-790273	2.	3. Recipient's Accession No. PB 80 134810

Title and Subtitle	5. Report Date
Statistical Analysis of the Response of Nonlinear Systems Subjected to Earthquakes (Report No. UILU 79-2016)	August 1979
	6.

7. Author(s)	8. Performing Organization Rept. No.
R. Riddell, N. M. Newmark	UILU 79-2016

9. Performing Organization Name and Address	10. Project/Task/Work Unit No.
University of Illinois at Urbana-Champaign Department of Civil Engineering Urbana, Illinois 61801	SRS 468
	11. Contract(C) or Grant(G) No.
	(C) AEN7508456
	(G) ENV7707190

12. Sponsoring Organization Name and Address	13. Type of Report & Period Covered
Engineering and Applied Science (EAS) National Science Foundation 1800 G Street, N.W. Washington, D.C. 20550	
	14.

15. Supplementary Notes

16. Abstract (Limit: 200 words)

The dynamic response of single degree of freedom nonlinear systems subjected to earthquake motions is considered with the purpose of deriving factors for constructing inelastic design spectra, and of evaluating the effect of damping combined with inelastic behavior and the influence of the type of material nonlinearity on inelastic response. Inelastic response spectra for elastoplastic systems with 2, 5, and 10 percent damping, and for bilinear and stiffness degrading systems with 5% damping, are computed for a number of frequencies ranging from about 0.03 cps to 35 cps, for ductility values from 1 to 10, and for ten strong-motion earthquake records. A statistical procedure is developed to analyze the data. From this analysis, factors for deriving the characteristic trapezoidal design spectrum are obtained.

17. Document Analysis a. Descriptors

Nonlinear systems
Statistical analysis
Dynamic structural analysis
Structural engineering

Dynamic response
Design criteria
Earthquakes
Ductility

Models
Damping
Degradation

b. Identifiers/Open-Ended Terms

Response spectra

c. COSATI Field/Group

18. Availability Statement	19. Security Class (This Report)	21. No. of Pages
NTIS		312
	20. Security Class (This Page)	22. Price PC A10 MF A01

i

STATISTICAL ANALYSIS OF THE RESPONSE OF NONLINEAR SYSTEMS SUBJECTED TO EARTHQUAKES

by

RAFAEL RIDDELL

and

NATHAN M. NEWMARK

UNIVERSITY OF ILLINOIS

Urbana, Illinois

August, 1979

ACKNOWLEDGMENT

TABLE OF CONTENTS

LIST OF TABLES

LIST OF FIGURES

Page

CHAPTER 1

INTRODUCTION

1.1 Background and motivation

Earthquake resistant design procedures recognize, either implicitly or explicitly, that structures may respond inelastically even to moderate intensity ground motions. Insofar as earthquake motions are of an extremely complex nature, a number of structural factors influence the response as well.

Admitting that detailed nonlinear dynamic computations can be carried out, in principle, no matter how complicated the motion and the system may be, and regardless of the valuable information that may be so obtained, one can achieve reliable results only by calculating responses to several representative ground motions and examining the statistics of the response. On the other hand, since the present knowledge on nonlinear dynamic characteristics of structural materials does not seem to permit an accurate description of a structure, a number of analyses may also be required to account for variations in structural properties and different modeling techniques. Designs based on inelastic time history analyses of multi-degree of freedom systems may be justified in some circumstances; they may not be feasible for the vast majority of structures, however.

Particularly attractive for its simplicity is the design spectrum approach. The method is based on the approximation that nonlinear effects can be accounted for by a linear analysis of

the structure using design coefficients determined from inelastic design spectra for single degree of freedom systems (67,70). Even if a more rigorous procedure is deemed necessary for a particular application, the design spectrum method is ideally suited for preliminary design.

The advantage of using single degree of freedom systems is that response computations for a large number of actual earthquake motions, combined with a range of values for structure related parameters, can be carried out at a reasonable cost. In this manner, the influence of the various factors affecting the response, as well as their relative importance, can be assessed. This information is conveniently summarized in the form of response spectra, wherefrom rational estimates of the response of more complex systems can be made. On the other hand, examination of the characteristics of earthquake response spectra, combined with observations of the effect of damaging earthquakes on real structures, and consideration of a number of factors regarding expected earthquake intensities at a given site, permit one to develop a set of simplified design rules that are synthesized in the form of design spectra.

Response spectra for single degree of freedom elastic systems have been computed for various input motions including simple ground disturbances and earthquake accelerograms (17,26, 48,115,116); average elastic spectra (47), and statistical analyses of elastic response spectra (38,41,65,71,77,98), have also been reported. Primary attention is given in these studies to the amount of damping of the systems. Although inelastic

response spectra for simple elastoplastic systems subjected to earthquake and ground shock motions have been obtained (91,114, 115,116), statistical analyses consistent with the procedures developed for the elastic case have not been reported.

On the basis of the findings of some of the above elastic and inelastic response studies, and from consideration of other pertinent information, Newmark and Hall have proposed recommendations to derive design spectra for various conditions (73,74,75).

Because of the limited data available, coefficients independent of the damping factor are used to derive inelastic spectra from the elastic spectrum, which is equivalent to the assumption that damping has a similar effect on both linear and nonlinear responses. There are some indications to the contrary, however. Thus, it appears necessary to consider additional data to account for damping in an explicit manner.

Considerable effort has been devoted recently to the study of the behavior of structural materials and components under cyclic loading. Special attention has been given to reinforced concrete elements that may deteriorate, in the sense of losing stiffness and strength, under load reversals. It is of interest to examine the significance of these effects in terms of inelastic response spectra. This has not been considered in detail heretofore.

1.2 Purpose and outline of the study

The dynamic response of single degree of freedom nonlinear systems subjected to earthquake excitations is considered to

estimate the effect of structural damping combined with inelastic behavior and the effect of various types of material nonlinearity.

Inelastic response spectra, obtained for a range of conditions, are analyzed statistically to make quantitative estimates of the effect of the various parameters, and with the purpose of deriving improved rules for constructing inelastic design spectra. In turn, a great deal of insight on the nature of nonlinear responses is gained.

In Chapter 2, experimental results available in the literature on structural behavior under cyclic loading are reviewed with the purpose of defining the resistance functions and range of damping values used in the study. On this basis, three types of nonlinear model are chosen: elastoplastic, bilinear, and stiffness degrading; the latter was specially developed for this study and has some advantages over other relationships available. Relative damping values of 2, 5, and 10 percent of critical are selected in combination with the elastoplastic model; damping of 5 percent is used for bilinear and stiffness degrading systems to permit comparisons with the elastoplastic case.

In Chapter 3, a description is given of the systems considered and of the ten earthquake records used as base motion. The procedure used to compute responses is described, and the corresponding results are summarized in the form of inelastic response spectra. These results are discussed and observations are made regarding the influence of the parameters under study.

A procedure for the statistical analysis of the data is developed in Chapter 4. From this analysis, factors for deriving the characteristic trapezoidal spectrum are obtained. As an intermediate step in the statistical analysis, single frequency statistics that are relevant for a number of reasons are obtained; in particular, average spectra can be constructed from which general conclusions can be reached regarding the effects of damping and the type of nonlinearity on inelastic response.

The various factors involved in the establishment of earthquake design spectra are presented in Chapter 5. A key point, the estimation of the earthquake hazard at a given site, is discussed in some detail. Rules for the construction of design spectra, and particular examples are given. Comparisons are made of design spectra and actual response spectra.

Chapter 6 contains a summary of the conclusions of the study.

1.3 Notation

The symbols used in the text are defined where they are first introduced. For quick reference, a list of the most important ones follows:

A   = peak ground acceleration; also used as a subscript to indicate normalization to ground acceleration

a   = subscript referring to the acceleration axis of the spectrum

C   = damping constant

COV = coefficient of variation

D   = peak ground displacement; also used as a subscript to indicate normalization to ground displacement

d = subscript referring to the displacement axis of the spectrum

f = undamped natural frequency in cycles per second

f_{dv} = frequency at the knee between the displacement and the velocity regions of the spectrum

f_{va} = frequency at the knee between the velocity and the acceleration regions of the spectrum

k = stiffness of elastic systems or initial stiffness of inelastic systems

k_s = strain hardening stiffness of bilinear and stiffness degrading systems

m = mass of the system

p = parameter in the general expressions for deamplification factors

p = probability level

Q = general designation for any of the peak ground motion parameters (A, V, or D); also used as a subscript to indicate the nature of normalized quantities

q = parameter in the general expressions for deamplification factors

R = resistance function, force in the spring

R_m = maximum resistance

R_y = yield point resistance

r = parameter in the general expressions for deamplification factors

S = any spectral quantity

S_a = spectral acceleration

S_e = ordinates of the elastic design spectrum

S_d = spectral displacement

S_v = spectral velocity

S_μ = ordinates of the inelastic design spectrum for a ductility value μ

s = ratio between the strain hardening stiffness and the elastic stiffness, taken as 0.03 in this study

T = natural period of vibration

u = relative displacement of the system with respect to the ground

$\dot{u}$ = relative velocity of the system

$\ddot{u}$ = relative acceleration of the system

u_e = maximum relative displacement of an elastic system

u_m = maximum relative displacement

u_m^+ = maximum relative displacement in the positive direction of motion

u_m^- = absolute value of the maximum relative displacement in the negative direction of motion

u_y = deformation corresponding to the yield point

V = peak ground velocity; also used as a subscript to indicate normalization to ground velocity

Var = frequency band variance

$\tilde{\text{Var}}$ = single frequency variance

v = subscript referring to the velocity axis of the spectrum

x = absolute displacement of the system

$\dot{x}$ = absolute velocity of the system

$\ddot{x}$ = absolute acceleration of the system

y = absolute displacement of the ground

$\dot{y}$ = absolute velocity of the ground

$\ddot{y}$ = absolute acceleration of the ground

β = damping factor as a fraction of the critical damping

δ_p = deviation from the mean for probability level p

λ_μ = correction factor to account for the difference between $\phi_{p\mu}$ and ϕ_μ

μ = ductility factor

σ = frequency band standard deviation, also indicated as σ_μ

$\tilde{\sigma}$ = single frequency standard deviation

ϕ_e = factors that applied to the ground motion estimates give the ordinates of the elastic design spectrum

ϕ_μ = deamplification factors that applied to the elastic design spectrum give the ordinates of the inelastic design spectrum

$\phi_{p\mu}$ = deamplification factor for probability level μ

Ψ_μ = factors that applied to the ground motion estimates give the ordinates of the inelastic design spectrum

$\overline{\Psi}$ = frequency band average, equal to Ψ_μ

ψ = any normalized spectral quantity

$\overline{\psi}(f)$ = average of ψ values at frequency f

Ω = frequency band coefficient of variation, also indicated as Ω_μ

$\tilde{\Omega}$ = single frequency coefficient of variation

ω = undamped circular frequency in rad/sec

CHAPTER 2

BEHAVIOR OF STRUCTURES UNDER CYCLIC LOADING

AND MODELING FOR ANALYTICAL PURPOSES

2.1 Introduction

Structures subjected to earthquakes may undergo several reversals in direction of displacements. It is clear from the literature that in such circumstances the nonlinear behavior of the structure differs from that under monotonically increased loading. Stiffness and strength degradation phenomena, which may affect the energy absorption and energy dissipation capacities, are particularly relevant to earthquake resistant design.

An important number of experimental results are already available from tests on a wide variety of structural systems, ranging from simple beams to entire buildings, and various models for load deformation relationships have been suggested to analytically predict the actual response of the corresponding systems. It must be pointed out, however, that experimental work on structural hysteresis has not yet produced all the information required for the solution of the problem regarding the mechanical behavior of a real structure under severe dynamic loading.

Real buildings have been instrumented and measurments have been obtained during actual earthquakes or in forced and free vibration tests (37,103). Notwithstanding the fact that this information has led to significant results concerning member strains, variation of natural periods, degree of damping, and

soil-structure interaction effects, data have been generally obtained under moderate excitations which have not induced important inelastic deformations. It has been pointed out that information on the nonlinear behavior of actual buildings and their surrounding soil is needed (11), but too few results are available (83).

Laboratory tests on members, subassemblages and reduced scale models, using shaking tables or quasi-static load reversals, are the natural option. It is unfortunate, though, that the results of dynamic tests are given, in most cases, in the form of force or displacement time histories instead of force displacement curves, thus, the hysteretic behavior cannot be readily assessed. Several hundred papers on pseudostatic testing have been published during the last few years. A comprehensive review of the literature would be a tremendous task. Instead, a few specific contributions will be discussed with the purpose of defining the load deformation functions and range of damping values used later on in this study.

2.2 Reinforced Concrete Members and Frames

Consider first a doubly reinforced concrete member whose behavior is controlled by flexure, i.e., stresses relate primarily to bending, and assume premature crushing is prevented by means of an under-balanced reinforcement ratio. The general characteristics of the behavior of such an element, under quasi-static load reversals, are qualitatively illustrated by the load deflection curve shown in Figure 2.1. Notably, there is a

degradation in the reloading stiffness when the element is subjected to a new cycle exceeding the maximum deformation attained in the previous one.

The factors which influence the shape of the hysteresis loop, thoroughly discussed by Sozen (104) and Bresler (19), are the following: (a) Amount of longitudinal reinforcement in relation to the concrete area and the stress-strain properties of the reinforcing steel, (b) amount of cracking in terms of the distribution and width of cracks, (c) effectiveness of bond between steel and concrete, (d) shear stresses and amount of web reinforcement, (e) local and overall distortions at joints, and (f) instability of longitudinal reinforcing bars.

It has been pointed out that, while some of the above factors are inherent to hysteretic behavior, others constitute deficiencies which should be considered only to be avoided (104). Typical of the latter are inadequately proportioned joints, insufficient web reinforcement for shear and stability of longitudinal bars, and lack of adequate detailing for bond resistance. For example, Figure 2.2.a shows the load deflection curve for a reinforced concrete member without adequate web reinforcement; the decay in strength with cycling is notable. Figure 2.2.b features a typical slip loop due to loss of anchorage after two complete cycles.

A word of caution is necessary when referring to "adequate" web reinforcement. Acceptable results have been obtained, in terms of no shear strength decay with cycling, by assigning all the shear to the transverse reinforcement while neglecting the

contribution of the concrete (94,121). However, this appears to be the case only for members with moderate to slender proportions. The shear-span to depth ratio M/Vd, where M and V are the moment and the shear at the critical section, seems to be a reasonable classification criterion. Referring to columns, Sozen (105) has mentioned a value of 2 as the limit below which the member should be referred to as a "shear column." For such members, even large amounts of transverse reinforcement do not seem always to prevent the strength decay with cycling (20,107); there is need to determine the maximum moment capacity that can be developed while ensuring stable hysteretic response under high shear stresses.

The effect of axial load must also be discussed. Wight and Sozen (121) tested members with a shear-span to depth ratio of about 3 and axial forces applied in such a way that the possible P-δ effect was minimal. They observed that increasing the axial load from zero to one half the balance load tended to retard the decay in stiffness and strength with cycling. This bears out the intuitive behavior. Elements with no axial load present wider cracks which may not close properly when the load is reversed because of permanent elongation of the reinforcement; this may result in through-the-depth cracks carrying shear by aggregate interlocking resistance. This kind of resistance rapidly deteriorates under load reversals by abrasion of the contacting surfaces. Moderate axial loads would then be beneficial in providing confinement to arrest, to some degree, the otherwise rapid deterioration. On the other hand, axial compression has a

positive effect on the moment capacity of typically proportioned flexural sections (under balanced condition); the ultimate curvature decreases though.

Atalay and Penzien (8) tested members with shear span to depth ratios of 5.5 and axial forces ranging from 25 to 75 percent of the balance load. They concluded that increasing the axial load decreases the ultimate lateral displacement capacity and enhances strength and stiffness degradation. It must be pointed out however that the testing configuration was such that the P-δ effect was present and partly responsible for the strength decay featured by the load deflection curves at large cyclic amplitudes.

The P-δ effect is schematically illustrated in Fig. 2.3. The curve denoted by P=0 represents an ideal force deformation relationship for a member without axial load; M_y is the yield moment of the cross section. The effect of a constant axial load may be taken into account by substracting the dashed line "b" representing the geometric stiffness P/h, from the dashed line denoted by "a". The latter corresponds to the load deformation relation obtained by computing the moment capacity of the section including the favorable effect of compressive stresses. It is apparent that the lateral load capacity of the column declines as the lateral displacement increases; the strength of the section, however, is fully developed. If no deterioration ocurred, the curve labeled P$\neq$0 would envelope the loops resulting from load reversals. On the contrary, if strength is not sustained, the loops will not reach such envelope.

P-δ effects make inverted pendulum structures particularly vulnerable to earthquakes. In the case of frame buildings, however, the predominant design philosophy is one of strong column, weak girder (6). Special code provisions (4) are intended to insure that yielding occurs in the beams rather than in the columns. Even though this does not guarantee that all columns will remain elastic during a strong earthquake (14,86), the chance of instability problems is substantially diminished.

The effect of alternating loads on the behavior of reinforced concrete frames is similar to that observed in members. If proportions and detailing are such that failures other than by flexure are prevented, the lateral capacity is almost insensitive to the repetition of loading; in contrast, the stiffness deteriorates rapidly as the amplitude of the deformations and the number of cycles increase (16,39,87). Typical hysteresis loops for frames are shown in Figures 2.4 and 2.5.

Various studies have pointed out the importance of bond and anchorage of reinforcing bars (39,92). A particularly critical bond demanding situation arises in beam column joints of frames under lateral loading as the main reinforcement is pulled from one side of the joint while being pushed from the other. Slippage of the reinforcement may cause pronounced degradation of the hysteresis loops, not only regarding stiffness but strength as well, even in absence of shear problems.

Corner connections presenting commonly used reinforcement details have been found to fail, even under static loading, at a small fraction of the capacity of the adjoining members (80). In

structures required to dissipate energy under load reversals, the full capacity of the members adjacent to a connection must be developed and sustained during inelastic excursions. Extensive discussion on the behavior of beam column joints, the essential requirements for satisfactory performance and recommendations for proportioning and detailing are available (5,87). Limitations of the recommendations and areas of needed research have also been pointed out (5).

2.3 Reinforced Concrete Walls

Because reinforced concrete walls are frequently the principal elements resisting lateral loads in multistory buildings, they have been called shear walls. As Park and Pauley point out (87), the name is an unfortunate one; in seismic design the main concern is for relatively tall walls that behave essentially in flexure. Again, ductility is realized by preventing shear, anchorage or crushing modes of failure prior to a bending failure. Short walls, or "true shear walls" (92), are subjected to low flexural stresses and have large shear capacity, so that their load-deflection curve is practically linear up to a basically brittle failure; they should be designed and analyzed for elastic behavior only.

There is no general consensus on the delimitation between the two wall categories. Walls having a height to depth ratio of less than 0.5 to 1.0 have been classified as "short" or pure shear type; it must be noted though, that the shear span to depth ratio is a more appropiate index for classification (92) since

the former does not provide information on the existing combination of shear and flexural stresses. The following discussion refers to the behavior of flexural walls.

As the initial part of an extensive experimental program at the Portland Cement Association (81), eight 1/3 scale walls were tested under cyclic loading. Controlled variables included the shape of the cross section (rectangular, barbell and flanged), the amount of flexural reinforcement, and the amount of hoop reinforcement around the main flexural reinforcement. Shear reinforcement was provided according to the ACI 318-71 Code (4). All specimens had shear span to depth ratios of about 2.4. Load deformation curves for two rectangular and two barbell specimens are shown in Figure 2.6. All these specimens had the same horizontal and vertical web reinforcement; the main flexural reinforcement, concentrated at the edges of the wall, and the special confinement reinforcement varied as indicated in the figure. Detailed discussion of the performance of the specimens is given in the original report. It is of interest to remark here that the behavior of the walls in Figure 2.6 is essentially that of a ductile flexural member; defining as yield displacement that corresponding to the load which produces yielding of all the main reinforcement, and taking as maximum displacement that corresponding to the last cycle before strength deterioration, ductility factors ranging from about 6 to 10 are obtained. It must be borne in mind however that such ductilities are smaller than those expected in slender flexural members. The characteristic stiffness degradation and pinching of the

hysteresis loops is also apparent.

Similar observations can be made from tests conducted at the University of California, Berkeley (120). One-third scale walls corresponding to the lower three stories of a ten-story prototype building were tested. Special emphasis was placed on simulating, in a pseudostatic manner, the effect of actual earthquake loading conditions by applying gravity forces and overturning moments as shown in Figure 2.7.b. The figure also shows the general dimensions and details of the wall specimens as well as the lateral loading histories and the resulting hysteretic diagrams. These walls attained maximum ductilities of the order of 4 and 6. The shear span to depth ratio was about 2.3.

Due to functional requirements, structural walls in multistory buildings are often pierced by vertical rows of openings. This frequently results in relatively short and deep spandrel beams. Experiments have shown that the strength and ductility of coupling beams can be improved if diagonal reinforcement is used instead of the conventional arrangement of longitudinal bars and vertical stirrups (9,87). Two 1/4 scale seven-story coupled walls -one with conventionally reinforced beams, the other with diagonally reinforced beams- were tested to verify the overall structural behavior in terms of stiffness degradation, ductilities attained, and energy dissipation capacity (87,89). In every respect, the wall with diagonally reinforced beams performed better. The load deformation histories for the two walls are reproduced in Figure 2.8.

In a similar fashion, suitable detailing of the beam rein-

forcement at beam-wall junctions in frame-wall assemblies has been proved effective in improving the overall hysteretic response of the structure (88).

2.4 Masonry Construction

Even though masonry is historically one of the oldest costruction materials, and regardless of its widespread geographic employment, its seismic behavioral characteristics are perhaps the most poorly known of all structural materials. The reasons for this limited knowledge are presumably due to a number of factors. First, and perhaps the most important, masonry refers to a vast range of materials such as stone, adobe, clay, and concrete units, each of which in turn varies widely in geometrical and mechanical properties. In addition, reinforcement, grouting and enclosing frames may or may not be provided, thus further broadening the variety of masonry forms. This evidently makes difficult the process of using past experience and interpreting experimental data into comprehensible models of some generality. A second factor is the orthotropic and nonhomogeneous character of masonry. This has led to a wide variety of testing techniques as a result of the efforts made for obtaining load configurations and boundary conditions compatible with the material properties under study. For example, Omote et al.(82) elaborate on the various methods used and relationships formulated in relation to shear strength. Furthermore, even the standard procedure for determining the compressive strength has been questioned (45). Finally, the unsatisfactory performance of

some types of masonry during earthquakes has probably given a negative image to all masonry forms regarding their ability as seismic resistant materials. However, it is indeed gratifying that extensive research programs on masonry buildings are being carried out (64).

The behavior of unreinforced, unconfined masonry panels under cyclic loads is not of particular interest. Below a certain stress level the walls behave in a practically linear fashion, at higher stresses the panels fail in a brittle manner (79). In the following, the cyclic behavior of reinforced masonry walls, and masonry infilled reinforced concrete frames will be discussed.

At present, there is not sufficient information for predicting the behavior of reinforced masonry walls. Mayes and Clough (63) summarized the scarce results available on load capacity and performance under cyclic loads. Such results correspond to walls with height to depth ratios of less than or about two. Their principal conclusions are summarily reproduced in the following: (a) There are two major modes of failure, a shear or diagonal tension failure characterized by diagonal cracking, and a flexural failure characterized by yielding of the tension steel and compressive failure at the toe of the wall; (b) ultimate strength can be predicted with reasonable accuracy in the flexural mode of failure; there is no adequate method for predicting the ultimate capacity in the shear type of failure, however, some simplified criteria are available for some kinds of panels under certain loading conditions; (c) the flexural mode of

failure has a more stable inelastic cyclic behavior and ductilities of at least 2 can be attained, continued loading to deflections consistent with maximum ductility leads to severe strength and stiffness degradation; (d) masonry walls in the shear failure mode have essentially no ductility and experience significant load and stiffness losses after the ultimate capacity is reached; such walls should be designed for elastic behavior.

Filler walls are often used as partitions or exterior walls. Unless adequately isolated to prevent interaction with the frame, filler walls must be considered active structural elements. It is generally known that the behavior of the frame-wall composite cannot simply be obtained from a superposition of the behavior of its individual components. On the other hand, infilled frames are several times stiffer and stronger than bare frames, and can, if properly designed, dissipate considerable amounts of energy after panel cracking.

Although Fiorato et al.(36) used monotonic loading, their study is worth mentioning here since it seems to be the first including a number of multistory systems. They tested eight one-story one-bay specimens, twelve five-story one-bay specimens, and six two-story three-bay specimens representing 1/8 scale models of full scale frames; unreinforced clay masonry infill was used and some panels presented openings. The five story models behaved initially in a flexural manner; shear cracking of the wall panels at later stages of loading did not preclude the development of yielding in the frame reinforcement. Actually, observed ultimate loads showed reasonably good agreement with the

capacities calculated on the basis of yielding of the column reinforcement. After initiation of shearing cracks, shear was resisted by the columns with the intact portions of the wall acting as braces; failure resulted by either shearing of both columns or shearing of the compression column only while the flexural capacity of the tension column developed. Five-story specimens with a low amount of reinforcement in the columns, about one percent, failed by yielding before shear cracks developed in the walls. The behavior of the one-story specimens was governed, from the beginning, by the shear rigidity of the wall. This points to the need for determining the proper combination of shear and bending stresses and the conditions for ductile behavior with maximum utilization of the shear capacity.

Esteva (31) investigated the cyclic behavior of full scale one-story one-bay unreinforced masonry panels confined by reinforced concrete frames. It was found that tension cracking at the corners of the frame greatly impairs the capacity of the system for resisting further load cycles. Even though development of the shear capacity of the panel was not affected by the resistance of the frame, stable hysteresis loops were observed only when failure of the frame was prevented by providing additional transverse reinforcement at and near the corners.

Klingner and Bertero (56) tested 1/3 scale models representing subassemblages of an eleven-story moment resisting reinforced concrete frame; one bare frame and three infilled frames were subjected to axial loads plus quasi-static cycles of reversed shear and overturning moment, simulating the action of

gravity and earthquake loads in the prototype structure. The specimens were specifically designed and constructed so as to obtain frame members with high rotational ductility and resistance to degradation. Closely spaced infill reinforcement was used to achieve gradual panel degradation. The panel thickness was limited so that the infill cracking resistance was smaller than the combined shear capacity of the columns and much smaller than the shear associated with overall flexural failure. It was concluded that infilled frames so designed had several advantages over comparable bare frames. Besides their larger stiffness and strength, the increase in energy absorption and dissipation capacities was so important that it far exceeded the negative effect of larger inertial forces due to the increase in stiffness. A typical load deflection curve is shown in Fig. 2.9. As progressive panel deterioration occurred, the system asymptotically approached the strength of the corresponding bare frame mechanism.

The foregoing studies indicate that, in contrast to unbounded masonry walls, masonry infilled frames may present desirable characteristics from the earthquake resistant design point of view. The observed cyclic behavior is susceptible of modeling for analysis, however, there is still need for further research to establish, in a more definitive manner, the effect of the various parameters involved and their influence on the possible modes of behavior.

2.5 Structural Steel Systems

Results from experiments by Popov and Stephen (95) serve to illustrate the behavior of steel beams. They tested wide-flange section cantilever beams connected to a column stub fixed to a reaction frame. All specimens exhibited stable hysteresis loops as shown in Figure 2.10.a. Most of the specimens finally failed by local buckling of the flanges.

Similarly shaped hysteresis loops are characteristic of unbraced steel frames subjected to cyclic horizontal loads (23), as shown in Fig. 2.10.b. This will be the case, in general, provided that ductile connections can be achieved, lateral instability and local buckling are avoided and second order effects (P-δ) are not important.

Improperly designed joints may not permit development of the full capacity of the individual elements of a frame. Krawinkler (58) has discussed the findings of various experimental studies on beam-column joints and made suggestions for improved design criteria. Studies have also shown that the development of local buckling and lateral torsional buckling is severely accelerated and accentuated by load reversals (15); consequently, use of sections with low width to thickness ratios was recommended.

The behavior of beam-columns and unbraced frames subjected to relatively high vertical load in addition to cyclic lateral loading is illustrated in Fig. 2.10.c. In the first cycle, the maximum capacity is smaller than that of the case with no axial load; the negative slope of the load deflection curve is due to the P-δ effect. In subsequent cycles, the load carrying capacity

increases steadily as a result of strain hardening of the steel (93,117).

The cyclic behavior of braced frames has been studied by Wakabayashi (118). The typical pinching of the hysteresis loops, shown in Fig. 2.11.a, is due to the lateral deflection necessary for the buckled brace to be effective again. This behavior can be predicted by analysis; for this purpose, detailed studies of the individual behavior of the bracing elements have been conducted (119).

An alternate bracing system has been developed with the purpose of increasing the ability of braced frames to dissipate energy (100). The idea was basically motivated by the interest in reducing the previously described pinching effect. Two eccentrically braced frames were tested and found to have excellent energy dissipation capabilities. A typical load deformation curve is shown in Figure 2.11.b.

2.6 Nonlinear load-deformation models.

The studies reviewed in the foregoing sections reveal that there is a wide spectrum of hysteretic forms. The various researchers have not only attempted to explain the effect of the diverse parameters involved, but, ingeniously, experimented new alternatives to correct or eliminate some of the detrimental effects of cyclic loading. Even though not all the answers are available yet, a wide variety of models have been proposed to simulate behavioral phenomena observed under diverse circum-stances. Before elaborating on the particular characteristics of

the models used in this study, the bases for their selection must be established.

In first place, the scope of the model needs to be specified. One possible approach is to start modeling at the material level for predicting the behavior of sections, then members, and finally the structure. Attempts have also been made to start at the section level and model only those regions of the structure expected to reach the inelastic range by means of moment curvature relationships for example. Alternatively, one may consider a model as representative of a complete subassemblage or an entire structure. The latter approach is the most appropriate for this study because of the following reasons: (a) It is consistent with the assumptions underlying the use of the inelastic spectrum method, i.e., a complex structure is represented by a single degree of freedom system. The force restoring characteristics of such system must be in accordance with the overall behavior of the structure; (b) It is of main concern to gain insight on the general trends of the response of nonlinear systems. The model should then be representative of a family of structures rather than a particular one. Regardless of the valuable information that can be obtained from the lower-level approaches, they are necessarily related to specific designs since sectional properties are needed to define the corresponding load deformation functions; (c) Presumably, the resistance function of a complete structure is not particularly sensitive to local deficiencies. Local imperfections at a particular connection or excessive cracking of an individually

overloaded member should not compromise the behavior of the entire structure. It is reasonable to expect that such defects will be filtered out and will not affect the shape of the load deflection relationship to a great extent.

On this basis, let us consider the various shapes of hysteresis loops sketched in Fig. 2.12. Type I is the upper bound, regarding loop area, that can be attained. This behavior, characteristic of intrinsically ductile, nondeteriorating systems, can be modeled by means of Ramberg-Osgood skeleton curves (97) completed with rules for unloading and reloading (54,62). Although approximated, the bilinear model has been widely used because of its simplicity. Type II characterizes the behavior of stiffness degrading structures; there can be some differences in the behavior from one system to another, but the illustrated shape has a certain degree of generality. It has been represented by the well known Clough's and Takeda-Sozen's models (27,108). Type III is in general representative of behavior under high shear and typical of slip phenomena in connections.

It must be noted, however, that the loops shown in Figure 2.12 do not present strength deterioration, i.e., all of them reach the spine curve and would follow it if the deformation increased. Naturally, as discussed earlier, some systems can not maintain the maximum load after a few yielding excursions. This is undesirable and efforts must be made to avoid it, unless there is another source of strength in the structure to prevent collapse.

It is of primary interest to study the earthquake response

of systems of types I and II since these cover a wide range of structural behavior. A bilinear model will be used to represent the first type. Two reasons support this selection: first, simplicity, and second, the bilinear model is the next step from the elasto-plastic model, the only change being the non-zero second branch stiffness. A further step could be to consider the rounded Ramberg-Osgood curves, but this will not be included in this study.

The selection of the model for stiffness degrading structures belonging to Type II requires some additional comments. As observed in the previous review of experimental studies, as well as in most of the available evidence, the specimens are driven through successive full yielding cycles. However, under earthquake excitation, structures undergo a fairly large number of small loading cycles before, between and after yielding cycles. Model deficiencies, leading to spurious results, are often encountered in the literature as a consequence of the lack of provisions for treating incomplete and small amplitude loops. This problem has been discussed in more detail elsewhere (99). The Takeda-Sozen model, which has checked very favorably against experimental dynamic responses, is a good example of the many constitutive rules that may be needed for defining an unambiguous model; sixteen rules govern the different stages of loading indicated in Figure 2.13 (84). Otani and Sozen (84,85) have also used a simplified version of the previous model, as shown in Fig. 2.14. Basically, the initial tri-linear spine and the varying unloading stiffness were excluded; a total

of eleven rules were needed in this case.

A new model was developed for this study. Although a close relative of the Otani-Sozen model, the new model was conceived to fulfill the following objectives: (a) Generality of the constitutive rules. This is desirable not only for comprehensibleness but also because additional features can be implemented in the future without disrupting the general structure of the model. In turn, it results in shorter and clearer computer code; and (b) Avoidance of inconsistencies arising from unclosed loops (99).

The new stiffness degrading model, illustrated in Fig. 2.15, consists of an initially bilinear spine and loading occurs either on the strain hardening branch or towards the furthest point attained in the previous cycle. Thus, at any point in time the resistance and possible path are given by the current spine, represented by the dashed lines in the examples of Figure 2.15. For this study, unloading was set to be parallel to the elastic stiffness k.

In summary, the three nonlinear models used in this study are as shown in Fig. 2.16. The strain hardening stiffness k_s was taken as 3 percent of k. It is not uncommon to find larger strain hardening slopes, however, only a moderate influence of this factor was desired here.

2.7 Structural Damping

In addition to the energy dissipated by the structure by inelastic behavior, in the structural mechanics sense, there are

energy losses even in the "elastic" range. The latter are customarily taken into account by means of a damping factor. Energy dissipation may also take place through feed-back into the ground; in a certain sense this effect is of the nature of damping, but it should be better taken into account, when pertinent, by means of soil-structure interaction techniques.

The degree of damping depends on the type of structure, the materials used, the intensity of motion and stress level within the material, and the amount of deterioration already experienced by the structure. For example, the damping coefficient for a cracked concrete beam will be several times larger than that of a similar uncracked beam, when both are subjected to the same excitation at a below-yielding stress level. The difference is explained by the additional energy dissipated by friction between the sides of the cracks that can move relative to each other. On the other hand, even for a homogeneous material like structural steel, the degree of damping increases as the intensity of motion does. This may be attributed to the intensification of the sources of damping at a microscopic scale, such as internal friction and nonlinearities resulting from stress concentrations and residual stresses.

As mentioned earlier, data on damping are available from reports on forced and free vibration tests of actual structures, and also from measurements obtained during real earthquakes. Portillo and Ang (96) summarized the data for reinforced concrete buildings and presented average damping factors for the various levels and types of excitations; the values ranged from 1.2

percent of critical for low amplitude man-excited vibrations to 5.7 percent for blast exposed structures. In each category, the coefficient of variation of the data was of the order of 50 percent.

A wider sample of data, including reinforced concrete, steel and composite buildings, has been analyzed by Haviland (43). With regard to the intensity of excitation, the information was classified in two groups: small and large amplitude. The mean damping value and its coefficient of variation for reinforced concrete buildings were 4.26 percent and 0.76 respectively for small amplitude, and 6.63 percent and 0.64 for large amplitude. In the case of steel buildings, a mean of 1.68 percent and a COV of 0.65 were computed for small amplitude vibrations, and 5.65 percent and 0.45 for large amplitude.

Newmark and Hall (72) have also recommended damping values as a function of the stress level and the type and condition of the structure; for reinforced concrete structures, damping values ranging from 0.5 to 1, 2 to 5, and 7 to 10 percent were associated, respectively, with stress levels below 1/4 of the yield point, about 1/2, and at or just below the yield point. For the same stress levels, but for welded steel structures, they indicated damping factors of 0.5 to 1, 2, and 5 percent respectively; for bolted or riveted steel the corresponding values were 0.5 to 1, 5 to 7 and 10 to 15 percent.

A great deal of judgement is involved in interpreting the above data. It is not a simple matter to select a value for use in a particular application, not only because of the observed

variability but also because damping varies with time. It is probably safer to consider a range of values rather than a specific one; for this purpose the foregoing data can be used as a general guideline.

There is no evidence available indicating what degree of damping should be used when inelastic behavior is explicitly considered by means of a nonlinear resistance function. However, since in this case damping is meant to represent the energy dissipation associated with "elastic" stages of response, it is reasonable to consider values corresponding to moderate stress levels, say about 1/2 the yield point. With this in mind, and considering the variability observed in actual structures, a damping range from 2 to 10 percent seems to cover most of the cases.

On this basis, damping factors of 2, 5 and 10 percent of critical are used in this study in combination with the elasto-plastic model. The intermediate value of 5 percent is used with the bilinear and stiffness degrading resistance functions, so that the results can be compared with the elastoplastic case.

CHAPTER 3

RESPONSE OF INELASTIC SYSTEMS TO EARTHQUAKE MOTIONS

3.1 Introduction

The initial sections of this chapter give a general description of the systems and ground motions considered, and the procedure used to compute responses. Then the results are summarized in the form of response spectra.

Finally, by means of comparisons of spectra for particular records, observations are made regarding the effect of damping and the type of nonlinearity on inelastic responses. Force deformation curves and response time histories for a few cases are studied in detail to explain some of the differences and similarities found in the spectra. In addition to being useful for this purpose, the response time histories provide a great deal of insight into the behavior of nonlinear systems. Furthermore, the observations and comments made in the discussion of results will aid in the interpretation of the general analysis of the data presented in the next chapter.

3.2 System considered

A simple one-degree-of-freedom system is considered, as shown in Fig. 3.1. The concentrated mass m is connected to the ground by a weightless spring and a dashpot; the absolute displacement of the mass is denoted by x, the absolute displacement of the ground by y, and the spring deformation, or

relative displacement of the mass with respect to the ground, is denoted by u, such that

$$u = x - y \qquad (3.1)$$

The force in the spring, or resistance function R, depends on the relative displacement u, as shown in Fig. 2.16. Hereafter, depending on the type of resistance function, the systems will be simply referred to as "elastoplastic," "bilinear" or "degrading."

The dashpot represents viscous damping and exerts a resisting force proportional to the relative velocity $\dot{u}$. The damping constant C is seldom specified in absolute terms but as a fraction of the critical damping, $2\omega m$, of the corresponding system. Such a fraction will be normally referred to as the damping factor and will be designated as β, so that

$$C = 2\omega m\beta \qquad (3.2)$$

where ω is the undamped circular frequency of the system. In turn, the circular frequency relates to the frequency f and the period T as follows

$$\omega = \sqrt{k/m} = 2\pi f = \frac{2\pi}{T} \qquad (3.3)$$

noting that the frequency of inelastic systems is defined as that computed using the initial elastic stiffness.

The equation of motion of the system is

$$\ddot{u} + 2\beta\omega\dot{u} + \frac{R}{m} = -\ddot{y} \qquad (3.4)$$

where the dots denote differentiation with respect to time.

3.3 Ground motion

Ten earthquake records are used as input motion. Information regarding the seismic events and site characteristics is given in Tables 3.1 and 3.2. No attempt of selecting or grouping the records according to similar characteristics was made; this would have required a prohibitively large sample of records, besides the problem of finding records to fill adequately the very many categories that one can conceive. Naturally, the interest of considering specific groups in future research must not be disregarded.

The ground motions selected cover a variety of situations regarding site conditions, intensity, distance to fault, duration of motion, etc. The only common factor is that all of them have a peak ground acceleration greater than 0.1 g. Most of them were recorded in the free field or in relatively small buildings. The ground acceleration time histories, as well as integrated ground velocities and displacements, are shown in Figures 3.2 to 3.11; ground motion maxima are also summarized in Table 3.3.

With the exception of the Managua record, the rest correspond to standard corrected accelerograms issued by the California Institute of Technology (21) or the U.S. Geological Survey (18,102,111). Both institutions use the corrective procedure developed at Caltech (109). The Managua record corresponds to an uncorrected version that was adjusted for this study by fitting a parabolic base line so that the mean square error of the ground velocity time history was minimized (10).

3.4 Response computations

The equation of motion (Eq. 3.4) was integrated numerically using Newmark's method (66). The interval of integration was given by the spacing of the ground motion data or as T/20, whichever was smaller.

The details about calculations for nonlinear response spectra are well known. Nevertheless, there are a few points that call for further explanation, which will be topics for the next sections: (a) Special treatment of earthquake records with specified non-zero initial conditions for ground velocity and ground displacement, (b) selection of frequencies and duration of input motion for nonlinear responses, and (c) procedure for obtaining responses associated with desired ductility factors.

3.4.1 Use of records with non-zero initial conditions

As mentioned earlier, the accelerograms used correspond to records corrected by means of the Caltech procedure. This procedure leads to initial values for the ground motion that result from the fact that some portion of the motion is lost since a certain input level is required to trigger the recording device.

When records with initial conditions are used to compute response spectra a difficulty arises because the initial conditions for the oscillator are not known. In fact, denoting the time at the beginning of the recorded motion as t_o, the initial conditions are:

$$u(t_o) = x(t_o) - y(t_o) \qquad\qquad (3.5a)$$

$$\dot{u}(t_o) = \dot{x}(t_o) - \dot{y}(t_o) \qquad\qquad (3.5b)$$

where $y(t_o)$ and $\dot{y}(t_o)$ are the specified ground displacement and velocity, but $x(t_o)$ and $\dot{x}(t_o)$ are unknown since they depend on the response to the lost portion of the ground motion.

The customary procedure of using zero relative velocity and displacement, i.e., $\dot{u}(t_o)=0$ and $u(t_o)=0$, leads to distortions of the response spectrum in the low frequency range. Spurious low frequency effects are particularly serious in the case of nonlinear responses.

A method for removing such distortions is to prefix a short acceleration pulse to the original accelerogram (90). The pulse starts from zero acceleration and yields the prescribed initial conditions of the ground at the end of the pulse (t_o). The rest of the accelerogram, and the corresponding integrated velocity and displacement time histories remain unaltered. This procedure was used in this study; the records containing a prefixed pulse are indicated in Table 3.3. For these records, the first two seconds of motion shown in Figures 3.2 to 3.9 correspond to the prefixed pulse.

3.4.2 Selection of frequencies and duration of input motion

Important savings in computational time can be made if one reduces both the number of frequencies considered and the duration of the input motion, provided that the shape of the response spectrum is not greatly affected.

Since there seems to be no universally accepted definition of significant duration, it has been a common practice to clip the accelerogram at a point close to the end of the strong phase of motion. This is in general appropriate when the problem under consideration lies in the relatively high frequency region. However, response spectra computed using only the strong portion of motion are likely to be inaccurate, on the unconservative side, for intermediate and low frequencies.

Due to the nature of this study, the main concern aimed at savings in nonlinear response calculations. For this reason, elastic spectra were computed first for a relatively large number of frequencies and a rather long duration of motion. The times when maxima occurred were observed, and responses for a few inelastic systems computed, to check if the same trends were noted. Then, the record durations indicated in Table 3.3 were selected. It may be noted that the tabulated durations are not rounded numbers; this is because points corresponding to zero velocity were chosen so that the ground was at rest at the end of the record. Response calculations were continued for one-half period of free vibration following the ground motion, since some systems experience their maximum response after the ground motion ceases.

It can be seen in Table 3.3 that the duration required at high frequencies is sometimes about one half or two thirds of that needed at low frequencies; indeed, one is interested in shorter durations for high frequency systems since they require smaller intervals of integration.

One additional remark is necessary with regard to the San Juan record. In this case, a very weak portion of motion at the beginning of the record was removed; thus, t=0 in Fig. 3.11 corresponds to t=11.8 seconds in the original record.

The set of frequencies used for each record was selected after observing the shape of the elastic spectrum, so that larger spacing could be used in smoother areas. In irregular regions, frequencies were chosen so as to include the most important features of the spectrum -peaks and troughs- and so that the spectrum varied smoothly between the selected frequencies. The set of frequencies used for each record, for inelastic responses, are tabulated in Table 3.4.

3.4.3 Procedure to obtain responses for specified ductilities

Denoting the yield point deformation by u_y, and the maximum deformation, without regard to sign, by u_m, the ductility factor is defined as

$$\mu = \frac{u_m}{u_y} \qquad (3.6)$$

For plotting inelastic spectra one is interested in responses associated with predetermined values of the ductility factor. In particular, the following values were selected for this study: 1 (elastic), 1.5, 2, 3, 5, and 10.

An interpolative procedure is normally involved since the responses of systems with arbitrarily selected yield levels will seldom correspond to the desired ductility values. Furthermore,

the results of a single interpolation may err considerably. The difficulty arises from the fact that the ductility factor varies irregularly as the yield level is progressively reduced, for fixed values of the frequency parameter, as in the examples shown in Figures 3.12 and 3.13. In these figures, the yield displacement is expressed as a fraction of u_e, the maximum response of the elastic system with the same natural frequency.

Hence, an iterative procedure is required to obtain the specified ductilities. After each interpolation, responses were computed to check the accuracy of the interpolated points. The results were considered satisfactory if within 1% of the desired ductility. The interpolations were performed assuming a linear relation between $\log(u_y)$ and $\log(\mu)$, which is approximately the case for many frequencies, or, at least, it holds over important segments of the range of interest when irregularities are present, as shown in Figures 3.12 and 3.13.

It should be noted that ductility does not always increase monotonically as the yield level decreases, thus, there can be more than one yield level corresponding to a given value of μ. For example, the case f=4 in Fig. 3.13 features three yield levels corresponding to a ductility factor of 10. This peculiar phenomenon, already brought out by Veletsos and Newmark (115), can be explained on physical grounds that are paramount in the understanding of the nature of nonlinear response. The ductility factor, represented by the solid line in Figs. 3.12 and 3.13, results from the larger of u_m^+/u_y and u_m^-/u_y, where u_m^+ is the maximum relative displacement in the positive direction of motion

and u_m^- the absolute value of the maximum displacement in the negative direction; the dashed lines correspond to whichever was the smaller of the previous ratios. Indeed, the relative magnitudes of u_m^+ and u_m^- vary as the yield displacement decreases, so that at some level $u_m^+=u_m^-$, in which case the system dissipates energy more efficiently. This often corresponds to a local minimum of the ductility factor, as it occurs for example for u_y/u_e values of 0.55 and about 0.25 for f=0.15 in Figure 3.12.

Back to the discussion of the interpolative procedure, it must be noted that in the case of multiple solutions the method leads to whatever solution it hits first. In very special situations, for instance for a target ductility of 2 for the case f=0.65 in Fig. 3.12, the accuracy criterion may be satisfied by a large number of points.

3.5 Presentation of results

A simple means of representing structural response to a given motion is through the response spectrum. It consists of curves that represent the maximum numerical values of the responses as functions of the natural frequency and other parameters such as damping or ductility.

The choice of a tripartite logarithmic plot, with frequency plotted also logarithmically, is convenient because it permits the simultaneous plotting of three related quantities that give information on a number of aspects of the maximum response of the systems considered. Various quantities can be plotted depending on the type of spectrum one is interested in; in general, these

quantities will be denoted by S_d, S_v, and S_a, and will be referred to as spectral displacement, spectral velocity and spectral acceleration, by virtue of the dimensional nature of the quantities they represent. Correspondingly, the axes of the plot will be referred to as the velocity axis, which is perpendicular to the frequency axis, and the displacement and acceleration axes at 45 degree angles. The spectral quantities are interrelated as follows:

$$S_v = \omega S_d \qquad\qquad (3.7a)$$

$$S_a = \omega S_v = \omega^2 S_d \qquad\qquad (3.7b)$$

In the case of linearly elastic systems, the Elastic Spectrum features the maximum relative displacement, u_e, in the displacement axis. The spectral velocity, ωu_e, often referred to as pseudovelocity, is nearly the same as the maximum relative velocity for intermediate frequencies and low damping, but differs substantially for very low frequencies and high damping. The pseudovelocity is related to the maximum energy absorbed by the elastic system, E, by the equation

$$E = \frac{1}{2}m(\omega u_e)^2 = \frac{1}{2}ku_e^2 \qquad\qquad (3.8)$$

The spectral acceleration, $\omega^2 u_e$, or pseudoacceleration, is equal to the maximum absolute acceleration when there is no damping; they differ, especially for low frequencies, when damping is present. However, one is indeed more interested in the pseudoacceleration since by multiplying by the mass one obtains, precisely, the maximum force in the spring.

Elastic Spectra for the 10 records considered in this study, and for damping factors of 2, 5, and 10 percent of critical, are shown in Figures 3.14 to 3.23.

The response of nonlinear systems can be best represented graphically by means of the Inelastic Yield Spectrum (IYS). In this case, the yield deformation, u_y, necessary to limit the maximum deformation of the system to a specified multiple of the yield deformation itself, $u_m = \mu u_y$, is plotted on the displacement axis. The spectral acceleration, $\omega^2 u_y$, multiplied by the mass gives the yield resistance R_y

$$R_y = m\omega^2 u_y = k u_y \tag{3.9}$$

which in the case of elastoplastic systems is also the maximum force in the spring. For bilinear and degrading systems with strain hardening slope sk, the maximum force in the spring, R_m, is obtained from the expression

$$R_m = m\omega^2 u_y [1 + s(\mu-1)] \tag{3.10}$$

Alternatively, in instances where it is desirable to deal directly with maximum forces, it is possible to plot R_m/m on the acceleration axis to obtain Inelastic Acceleration Spectra (IAS) for systems with strain hardening. In this case, the quantities on the displacement and velocity axes are meaningless. Obviously, IYS and IAS are identical for elastoplastic systems.

In a similar fashion, if one is concerned with maximum deformations, Total Deformation Spectra (TDS) featuring the

maximum relative displacement u_m in the displacement axis can be drawn, in which case the quantities on the velocity and acceleration axes are irrelevant.

It is clear from the foregoing that the information in the IAS and the TDS are readily determined from the IYS by multiplying by $[1+s(\mu-1)]$ and μ respectively; hence, besides being convenient for illustrative purposes, there seems to be no particular advantage in deriving IAS or TDS for the purpose of this study.

The results of response computations are then presented in term of IYS. For each earthquake record, there are five spectra corresponding to elastoplastic systems with 2, 5, and 10 percent damping, and bilinear and degrading systems with 5 percent damping. For illustration, IAS are included for the case of the El Centro record, and TDS are presented for the first five records listed in Table 3.3. The various spectra are shown in Figures 3.24 to 3.80.

3.6 Discussion of results

In this section, observations are made regarding the effect of damping and the influence of different types of resistance functions on inelastic behavior. The results presented in the preceding section are discussed, in qualitative terms, on the basis of comparisons of spectra for particular records. Then, force deformation curves and response time histories for a few systems are examined to explain some of the differences observed in the spectra.

The spectra in Fig. 3.81 for the Pacoima Dam record is typical of the effect of damping combined with inelastic behavior. It is apparent that:

(a) the effect of damping is quite different in the various regions of the spectrum. In particular, in the very low frequency range the effect of damping may be considered to be negligible, whereas it is still somewhat effective in reducing the magnitude of the response of very rigid systems. In turn, damping is most efficient in the intermediate frequency range, say between 0.2 to 10 cps.

(b) The effect of damping lessens as inelastic deformations increase. For instance, in the previously mentioned frequency range, the percentage response reduction resulting from increasing the damping factor from 2% to 10% for systems with ductilities larger than 3 is, on the average, about one half of that for elastic systems.

Inelastic Yield Spectra for elastoplastic, bilinear and degrading systems subjected to the El Centro, Olympia, and Pacoima Dam records are compared in Figures 3.82 to 3.87. These plots feature characteristics which are representative of the spectra for all the records considered in this study. The following observations can be made:

(a) The response of very low frequency systems is independent of their force deformation law.

(b) Some differences can be noted for high frequency systems (f greater than 10 cps), but they are negligible for ductility factors less than about 5, and not substantial for larger

ductilities.

(c) For intermediate frequencies, the responses of bilinear systems with ductility less than or equal 2 are practically identical to those of elastoplastic systems with the same yield level. For larger ductilities, the maximum responses of bilinear systems are in general smaller than those of the associated elastoplastic systems.

(d) All frequencies considered, the ordinates of the spectra for elastoplastic systems seem to be, on the average, larger than those of the spectra for stiffness degrading systems.

(e) Spectra for stiffness degrading systems are smoother than spectra for elastoplastic systems. Notably, the former have a tendency to go below the peaks and above the troughs of the latter.

The last observation points to a remarkable difference in the behavior of elastoplastic and degrading systems. Before attempting to explain why, it is worth emphasizing that the observations regarding degrading systems reveal that stiffness degradation is not as much a detrimental phenomena as one might expect, a priori. It is necessary to recall too that the degrading model under consideration does not include strength deterioration nor softening of the unloading stiffness, wherefore one must restrain from extending the conclusions reached herein beyond their scope.

Consider for example the spectra for El Centro shown in Fig. 3.83; the largest differences between elastoplastic and degrading systems occur for a frequency of 0.15 cps and

ductilities between 3 to 5. Figure 3.82 also features an important difference at the same frequency and for a ductility factor of 5. The variation of ductility as the yield level decreases, for the three types of resistance functions, is shown in Fig. 3.88; notably, the curve for degrading systems is smoother than the others. It is of interest to examine the case $u_y/u_e=0.3$, or $u_y=5.73$ inches, for which the response of the elastoplastic system is about 2 times that of the degrading system. The relative displacement and spring force time histories, as well as the corresponding hysteresis curves, are shown in Figures 3.89 and 3.90; the maximum displacements of the elastoplastic, bilinear, and degrading systems are 27.44, 23.44, and 14.28 inches respectively, which correspond to ductilities of 4.8, 4.1, and 2.5. It is apparent that:

(a) The stiffness degrading system was the most efficient regarding energy dissipation capacity. The maximum displacement attained in the first yield excursion was barely exceeded, once, at a later time.

(b) The elastoplastic system was driven through successive yielding cycles, with plastic deformations occurring predominantly in one direction.

(c) Although the bilinear system behaved in a manner similar to that of the elastoplastic system, it was somewhat more efficient.

(d) After first yielding, the degrading system was capable of recovering, further than the others, in the opposite direction. This mechanism prevented the one-sided behavior

experienced by the elastoplastic system, and led to the smallest permanent plastic deformation after the end of the ground motion. The permanent set of the degrading system was about 5 inches, against about 17 and 22 inches for the bilinear and elastoplastic systems respectively.

It is also instructive to consider systems presenting larger ductilities, such as the case $u_y/u_e=0.04$, or $u_y=0.764$ inches, in Fig. 3.88. The response time histories and hysteresis curves are shown in Figures 3.91 and 3.92. In this case, the three systems yield significantly in both the positive and negative directions; the maximum relative displacements are, in the positive and negative directions respectively, 11.2 and -7.6 inches for the elastoplastic system, 12.8 and -7.92 inches for the bilinear system, and 10.4 and -8.1 inches for the degrading system. These responses correspond to maximum ductilities of 14.6, 16.7, and 13.6 for the elastoplastic, bilinear, and degrading systems respectively. Ostensibly, the degrading system yielded, in the sense of reaching the bilinear spine, a fewer number of times and was competent to dissipate energy through hysteresis loops associated with moderate spring forces. The degrading system also shows better balance with regard to positive and negative deformations. It is reasonable to presume that the behavior of the degrading system was mainly dominated by the softening resulting from stiffness degradation, rather than by the effect of the additional strength provided by its strain hardening slope. Indeed, the associated bilinear system presented the largest maximum deformation. It may be also noted that the

degrading system presents the smallest permanent set at the end of the ground motion.

Unlike the situation observed in the first example mentioned above, it can be seen in Fig. 3.83 that for a frequency of 1.1 cps, the degrading system attains a ductility of 2 for a yield level much larger than that required by the elastoplastic system to have the same response ductility. A yield displacement of 1.28 inches results in maximum negative and positive displacements of -2.56 and 1.84 inches for the degrading system, -1.98 and 2.02 inches for the elastoplastic, and -2.06 and 2.0 inches for the bilinear system. Respectively, these responses correspond to maximum ductilities of 2.0, 1.58, and 1.61. It is apparent that the response of the elastoplastic system was the best balanced, thus leading to the lowest ductility. The response time histories and force displacement curves for this case are shown in Figures 3.93 and 3.94.

Finally, it is worthwhile to study a couple of cases wherein the maximum responses of the three models are practically the same as a result of a peculiar feature of the ground motion itself, rather than as a consequence of the energy dissipation mechanism. Consider systems with 5% damping, frequency of 0.75 cps, and yield displacement of 9.44 inches, subjected to the Pacoima Dam record (see Figures 3.86 and 3.87). Besides a virtually unnoticeable difference due to the hardening of the bilinear and degrading systems, a ductility of 2 is obtained for all the models. The relative displacement time histories shown in Fig. 3.95 indicate that the three models attained their

maximum responses at the the same time for the first and only important yield excursion; the corresponding hysteresis curves are shown in Fig. 3.96.

For the same frequency but a yield displacement of 1.685 inches, a ductility factor of 10 is obtained for bilinear and degrading systems, and slightly larger, 10.33, for the elasto-plastic system. The maxima ocurred, after considerable yielding, in the first drive into the inelastic range (see Figures 3.97 and 3.98). As in the previous case, the systems were apparently impelled by a relatively long acceleration pulse in the Pacoima Dam record, starting at t=4.4 seconds in Fig. 3.7. Notably, this pulse greatly influences the behavior of systems whose natural frequencies are near that of the pulse itself; this is clearly perceptible in the spectra shown in Figures 3.86 and 3.87. Notably too, in this and the previous example, the elastoplastic systems feature the largest permanent deformations. The danger of incremental collapse due to the accumulation of inelastic deformations during a sequence of long acceleration pulses has been pointed out by Bertero (12,13).

From the few cases discussed above, it is concluded that the characteristics of the response of particular systems can be explained, a posteriori, on physical grounds. It is also clear that the variety of situations one may encounter is such that one cannot precisely predict the response of a particular system to a particular ground motion. The discussion in Section 3.4.3 best dramatizes the problem that even systems with the same type of resistance function, same degree of damping, and subjected to the

same ground motion, may behave in entirely different manners, depending on how energy is dissipated at the various yield levels. Furthermore, when the responses of different nonlinear models are compared, it is apparent that the conditions for any of them to be "better" than the others, strongly depend on an intimate interaction between the hysteretic behavior itself and the particular characteristics of the ground motion being input.

Although no conclusive statements can be made from the observation of particular systems, the comparisons of inelastic spectra presented above suggest some general trends. Naturally, these trends can only be confirmed by means of average spectra for a number of records, as will be discussed in the next chapter.

CHAPTER 4

STATISTICAL ANALYSIS OF THE DATA

4.1 Introduction

The purpose of the statistical analysis is twofold: (a) to determine factors for constructing design spectra when estimates can be made of the possible peak ground motion parameters for future earthquakes affecting a site, and (b) to make observations regarding the effect of damping combined with inelastic behavior and the effect of different types of nonlinearities, on the basis of average spectra.

To summarize, in the elastic case, the statistical procedure consists in determining factors ϕ_e that, applied to the ground motion estimates Y, give the spectral ordinates S_e, for each of the three characteristic regions of the spectrum:

$$S_e = \phi_e \, Y \qquad (4.1)$$

Values of ϕ_e for various damping factors and probability levels have been presented by Newmark et al, (41,65,71,77,98). In a similar fashion, the inelastic spectrum S_μ can be obtained by applying factors ψ_μ to Y:

$$S_\mu = \psi_\mu \, Y \qquad (4.2)$$

Alternatively, the inelastic spectrum S_μ can be obtained by deamplifying the elastic spectrum S_e, so that

$$S_\mu = \phi_\mu \, S_e \qquad (4.3)$$

Evidently, the foregoing factors are related as follows

$$\Psi_\mu = \phi_\mu \phi_e \qquad\qquad (4.4)$$

where the subscript "e", denoting elastic conditions, corresponds to the particular case $\mu = 1$, so that

$$(\Psi_\mu)_{\mu=1} = \phi_e \qquad\qquad (4.5.a)$$

$$(S_\mu)_{\mu=1} = S_e \qquad\qquad (4.5.b)$$

$$(\phi_\mu)_{\mu=1} = 1 \qquad\qquad (4.5.c)$$

In the next sections, Ψ_μ and its statistics will be determined. Then, ϕ_μ factors corresponding to a presentation of the form of Eq. 4.3 are computed using Eqs. 4.4 and 4.5.a. This type of presentation is convenient because it is consistent with previous recommendations currently in use (73), and especially, because ϕ_μ is found to be practically independent of the probability level associated with the inelastic spectrum, whereas Ψ_μ is not; thus, the same ϕ_μ can be used regardless of the character of S_e.

Finally, the results are discussed with regard to the effect of damping and the influence of the type of nonlinearity on inelastic response.

4.2 Normalization of the data

Results in the form of Inelastic Yield Spectra are used for the analysis. As mentioned earlier, this type of spectrum contains all the information necessary to describe the maximum

inelastic response of any system. It is convenient to recall that every spectral point S depends on a number of parameters,

$$S_i = S_i(f,\beta,\mu,R) \qquad (4.6)$$

where f, β, μ, and R correspond to frequency, damping factor, ductility, and resistance function respectively, and i denotes the various input motions used.

For simplicity, the parameters β, μ, and R will not be carried through the analysis explicitly, on the understanding that the same procedure will be carried out separately five times, i.e., for the three damping factors associated with elastoplastic systems, for bilinear systems, and for degrading systems. Similarly, for each of these cases, the ductility factor can take any of the six selected values. Hence, Eq. 4.6 can be rewritten as

$$S_i = S_i(f) \qquad i=1,2,\ldots 10 \qquad (4.7)$$

Since the ground motions for earthquake records differ from each other, the computed responses connot be compared on an absolute basis. In order to make meaningful comparisons, it is customary to scale the spectra to some predetermined parameter. In this study, normalizations are made either to maximum ground acceleration, maximum ground velocity, or maximum ground displacement, over the entire range of frequencies; but primary consideration is given to normalization relative to maximum acceleration for high frequencies, to maximum velocity for intermediate frequencies, and to maximum displacement for low

frequencies. This sort of normalization is implicit in the general formulation presented in Section 4.1, i.e., when factors are applied to estimates of the three peak ground motion parameters. On the other hand, the procedure leads to a minimization of the dispersion of the data, as will be discussed later. The normalized spectral ordinates are defined as:

$$\psi_{Qi}(f) = \frac{S_i(f)}{Q_i} \qquad i=1,2,\ldots10 \qquad (4.8)$$

where Q_i can be either A_i, V_i, or D_i, the peak ground acceleration, peak ground velocity, and peak ground displacement of the ith record respectively; in turn, to indicate the parameter used in the normalization, ψ is subscripted with Q equal to A, V, or D, as the case may be.

It is worth noting that when a single response spectrum is normalized to one of the three ground motion parameters, the spectral ordinates at the various frequencies are divided by a constant; therefore, the shape of the normalized spectrum is identical to that of the original spectrum. At any frequency, the ordinates of the response spectra obtained by normalizing to each of three parameters are proportional to each other, the proportionality factor being the ratio of two of the three ground motion peaks; for example:

$$\frac{\psi_{Ai}(f)}{\psi_{Vi}(f)} = \frac{V_i}{A_i} \qquad (4.9)$$

Furthermore, the general relationships between the spectral quantities (Eqs. 3.7) are obviously valid for the normalized

spectrum, regardless of the scaling parameter, i.e.,

$$\psi_{Qvi}(f) = \omega\psi_{Qdi}(f) \qquad (4.10.a)$$

$$\psi_{Qai}(f) = \omega\psi_{Qvi}(f) \qquad (4.10.b)$$

where the subscripts a, v, and d refer to the spectral quantities being considered.

4.3 Single frequency statistics

Although the final objective is to determine response statistics associated with frequency bands, single frequency statistics are relevant for a number of reasons. First, the appropriateness of the normalization procedure, adopted from studies of elastic spectra, is verified for the inelastic case. Second, observation of mean spectra is paramount to devise a procedure to define the spectral regions for which frequency band statistics are computed. Lastly, comparisons of mean spectra for the various conditions considered in this study lead to important conclusions regarding the characteristics of the response of inelastic systems; observations in this regard will be made later in a separate section for the sake of continuity of the statistical analysis.

Let F_i be the set of frequencies at which responses were computed for record i. It is desirable to compute ensemble averages for every frequency f belonging to the set F, where

$$F = \bigcup_{i=1}^{n} F_i \qquad (4.11)$$

includes all the different frequencies in Table 3.4. For each frequency, the sample mean, variance, standard deviation, and coefficient of variation are, respectively, computed as follows:

$$\bar{\psi}_Q\,(f) = \frac{1}{n}\sum_{i=1}^{n}\psi_{Qi}(f) \tag{4.12}$$

$$\tilde{V}\text{ar}[\psi_Q(f)] = \frac{1}{n}\left(\sum_{i=1}^{n}\psi_{Qi}^2(f) - n\bar{\psi}_Q^2(f)\right) \tag{4.13}$$

$$\tilde{\sigma}[\psi_Q(f)] = \sqrt{\tilde{V}\text{ar}[\psi_Q(f)]} \tag{4.14}$$

$$\tilde{\Omega}[\psi_Q(f)] = \frac{\tilde{\sigma}[\psi_Q(f)]}{\bar{\psi}_Q(f)} \tag{4.15}$$

where n is the number of records, and the subscript Q can be either A, V, or D depending on the character of the normalized data. It should be pointed out that prior to computing the above statistics, responses must be defined for each sample spectrum for every frequency belonging to F. The necessary additional values are obtained by interpolation, which is justified by the manner in which the frequencies were selected for each record, as explained in Section 3.4.2. It should also be noted that Eq. 4.13 gives the so called "biased" estimate of the population variance; this bias can be simply removed by dividing by (n-1) instead of n in Eq. 4.13 (7); however, for present purposes, as stated at the beginning of this section, the distinction is immaterial.

Mean and mean plus one standard deviation spectra for elastoplastic systems with 5% damping are shown in Figures 4.1 to

4.3. Mean spectra for elastoplastic systems with 2% and 10% damping, and for bilinear and stiffness degrading systems with 5% damping are presented in Figures 4.6 to 4.17. There are several observations to make from these plots, which will be discussed next.

Referring to Figs. 4.1 to 4.3, and noting that the distance between the solid and the corresponding dashed lines gives an indication of the coefficient of variation of the data, the observation can be made that normalization to peak ground acceleration gives a COV that is minimum for high frequencies and increases towards the low frequency region, whereas the opposite occurs for normalization to ground displacement. Normalization to ground velocity leads to a more uniform COV over the entire frequency range. This is confirmed by directly plotting the COV against frequency for the three normalization parameters, as shown in Figures 4.4 and 4.5. Furthermore, the same trend is observed regardless of the value of the ductility factor, thus indicating that the normalization procedure, as used in elastic studies (41,77), is adequate for the analysis of nonlinear spectra.

Mean spectra for elastic conditions ($\mu=1$) feature segments that are approximately parallel to the horizontal and 45 degree lines of the logarithmic plot. For instance, in spectra normalized to ground acceleration (Figs. 4.1, 4.6, and 4.9), the spectral acceleration is nearly constant for frequencies ranging from about 3 cps to 8 cps. Also, in this range the COV has a tendency to stabilize around a constant value. It can be seen in

Fig. 4.4 that the COV oscillates around a value of about 0.22 for frequencies between 2.5 and 9 cps; the same observation can be made for other damping factors, although the COV will in general increase for lower damping and vice versa. Above 8 cps the spectral acceleration decreases fairly uniformly to intersect the ground motion acceleration at a frequency of about 35 cps.

Similarly, elastic spectra normalized to ground velocity (Figures 4.2, 4.7, and 4.10) are approximately uniform for the intermediate range of frequencies, say between 0.4 and 3 cps, although some tendency to increase toward higher frequencies is observed; in turn, in this range, the COV remains at a low level (Fig. 4.4).

At lower frequencies, mean spectral displacements are approximately constant for frequencies ranging from about 0.1 to 0.4 cps (Figs. 4.3, 4.8, and 4.11); below 0.1 cps there is a transition region decreasing to the maximum ground displacement at a frequency of about 0.03 to 0.04 cps. Unlike in the other regions, the COV of elastic spectra normalized to ground displacement does not keep a uniform level (Fig. 4.4), although it is in general lower than that obtained if the other scaling parameters were used. The explanation for the irregular COV in the displacement region presumably is based on the fact that responses in that region, as well as integrated ground displacements, are particularly sensitive to base line adjustments of earthquake records, thus constituting less reliable quantities.

A conclusion apparent in the preceding considerations is

that in the case of average elastic spectra it is both possible and appropriate to define regions of response amplification by simple inspection. Actually, the above mentioned frequency bands are in general agreement with those selected in previous studies (41,77). However, in the case of inelastic responses the corresponding regions are more difficult to visualize, especially for large ductilities. For example, observation of spectra for a ductility factor of 10 reveals a shift of the velocity region towards higher frequencies. Therefore, spectral regions inferred from observation of elastic spectra are not suitable for computing frequency band averages for inelastic conditions.

To eliminate arbitrariness in the determination of the boundaries between the three spectral regions, a procedure consisting in fitting trapezoidal lines to the mean spectra is developed in the next section.

4.4 Determination of spectral regions

Consider the average spectrum $\bar{\psi}_Q(f)$ shown in Fig. 4.18, and assume it corresponds to any of the spectra computed according to Eq. 4.12 presented above. It is desired to fit a trapezoidal line to $\bar{\psi}_Q(f)$ between lower and upper frequency limits set at 0.1 and 8 cps respectively. This limits comprise the most important portion of the spectrum with regard to response amplification, and exclude the transition regions above 8 cps and below 0.1 cps.

The trapezoidal line becomes determinate if its three spectral ordinates and the knee frequencies f_{dv} and f_{va} are known (see Fig. 4.18). The frequencies f_{dv} and f_{va} are the boundaries

between the displacement and velocity regions, and the velocity
and acceleration regions respectively.

It is worth reiterating that for any frequency such as f_o in
Fig. 4.18, $\overline{\psi}_Q(f_o)$ can be referred to in terms of any of the three
spectral quantities $\overline{\psi}_{Qa}(f_o)$, $\overline{\psi}_{Qv}(f_o)$, and $\overline{\psi}_{Qd}(f_o)$, which are, of
course, related to each other (Eqs. 3.7).

It should be also noted that $\overline{\psi}_Q(f)$ is defined for the set of
frequencies F as indicated by Eq. 4.11. The frequencies
belonging to F are not necessarily evenly spaced; although they
cover the frequency axis in a reasonable manner, a few points of
clustering can be identified. On the other hand, recalling the
manner in which the frequencies were selected for each record,
most of them correspond to points of local spectrum extrema.
From these considerations one can draw the conclusion that, for
the purpose of computing frequency band averages, it is
convenient to treat $\overline{\psi}_Q(f)$ as a piecewise linear function of f.
Consideration of $\overline{\psi}_Q(f)$ as a discrete function of f would be
equivalent to assign the same weight to all data points
regardless of their actual spacing; on the other hand, it would
lead to overestimated measures of the dispersion of the data.

Naturally, the distinction between the discrete or continu-
ous character of the mean spectra would be trivial, for all prac-
tical purposes, if data for a substantially larger number of
frequencies were available, but it seems pertinent herein. The
assumption of piecewise linearity is compatible with the smooth
variation between the selected frequencies indicated in Section
3.4.2, besides being the simplest one can make.

The fitting of the trapezoidal lines proceeds iteratively as described next. Assume values for f_{dv} and f_{va} and compute frequency band averages for the spectral regions so determined as follows:

$$\overline{\psi}_{Qd}^{(j)} = \frac{\displaystyle\int_{0.1}^{f_{dv}^{(j)}} \overline{\psi}_{Qd}(f) \; df}{f_{dv}^{(j)} - 0.1} \qquad (4.16.a)$$

$$\overline{\psi}_{Qv}^{(j)} = \frac{\displaystyle\int_{f_{dv}^{(j)}}^{f_{va}^{(j)}} \overline{\psi}_{Qv}(f) \; df}{f_{va}^{(j)} - f_{dv}^{(j)}} \qquad (4.16.b)$$

$$\overline{\psi}_{Qa}^{(j)} = \frac{\displaystyle\int_{f_{va}^{(j)}}^{8} \overline{\psi}_{Qa}(f) \; df}{8 - f_{va}^{(j)}} \qquad (4.16.c)$$

where the superscript j indicates the jth iteration. Noting that the subscript Q can be either A, V, or D, depending on the character of the normalized data under consideration, three sets of equations of the form of Eqs. 4.16 can be written.

Next, compute the new knee frequencies as:

$$f_{dv}^{(j+1)} = \frac{1}{2\pi} \frac{\overline{\psi}_{Qv}^{(j)}}{\overline{\psi}_{Qd}^{(j)}} \qquad (4.17.a)$$

$$f_{va}^{(j+1)} = \frac{1}{2\pi} \frac{\overline{\psi}_{Qa}^{(j)}}{\overline{\psi}_{Qv}^{(j)}} \qquad (4.17.b)$$

Then, averages are computed for the new regions, and so on, until

$$f_{dv}^{(j+1)} = f_{dv}^{(j)} \qquad (4.18.a)$$

$$f_{va}^{(j+1)} = f_{va}^{(j)} \qquad (4.18.b)$$

up to a desired number of significant figures. In general the procedure converges in about half a dozen iterations.

The resulting knee frequencies and fitted trapezoidal lines for the case of elastoplastic systems with 5 percent damping are shown in Figs. 4.19, 4.20 and 4.21. It may be observed that the knee frequencies vary somewhat depending on the normalization parameter used, however, the same trend is observed regarding the rightward shift of the velocity region as the ductility increases.

The relative ordinates of the fitted lines do not vary significantly with the different normalizations. To make a meaningful comparison, the band averages for the various ductilities in each region are divided by the average for $\mu=1$ in the same region; these ratios, along with the corresponding limiting frequencies, are presented in Table 4.1. This result is expected since the ratios must reflect an essential attribute of the original spectra, and thus be independent of the sets of coefficients used to scale the data. Incidentally, these ratios actually correspond to deamplification factors consistent with the form of Eq. 4.3; later on, they will be presented and discussed for the various conditions considered in this study.

4.5 Frequency band statistics

Henceforth, in each spectral region, the attention will be focused in the data normalized to the ground motion parameter corresponding to that region; for instance, out of the nine averages defined by Eqs. 4.16, the concern will be on the terms $\overline{\Psi}_{Dd}$, $\overline{\Psi}_{Vv}$, and $\overline{\Psi}_{Aa}$. Thus, the subscripts can be dropped for simplicity.

On this basis, the frequency band average, variance, standard deviation and coefficient of variation are, respectively computed as follows:

$$\overline{\Psi} = \frac{1}{n} \sum_{i=1}^{n} \frac{\int_{f_\ell}^{f_u} \psi_i(f)\, df}{(f_u - f_\ell)} \tag{4.19}$$

$$\mathrm{Var}(\psi) = \frac{1}{n} \sum_{i=1}^{n} \frac{\int_{f_\ell}^{f_u} (\psi_i(f) - \overline{\Psi})^2\, df}{(f_u - f_\ell)} \tag{4.20}$$

$$\sigma(\psi) = \sqrt{\mathrm{Var}(\psi)} \tag{4.21}$$

$$\Omega(\psi) = \frac{\sigma(\psi)}{\overline{\Psi}} \tag{4.22}$$

where n is the number of records and f_ℓ and f_u are the lower and upper limit of each frequency band determined by the previosly fitted trapezoidal lines. It is worth noting that the averages computed with Eq. 4.19 are identical to those obtained by means of Equations 4.16; substitution of Eq. 4.12 into the latter only reveals a reversed order of summation and integration.

The frequency band averages $\overline{\Psi}$ correspond to the desired ψ_μ

factors defined by Eq. 4.2. Similarly, to emphasize their dependence on the ductility factor, hereafter the standard deviation and the COV defined by Eqs. 4.21 and 4.22 will be designated as σ_μ and Ω_μ. The calculated statistics, along with f_ℓ and f_u, are summarized in Tables 4.2 and 4.6 for the various ductility factors, resistance functions, and damping factors considered in this study. The Ψ_μ factors are also shown in Figs. 4.22 to 4.27; observations regarding the effect of the various parameters involved will be made in Section 4.7.

A comparison of the results for elastic systems with those obtained in a previous study of elastic spectra (77) is instructive. It can be seen in Table 4.7 that the results are in general agreement, despite the differences in the ground motions used in the studies. In the Newmark-Hall-Mohraz study, 14 earthquakes were considered, with two components of horizontal motion being used for each earthquake, thus giving a total of 28 records. Only four of the latter are included among the ten records used in this study, and even these four records may be somewhat different since different versions were used in each study; in Ref. 77, the originally uncorrected records were adjusted assuming a segmentally parabolic acceleration base line. Although the procedures used in the studies involved some differences in the arrangement of frequencies, determination of frequency bands, and computation of band averages, the formulation of the problem was conceptually the same.

The coefficients of variation in Tables 4.2 to 4.6 give an indication of the variability of the normalized responses. It

can be seen that Ω_μ does not vary significantly for the various damping factors, ductilities, and resistance functions; although not consistently, Ω_μ seems to decrease as damping and ductility increase. It is notably different for the various spectral regions: between about 15-20% in the acceleration region, 30-40% in the velocity region, and 40-50% in the displacement region.

It must be emphasized that the calculated Ω_μ does not include all the uncertainties associated with predicted spectral ordinates. In fact, a large degree of uncertainty is involved in the estimation of the possible ground motion peaks resulting for future earthquakes affecting a site. The uncertainties underlying such estimates depend not only on a number of factors but also on the amount and quality of the information available for a given site, as will be discussed in the next chapter.

4.6 Deamplification factors

As stated before, it is customary to derive inelastic spectra by reducing the ordinates of the elastic spectrum (73, 114,116) as symbolically indicated by Eq. 4.3. Deamplification factors ϕ_μ associated with mean level responses can be simply obtained as:

$$\phi_\mu = \frac{\Psi_\mu}{\Psi_{\mu=1}} \qquad (4.23)$$

which follows from Eqs. 4.4 and 4.5.a. The computed ϕ_μ for the various resistance functions, ductilities, damping factors, and spectral regions are presented in Tables 4.2 to 4.6 and plotted

in Figures 4.28 to 4.33.

For practical applications, ϕ_μ values can be read or interpolated directly from the figures. For the case of ealastoplastic systems, and in order to facilitate calculations for intermediate ductility values and damping factors, it is useful to have expressions for ϕ_μ in terms of these parameters. General expressions of the form

$$\phi_\mu = (p\mu-q)^{-r} \tag{4.24}$$

for the acceleration and velocity regions, and

$$\phi_\mu = p\mu^{-r} \tag{4.25}$$

for the displacement region were derived by means of multivariate nonlinear regression analyses. For this purpose, a modified Levenberg-Marquardt algorithm was used (52,60); the sum of the squares of the logarithm of the residuals was used as objective function rather than the simple sum of the squares since the former leads to more uniform relative errors. The resulting coefficients are indicated in Figures 4.28 to 4.30. The general expressions are accurate within 2% or less, and can be conveniently used if a pocket calculator is available.

If a greater degree of conservatism is desired, factors associated with smaller probabilities of exceedance can be used. In other words, one is interested in determining p-percentile $\Psi_{p\mu}$ factors so that the probability that the response amplification will not exceed $\Psi_{p\mu}$ is p. Assuming normal distribution, the

percentile amplification factors are computed as

$$\Psi_{p\mu} = \Psi_\mu + \delta_p \sigma_\mu \qquad (4.26)$$

where the coefficient δ_p, indicating the deviation from the mean, can be obtained, for the corresponding probability level p, from tables of standard normal probability (7). For instance, δ_p is equal to 0, 1, and 2 for p equal to 0.5, 0.841, and 0.977 respectively; the associated factors correspond to the 50-percentile, 84.1-percentile and 97.7-percentile values. It has been recommended that amplification factors should in general be chosen for the 84.1 probability level, unless a greater or lesser degree of conservatism can be justified for the particular case under consideration (40).

Deamplification factors $\phi_{p\mu}$ corresponding to a probability level p can be obtained as

$$\phi_{p\mu} = \frac{\Psi_\mu + \delta_p \sigma_\mu}{\Psi_{\mu=1} + \delta_p \sigma_{\mu=1}} \qquad (4.27)$$

whence

$$\phi_{p\mu} = \frac{(1 + \delta_p \Omega_\mu)}{(1 + \delta_p \Omega_{\mu=1})} \phi_\mu \qquad (4.28)$$

For δ_p values from 0 to about 1, the difference between $\phi_{p\mu}$ and ϕ_μ is not very significant. In particular, for the recommended 84.1% probability level, i.e., $\delta_p = 1$, the correction factor

$$\lambda_\mu = (1 + \Omega_\mu)/(1 + \Omega_{\mu=1}) \qquad (4.29)$$

is in general close to 1, as can be seen in Tables 4.2 to 4.6. Therefore, as a reasonable approximation, ϕ_μ factors can be used regardless of the probability level. It should be also noted that using ϕ_μ instead of $\phi_{p\mu}$ is conservative when λ_μ is less than 1, which is always the case in the acceleration and velocity regions of the spectrum.

4.7 Discussion of results

In this section, observations are made from the previously presented factors and average spectra with regard to the effect of damping combined with inelastic behavior and the influence of different types of resistance functions on nonlinear responses.

It can be seen in Figures 4.22 to 4.24 that the effect of damping on inelastic response becomes less important as ductility increases. In the velocity region for example, the response of elastic systems is reduced, on the average, by about 41% when damping increases from 2 to 10 percent of critical, while for elastoplastic systems with displacement ductility of 10 the mean response decreases by only 16% for the same damping range. Similarly, in the acceleration region, $\Psi_{\mu=1}$ decreases by 42% while $\Psi_{\mu=10}$ reduces by 22% when damping increases from 2 to 10 percent of critical.

In the displacement region, the effect of damping is more uniform for the various ductility values. Comparing the Ψ_μ factors for 2 and 10 percent damping, a reduction of 27% is observed for elastic systems, 22% for systems with ductility of 1.5, and an aproximately constant reduction of 20% for

ductilities between 2 and 10. For this reason, a relationship corresponding to straight lines with constant slope in the logarithmic plot was used for the deamplification factor ϕ_μ in the displacement region (Eq. 4.25, Fig. 4.28).

The same conclusions can be reached by observing the mean spectra for elastoplastic systems with 2, 5, and 10 percent damping shown in Figures 4.34 and 4.35. It is also worth noting that at the low frequency end of the spectrum, 0.03 cps, the effect of damping is negligible regardless of the ductility level. The same is in general true at the high frequency end, 35 cps; however, there is still some reduction for a ductility factor of 10 (Fig. 4.35).

With regard to the effect of the type of resistance function on inelastic responses, it is instructive to compare mean spectra for elastoplastic, bilinear, and degrading systems with the same amount of damping, as shown in Figures 4.36 to 4.38.

First, it is apparent that the ordinates of the mean spectra do not vary very significantly when various nonlinear models are used; differences occur mainly for intermediate frequencies and large ductilities, and are practically negligible at the low and high frequency ends of the spectrum. And second, use of the elastoplastic idealization provides, in almost every case, a conservative estimate of the maximum response.

CHAPTER 5

INELASTIC SPECTRA FOR EARTHQUAKE RESISTANT DESIGN

5.1 Introduction

Currently available methods of structural analysis permit calculation of structural responses to deterministic dynamic loadings. From the results of such calculations, and from application of judgment and experience, the margin of safety or adequacy of the corresponding design may be assessed. Unfortunately, because a specific ground motion may not be representative of the variety of earthquake excitations the structure may possibly experience during its useful life, reliable results can be achieved only by examining the statistics of the response to several ground motion time histories. Since a number of nonlinear analyses may be an impractical requirement in the design of most structures, there is need to infer a more general and simpler loading condition.

One approach to this goal is the development of design spectra. Combining estimates of the possible intensities of future earthquakes, with information on the characteristics of the response of simple systems to a number of previously recorded ground motions, design spectra can be derived to prescribe design coefficients. Like response spectra, design spectra are not constructed to represent a single system but for a range of structure related parameters.

The basic steps for deriving design spectra involve: (a)

Selection of the earthquake hazard in terms of estimates of the expected peak ground acceleration, velocity, and displacement at the site under consideration; (b) estimation of structure related parameters; (c) construction of the Elastic Design Spectrum by applying amplification factors to the ground motion maxima; and (d) construction of the Inelastic Design Spectrum by deamplifying the Elastic Spectrum to take into account the effect of nonlinear behavior.

The various factors involved in the selection of the earthquake hazard are discussed first. Such a selection can not be treated as an isolated entity, but as an integral part of the design process. Although some design considerations are made along the presentation, a review of earthquake resistant design procedures is not intended here; discussions of general design concepts and procedures applicable to buildings (69,70), and to specialized systems (76) are available.

A formal derivation of the factors necessary for the last two steps above was given in Chapter 4. In this chapter, the information is summarized with a view towards the mechanics of the construction proper. Some additional aspects are discussed for the completion of the spectrum in the high and low frequency ends. Finally, some comparisons are made of derived design spectra with computed response spectra.

5.2 Estimation of ground motions

The earthquake motions for which a design is to be accomplished, or even the occurrence of a given size earthquake

affecting the site, are not amenable to precise determination and must be considered as probabilistic matters.

Procedures for a quantitative evaluation of the seismicity of a region and assessment of earthquake risk are available (28,29,32,34,59,79). Estimation of the earthquake risk at a particular site requires first to determine seismic activity levels associated with given volumes of the earth crust or with geologic features that can be identified as potential earthquake sources, such as active faults. This implies determination of the parameters of assumed probability distributions modeling earthquake magnitudes and rates of occurrence. Then, by means of attenuation expressions relating the desired ground motion characteristic (peak acceleration, peak velocity, etc) to earthquake magnitude and distance to the source, the seismic risk at the site is obtained by integration of the contributions of all significant sources, and expressed in terms of probabilities of exceedance of given intensities during given periods of time. When this procedure is repeated for a number of sites, the results can be presented in the form of regional seismicity maps showing contour levels for peak ground motion parameters that correspond to various return periods (1,33).

Earthquake risk analyses have not seldom been object of severe criticism. While the validity and limitations of the probabilistic models are discussed in most of the aforementioned references, the main weaknesses arise from the incomplete understanding of the mechanics of the natural process, and, undoubtedly, from the lack of adequate data.

One could even start by mentioning that reported magnitudes, for the same earthquake event, may vary by more than one point in the Richter scale depending on the reporting seismological station; on the other hand, it has been only since the 60's that the network of seismographic stations around the world has the capacity to locate earthquake epicenters to within a few kilometers (50).

A substantially higher degree of uncertainty underlies empirically derived attenuation expressions. As a consequence of the limited knowledge of the physical process related to liberation and propagation of seismic energy, at the present time, magnitude and distance are the only parameters used to describe the effect of various source and travel path factors on ground motion parameters. Furthermore, earthquake magnitude definitions have not been used consistently in the literature, and even the definition of distance between the site and the source is not a straightforward matter. These and several other aspects are discussed by Idriss (51) in a comprehensive review of recently proposed attenuation formulae. The effect of soil conditions will be briefly discussed later on.

The most important limitation, perhaps, arises from the fact that the period of documented seismic activity spans an insignificant portion of the natural tectonic process. Allen (2) has pointed out that, for most parts of the world, neither the local instrumental data, nor the historical record of felt earthquakes cover a sufficiently long time to allow valid extrapolations of future seismicity, except on very broad

regional scales. It is apparent that strong earthquake activity is subject to marked temporal fluctuations, so that several centuries long quiescent periods may precede or follow highly active terms. Moreover, segments of seismic zones that have not experienced a large earthquake recently have been identified as likely locations for future major shocks (55).

It has been also argued that geological evidence can be used to supplement or even supersede the historic record in estimating seismicity and associated earthquake hazards (2). Although a criterion based on the application of Bayesian statistics has been proposed to conciliate hard data with relevant geological, geophysical, and other nonstatistical evidence (32,34), it has not been extensively used.

Consequently, one must be extremely cautious in interpreting the results of seismic risk analyses based on limited data. It is believed nevertheless, that the procedure is consistent with the present state of knowledge and provides a rational means for synthesizing the available information.

In many regions of the world, where the occurrence of earthquakes is not associated with superficial geologic features, or when recorded ground motions are scarce, estimates of a similar nature can be inferred but are much more uncertain. Under these conditions, it is necessary to correlate peak ground motions to a qualitative measure of earthquake intensity, such as the Modified Mercalli scale. On the basis of several observations, it has been suggested that the maximum ground acceleration and maximum ground velocity are 0.167g and 8 in/sec,

respectively, for Modified Mercalli Intensity VIII, and change by a factor of 2 with each unit drop in MM Intensity; above MM VIII, acceleration and velocity increase more slowly, by a factor somewhat lower than 2. These relationships represent mean values with standard deviations corresponding at least to a factor of 2 (75).

It should be noted that MMI is a subjective measure in large part, so that intensity rating practices vary from one locality to another; hence, general rules may not be directly applicable to all seismic areas. Therefore, the few instrumental data that may be available become valuable elements in adapting the above recommendations to the corresponding local conditions. Likewise, it may be convenient to estimate attenuation rates from the particular shapes of isoseismal lines for local past earthquakes. These lines may reveal directional attenuation patterns resulting from local geologic conditions.

It is also worth to remark that assigning MMI is a viable way of incorporating noninstrumental historical evidence in a quantitative analysis, thus extending the length of the record beyond the time covered by instrumental observations.

The regional motions that one obtains from the methods described in the above must be modified to take account of the soil conditions of the site. Nevertheless, it must be kept in mind that the attenuation formula used may already contain soil effects or may apply only to the type of soils corresponding to the data used in its derivation. On the other hand, the type of soil is to some extent implicitly considered in the observation

of damage or in the observational data leading to reported MM intensities.

It has been only in the last five or six years that statistical studies on the effect of site conditions on ground motions have become available. Various relationships for peak ground motion parameters, explicitly including local soil conditions, have been proposed; these have been summarized by Idriss in the previously mentioned reference.

It is generally found that ground velocities and ground displacements are more affected than ground accelerations. Peak accelerations on rock are essentially equal to those on stiff soil deposits, especially for distances of about 30 kilometers. However, large accelerations may be attenuated by a soil profile, whereas small accelerations may be amplified; thus, rock accelerations are generally larger than accelerations in soil sites for short distances, and vice versa for large distances. These trends intensify in the case of soft and deep cohesionless soils. In turn, peak ground velocities and displacements are somewhat higher on soil sites than on rock sites at short distances, and substantially higher at large distances.

The significance of relationships between the ground motion parameters, such as V/A and AD/V^2, has been pointed out (41,77, 79). When only the peak acceleration is given to characterize the seismic hazard, as is often the case, these expressions can be used to estimate associated ground velocities and displacements. The dispersion of these ratios is about the same as that of the individual parameters themselves.

The V/A ratio depends on the site characteristics and varies roughly in about 25% per unit change in magnitude; it increases, although not very significantly, with the distance to the source. Values of the V/A ratio of 48 in/sec/g for firm ground, and 32 to 36 in/sec/g for rock are recommended for magnitudes of about 6.5 and moderate distances. Although an average value for rock of about 22 was obtained for the data considered in reference 77, a somewhat more conservative value was recommended because of the limited rock data available.

It has been established that AD/V^2 must approach 1 as the distance tends to infinity, and should increase rapidly as the distance tends to zero (79). While several recent studies are in agreement with the previous limits, others are not; there are also contradictions regarding the variation of AD/V^2 with magnitude (51). It varies between 3 to 15 for most earthquakes. Average values of about 5.5 were found for a number of records used in statistical analyses of elastic spectra, and a value of 6 was suggested as adequately conservative, regardless of soil conditions (41,77).

For illustration, the V/A and AD/V^2 ratios for the records used in this study are given in Table 5.1.

It has also been pointed out that under certain circumstances it may be reasonable to base design spectra on "effective" ground acceleration values that are somewhat lower than acceleration intensities inferred from actual instrumental data as discussed above (68,76). Although very few recordings have been obtained in the vicinity of earthquake sources,

observation of damage associated with extremely close, short duration earthquakes, does not seem to be consistent with the high ground acceleration readings, and appears to be much less than that associated with even lower accelerations resulting from more distant and/or longer earthquakes.

The observation has also been made that heavy structures on large foundations appear to respond to earthquakes in a less intense manner than do smaller structures, or, more specifically, than free field instrumentation would predict (68,78). This becomes apparent when peak acceleration values and response spectra computed for records obtained in the basement of the Hollywood Storage Building and in the adjacent parking lot are compared. The high frequency content of the free field motion seems to be filtered, to some extent, by the relatively large dimensions of the foundation of the structure, thus explaining the lower peak accelerations and lower spectral ordinates in the high frequency region corresponding to the record in the building. On the other hand, no significant changes in ground velocities and displacements, nor in spectral ordinates in the low frequency region are observed; furthermore, little reduction in the acceleration region results from distant earthquakes, which is indicative of unaffected long period waves.

For the previous reasons, it is considered appropriate to reduce high intensity motions, especially those arising from near sources, to values below those inferred without consideration of aspects related to earthquake effects on structures. The effective motions for which design spectra are drawn may be as

little as one half of the expected peak instrumental values for near earthquakes, ranging up to the latter values for distant earthquakes (70,76).

Naturally, the selected motions and the corresponding return periods will also depend on the use and characteristics of the structure under consideration as well as on the implications of its failure. This involves consideration of socioeconomic factors to compromise the level of risk society is willing to accept with the related cost of protection. Thus, the earthquake hazard for which the design is to be accomplished must be specified accordingly; a much lower level of safety, or shorter return periods, might be permissible for an apartment building than for a school or a hospital building; a higher factor of safety may be required for a dam, and even higher margins of conservatism might be required for nuclear reactors, where damage may involve exposure of a large number of people to excessive radiation (75). For example, in the design of exceptionally critical facilities, such as nuclear power plants, it is also necessary to make some estimate of the maximum intensity of an earthquake that could be expected, the so called "maximum credible earthquake." This is even more difficult to determine since such an earthquake may have never occurred in the past and certainly not during the period of recorded history. It is generally considered desirable to provide resistance against a major earthquake at yield levels or limit conditions (75).

From the foregoing discusion, it is concluded that there are a number of parameters and criteria that must be considered to

arrive at design ground motions. Such estimates are subjected to wide margins of uncertainty arising from the various sources mentioned earlier. Although it is desirable to have an assured margin of safety in the combined design conditions, it is not proper to make conservative allowances for each of the parameters involved in every step of the design process. It is considered reasonable to take values close to the mean or expected values of the ground motion parameters, or values associated with mean recurrence periods; in turn, these values are generally combined with factors for deriving design spectra taken at the mean plus one standard deviation level.

5.3 Structure related parameters

The system parameters, as defined earlier in this study, are the natural period or frequency, the degree of damping, the type of resistance function, and the ductility factor.

The natural frequency is not of great concern at this point since spectra will be derived for the entire frequency band of interest. It should be noted, however, that the period of a structure can not be determined as accurately as one may wish; furthermore, it is also well known that important changes in the fundamental period of a multistory building may occur due to earthquake exposures. A number of aspects regarding resistance function models and damping factor were discussed in Chapter 2. Naturally, one seeks the best possible representation of the actual structure under consideration, however, selection of a range for the mentioned parameters may be necessary.

The case of the ductility factor requires further discussion. In modifying the elastic design spectrum to obtain the inelastic design spectrum in accordance with the procedures given in the following sections, one must keep in mind that the ductility level is associated with the load deformation relationship for the structure as a whole (see Section 2.6), rather than with the moment rotation capacity at a particular joint or in a particular member or component of the structure. The design ductility level is generally lower than local ductilities at connections and elements. Such a difference depends on the type of structure and the number of members contributing to dissipate energy by inelastic action.

A corollary is that the design should be conducted in such a way that there is no major disparity in the distribution of resistances within the structure, so that energy is dissipated uniformly.

On the other hand, in accordance with the concept of design spectrum, the ductility is not a response quantity but a measure of the ductility requirements corresponding to the associated design forces. Thus, one should make sure that the structure will be capable of mobilizing the required ductilities at the overall and local levels.

Design ductilities of the order of 4 to 6 have been suggested for multistory reinforced concrete buildings (17). In a moment resisting frame for example, the design ductility generally represents an average of the interstory ductilities; to develop an overall ductility of 4 to 6, some stories may have to

develop ductilities between 1.5 or 2 times larger, and even larger ductilities may have to be developed at joints or individual members.

5.4 Construction of Design Spectra

Consider first the construction of the Elastic Design Spectrum. Referring to Fig. 5.1, assume that D, V, and A correspond to the design ground motions. By multiplying the latter by the amplification factors summarized in Table 4.7 one determines the lines JK, KL and LM, noting that points J and M correspond to frequencies of 0.1 and 8 cps respectively. As mentioned earlier, amplification factors corresponding to mean plus one standard deviation levels are generally recommended; however, lower or higher values may be also taken depending on the degree of conservatism that may be justified for the particular application under consideration.

The transition lines IJ and MN are determined by the points I and N at 0.03 and 33 cps respectively. Below 0.03 cps the elastic spectrum coincides with the ground displacement line, and above 33 cps it coincides with the ground acceleration line.

As discussed in Section 4.6, deamplification factors ϕ_μ, independent of the probability level associated with the amplification factors taken to derive the elastic spectrum, are used to determine the segments J'K', K'L', and L'M' of the Inelastic Design Spectrum, as shown in Figure 5.2. For the corresponding damping factor, ductility factor, and resistance function, ϕ_μ factors can be read in Tables 4.2 to 4.6, or in

Figures 4.28 to 4.33, or, in the case of elastoplastic systems, the expressions indicated in Figures 4.28 to 4.30 may be used. Since the factors for elastoplastic systems are generally conservative, they are recommended for general purposes.

Before proceeding with the construction of the inelastic spectrum, it is instructive to compare the recommendations given herein with previous rules for the same purpose (73). In the earlier procedure, the inelastic spectrum was obtained dividing the elastic spectrum by μ in the displacement and velocity regions, and by $\sqrt{2\mu-1}$ in the acceleration region. These factors, which are independent of the amount of damping, are compared with the ϕ_μ factors for elastoplastic systems developed herein in Figures 5.3 to 5.5. It is apparent that, with the exception of the displacement region, the old factors are on the unconservative side for damping larger than 5% and for ductilities larger than 3. It may be noted, though, that the old rule for the acceleration region is still quite a good approximation for the 5% damping case. It is believed, however, that the new recommendations are more reliable than the previous rules because they are consistent with a larger number of observations and take into account parameters not considered before.

Following with the construction, point I' is obtained dividing the elastic ordinate at I by μ; this is based on the fact that at very low frequencies the maximum deformation of elastic and inelastic systems are the same. Then join points I' and J'.

The ordinate of the inelastic spectrum at 33 cps can be taken, conservatively, equal to that of the elastic spectrum, i.e., point N. However, all the response spectra given in the previous chapters show some reduction from the ground acceleration level represented by point N. Mean and mean plus one standard deviation values at the highest frequency considered in this study are summarized in Table 5.2 (these values are computed as indicated in Section 4.3). Table 5.2 also shows the values obtained from approximate relationships of the form $\mu^{-\alpha}$ that can be used to determine point N' at 33 cps. For elastoplastic systems with 2 and 5 percent damping, the parameter α takes the values 0.07 and 0.10 for mean plus one standard deviation and mean spectra, respectively. For bilinear and degrading systems with 5% damping, and for elastoplastic systems with 10% damping, α =0.10 corresponds to the mean plus one standard deviation level, and α =0.13 corresponds to the mean level.

Finally, join points M' and N'. When the ordinate of point L' results lower than the ground acceleration (point N), it is more appropriate to join directly L' and N', as indicated in the lowest spectrum in Figure 5.2.

Beyond point N', the inelastic spectrum is tentatively drawn as indicated by the dashed lines in Fig. 5.2. No data are available at such high frequencies so as to make a definitive recommendation; the elastic spectrum represents a conservative upper bound, however.

5.5 Example

Assume that design spectra for firm ground, for systems with 5% damping, and ductility factors of 1 (elastic), 3, and 10 are desired. For convenience, a peak ground acceleration of 1g is used; for different design acceleration values, spectra can be obtained proportionally with no difficulty. Consider also that no specific estimates for the design ground velocity and displacement are provided; thus, recommended average values for the V/A and AD/V^2 ratios are used. Amplification factors corresponding to the 84.1 probability level are used to draw the elastic spectrum, and deamplification factors for elastoplastic systems are used, as recommended for general purposes. The various steps for the solution shown in Figure 5.6 are the following:

(1) Draw the ground motion maxima, denoted as A, V, and D, using V/A=48 in/sec/g and AD/V^2=6. For A=1g, V=48 in/sec and D=36 inches are obtained.

(2) Draw the elastic spectrum between 0.1 and 8 cps using amplification factors from Tables 4.3 or 4.7. These tables give mean plus one standard deviation values of 2.1, 2.15, and 2.77 for the displacement, velocity, and acceleration regions, respectively. Therefore, the ordinates of the elastic spectrum are 75 inches, 103 in/sec, and 2.77g. Complete the construction with transition regions dropping to the ground motion values at 0.03 and 33 cps.

(3) Draw the inelastic spectra between 0.1 and 8 cps using deamplification factors from Table 4.3 or Figures 4.28 to 4.30.

For a ductility factor of 3, use the factors 0.3, 0.33, and 0.45 for the displacement, velocity, and acceleration regions; and 0.08, 0.14, and 0.26 for a ductility factor of 10. Hence, the ordinates of the inelastic spectrum for a ductility of 3 are 23 inches, 34 in/sec, and 1.25g; the corresponding values for a ductility of 10 are 6 inches, 14 in/sec, and 0.72g. Since the latter value is less than the ground acceleration value, use it to determine the intercept with the line for the velocity region and join the point so determined directly with the ordinate at 33 cps.

(4) Complete the spectra in the high frequency region using the expression $\mu^{-0.07}$ to determine the ordinates at 33 Hertz. This gives 0.93g and 0.85g for ductilities of 3 and 10, respectively. In the very low frequency region, apply the factor $1/\mu$ to the ground displacement value to obtain the ordinates below 0.03 cps; this results in values of 12 inches and 3.6 inches for ductilities of 3 and 10, respectively. Finally join the points corresponding to 0.03 and 0.1 cps.

It is illustrative to compare the previous design spectrum for firm ground with actual response spectra. In Figures 5.7, 5.8, and 5.9, computed yield spectra for the El Centro, Olympia, and Santiago records, for elastoplastic systems with 5% damping, and scaled to a 1g ground acceleration, are compared with the design spectrum shown in Figure 5.6.

The spectra for the El Centro record show an extremely good fit with the design spectra, the implications of which should not be improperly interpreted. It is not expected, nor implied, that

responses for any single earthquake should match the design spectrum. In fact, the spectra for the Olympia record lie below the design spectra for all frequencies, while spectra for the Santiago record nearly reach or exceed the design spectra at some points in the acceleration and displacement regions, but fall well below the design spectra in the velocity region.

It should be noted that the design spectrum was drawn for the mean plus one standard deviation conditions, thus the response to El Centro is about one standard deviation above the mean for all records, especially in the velocity and displacement regions.

If design spectra using factors corresponding to the mean level were constructed, the spectra for the Olympia record would show better fit in the acceleration region, but would still lie below the mean design spectra in the velocity and displacement regions.

In general, spectra for particular records may present different levels of amplification in the various spectral regions, as well as different V/A and AD/V^2 values than those corresponding to the average conditions used to derive design spectra. The V/A and AD/V^2 ratios are directly related to the shape of the spectrum. The V/A ratio determines the position of the spectrum within the frequency band; a reduction of the V/A ratio results in a rightshift of the velocity region. The AD/V^2 ratio is a measure of the wideness of the spectrum; large AD/V^2 values correspond to flat shaped spectra, whereas small AD/V^2 ratios correspond to narrow velocity regions, i.e., narrow band

spectra.

In summary then, the design spectrum recommended herein is intended to represent, at a given probability level, response characteristics associated with a family of earthquakes. It is believed that a smoothed design spectrum is a more appropriate basis for design than either a spectrum or a time history for a single ground motion, since it takes into account the random nature of earthquake responses as well as earthquake motions.

CHAPTER 6

SUMMARY AND CONCLUSIONS

6.1 Summary

Inelastic response spectra for ten earthquake records were analyzed statistically to review previous recommendations for deriving inelastic design spectra and to evaluate the effect of damping combined with nonlinear behavior and the influence of the type of material nonlinearity on inelastic response.

Three nonlinear models were used. The well known elastoplastic and bilinear idealizations, and a stiffness degrading model specifically derived for this study. Damping factors of 2, 5, and 10 percent of critical were considered in combination with the elastoplastic model; a damping factor of 5 percent of critical was used for bilinear and stiffness degrading systems. For each earthquake record, responses were computed for about 40 different frequencies, and for 6 preselected ductility factors: 1 (elastic), 1.5, 2, 3, 5, and 10; an iterative procedure was used to obtain inelastic responses accurate to within 1% of the desired ductility values.

Considering the various conditions and ground motions used, results for about 12000 different cases were obtained and summarized in the form of inelastic response spectra. A statistical procedure was developed to analyze the data for the purpose of deriving factors for the construction of inelastic design spectra. This procedure is a generalization of available

methods that have been previously used in elastic spectra studies.

6.2 Conclusions

1. Observation of inelastic response spectra for elastoplastic systems indicates that the effect of damping combined with nonlinear behavior is different in the various regions of the spectrum. In the very low frequency range, say below 0.05 cps, the effect of damping may be considered to be negligible, whereas it is still somewhat effective in reducing the response of very rigid systems, specially for large ductilities. Damping is more effective in the intermediate frequency range, specifically, in the region between 0.4 and 8 cps where elastic spectra present larger response amplification. On the other hand, the effect of damping lessens as inelastic deformations increase.

2. Observation of average inelastic response spectra corroborates the previous remarks. In particular, the estimation can be made that increasing the damping factor from 2 to 10 percent of critical results in about 40% reduction of the spectral ordinates in the region between 0.4 and 8 cps; for the same conditions, however, the response of elastoplastic systems with a ductility factor of 10 is reduced, on the average, by only about 20 percent.

3. Comparisons of inelastic response spectra for elastoplastic, bilinear, and stiffness degrading systems, with the same amount of damping, reveals that: (a) At the low

frequency end of the spectrum, say below 0.05 or 0.1 cps depending on the ground motion record, responses are practically independent of the force deformation law; (b) some differences exist for frequencies greater than 10 Hertz, but they are negligible for ductility factors less than about 5, and not substantial for larger ductilities; (c) for intermediate frequencies, the responses of bilinear systems with ductilities less than or equal to 2 are almost identical to those of elastoplastic systems with the same yield level, while for larger ductilities, the maximum responses of bilinear systems are generally smaller than those of the associated elastoplastic systems; (d) for intermediate frequencies, the responses of stiffness degrading systems are generally between about 0.5 to 1.5 times the response of the associated elastoplastic systems; and (e) notably, spectra for degrading systems have a tendency to go below the peaks and above the troughs of spectra for elastoplastic systems.

4. The differences or similarities in the responses of systems with different types of resistance, for all other parameters the same, can be explained by means of the corresponding response histories. The latter reveal that the energy dissipation mechanism and the particular characteristics of the ground motion itself interrelate in an extremely complex manner, thus making it practically impossible to predict, accurately, the response of a particular system to a particular earthquake motion. Furthermore, even systems with the same type of nonlinearity and amount of damping, and excited by the same

ground motion, may present hysteretic behavior of an entirely different nature depending on their yield point resistances.

5. From a comparison of average spectra for elastoplastic, bilinear, and stiffness degrading systems, more definitive conclusions can be reached. First, the ordinates of the average spectra do not vary significantly when various nonlinear models are used; differences occur mainly for frequencies between 0.1 and 10 cps and for large ductilities, and are practically negligible at the low and high frequency ends of the spectrum. And second, use of the elastoplastic idealization provides, in almost every case, a conservative estimate of the average response to a number of earthquake motions.

6. On the basis of the previous observations, inelastic design spectra may be constructed using factors derived for elastoplastic systems. It is particularly significant that, on the average, the stiffness degradation phenomenon is not as critical as one might expect. There is still need, however, to consider a somewhat more sophisticated deteriorating model; for future research, it is of interest to include strength degradation and softening of the unloading stiffness, with both effects increasing progressively as inelastic deformations increase.

7. A comparison of the factors for constructing inelastic design spectra derived in this study, with available rules for the same purpose, indicates that, with the exception of the displacement region of the spectrum, the old factors are on the unconservative side for damping larger than 5 percent and for

ductilities larger than 3. It is believed that the new recommendations are more reliable than the previous ones because they are consistent with a larger number of observations and take into account parameters not considered before.

8. A critical step in the derivation of design spectra for particular applications is the determination of the earthquake hazard at the site of interest. Information related to various scientific disciplines must be considered to arrive at the ground motions upon which the design spectrum is based. Earthquake risk procedures promise a viable way of synthesizing the available information. At the present time, however, serious limitations arise from the irremediable scarcity of data on previous earthquake activity, and from the incomplete understanding of the physical process governing the release and propagation of seismic energy. Furthermore, it is often necessary to adjust the ground motion values inferred from instrumental data to effective design values compatible with past experience regarding observed structural damages, or to account for factors that may have not been explicitly considered in the analysis. There is an urgent need to evaluate the current knowledge and practices in the determination of design ground motions in order to propose topics and priorities for future research.

LIST OF REFERENCES

1. Algermissen, S.T., and Perkins, D.M., "A Probabilistic Estimate of Maximum Acceleration in Rock in the Contiguous United States," United States Geologic Survey, Open File Report No. 76-416, 1976.

2. Allen, C.R., "Geological Criteria for Evaluating Seismicity," Chapter 3 in "Seismic Risk and Engineering Decisions," C. Lomnitz and E. Rosenblueth editors, Elsevier, Amsterdam, 1976, pp. 31-69.

3. Allen, C.R., et al., "Main Shock and Larger Aftershocks of the San Fernando Earthquake, Feb. 9 through March 1, 1971," Geological Survey Professional Paper 733, U.S. Dept. of the Interior and U.S. Dept. of Commerce, Joint Publication, 1971.

4. American Concrete Institute, "Building Code Requirements for Reinforced Concrete ACI 318-71," November 1971.

5. American Concrete Institute, ACI-ASCE Committee 352, "Recommendations for Design of Beam Column Joints in Monolithic Reinforced Concrete Structures," ACI Journal, July 1976.

6. Anderson, J.C., and Bertero, V.V., "Seismic Behavior of Multistory Frames Designed by Different Philosophies," Earthquake Engineering Research Center, Report No. 69-11, University of California, Berkeley, October 1969.

7. Ang, A.H-S., and Tang, W.H., "Probability Concepts in Engineering Planning and Design," Vol. I, Basic Principles, John Wiley, 1975.

8. Atalay, M.B., and Penzien, J., "The Seismic Behavior of Critical Regions of Reinforced Concrete Components as Influenced by Moment, Shear and Axial Force," Earthquake Engineering Research Center, Report No. 75-19, University of California, Berkeley, December 1975.

9. Barney, G.B., et al., "Earthquake Resistant Structural Walls, Tests of Coupling Beams," Construction Tech. Laboratories, Portland Cement Association, Skokie, Illinois, January 1978.

10. Berg, G.V., and Housner, G.W., "Integrated Velocity and Displacement of Strong Earthquake Ground Motion," Bulletin of the Seismological Society of America, Vol. 51, No. 2, April 1961, pp. 175-189.

11. Bertero, V.V., "Identification of Research Needs for Improving Aseismic Design of Building Structures," Earthquake Engineering Research Center, Report No. 75-27, University of California, Berkeley, September 1975.

12. Bertero, V.V., "State of the Art in Establishing Design Earthquakes," Workshop on Earthquake Resistant Reinforced Concrete Building Construction, University of California, Berkeley, July 11-15, 1977, Vol. II, pp. 315-345.

13. Bertero, V.V. and Bresler, B., Panel Paper: "Failure Criteria -Limit States," 6th. World Conference on Earthquake Engineering, New Delhi, India, January 1977, Vol. I, pp. 77-87.

14. Bertero, V.V., and Kamil, H., "Nonlinear Seismic Design of Multistory Frames," Canadian Journal of Civil Engineering, Vol. 2, 1975, pp. 494-516.

15. Bertero, V.V., Krawinkler, H., and Popov, E.P., "Further Studies on Seismic Behavior of Steel Beam Column Subassemblages," Earthquake Engineering Research Center, Report No. 73-27, University of California, Berkeley, December 1973.

16. Bertero, V.V., and McClure, G., "Behavior of Reinforced Concrete Frames Subjected to Repeated Reversible Loads," Journal of the ACI, Vol. 61, No. 10, Oct. 1964, pp. 1305-1329.

17. Blume, J.A., Newmark, N.M., and Corning, L.H., "Design of Multistory Reinforced Concrete Buildings for Earthquake Motions," Portland Cement Association, Skokie, Illinois, 1961.

18. Brady, A.G., and Perez, V., "Strong Motion Earthquake Accelerograms, Digitization and Analysis, Records from Lima, Peru, 1951 to 1974," U.S. Geological Survey, Report No. 77-587, Menlo Park, California, April 1977.

19. Bresler, B., "Behavior of Structural Elements, A Review," Building Practices for Disaster Mitigation, Building Science Series 46, U.S. Department of Commerce, NBS, Washington, D.C., February 1973, pp. 286-351.

20. Building Research Institute of Japan, "A List of Experimental Results of Deformation Ability of Reinforced Concrete Columns under Large Deflections (No.3)," February 1978.

21. California Institute of Technology, Earthquake Engineering Research Lab., Volume II Tape, Corrected Accelerograms and Integrated Velocity and Displacement Curves, Pasadena, Ca.

22. California Institute of Technology, Earthquake Engineering Research Lab., "Strong Motion Earthquake Accelerograms, Digitized and Plotted Data," Vol. II, Part A, Report No. 71-50, 1971, and Part B, Report No. 72-50, 1972.

23. Carpenter, L.D., and Lu, L.W., "Repeated and Reversed Load Tests on Full-Scale Steel Frames," 4th. World Conference on Earthquake Engineering, Santiago, Chile, 1969, Vol.I, pp. B2, 125-136.

24. Castano, J.C., Director of Instituto Nacional de Prevencion Sismica, San Juan, Argentina, personal communication, June 1978.

25. Cloud, W.K., and Perez, V., "Accelerograms, Parkfield Earthquake," Bulletin of the Seismological Society of America, Vol. 57, No. 6, December 1967, pp. 1179-1192.

26. Clough, R.W., "Dynamic Effect of Earthquakes," Journal of the Structural Division, ASCE, Vol. 86, ST4, April 1960, pp. 49-65.

27. Clough, R.W., "Effect of Stiffness Degradation on Earthquake Ductility Requirements," Report No. 66-16, Dept. of Civil Engineering, University of California, Berkeley, Oct. 1966.

28. Cornell, C.A., and Vanmarcke, E.H., "The Major Influences on Seismic Risk," 4th World Conference on Earthquake Engineering, Santiago, Chile, 1969, Vol. I, pp. Al, 69-83.

29. Der Kiureghian, A., and Ang, A.H-S., "A Line Source Model for Seismic Risk Analysis," Civil Engineering Studies, Structural Research Series No. 419, University of Illinois, Urbana, October 1975.

30. Dewey, J.W., et al., "The Managua Earthquake of Dec. 23, 1972: Location, Focal Mechanism, Aftershocks and Relationship to Recent Seismicity of Nicaragua," Proceedings of the Earthquake Engrg. Research Institute Conference on the Managua Earthquake, Vol. I, pp. 66-88, San Francisco, California, November 1973.

31. Esteva, L., "Behavior under Alternating Loads of Masonry Diaphragms Framed by Reinforced Concrete Members," International Symposium on the Effects of Repeated Loading of Materials and Structures, Rilem - Instituto de Ingenieria, Vol.5, Mexico, September 1966.

32. Esteva, L., "Seismicity Prediction: A Bayesian Approach," 4th World Conference on Earthquake Engineering, Santiago, Chile, 1969, Vol I, pp. Al, 172-184.

33. Esteva, L., "Regionalizacion Sismica de Mexico para Fines de Ingenieria," Universidad Nacional Autonoma de Mexico, Instituto de Ingenieria, 246, April 1970. (In Spanish).

34. Esteva, L., "Seismicity," Chapter 6 in "Seismic Risk and Engineering Decisions," C. Lomnitz and E. Rosenblueth editors, Elsevier, Amsterdam, 1976, pp. 179-224.

35. Falcon, E., Castillo, O., and Valenzuela, M., "Hidrogeologia de la Cuenca de Santiago," Joint publication of the Instituto de Investigaciones Geologicas and Corporacion de Fomento de la Produccion, Santiago, Chile, 1970. (In Spanish).

36. Fiorato, A.E., Sozen, M.A., and Gamble, W.L., "An Investigation of the Interaction of Reinforced Concrete Frames with Masonry Filler Walls," Civil Engineering Studies, Structural Research Series No. 370, University of Illinois, Urbana, November 1970.

37. Freeman, S.A., Honda, K. and Blume, J.A., "Dynamic Response Investigations of Real Buildings," Workshop on Earthquake Resistant Reinforced Concrete Bldg. Construction, University of California, Berkeley, Vol. III, pp. 1517-1536, July 1977.

38. Garcia, F., and Roesset, J.M., "Influence of Damping on Response Spectra," Report R70-4, Dept. of Civil Engineering, Massachusetts Institute of Technology, Cambridge, January 1970.

39. Gulkan, P., and Sozen, M.A., "Response and Energy Dissipation of Reinforced Concrete Frames Subjected to Strong Base Motions," Civil Engineering Studies, Structural Research Series No. 377, University of Illinois, Urbana, May 1971.

40. Hall, W.J., Mohraz, B., and Newmark, N.M., "Statistical Analyses of Earthquake Response Spectra," Paper K1/6, Transactions, 3rd. International Conference on Structural Mechanics in Reactor Technology, BAM, Berlin, Vol. 4, Part K, Sept. 1975.

41. Hall, W.J., Mohraz, B., and Newmark, N.M., "Statistical Studies of Vertical and Horizontal Earthquake Spectra," U.S. Nuclear Regulatory Commission, NUREG-0003, January 1976.

42. Harding, S.T. and Rinehart, W.A., "The Parkfield, California, Earthquake of June 27, 1966," U.S. Government Printing Office, Washington, D.C., 1966, pp. 1-16.

43. Haviland, R., "A Study of the Uncertainties in Fundamental Translational Periods and Damping Values for Real Buildings," Dept. of Civil Engrg., Massachusetts Institute of Technology, Publication No. R76-12, February 1976.

44. Hays, W.W., et al., "Guidelines for Developing Design Earthquake Response Spectra," U.S. Geological Survey Study for U.S. Army Construction Engrg. Research Laboratory, Champaign, Illinois, Report No. M-114, June 1975.

45. Hegemier, G.A., et al., "Earthquake Response and Damage Prediction of Reinforced Concrete Masonry Multistory Buildings, Part II: Selected Results," 6th. World Conference on Earthquake Engineering, New Delhi, India, January 1977, Vol. III, pp. 3019-3024.

46. Higashi, Y., and Takeda, T., "Stiffness and its Influence on Dynamic Behavior," Proc. of the International Conference on

Planning and Design of Tall Buildings, Lehigh University, August 1972, Vol. III, pp. 655-670

47. Housner, G.W., "Behavior of Structures During Earthquakes," Journal of the Engineering Mechanics Division, ASCE, Vol. 85, EM4, October 1959, pp. 109-129.

48. Housner, G.W., Martel, R.R., and Alford, J.L., "Spectrum Analysis of Strong Motion Earthquakes," Bulletin of the Seismological Society of America, Vol. 43, No. 2, 1953.

49. Hudson, D.E., editor, "Strong-Motion Instrumental Data on the San Fernando Earthquake of Feb. 9, 1971," Earthquake Engrg. Research Lab., California Institute of Technology and Seismological Field Survey, U.S. Department of Commerce, September 1971.

50. Hudson, D.E., "Destructive Earthquake Ground Motions," Applied Mechanics in Earthquake Engineering, ASME, AMD8, 1974, pp. 1-33.

51. Idriss, I.M., "Characteristics of Earthquake Ground Motions," Specialty Conference on Earthquake Engineering and Soil Dynamics, ASCE, Pasadena, California, June 1978.

52. International Mathematical and Statistical Libraries, Inc., CDC version, 6th. Edition, Houston, Texas, July 1977.

53. Instituto Nacional de Prevencion Sismica, "El Terremoto de San Juan del 23 de Noviembre de 1977," Informe Preliminar, San Juan, Argentina, Diciembre 1977. (In Spanish).

54. Jennings, P.C., "Earthquake Response of a Yielding Structure," Journal of the Engineering Mechanics Division, ASCE, Vol. 91, EM4, August 1965, pp. 41-68.

55. Kelleher, J., Sykes, L., and Oliver, J., "Possible Criteria for Predicting Earthquake Locations and Their Application to Major Plate Boundaries of the Pacific and Caribbean," Journal of Geophysical Research, Vol. 78, No. 14, May 1973.

56. Klingner, R.E., and Bertero, V.V., "Infilled Frames in Earthquake Resistant Construction," Earthquake Engineering Research Center, Report No. 76-32, University of California, Berkeley, December 1976.

57. Knudson, C.F., and Hansen, F., "Accelerograph and Seismoscope Records from Managua, Nicaragua Earthquakes," Proceedings of the Earthquake Engrg. Research Institute Conference on the Managua Earthquake, Vol.I, pp.180-205, San Francisco, Ca., Nov. 1973.

58. Krawinkler, H., "Shear in Beam-Column Joints in Seismic

Design of Steel Frames," Engineering Journal, AISC, 3rd. Quarter, 1978, pp. 82-91.

59. Lomnitz, C., "Global Tectonics and Earthquake Risk," Developments in Geotectonics 5, Elsevier, Amsterdam, 1974.

60. Marquardt, D.W., "An Algorithm for Least Squares Estimation of Nonlinear Parameters," Journal of the Society for Industrial and Applied Mathematics, Vol. II, No. 2, June 1963.

61. Martinez, A., and Porturas, F., "Planos Goetecnicos para Lima, Peru. Analisis y Vision en Ingenieria Sismica," Reunion Andina de Seguridad Sismica, Universidad Catolica del Peru, Centro Interuniversitario de Desarrollo Andino, Lima, 11-15 Agosto, 1975. (In spanish).

62. Matzen, V.C., and McNiven, H.D., "Investigation of the Inelastic Characteristics of a Single Story Steel Structure Using System Identification and Shaking Table Experiments," Earthquake Engineering Research Center, Report No. 76-20, University of California, Berkeley, August 1976.

63. Mayes, R.L., and Clough, R.W., "State of the Art in Seismic Shear Strength of Masonry - An Evaluation and Review," Earthquake Engineering Research Center, Report No. 75-21, University of California, Berkeley, October 1975.

64. Mayes, R.L., et al., "Seismic Research on Multistory Masonry Buildings at the University of California, Berkeley, 1972 to 1977," North American Masonry Conference, Boulder, Colorado, August 1978.

65. Mohraz, B., "A Study of Earthquake Response Spectra for Different Geological Conditions," Civil and Mech. Engrg. Dept., Southern Methodist University, Dallas, Texas, August 1975.

66. Newmark, N.M., "A Method of Computation for Structural Dynamics," Transactions, ASCE, Vol. 127, pp. 1406-1435, 1962.

67. Newmark, N.M., "Current Trends in the Seismic Analysis and Design of High Rise Structures," Chapter 16 in "Earthquake Engineering," R.L. Wiegel, editor, Prentice-Hall, New Jersey, 1970.

68. Newmark, N.M., "A Rationale for Development of Design Spectra for Diablo Canyon Reactor Facility," Report to U.S. Nuclear Regulatory Commission, N.M. Newmark Consulting Engineering Services, Urbana, Illinois, September 1976.

69. Newmark, N.M., "Earthquake Design Philosophies - Past Development and Future Trends," Seminar on Earthquake

Resistant Design, Fall Conference of Specialists Group for Bridges and Structural Engrg., Swiss Society of Engineers, Zurich, Switzerland, September 1978.

70. Newmark, N.M., "Earthquake Resistant Design and ATC Provisions," 3rd. Canadian Conference on Earthquake Engineering, Montreal, Quebec, June 1979.

71. Newmark, N.M., Blume, J.A., and Kapur, K.K., "Seismic Design Spectra for Nuclear Power Plants," Journal of the Power Division, ASCE, Vol. 99, No. PO2, November 1973, pp. 287-303.

72. Newmark, N.M., and Hall, W.J., "Seismic Design Criteria for Nuclear Reactor Facilities," 4th. World Conference on Earthquake Engineering, Santiago, Chile, 1969, Vol. II, pp. B4, 37-50.

73. Newmark, N.M., and Hall, W.J., "Procedures and Criteria for Earthquake Resistant Design," Building Practices for Disaster Mitigation, National Bureau of Standards, Building Science Series No. 46, pp. 209-236, February, 1973.

74. Newmark, N.M., and Hall, W.J., "Seismic Design Spectra for Trans-Alaska Pipeline," 5th World Conference on Earthquake Engineering, Rome, Italy, 1974, Vol. I, pp. 554-557.

75. Newmark, N.M., and Hall, W.J., "Earthquake Resistant Design of Nuclear Power Plants," Article for Intergovernmental Conference on Assessment and Mitigation of Earthquake Risk, UNESCO, February 1976.

76. Newmark, N.M., and Hall, W.J., "Development of Criteria for Seismic Review of Selected Nuclear Power Plants," Prepared for U.S. Nuclear Regulatory Commission, NUREG/CR-0098, N.M. Newmark Consulting Engrg. Services, Urbana, Ill., May 1978.

77. Newmark, N.M., Hall, W.J., and Mohraz, B., "A Study of Vertical and Horizontal Earthquake Spectra," Report WASH-1255, Directorate of Licensing, U.S. Atomic Energy Commission, Washington, D.C., April 1973.

78. Newmark, N.M., Hall, W.J., and Morgan, J.R., "Comparison of Building Response and Free Field Motion in Earthquakes," 6th World Conference on Earthquake Engineering, New Delhi, India, January 1977, pp. 972-978.

79. Newmark, N.M., and Rosenblueth, E., "Fundamentals of Earthquake Engineering," Prentice-Hall, Inc., 1971.

80. Nilsson, I.H.E., and Losberg, A., "Reinforced Concrete Corners and Joints Subjected to Bending Moment," Journal of the Structural Division, ASCE, Vol. 102, No. ST6, June 1976, pp. 1229-1254.

81. Oesterle, R.G., et al., "Earthquake Resistant Structural Walls - Tests of Isolated Walls," Construction Technology Laboratories, Portland Cement Assoc., Skokie, Illinois, 1976.

82. Omote, Y., et al., "Effect of Test Technique on Masonry Shear Strength," 6th. World Conference on Earthquake Engineering, New Delhi, India, January 1977, Vol. III, pp. 3208-3213.

83. Osawa, Y., et al., "Earthquake Measurements in and around a Reinforced Concrete Building," 4th. World Conference on Earthquake Engineering, Santiago, Chile, 1969, Vol. I, pp. B-1, 1-16.

84. Otani, S., "SAKE, a Computer Program for Inelastic Response of R/C Frames to Earthquakes," Civil Engineering Studies, Structural Research Series No. 413, University of Illinois, Urbana, November 1974.

85. Otani, S., and Sozen, M.A., "Behavior of Multistory Reinforced Concrete Frames During Earthquakes," Civil Engineering Studies, Structural Research Series No. 392, University of Illinois, Urbana, November 1972.

86. Park, R., "Members: Behavior as Related to Design Criteria," 6th. World Conference on Earthquake Engineering, New Delhi, India, January 1977, Vol. I, pp. 50-64.

87. Park, R., and Paulay, T., "Reinforced Concrete Structures," John Wiley, 1975.

88. Paulay, T., and Spurr, D., "Frame-Shear Wall Assemblies Subjected to Simulated Seismic Loading," 6th. World Conference on Earthquake Engineering, New Delhi, India, January 1977, Vol. II, pp. 1195-1200.

89. Paulay, T., and Santhakumar, A., "Ductile Behavior of Coupled Shear Walls," Journal of the Structural Division, ASCE, Vol. 102, No. ST1, January 1976, pp. 93-108.

90. Pecknold, D.A., and Riddell, R., "Effect of Initial Base Motion on Response Spectra," Journal of the Engineering Mechanics Division, ASCE, Vol. 104, No. EM2, April 1978, pp. 485-491.

91. Penzien, J., "Dynamic Response of Elastoplastic Frames," Journal of the Structural Division, ASCE, Vol. 86, ST7, July 1960, pp. 81-94.

92. Popov, E.P., and Bertero, V.V., "On Seismic Behavior of Two R/C Structural Systems for Tall Buildings," Structural and Goetechnical Mechanics, W.J. Hall editor, Prentice-Hall Inc., 1977, pp. 117-140.

93. Popov, E.P., Bertero, V.V., and Chandramouli, S., "Hysteretic Behavior of Steel Columns," Earthquake Engineering Research Center, Report No. 75-11, University of California, Berkeley, September 1975.

94. Popov, E.P., Bertero, V.V. and Krawinkler, H., "Cyclic Behavior of Three R/C Flexural Members with High Shear," Earthquake Engineering Research Center, Report No. 72-5, University of California, Berkeley, October 1972.

95. Popov, E.P., and Stephen, R.M., "Cycling Loading of Full Size Steel Connections," Earthquake Engineering Research Center, Report No. 70-3, University of California, Berkeley, July 1970.

96. Portillo, M. and Ang, A.H-S., "Evaluation of Safety of Reinforced Concrete Buildings to Earthquakes," Civil Engineering Studies, Structural Research Series No. 433 University of Illinois, Urbana, October 1976.

97. Ramberg, W., and Osgood, W.R., "Description of Stress-Strain Curves by Three Parameters," U.S. National Advisory Committee on Aeronautics, Technical Note 902, July 1943.

98. Riddell, R., and Newmark, N.M., "Statistical Study of Earthquake Response Spectra," 2nd Chilean Conference on Seismology and Earthquake Engineering, Santiago, Chile, July 1976, pp. B2, 1-15.

99. Riddell, R., and Newmark, N.M., "Commentary on Force Deformation Models for Nonlinear Analyses," Journal of the Structural Division, ASCE, to be published.

100. Roeder, C.W., and Popov, E.P., "Inelastic Behavior of Eccentrically Braced Steel Frames under Cyclic Loadings," Earthquake Engineering Research Center, Report No. 77-18, University of California, Berkeley, August 1977.

101. Rojahn, C., Brogan, G.E., and Slemmons, D.B., "Preliminary Report on the San Juan, Argentina, Earthquake of Nov. 23, 1977," Central American Conference on Earthquake Engrg., San Salvador, January 1978.

102. Rojahn, C., Digitized Data for the E-W component of the San Juan, Argentina record, personal communication, June 1978.

103. Shepherd, R., and Jennings, P.C., "Experimental Investigations, Correlation with Analysis," Workshop on Earthquake Resistant Reinforced Concrete Building Construction, University of California, Berkeley, July 1977, Vol. III, pp. 1537-1554.

104. Sozen, M.A., "Hysteresis in Structural Elements," Applied

Mechanics in Earthquake Engineering, ASME, AMD8, 1974, pp. 63-98.

105. Sozen, M.A., "Dynamic Behavior of Structural Elements," 6th. World Conference on Earthquake Engineering, New Delhi, India, January 1977, Vol. III, pp. 2983-2991.

106. Sozen, M.A., "A General Description of Structural Damage," Engineering Report on the Managua Earthquake of December 23, 1972, Part II, National Academy of Sciences, Washington, D.C., 1975.

107. Sozen, M.A., and Aoyama, H., "Uses of Observation in Earthquake Resistant Design of Reinforced Concrete," Structural and Geotechnical Mechanics, W.J. Hall editor, Prentice-Hall Inc., New Jersey 1977, pp. 305-332.

108. Takeda, T., Sozen, M.A., and Nielsen, N.N., "Reinforced Concrete Response to Simulated Earthquakes," Journal of the Structural Division, ASCE, Vol. 96, ST12, December 1970, pp. 2557-2573.

109. Trifunac, M.D., "Low Frequency Digitization Errors and New Method of Zero Baseline Correction of Strong Motion Accelerograms," Earthquake Engineering Research Laboratory, EERL 70-07, California Institute of Technology, Pasadena, Ca., 1970.

110. U.S. Coast and Geodetic Survey, U.S. Department of Commerce, "United States Earthquakes," issues corresponding to the years 1936 to 1940, 1949, 1957, and 1966, U.S. Government Printing Office, Washington, D.C.

111. U.S. Geological Survey, "Strong-Motion Earthquake Accelerograms, Digitization and Analysis, 1971 Records," Open File Report No. 76-609, Menlo Park, California, July 1976.

112. U.S. Geological Survey, "Western Hemisphere Strong-Motion Accelerograph Station List - 1976," Open File Report No. 77-374, Menlo Park, California, May 1977.

113. Valera, J.E., "Soil conditions and Local Soil Effects during the Managua Earthquake of December 23, 1972," Proceedings of the Earthquake Engineering Research Institute Conference on the Managua Earthquake, San Francisco, California, Nov. 1973, Vol. I, pp. 232-269.

114. Veletsos, A.S., and Newmark, N.M., "Effect of Inelastic Behavior on the Response of Simple Systems to Earthquake Motions," 2nd. World Conference on Earthquake Engineering, Japan, 1960, Vol. 2, pp. 895-912.

115. Veletsos, A.S., and Newmark, N.M., "Design Procedures for

Shock Isolation Systems of Underground Protective Structures," Vol. 3 - Response Spectra of Single Degree of Freedom Elastic and Inelastic Systems, Report No. RTD TDR 63-3096, Air Force Weapons Laboratory, New Mexico, June 1964.

116. Veletsos, A.S., Newmark, N.M., and Chelapati, C.V., "Deformation Spectra for Elastic and Elastoplastic Systems Subjected to Ground Shock and Earthquake Motions," 3rd. World Conference on Earthquake Engineering, New Zealand, 1965, Vol. 2, pp. 11-663 to 11-682.

117. Wakabayashi, M., "Frames under Strong Impulsive, Wind or Seismic Loading," Proceedings of the Conference on Planning and Design of Tall Buildings, Lehigh University, August 1972, Vol. II, pp. 343-363.

118. Wakabayashi, M., et al., "Inelastic Behavior of Steel Frames Subjected to Constant Vertical and Alternating Horizontal Loads," 5th. World Conference on Earthquake Engineering, Rome, Italy, 1974, Vol. I, pp. 1194-1197.

119. Wakabayashi, M., et al., "Hysteretic Behavior of Steel Braces Subjected to Horizontal Load due to Earthquakes," 6th. World Conference on Earthquake Engineering, New Delhi, India, January 1977, Vol. III, pp. 3188-3193.

120. Wang, T.Y., Bertero, V.V., and Popov, E.P., "Hysteretic Behavior of Reinforced Concrete Framed Walls," Earthquake Engineering Research Center, Report No. 75-23, University of California, Berkeley, December 1975.

121. Wight, J.K., and Sozen, M.A., "Shear Strength Decay in Reinforced Concrete Columns Subjected to Large Deflection Reversals," Civil Engineering Studies, Structural Research Series No. 403, University of Illinois, Urbana, August 1973.

TABLE 3.1   EARTHQUAKE DATA[*]

Location	Date and Time	Epicenter Coordinates	Focal Depth (km)	Surface-Wave Magnitude	Maximum MMI	Felt Area (km²)	Stations and Components Considered in this Study
Imperial Valley, California	May 18, 1940 20:37 PST (21)	32°44'00" N 115°27'00" W (21)	16	6.3 (22)	X (22)	155000 (110)	El Centro, E-W
Western Washington, Washington	Apr. 13, 1949 11:56 PST (21)	47°06'00" N 122°42'00" W (21)	**	7.1 (22)	VIII (22)	390000 (110)	Olympia, N86E
San Francisco, California	Mar. 22, 1957 11:44 PST (21)	37°40'00" N 122°29'00" W (21)	9	5.3 (22)	VII (22)	31000 (110)	Golden Gate Park, S80E
Parkfield, California	June 27, 1966 20:26 PST (21)	35°54'00" N 120°54'00" W (21)	5-10 (42)	5.6 (22)	VII (22)	52000 (110)	Cholame, Shandon, Station 5, N85E
San Fernando, California	Feb. 9, 1971 6:00 PST (21)	34°24'00" N 118°23'42" W (21)	13 to surface (3)	6.6 (49)	XI (49)	210000 (49)	Castaic, N21E Pacoima, S16E
Off Peru Coast	May 31, 1970 15:23 local (18)	9°12'00" S 78°48'00" W (18)	56 (18)	7.75 (18)	VIII (18)	104000 (18)	Lima, Instituto Geofísico, N82W
Off Central Chile Coast	July 8, 1971 23:03 local (111)	32°30'00" S 71°12'00" W (111)	58 (111)	7.5 (111)	X (111)	**	Santiago, U. of Chile, N10W
Managua, Nicaragua	Dec. 23, 1972 12:29 local (30)	12°09'00" N 86°15'36" W (30)	5 (30)	6.2 (30)	IX (30)	**	Managua, ESSO Refinery E-W
San Juan, Argentina	Nov. 23, 1977 6:26 local (53)	31°18'00" S 67°42'00" W 40 (53)	30 (101) (53)	7.4 (53,101)	IX (53)	1800000 (53)	San Juan, INPRES, E-W

[*]Numbers in parentheses refer to entries in the list of references

**Not available

TABLE 3.2 SITE INFORMATION[*]

Station	Coordinates	Epicentral Distance (km)	MMI at Site	Geology	Instrument Location and Structure Type
El Centro, Imperial Valley Irrigation District.	32°47'43"N 115°32'55"W (21)	10 (44)	VII-VIII (110)	30m Stiff clay over 900m shale (44)	First floor of 2-story, heavily reinforced concrete structure (77)
Olympia, Washington Hwy. Test Lab	47°02'00"N 122°54'00"W (21)	48 (44)	VIII (110)	**	Ground level, instrument shelter (112)
Golden Gate Park	37°46'12"N 122°28'42"W (21)	8 (44)	VII (110)	Siliceous sandstone (77)	Ground level, small shack used to house electrical equipment (77)
Cholame, Shandon Station 5	35°42'00"N 120°19'42"W (21)	5.5 (44)	**	Alluvium, 330m (25)	Ground level, instrument shelter (112)
Castaic, Old Ridge Route	34°33'18"N 118°39'24"W (21)	29 (49)	VI (49)	Sandstone (49)	Ground level, instrument shelter (112)
Pacoima Dam	34°20'06"N 118°23'48"W (21)	8 (49)	VIII-XI (49)	Highly jointed diorite gneiss (49)	Adjacent to dam abutment, instrument shelter (49)
Lima, Instituto Geofísico	12°04'12"S 77°02'24"W (18)	372 (18)	**	Alluvium, 100-200 m. (Estimated from Ref. 61)	Ground level, 1-story building (18)
Santiago, U. of Chile	33°28'12"S 70°40'12"W (111)	120 (111)	VI (111)	Alluvium, 250 m (Estimated from Ref. 35)	Basement, 3-story building (111)
Managua, ESSO Refinery	12°08'42"N 86°19'18"W (57)	6 (30)	VI (30)	Alluvium, about 1000 m (106,113)	Ground level, 1-story building (112)
San Juan, INPRES	31°31'34"S 68°33'29"W (24)	80 (101)	VII-VIII (53)	Alluvium, 250 m (53)	Ground level, isolated from floor, 2-story RC and masonry building (24)

[*] Numbers in parentheses refer to entries in the list of references

** Not available

TABLE 3.3   RECORD INFORMATION

Station, Component	Ground Motion Maxima						Record Duration used* (seconds), frequency range (cps).	Prefixed Pulse Used
	Acceleration (g)	Time (sec)	Velocity (in/sec)	Time (sec)	Displacement (in)	Time (sec)		
El Centro, E-W	.214	13.44	14.54	4.14	7.90	5.00	31.89 f<0.8 / 15.18 f>0.8	yes
Olympia, N86E	.280	21.62	6.73	10.46	3.69	9.30	26.67 all	yes
Golden Gate, S80E	.105	3.44	1.81	3.50	0.46	12.92	15.96 f<0.3 / 8.94 f>0.3	yes
Cholame, N85E	.434	9.50	10.02	9.60	2.71	8.44	21.31 f<1.7 / 13.91 f>1.7	yes
Castaic, N21E	.316	4.60	6.76	3.34	1.99	25.54	28.94 f<2.4 / 11.86 f>2.4	yes
Pacoima, S16E	1.171	9.74	44.58	5.04	16.50	9.78	18.20 f<3.0 / 12.48 f>3.0	yes
Lima, N82W	.107	10.96	1.85	5.36	1.36	31.16	31.60 f<3.5 / 20.81 f>3.5	yes
Santiago, N10W	.159	19.06	9.15	19.70	5.06	23.76	32.22 f<0.6 / 24.97 f>0.6	yes
Managua, E-W	.383	6.27	15.87	6.21	8.52	3.46	13.81 all	no
San Juan, E-W	.193	29.52	8.11	37.14	2.50	36.50	45.03+ f<2.8 / 32.19 f>2.8	no

* Includes prefixed pulse if any.
+ Does not include 11.8 seconds of initial weak motion removed.

TABLE 3.4 SET OF FREQUENCIES USED FOR EACH RECORD

El Centro	Olympia	G.G. Park	Cholame	Castaic	Pacoima	Lima	Santiago	Managua	San Juan
.020	.030	.05	.050	.030	.030	.050	.03	.030	.050
.035	.050	.07	.075	.050	.050	.070	.05	.050	.100
.050	.070	.10	.100	.080	.100	.080	.07	.075	.140
.070	.080	.12	.130	.100	.120	.090	.08	.100	.170
.100	.100	.15	.170	.140	.150	.100	.09	.125	.200
.120	.110	.20	.200	.160	.170	.120	.10	.150	.240
.150	.130	.30	.260	.180	.200	.140	.12	.180	.280
.200	.150	.40	.320	.200	.220	.160	.14	.200	.330
.220	.200	.50	.400	.220	.260	.180	.16	.230	.370
.330	.240	.65	.500	.300	.300	.200	.20	.270	.440
.430	.280	.75	.600	.400	.360	.240	.22	.300	.500
.500	.330	1.00	.700	.460	.400	.280	.24	.350	.575
.600	.400	1.20	.850	.500	.450	.350	.26	.420	.650
.800	.500	1.60	1.000	.600	.500	.400	.30	.500	.800
1.000	.550	2.00	1.200	.625	.575	.460	.33	.600	.900
1.100	.600	2.40	1.400	.675	.650	.550	.40	.700	1.000
1.500	.675	2.80	1.700	.770	.750	.625	.43	.800	1.100
1.800	.750	3.00	2.000	.950	.850	.700	.46	.900	1.300
2.400	.850	3.60	2.200	1.000	.950	.750	.55	1.000	1.500
2.600	1.000	4.30	2.700	1.300	1.100	.825	.60	1.200	1.800
3.600	1.200	4.60	3.000	1.600	1.300	.900	.65	1.400	2.000
4.000	1.400	5.00	3.300	2.000	1.500	1.000	.75	1.600	2.400
5.000	1.600	6.00	4.000	2.400	1.700	1.150	.80	1.800	2.600
7.000	1.800	6.50	4.500	3.000	1.900	1.300	.90	2.000	2.800
7.500	2.000	7.50	5.000	3.400	2.200	1.400	.95	2.400	3.200
8.000	2.200	8.00	6.000	4.000	2.600	1.600	1.10	3.000	3.700
13.000	2.400	10.00	7.000	4.333	3.000	1.800	1.20	3.500	4.300
15.000	2.800	15.00	8.000	5.555	3.400	2.000	1.30	4.000	5.000
16.000	3.200	20.00	10.000	6.000	3.700	2.200	1.40	4.500	5.500
20.000	3.800	35.00	13.000	7.000	4.000	2.600	1.80	5.500	6.000
25.000	4.400		20.000	8.000	4.670	3.000	2.00	6.200	6.500
35.000	5.000		35.000	10.000	5.500	3.500	2.40	7.000	7.000
	5.500			15.000	7.000	4.000	2.60	8.000	8.000
	6.000			20.000	8.000	4.500	3.00	10.000	10.000
	7.000			25.000	10.000	5.000	3.30	14.000	13.000
	8.000			35.000	15.000	5.500	3.70	20.000	20.000
	10.000				20.000	6.000	4.30	30.000	35.000
	14.000				35.000	6.600	5.00		
	20.000					7.400	6.00		
	35.000					8.000	7.00		
						9.000	7.50		
						10.000	8.00		
						12.500	9.00		
						15.000	13.00		
						20.000	15.00		
						30.000	20.00		
							35.00		
Total=32	40	30	32	36	38	46	47	37	37

TABLE 4.1 FREQUENCY BANDS AND RELATIVE ORDINATES OF FITTED
TRAPEZOIDAL SPECTRA FOR ELASTOPLASTIC SYSTEMS WITH
5% DAMPING

MEAN SPECTRA NORMALIZED TO PEAK GROUND DISPLACEMENT								
Ductility factor	DISPLACEMENT REGION			VELOCITY REGION			ACCELERATION REGION		
	from	to	ratio	from	to	ratio	from	to	ratio
1.	.1	.43	1.000	.43	3.45	1.000	3.45	8.	1.000
1.5	.1	.44	.604	.44	3.81	.621	3.81	8.	.687
2.	.1	.45	.448	.45	4.24	.461	4.24	8.	.568
3.	.1	.47	.299	.47	4.65	.328	4.65	8.	.442
5.	.1	.57	.171	.57	5.03	.227	5.03	8.	.331
10.	.1	.78	.080	.78	5.66	.144	5.66	8.	.236

MEAN SPECTRA NORMALIZED TO PEAK GROUND VELOCITY								
Ductility factor	DISPLACEMENT REGION			VELOCITY REGION			ACCELERATION REGION		
	from	to	ratio	from	to	ratio	from	to	ratio
1.	.1	.39	1.000	.39	3.22	1.000	3.22	8.	1.000
1.5	.1	.40	.608	.40	3.54	.622	3.54	8.	.684
2.	.1	.40	.451	.40	4.00	.460	4.00	8.	.572
3.	.1	.42	.306	.42	4.42	.328	4.42	8.	.449
5.	.1	.53	.170	.53	4.68	.229	4.68	8.	.332
10.	.1	.71	.079	.71	5.46	.143	5.46	8.	.243

MEAN SPECTRA NORMALIZED TO PEAK GROUND ACCELERATION								
Ductility factor	DISPLACEMENT REGION			VELOCITY REGION			ACCELERATION REGION		
	from	to	ratio	from	to	ratio	from	to	ratio
1.	.1	.32	1.000	.32	2.86	1.000	2.86	8.	1.000
1.5	.1	.32	.627	.32	3.11	.635	3.11	8.	.689
2.	.1	.32	.473	.32	3.48	.473	3.48	8.	.575
3.	.1	.32	.329	.32	3.92	.333	3.92	8.	.455
5.	.1	.40	.185	.40	4.22	.232	4.22	8.	.342
10.	.1	.58	.080	.58	5.05	.145	5.05	8.	.256

TABLE 4.2 SUMMARY OF FREQUENCY BAND STATISTICS FOR ELASTOPLASTIC SYSTEMS WITH 2% DAMPING

Spectral Region	Ductility (μ)	Frequency Band ($f_\ell - f_u$)	Mean (Ψ_μ)	Standard Deviation (σ_μ)	COV (Ω_μ)	ϕ_μ	λ_μ
Displacement	1	0.10 - 0.49	1.691	.825	.49	1.000	1.00
	1.5	0.10 - 0.46	1.000	.448	.45	.591	.97
	2	0.10 - 0.46	.722	.343	.48	.427	.99
	3	0.10 - 0.48	.477	.222	.47	.282	.98
	5	0.10 - 0.57	.273	.133	.49	.162	1.00
	10	0.10 - 0.76	.129	.064	.50	.076	1.01
Velocity	1	0.45 - 3.32	2.032	.845	.42	1.000	1.00
	1.5	0.42 - 3.79	1.143	.438	.38	.563	.98
	2	0.42 - 4.18	.817	.311	.38	.402	.97
	3	0.43 - 4.58	.565	.202	.36	.278	.96
	5	0.52 - 4.88	.385	.140	.36	.190	.96
	10	0.70 - 5.63	.239	.079	.33	.118	.94
Acceleration	1	2.96 - 8.00	3.075	.743	.24	1.000	1.00
	1.5	3.29 - 8.00	1.974	.421	.21	.642	.98
	2	3.68 - 8.00	1.572	.311	.20	.511	.96
	3	4.02 - 8.00	1.195	.232	.19	.389	.96
	5	4.39 - 8.00	.881	.164	.19	.287	.95
	10	5.21 - 8.00	.647	.119	.18	.210	.95

TABLE 4.3 SUMMARY OF FREQUENCY BAND STATISTICS FOR ELASTOPLASTIC SYSTEMS WITH 5% DAMPING

Spectral Region	Ductility (μ)	Frequency Band $(f_\ell - f_u)$	Mean (Ψ_μ)	Standard Deviation (σ_μ)	COV (Ω_μ)	ϕ_μ	λ_μ
Displacement	1	0.10 – 0.43	1.465	.635	.43	1.000	1.00
	1.5	0.10 – 0.44	.885	.363	.41	.604	.98
	2	0.10 – 0.45	.656	.291	.44	.448	1.01
	3	0.10 – 0.47	.439	.194	.44	.299	1.01
	5	0.10 – 0.57	.250	.122	.49	.171	1.04
	10	0.10 – 0.78	.117	.061	.52	.080	1.06
Velocity	1	0.39 – 3.22	1.552	.597	.39	1.000	1.00
	1.5	0.40 – 3.54	.966	.346	.36	.623	.98
	2	0.40 – 4.00	.714	.253	.35	.460	.98
	3	0.42 – 4.42	.508	.176	.35	.328	.97
	5	0.53 – 4.68	.355	.129	.36	.229	.98
	10	0.71 – 5.46	.222	.075	.34	.143	.96
Acceleration	1	2.86 – 8.00	2.281	.494	.22	1.000	1.00
	1.5	3.11 – 8.00	1.572	.290	.18	.689	.97
	2	3.48 – 8.00	1.311	.234	.18	.575	.97
	3	3.92 – 8.00	1.038	.174	.17	.455	.96
	5	4.22 – 8.00	.781	.134	.17	.342	.96
	10	5.05 – 8.00	.584	.097	.17	.256	.96

TABLE 4.4 SUMMARY OF FREQUENCY BAND STATISTICS FOR ELASTOPLASTIC SYSTEMS WITH 10% DAMPING

Spectral Region	Ductility (μ)	Frequency Band $(f_\ell - f_u)$	Mean (Ψ_μ)	Standard Deviation (σ_μ)	COV (Ω_μ)	ϕ_μ	λ_μ
Displacement	1	0.10 — 0.40	1.234	.478	.39	1.000	1.00
	1.5	0.10 — 0.41	.781	.292	.37	.633	.99
	2	0.10 — 0.43	.577	.238	.41	.467	1.02
	3	0.10 — 0.47	.384	.166	.43	.311	1.03
	5	0.10 — 0.58	.218	.107	.49	.177	1.07
	10	0.10 — 0.79	.103	.055	.54	.084	1.11
Velocity	1	0.36 — 3.25	1.201	.436	.36	1.000	1.00
	1.5	0.37 — 3.58	.778	.273	.35	.648	.99
	2	0.39 — 3.84	.612	.221	.36	.509	1.00
	3	0.42 — 4.25	.438	.152	.35	.365	.99
	5	0.54 — 4.56	.313	.113	.36	.260	1.00
	10	0.72 — 5.28	.200	.069	.35	.166	.99
Acceleration	1	2.87 — 8.00	1.784	.321	.18	1.000	1.00
	1.5	3.15 — 8.00	1.277	.212	.17	.716	.99
	2	3.43 — 8.00	1.087	.168	.15	.610	.98
	3	3.81 — 8.00	.871	.135	.15	.488	.98
	5	4.19 — 8.00	.681	.119	.17	.382	.99
	10	4.88 — 8.00	.505	.081	.16	.283	.98

TABLE 4.5   SUMMARY OF FREQUENCY BAND STATISTICS FOR BILINEAR SYSTEMS WITH 5% DAMPING

Spectral Region	Ductility (μ)	Frequency Band $(f_\ell - f_u)$	Mean (Ψ_μ)	Standard Deviation (σ_μ)	COV (Ω_μ)	ϕ_μ	λ_μ
Displacement	1	0.10 - 0.43	1.465	.635	.43	1.000	1.00
	1.5	0.10 - 0.44	.882	.361	.41	.602	.98
	2	0.10 - 0.44	.648	.286	.44	.442	1.01
	3	0.10 - 0.46	.423	.183	.43	.289	1.00
	5	0.10 - 0.55	.233	.109	.47	.159	1.02
	10	0.10 - 0.68	.108	.053	.49	.074	1.04
Velocity	1	0.39 - 3.22	1.552	.597	.39	1.000	1.00
	1.5	0.40 - 3.55	.960	.344	.36	.619	.98
	2	0.40 - 3.99	.701	.255	.36	.452	.98
	3	0.41 - 4.35	.475	.162	.34	.306	.97
	5	0.49 - 4.84	.308	.107	.35	.199	.97
	10	0.61 - 5.84	.177	.055	.31	.114	.95
Acceleration	1	2.86 - 8.00	2.281	.494	.22	1.000	1.00
	1.5	3.12 - 8.00	1.567	.287	.18	.687	.97
	2	3.50 - 8.00	1.285	.223	.17	.563	.96
	3	3.86 - 8.00	.963	.156	.16	.422	.95
	5	4.37 - 8.00	.704	.109	.15	.309	.95
	10	5.26 - 8.00	.493	.088	.18	.216	.97

TABLE 4.6   SUMMARY OF FREQUENCY BAND STATISTICS FOR DEGRADING SYSTEMS WITH 5% DAMPING

Spectral Region	Ductility (μ)	Frequency Band $(f_\ell - f_u)$	Mean (Ψ_μ)	Standard Deviation (σ_μ)	COV (Ω_μ)	ϕ_μ	λ_μ
Displacement	1	0.10 - 0.43	1.465	.635	.43	1.000	1.00
	1.5	0.10 - 0.44	.870	.348	.40	.594	.98
	2	0.10 - 0.45	.617	.226	.37	.421	.95
	3	0.10 - 0.47	.392	.131	.34	.268	.93
	5	0.10 - 0.57	.221	.081	.37	.151	.95
	10	0.10 - 0.74	.103	.039	.38	.070	.96
Velocity	1	0.39 - 3.22	1.552	.597	.39	1.000	1.00
	1.5	0.40 - 3.54	.939	.359	.38	.605	1.00
	2	0.40 - 3.96	.670	.240	.36	.432	.98
	3	0.43 - 4.75	.452	.149	.33	.291	.96
	5	0.51 - 5.53	.306	.100	.33	.197	.96
	10	0.67 - 6.96	.186	.059	.32	.120	.95
Acceleration	1	2.86 - 8.00	2.281	.494	.22	1.000	1.00
	1.5	3.15 - 8.00	1.532	.289	.19	.672	.98
	2	3.54 - 8.00	1.235	.207	.17	.542	.96
	3	4.21 - 8.00	.998	.147	.15	.438	.94
	5	4.99 - 8.00	.799	.110	.14	.350	.93
	10	6.24 - 8.00	.609	.101	.17	.267	.96

TABLE 4.7 COMPARISON OF RESULTS FOR ELASTIC SYSTEMS WITH NEWMARK'S ET AL. STUDY

Damping	Spectral Region	This Study			Reference 77		
		$\psi_{\mu=1}$	σ	COV	Mean	σ	COV
2%	Displacement	1.69	.83	.49	1.68	.83	.49
	Velocity	2.03	.85	.42	2.06	.92	.45
	Acceleration	3.08	.74	.24	2.76	.89	.32
5%	Displacement	1.47	.64	.43	1.40	.64	.46
	Velocity	1.55	.60	.39	1.66	.66	.40
	Acceleration	2.28	.49	.22	2.11	.49	.23
10%	Displacement	1.23	.48	.39	1.15	.47	.41
	Velocity	1.20	.44	.36	1.34	.47	.35
	Acceleration	1.78	.32	.18	1.65	.36	.22

TABLE 5.1   RELATIONSHIPS BETWEEN GROUND MOTION
PEAKS FOR THE RECORDS USED IN THIS STUDY

Station, Component	V/A in/sec/g	$\dfrac{AD}{V^2}$
El Centro, E-W	68	3.1
Olympia, N86E	24	8.8
Golden Gate, S80E	17	5.6
Cholame, N85E	23	4.5
Castaic, N21E	21	5.3
Pacoima, S16E	38	3.8
Lima, N82W	17	16.4
Santiago, N10W	58	3.7
Managua, E-W	41	5.0
San Juan, E-W	42	2.8
Average	35	5.9

TABLE 5.2 SPECTRAL ORDINATES AT 35 HERTZ FOR SPECTRA NORMALIZED TO GROUND ACCELERATION

	μ=1.5	μ=2	μ=3	μ=5	μ=10
	MEAN – MEAN PLUS ONE STANDARD DEVIATION				
Elastoplastic, β=2%	.941-.963	.920-.948	.895-.931	.862-.906	.810-.864
Elastoplastic, β=5%	.935-.959	.913-.943	.884-.921	.846-.891	.784-.838
Elastoplastic, β=10%	.928-.955	.902-.935	.868-.907	.821-.868	.742-.797
Bilinear, β=5%	.932-.957	.906-.936	.871-.907	.820-.863	.731-.782
Degrading, β=5%	.932-.957	.907-.937	.874-.909	.829-.870	.748-.794
μ $^{-0.07}$ [1]	.972	.953	.926	.893	.851
μ $^{-0.10}$ [2]	.960	.933	.896	.851	.794
μ $^{-0.13}$ [3]	.948	.914	.867	.811	.741

[1] Approximate relation for elastoplastic systems with β=2% and 5% at mean + sigma level.

[2] Approximate relation for elastoplastic systems with β=2% and 5% at mean level; and bilinear and degrading systems with β=5%, and elastoplastic systems with β=10%, at mean + sigma level.

[3] Approximate relation for bilinear and degrading systems with β=5%, and elastoplastic systems with β=10%, at mean level.
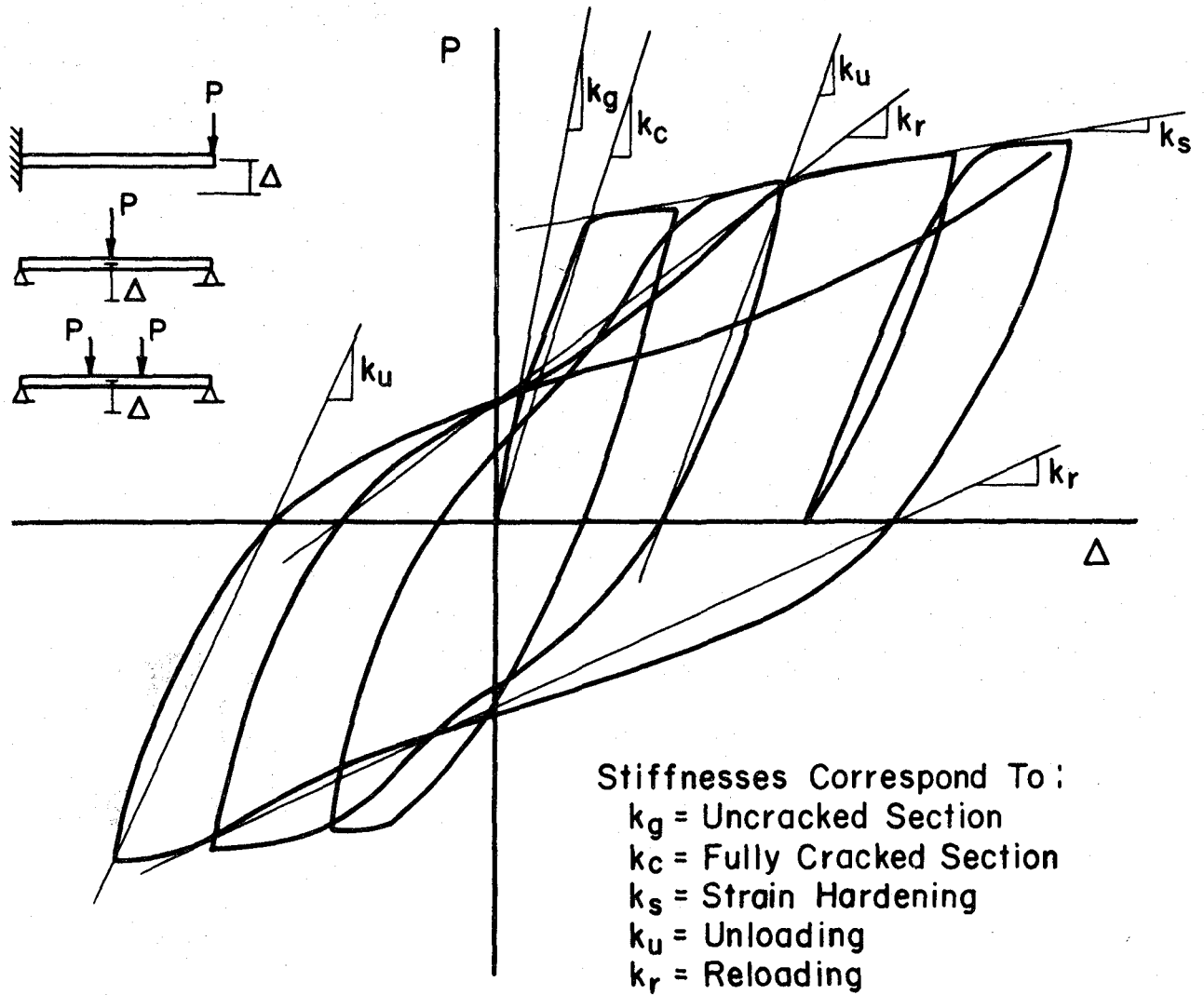
FIG. 2.1 HYSTERESIS FOR REINFORCED CONCRETE BEAMS
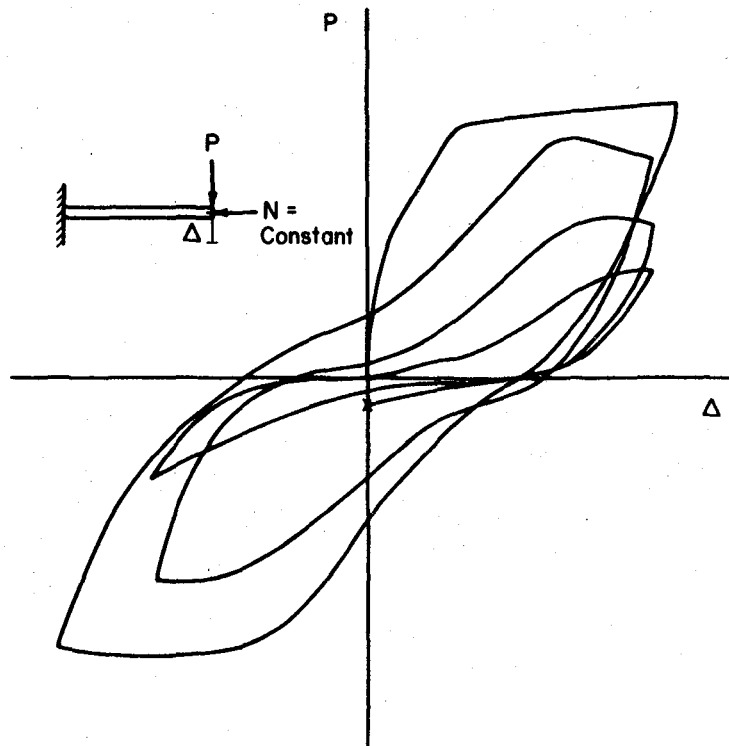
(a) Reinforced Concrete Member Without Adequate
Transverse Reinforcement. After Wight and Sozen (121).
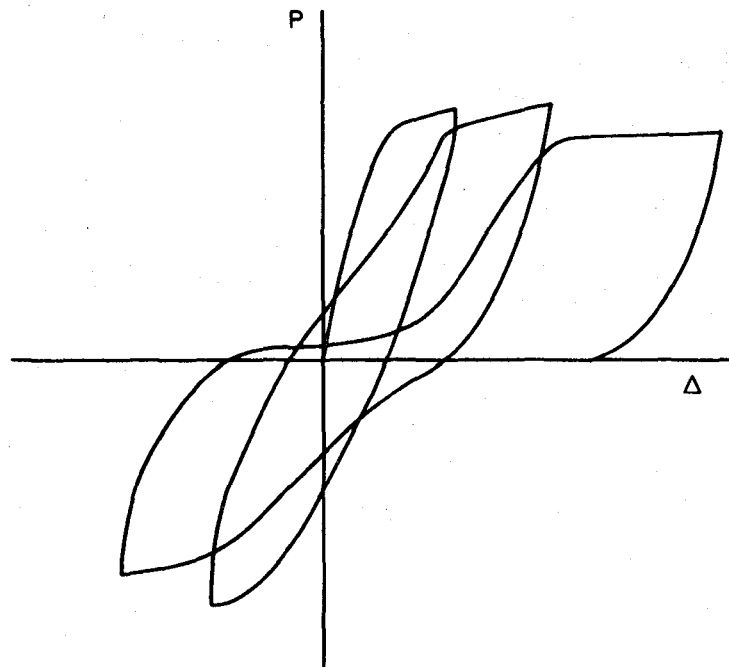
(b) Reinforced Concrete Member With Anchorage
Defect. After Higashi and Takeda (46).

FIG. 2.2 EFFECT OF REINFORCEMENT DEFICIENCIES ON HYSTERESIS LOOPS
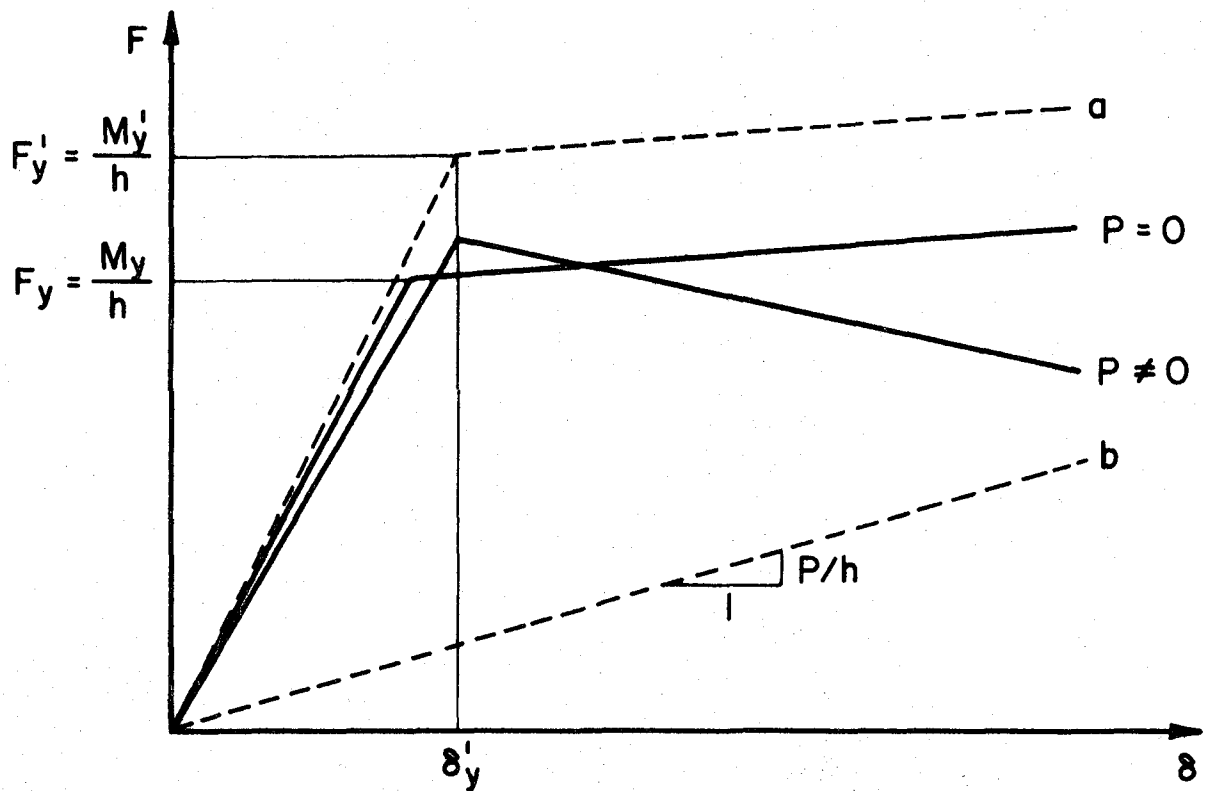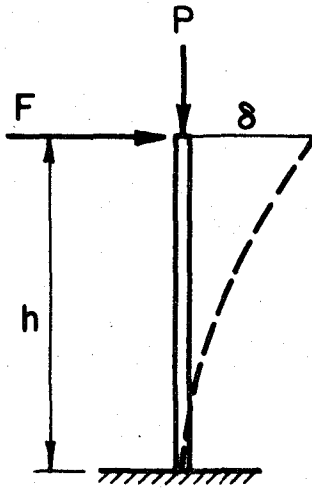
FIG. 2.3   P-δ EFFECT FOR IDEAL COLUMN SUBJECTED TO
LATERAL LOAD AND CONSTANT AXIAL FORCE
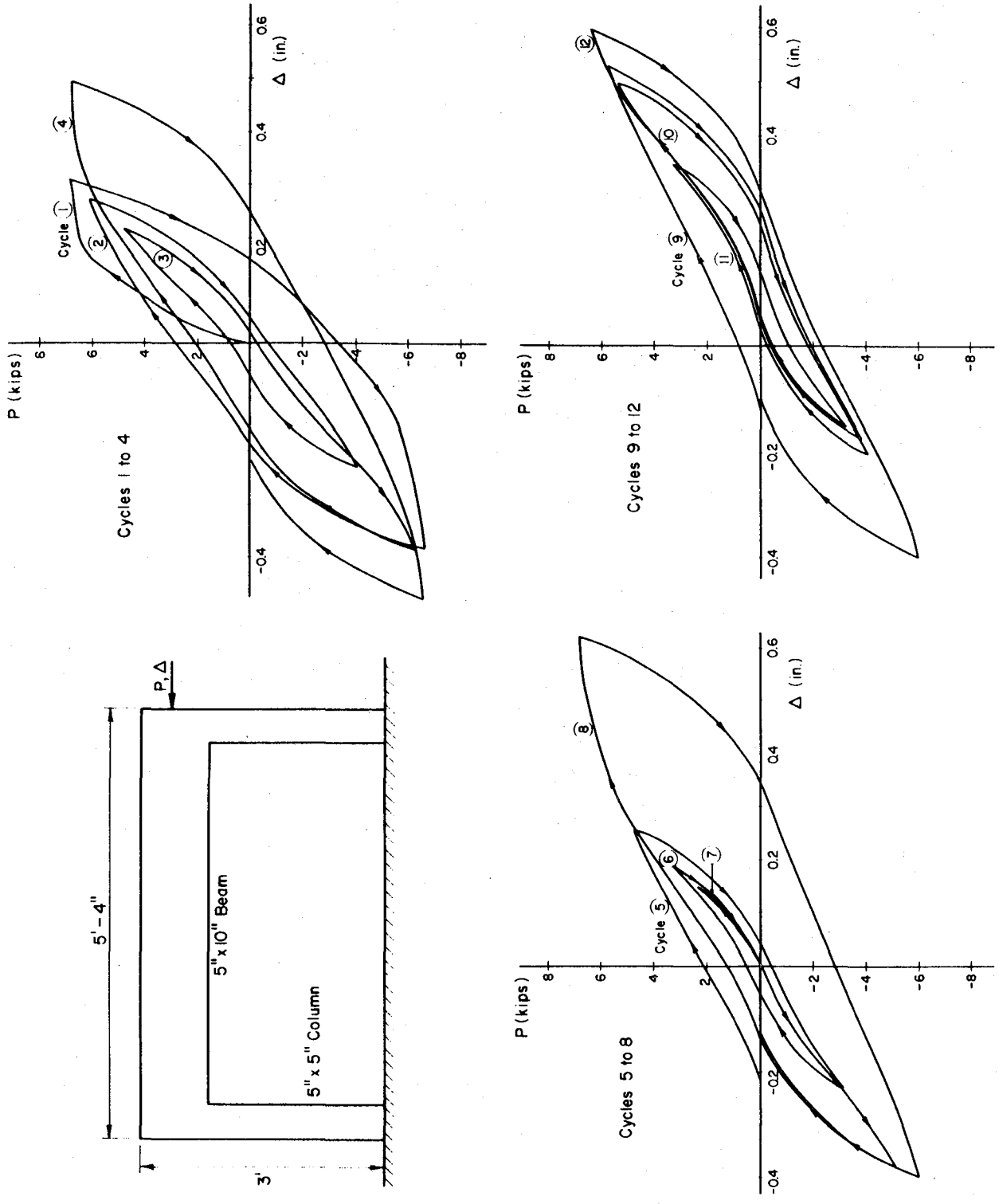
FIG. 2.4 LOAD-DEFLECTION CURVES FOR R/C FRAME MODEL. AFTER GULKAN AND SOZEN (39)

H/W

W = Total Weight

Lateral Deflection at
Top of Frame (in.)

b) Lateral Load-Deflection Curves for Model

Gravity Load 27 lb/ft²

0.357 H

0.214 H

0.171 H

2"x 2" Columns

0.129 H

0.086 H

0.043 H

1.2"x 2.4"
Beams

3'-4"

6 at 2'= 12'

3'-4"

Plan

3'-4"
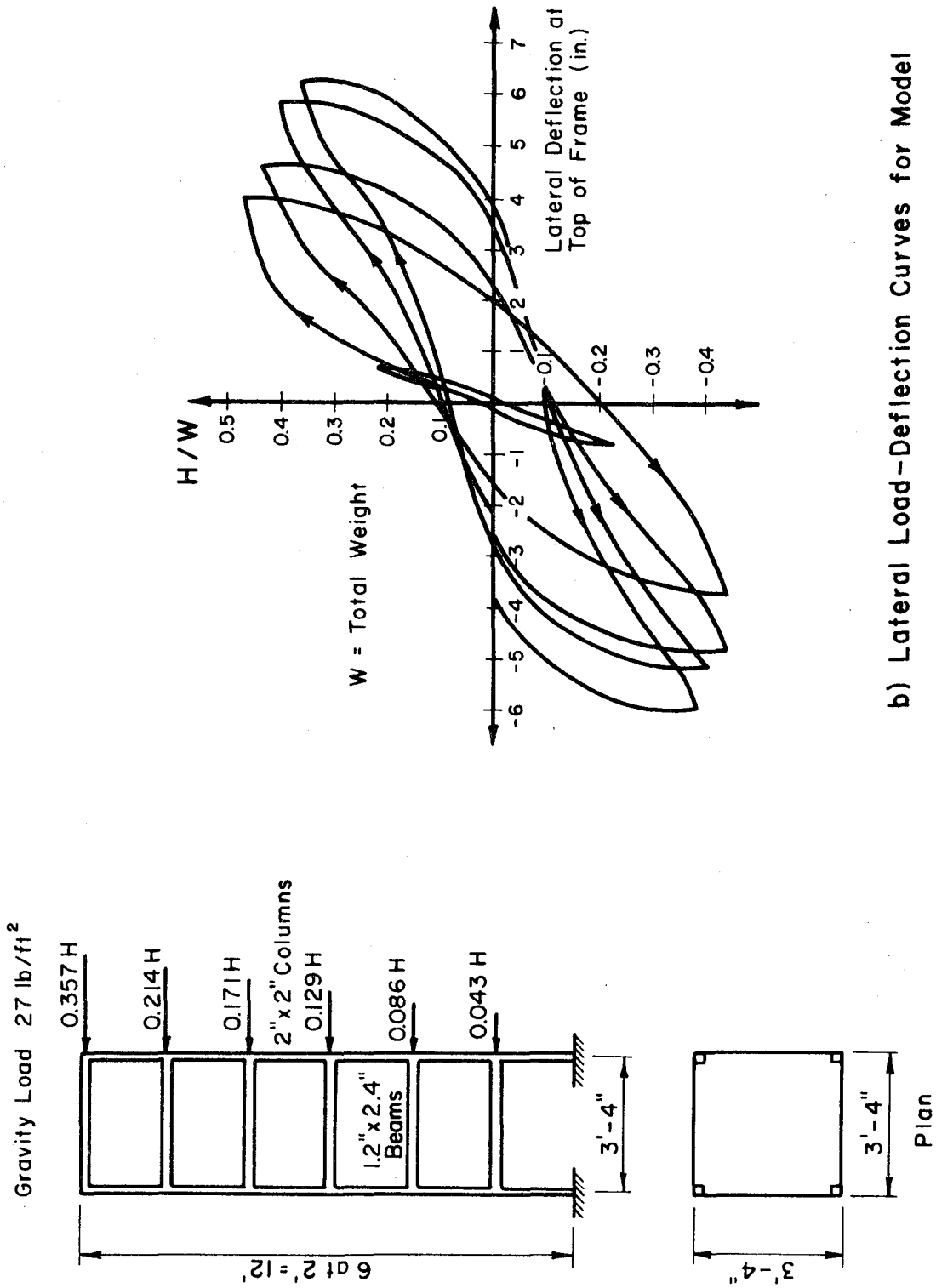
a) R/C Building Model

FIG. 2.5 REINFORCED CONCRETE BUILDING MODEL. AFTER PARK AND PAULEY (87)

123
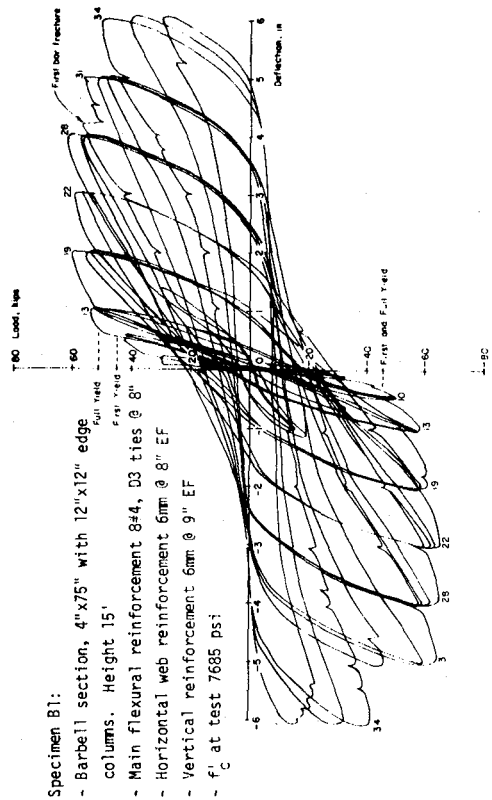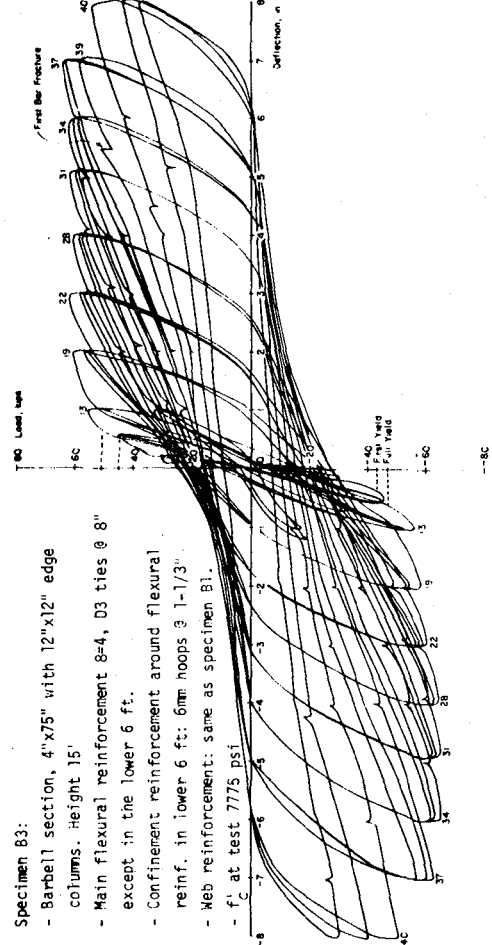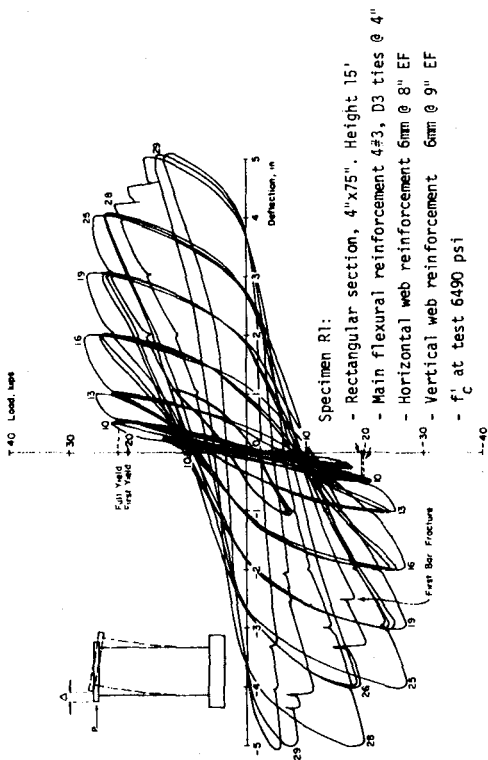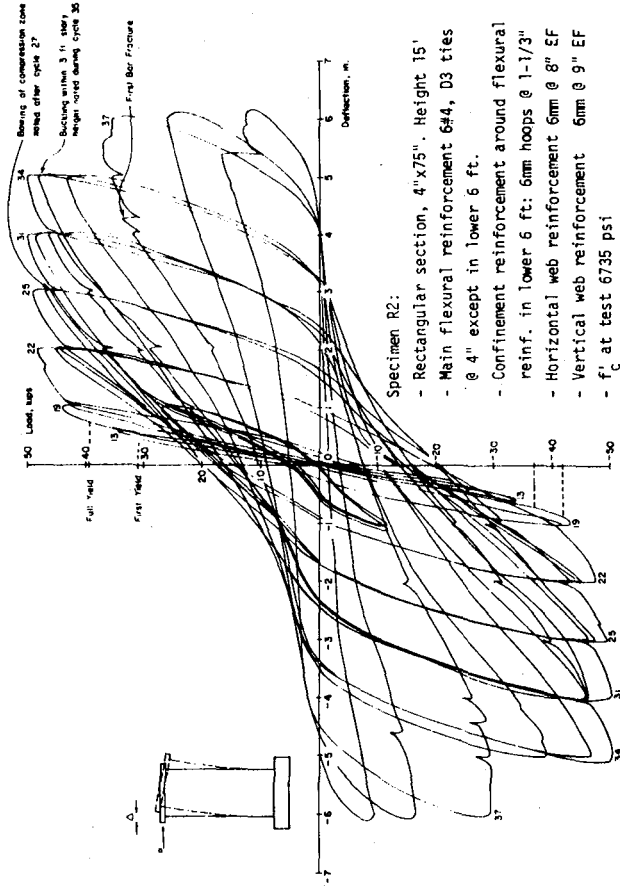
FIG. 2.6 LOAD-DEFLECTION CURVES FOR R/C WALLS. AFTER OESTERLE ET AL. (81)

124
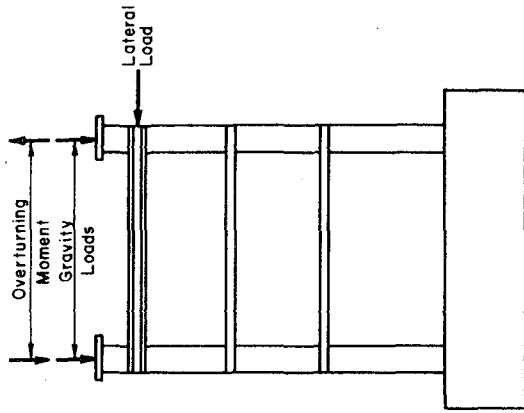
(b) Loading Configuration
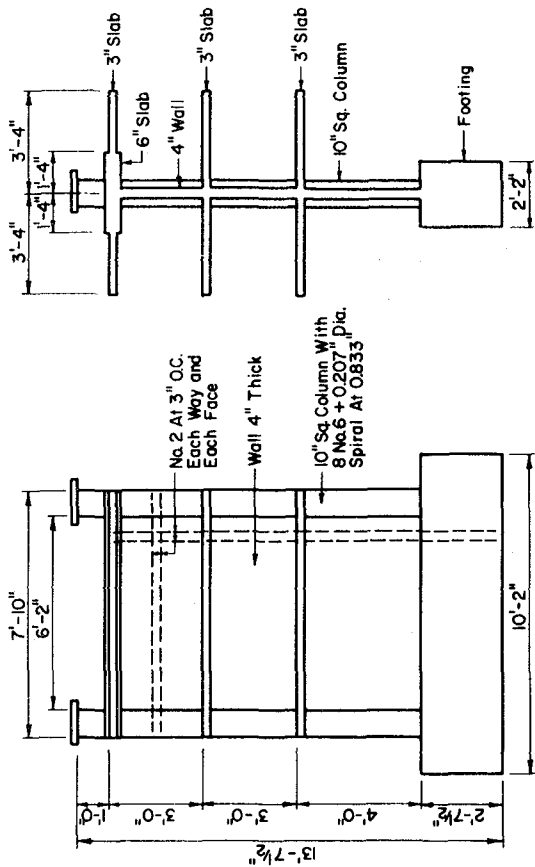
(a) Dimensions and Details of Wall Specimens
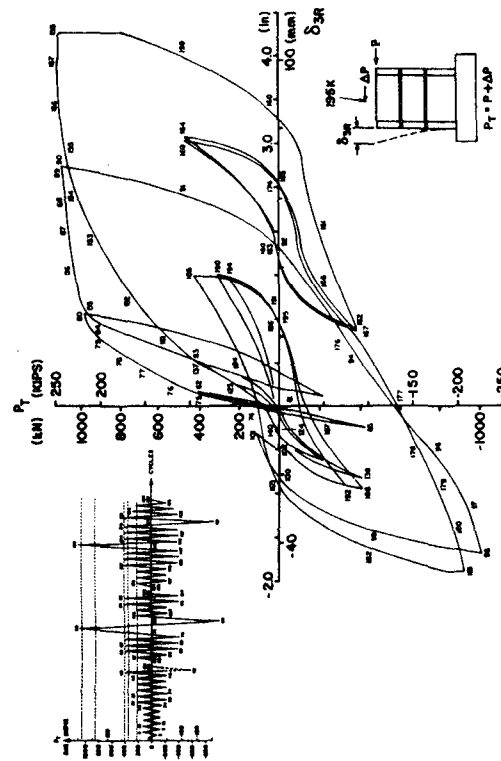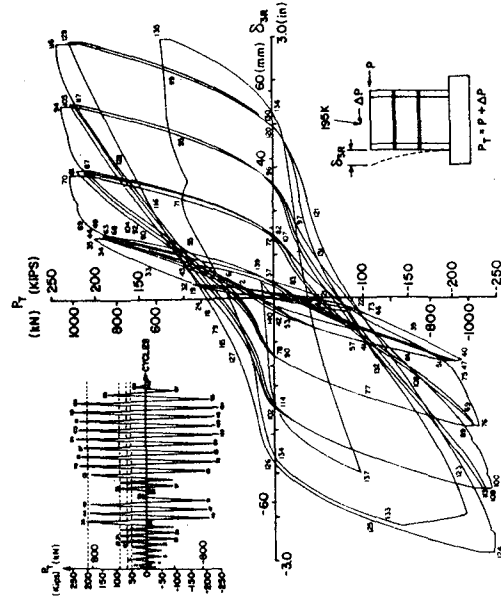
FIG. 2.7 LOAD-DEFLECTION CURVES FOR R/C WALL SUBASSEMBLAGES. AFTER WANG, BERTERO, AND POPOV (120).
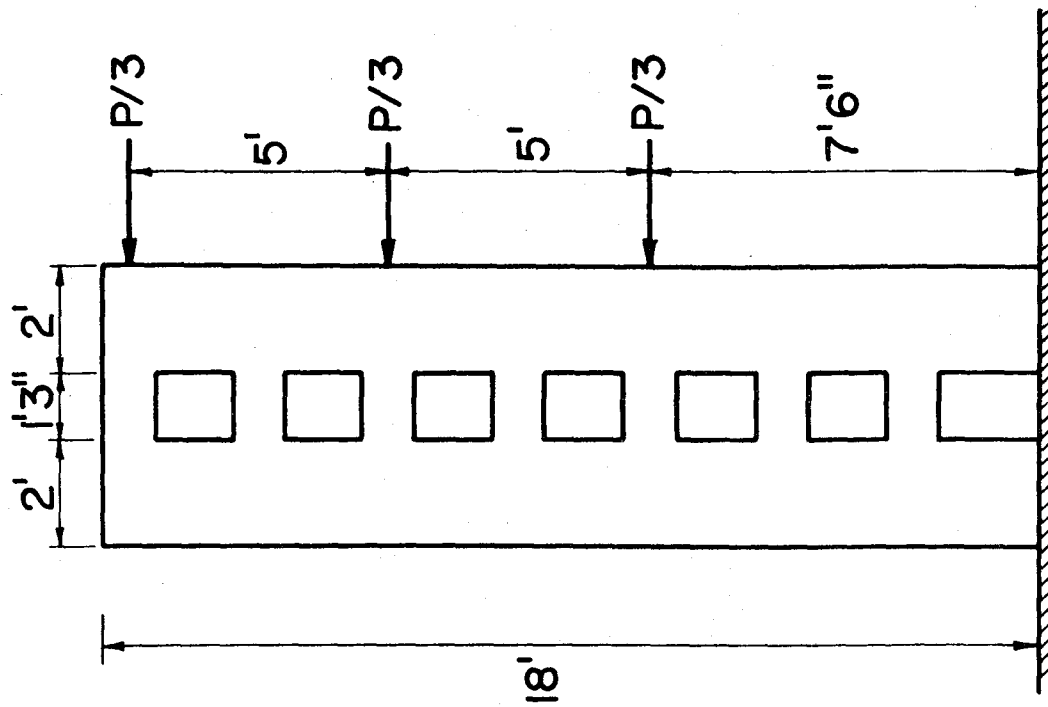
c) Coupled Wall Specimen
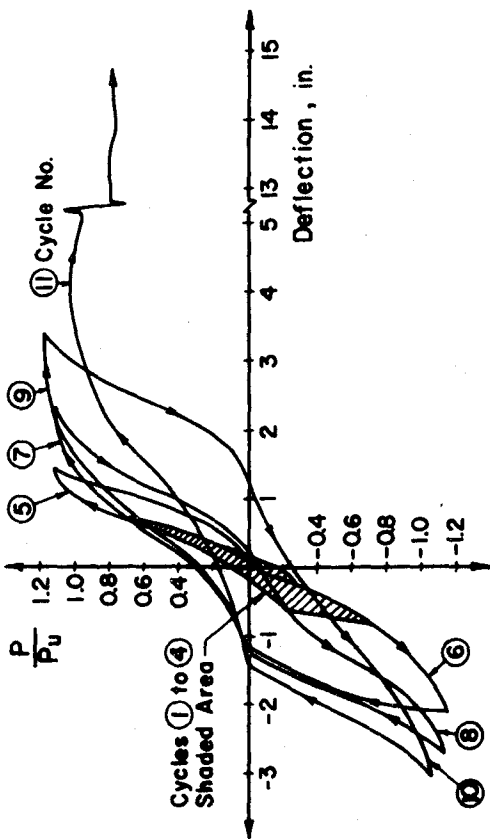
a) Wall with Conventionally Reinforced Coupling Beams
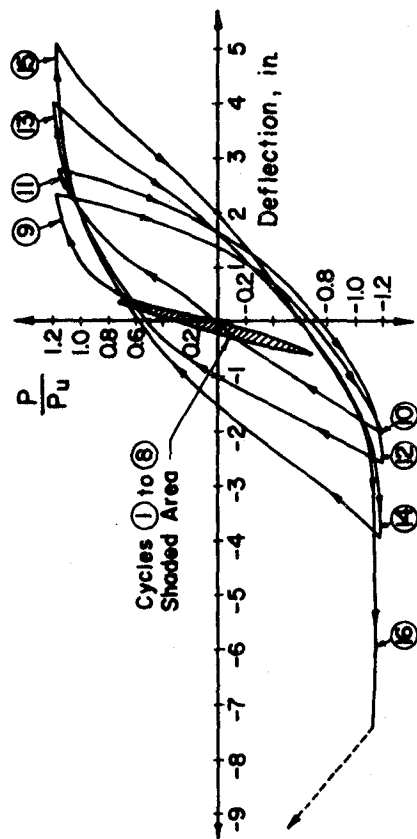
b) Wall with Diagonally Reinforced Coupling Beams

FIG. 2.8   LOAD-DEFLECTION CURVES FOR COUPLED R/C WALLS WITH DIFFERENT BEAM DETAILING.
AFTER PARK AND PAULAY (87), AND PAULAY AND SANTHAKUMAR (89).
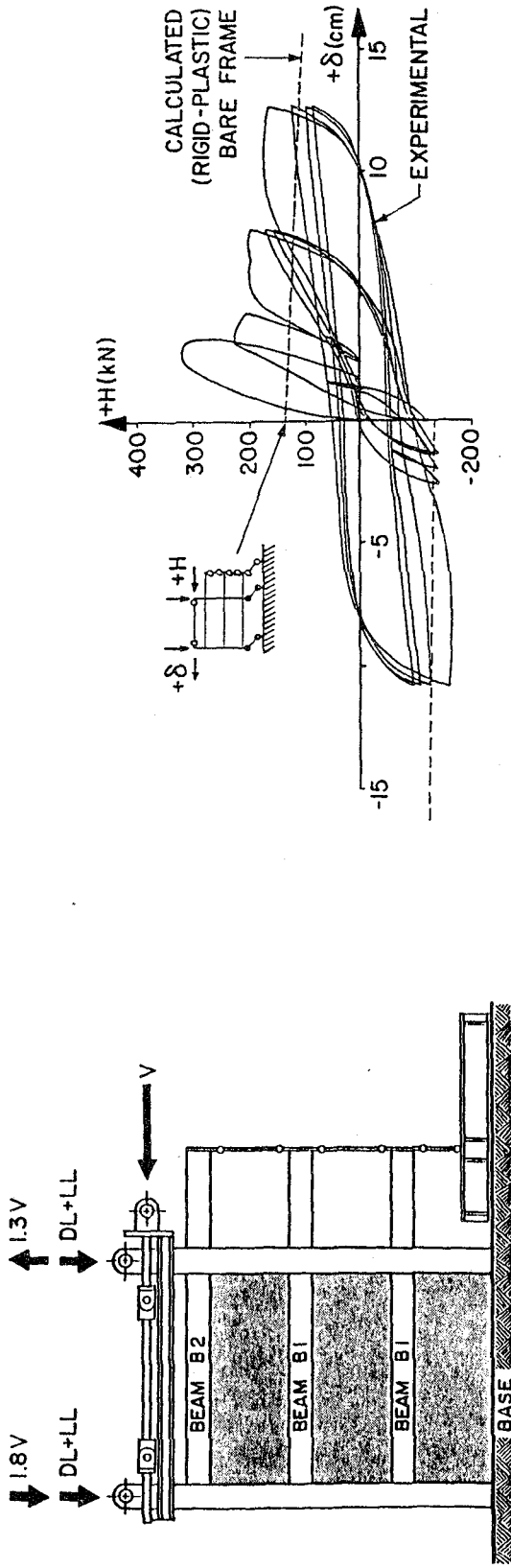
LATERAL LOAD-DEFLECTION RELATIONSHIP FOR FRAME WITH CLAY INFILL
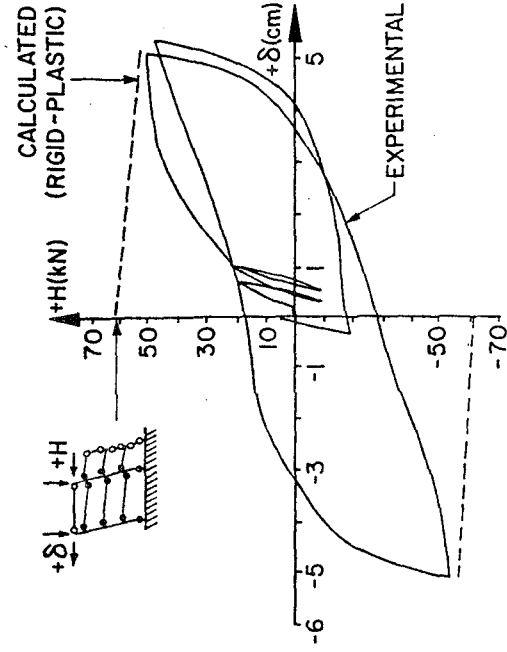
LATERAL LOAD-DEFLECTION RELATIONSHIP FOR BARE FRAME

LOADING PATTERN USED FOR INFILLED FRAMES
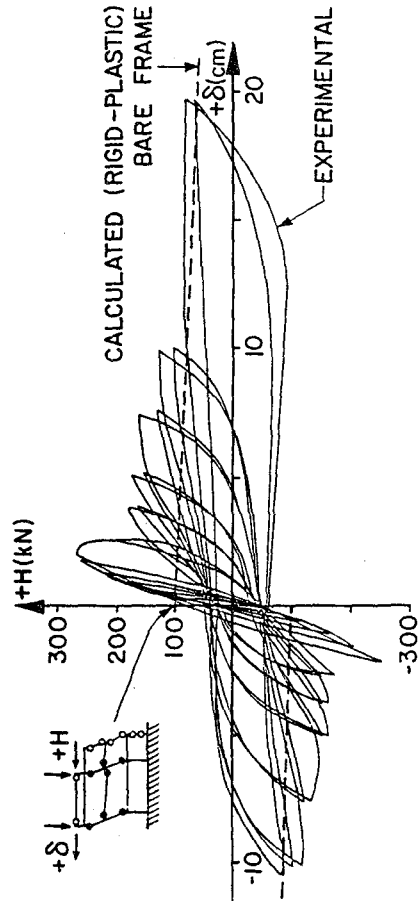
LATERAL LOAD-DEFLECTION RELATIONSHIP FOR FRAME WITH CONCRETE BLOCK INFILL

FIG. 2.9   LOAD-DEFLECTION CURVES FOR MASONRY INFILLED AND BARE R/C FRAMES.
AFTER KLINGNER AND BERTERO (56).
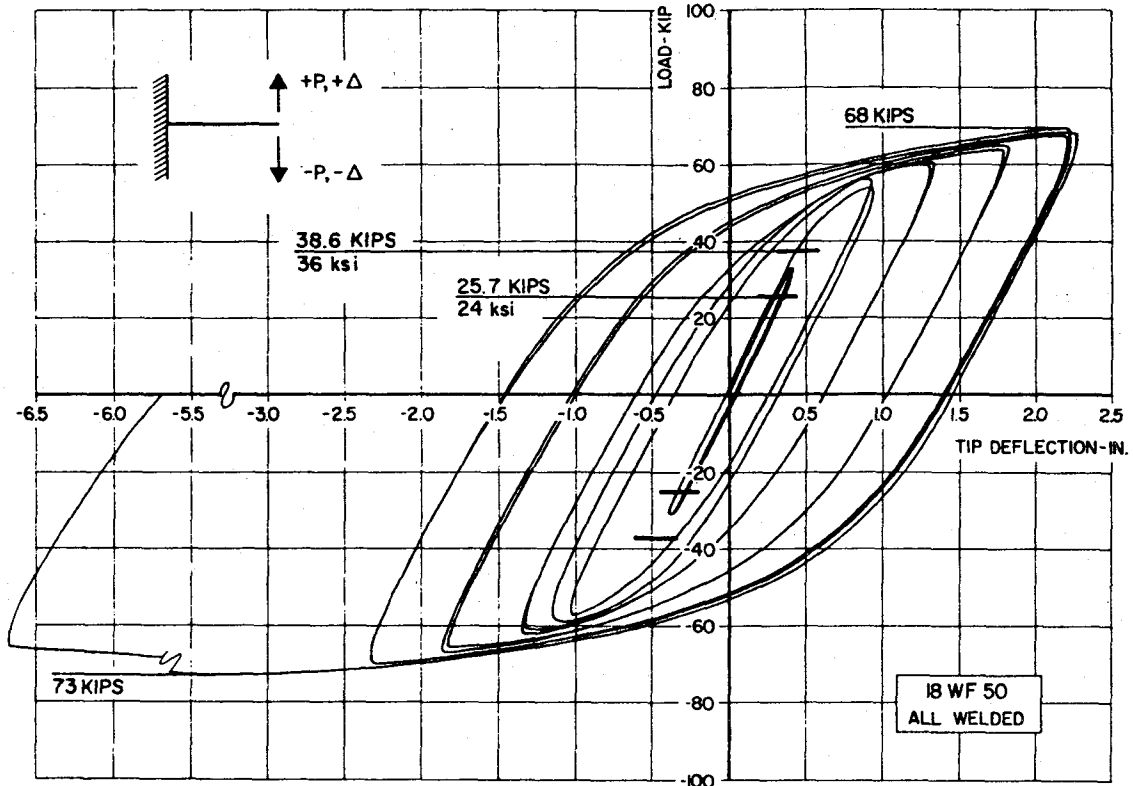
(a) Steel beam. After Popov and Stephen (95)
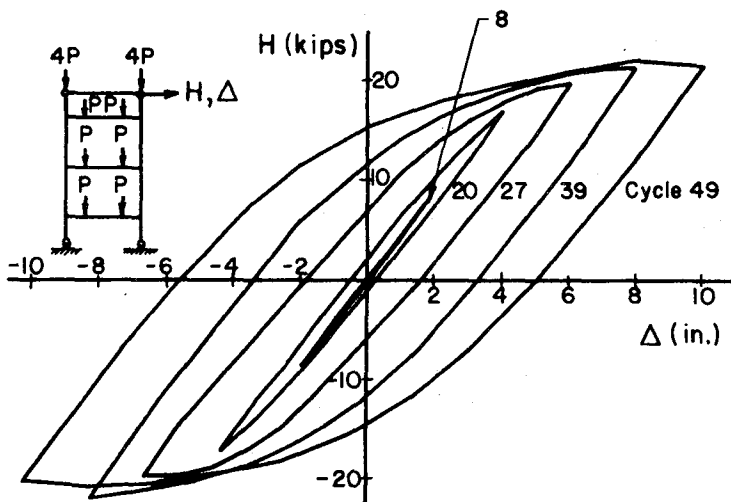
(b) Steel frame. After Carpenter and Lu (23)
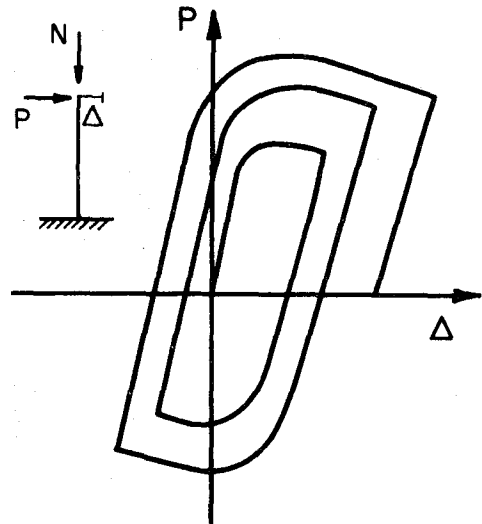
(c) Steel member with high axial force

FIG. 2.10 HYSTERESIS FOR STEEL MEMBERS AND UNBRACED STEEL FRAMES
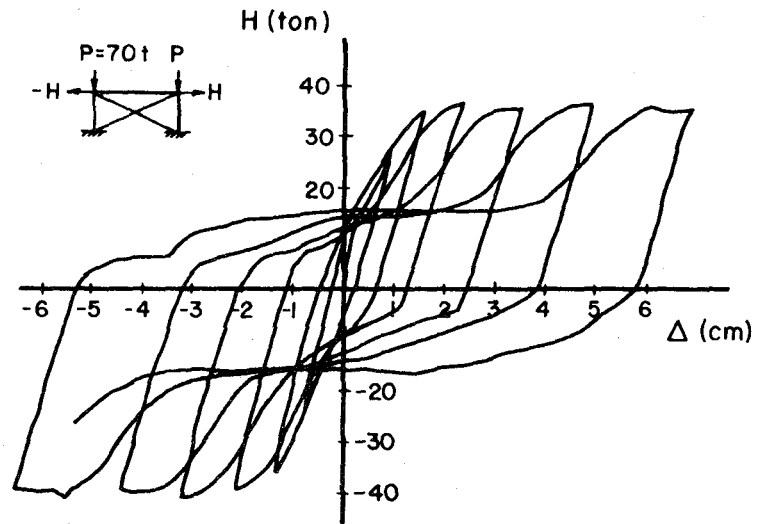
(a)   Braced steel frame.   After Wakabayashi (118).
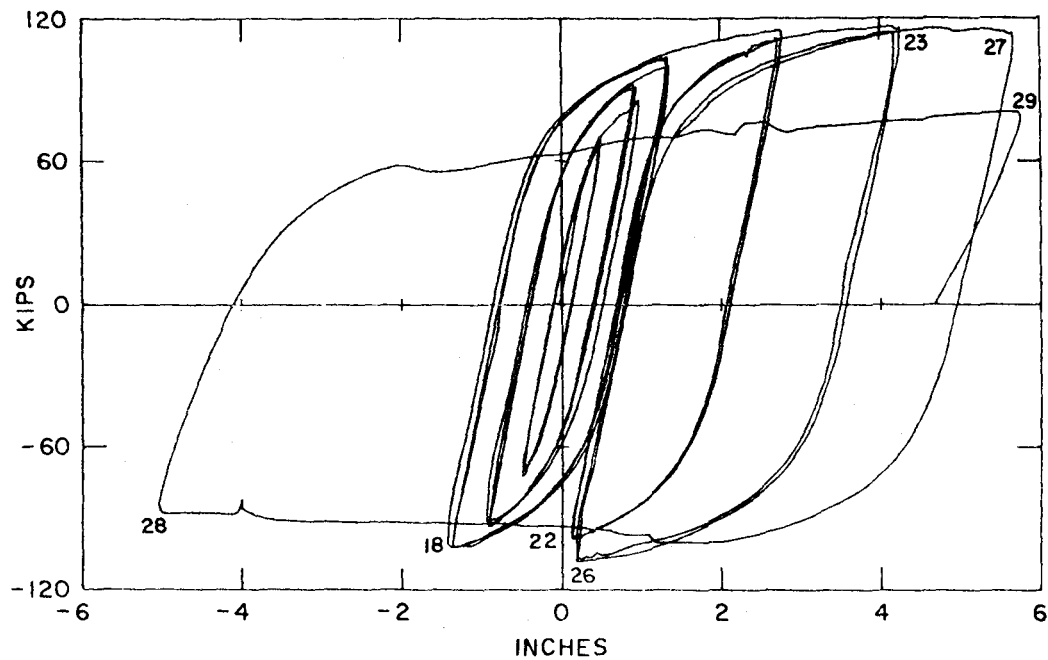
(b)   Eccentrically braced frame.   After Roeder and Popov (100).

FIG. 2.11   HYSTERESIS FOR BRACED STEEL FRAMES

Type I :
— Unbraced Steel Frames
  and Steel Members
  (Moderate Axial Load)
— Eccentrically Braced
  Steel Frames
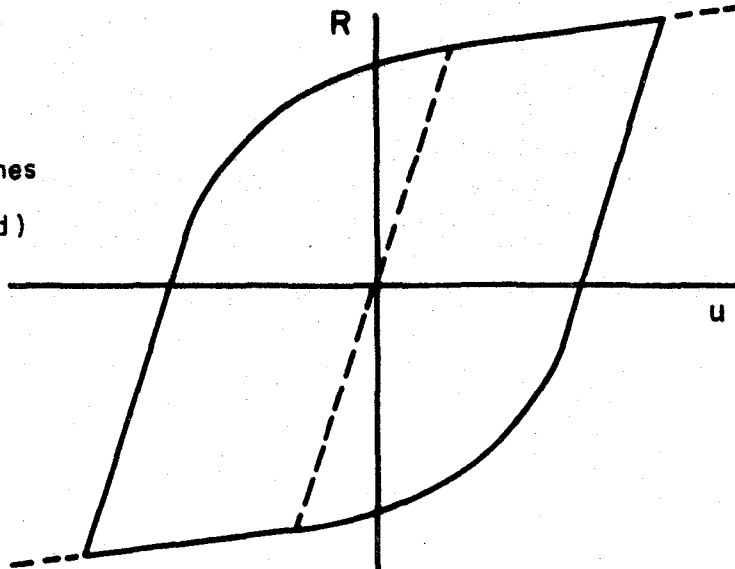
Type II
— Reinforced Concrete
  Members, Frames
  and Walls. (Flexural
  Behavior)
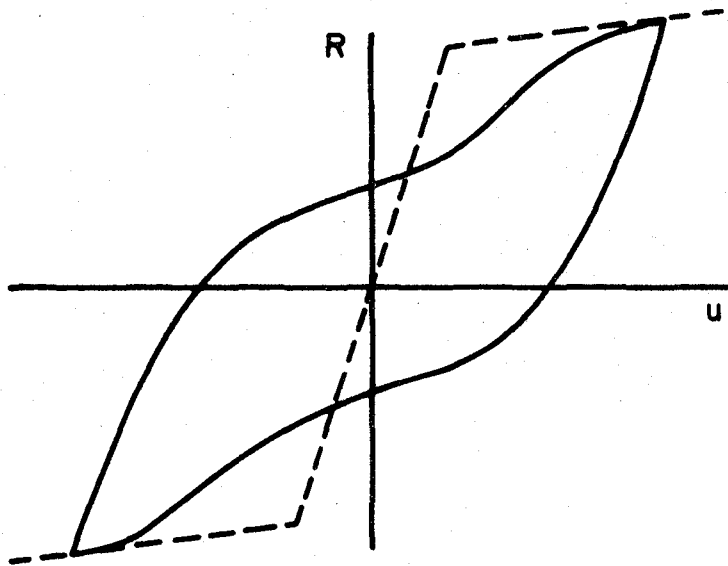
Type III
— Slip at R/C Joints
  or Bolted Steel
— Short R/C Members
— Concentrically Braced
  Steel Frames
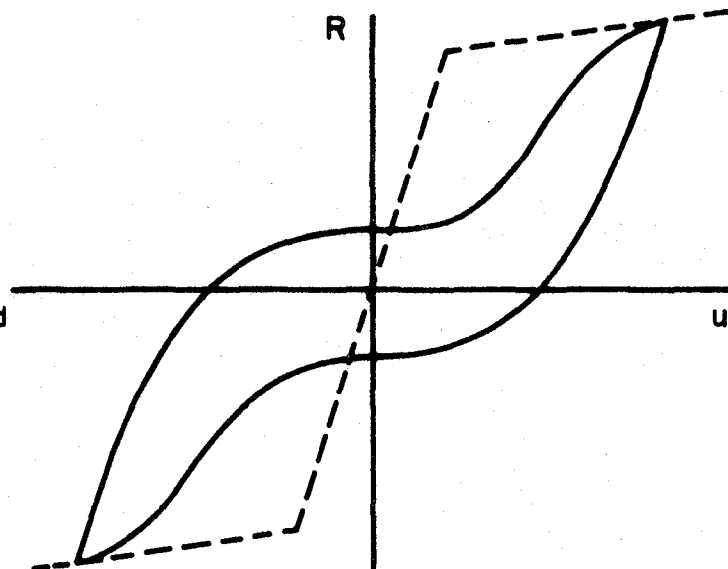
FIG. 2.12   SUMMARY OF HYSTERETIC SHAPES FOR STRUCTURES
WITHOUT STRENGTH DETERIORATION
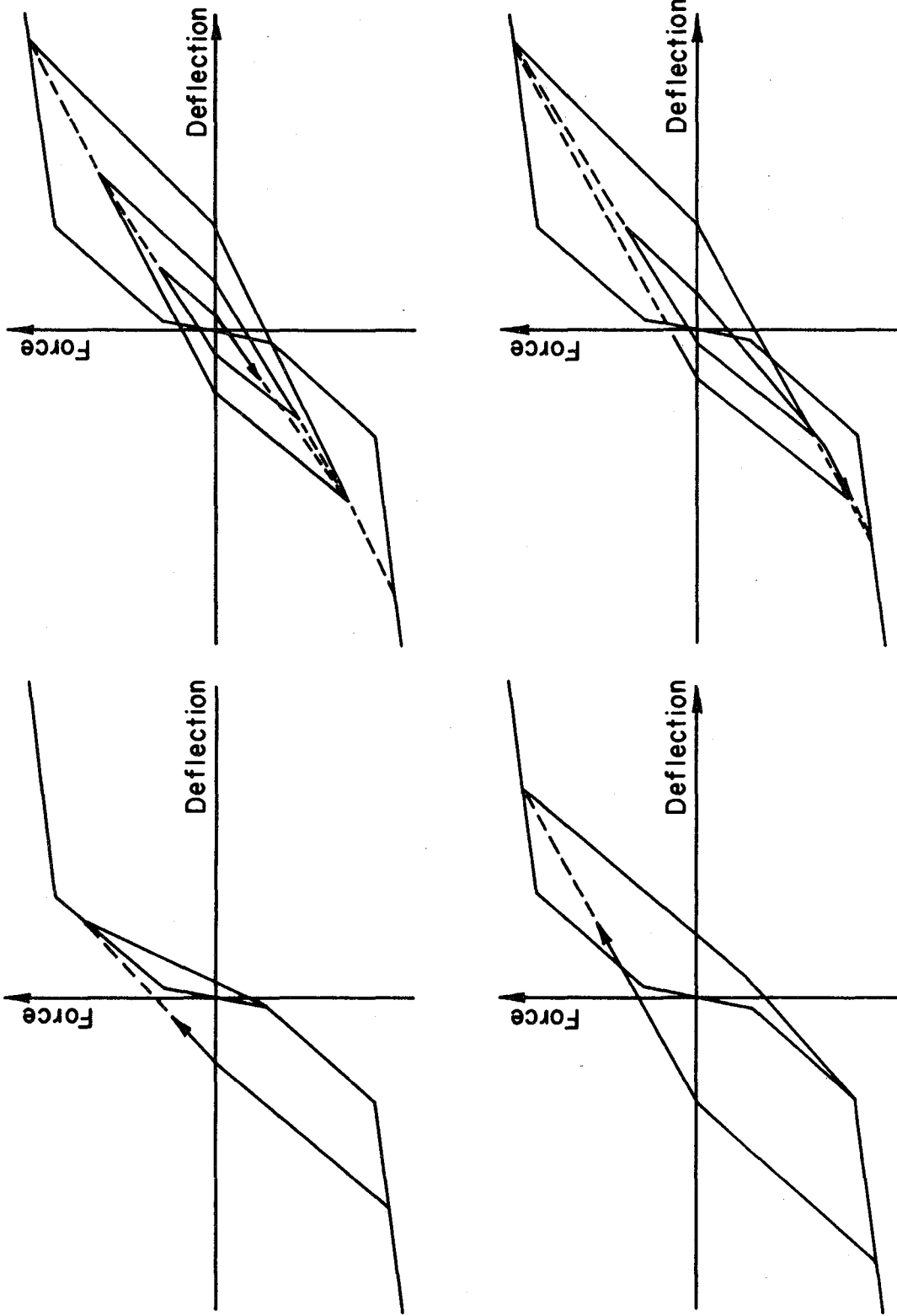
FIG. 2.13   THE TAKEDA-SOZEN STIFFNESS DEGRADING MODEL
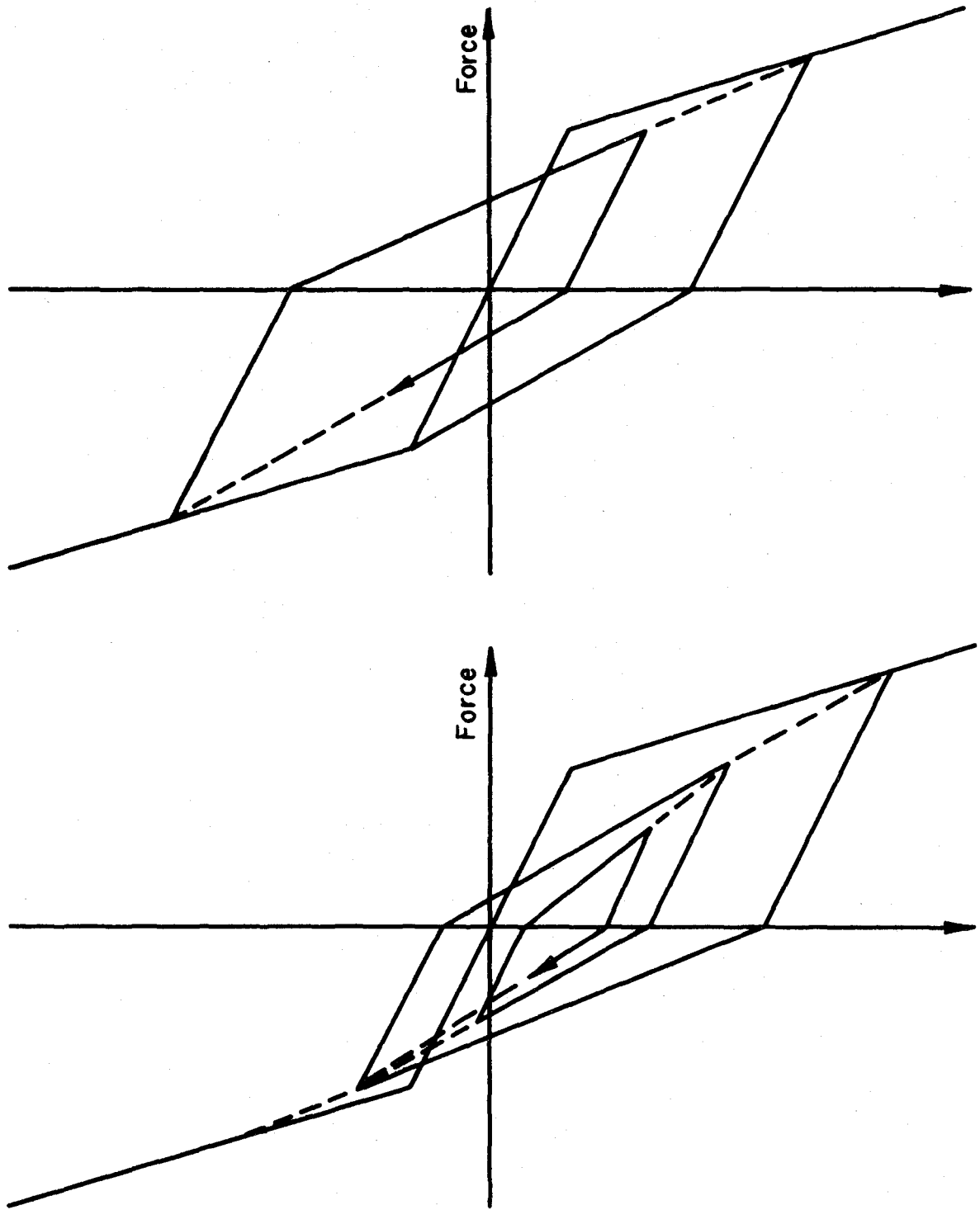
FIG. 2.14   THE OTANI-SOZEN STIFFNESS DEGRADING MODEL
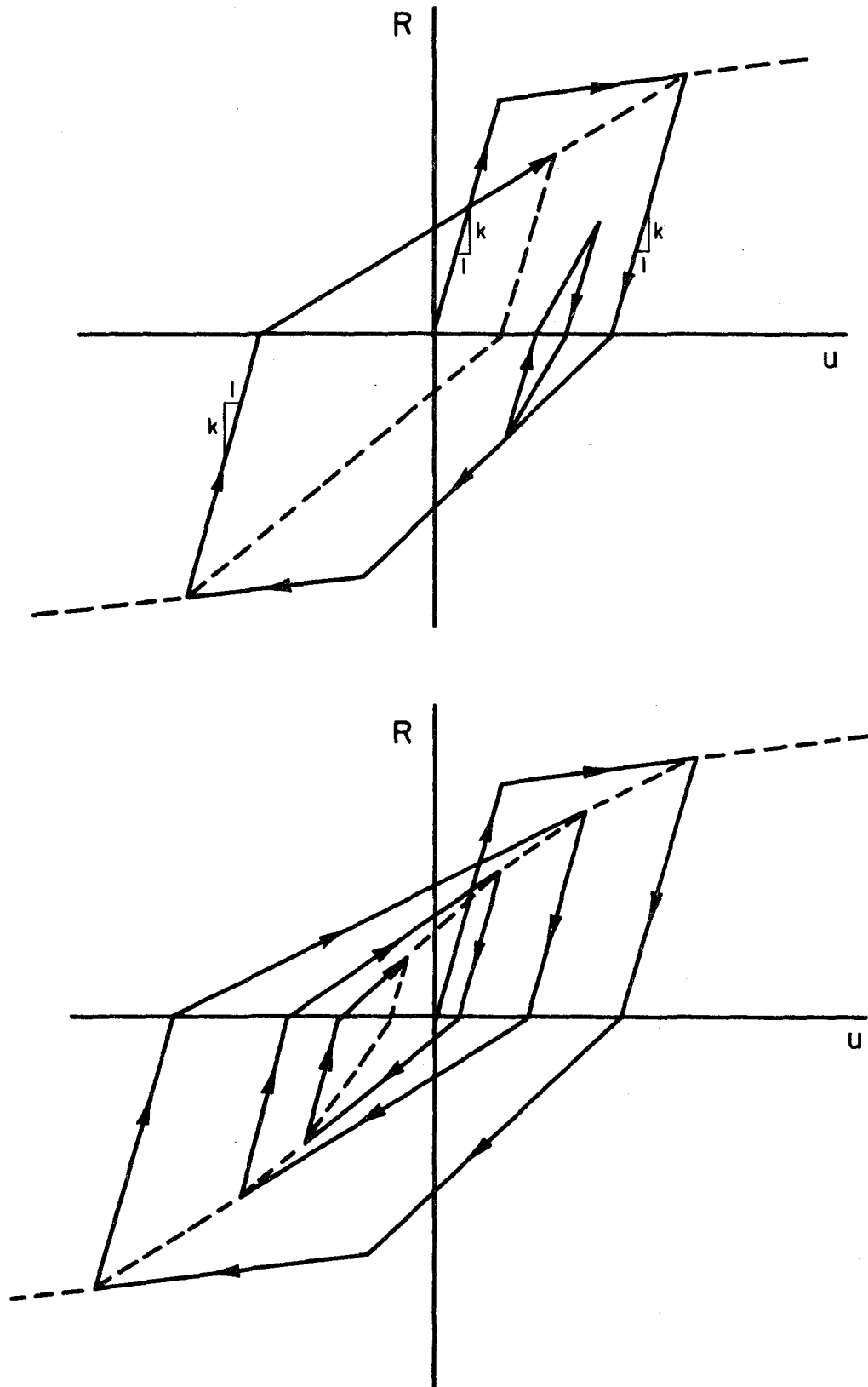
FIG. 2.15   STIFFNESS DEGRADING MODEL DERIVED FOR THIS STUDY
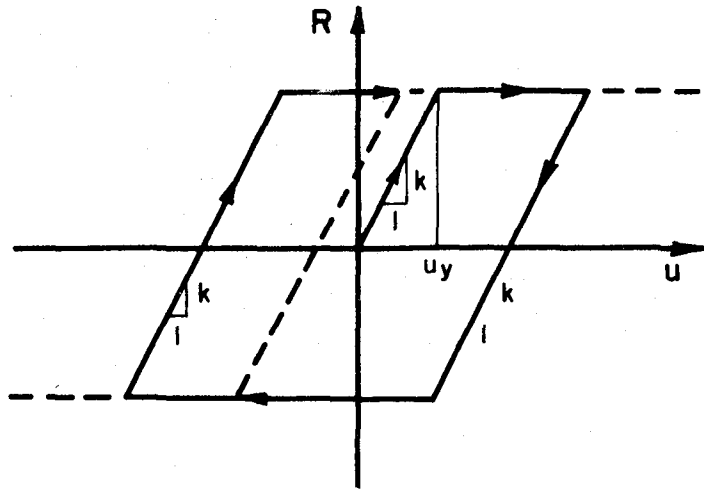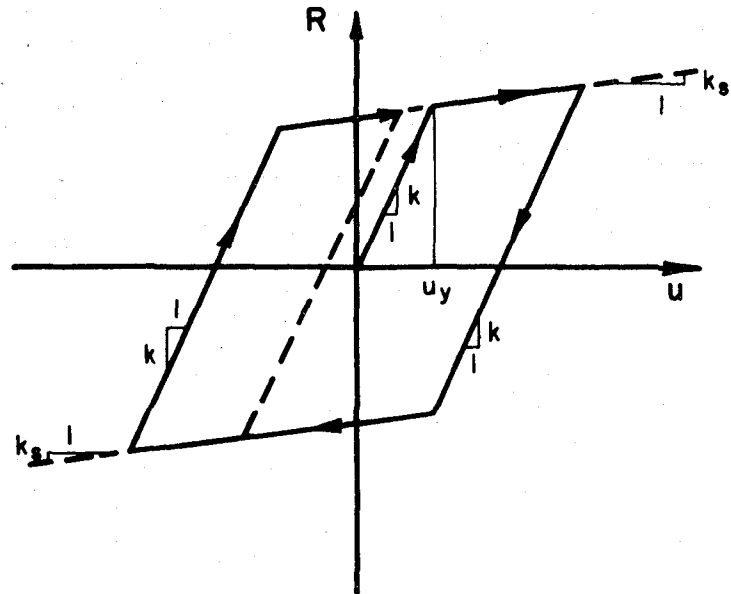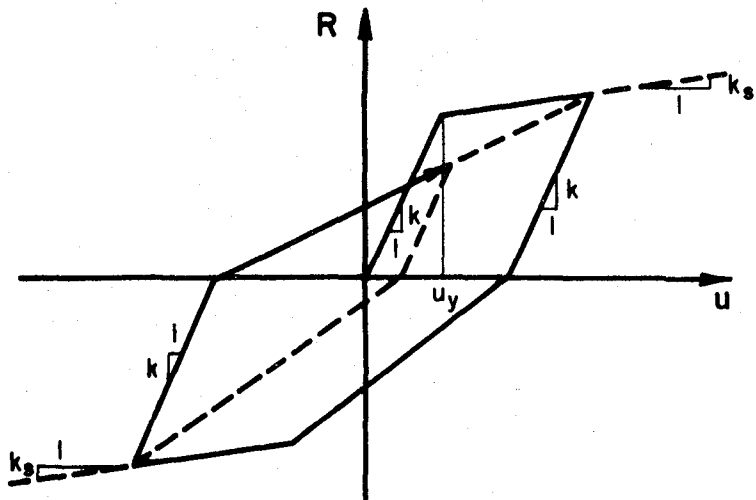
FIG. 2.16   NONLINEAR MODELS USED IN THIS STUDY
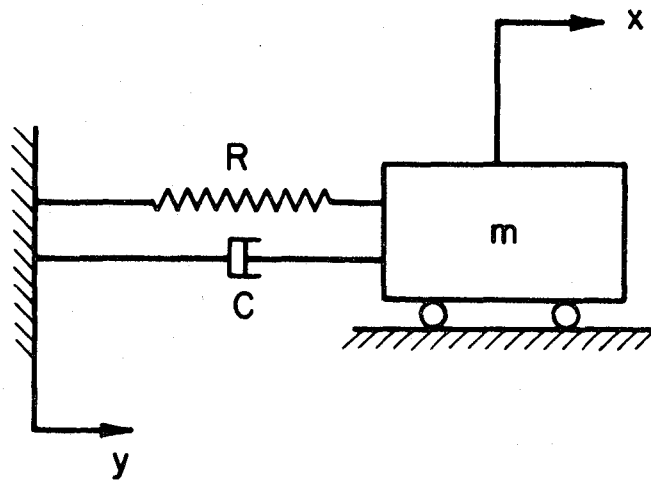
$$u = x - y$$

$$R = R(u)$$

$$C = 2\omega m \beta$$

FIG. 3.1   SYSTEM CONSIDERED IN THIS STUDY
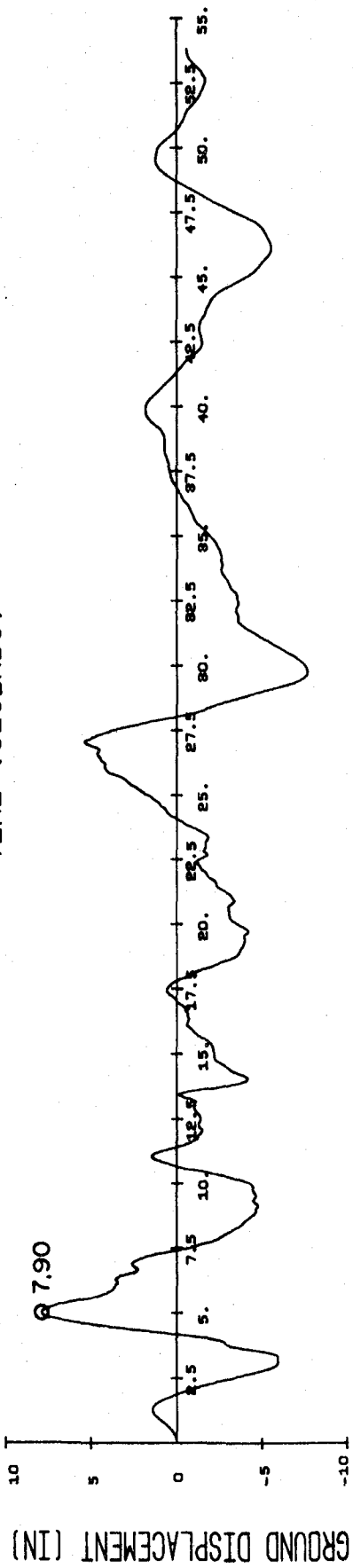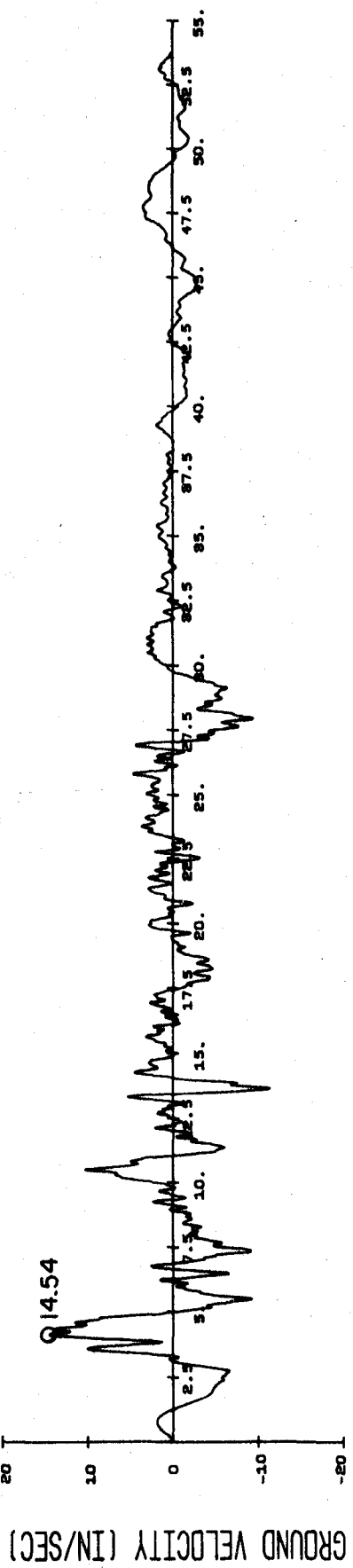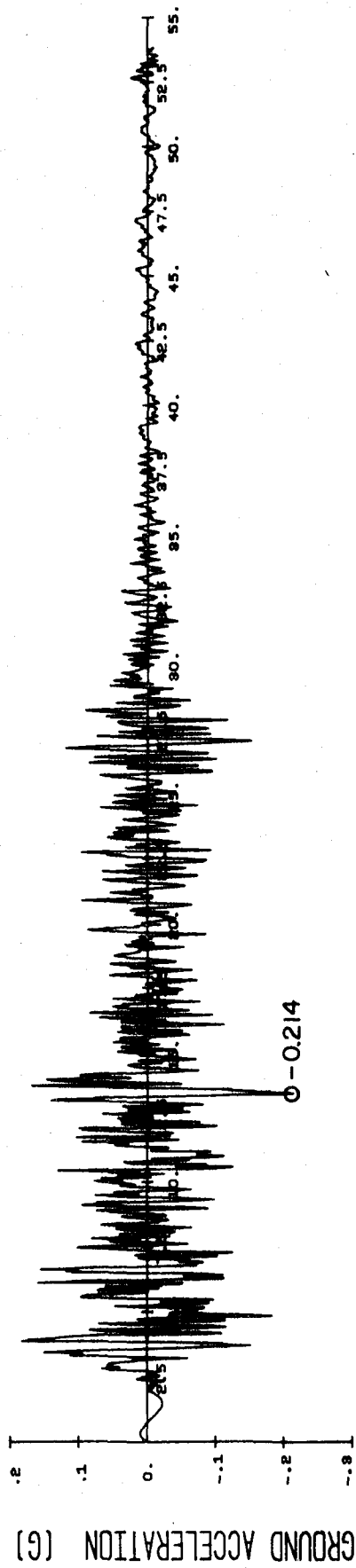
FIG. 3.2 GROUND MOTION FOR THE EL CENTRO RECORD OF MAY 18, 1940. E-W COMPONENT.
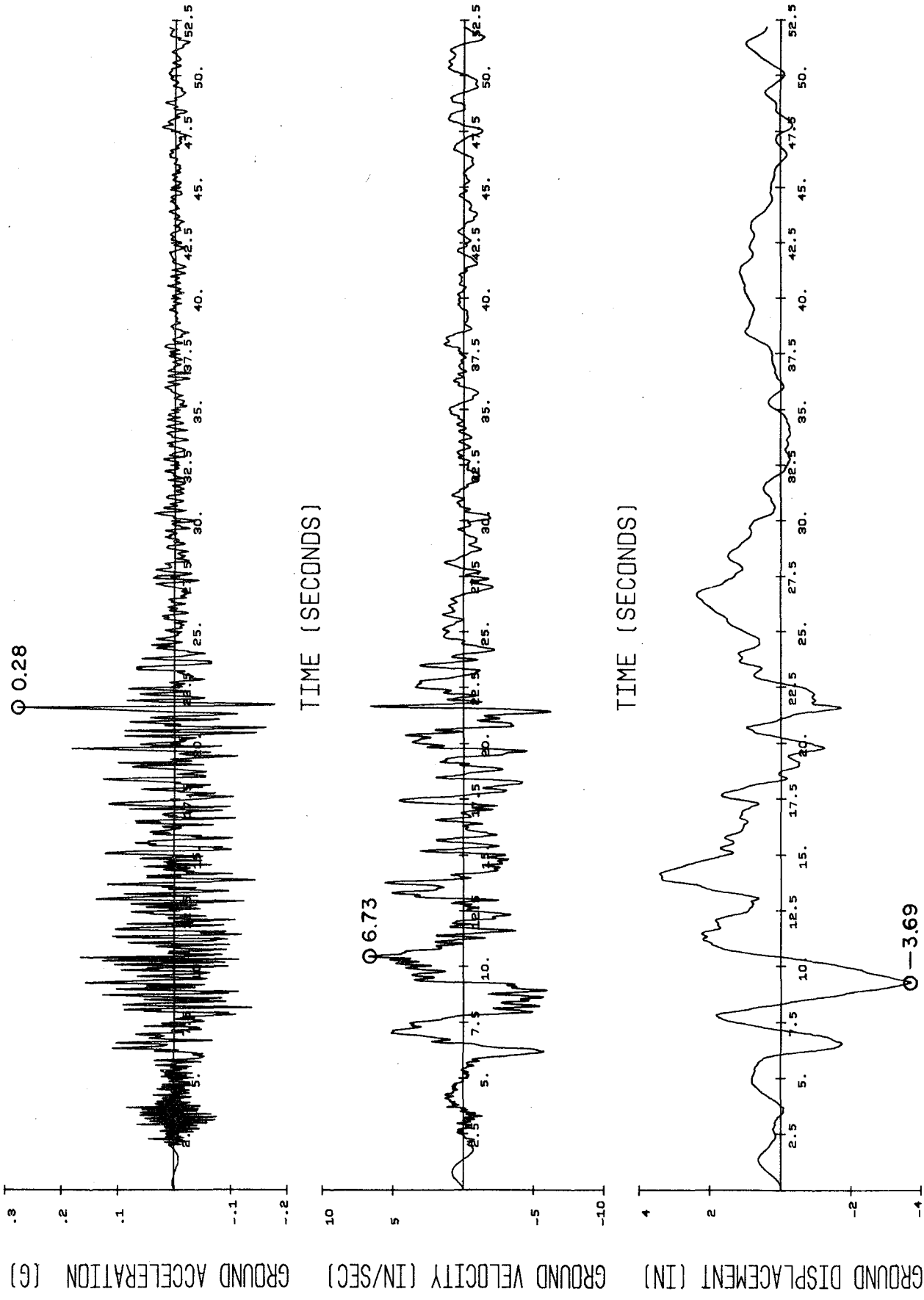
FIG. 3.3 GROUND MOTION FOR THE OLYMPIA RECORD OF APRIL 13, 1949. N86E COMPONENT.

137
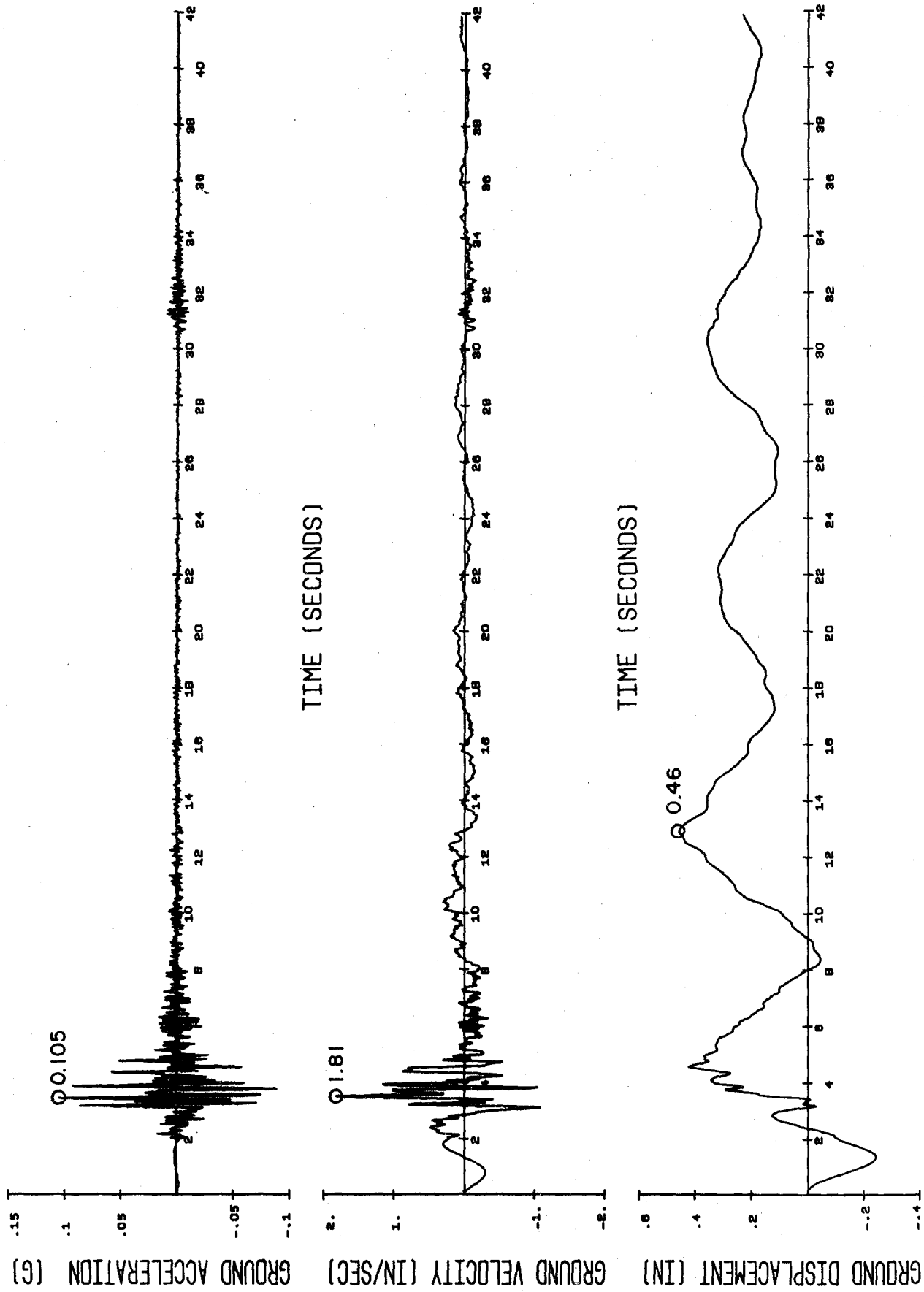
FIG. 3.4   GROUND MOTION FOR THE GOLDEN GATE PARK RECORD OF MARCH 22, 1957.   S80E COMPONENT.
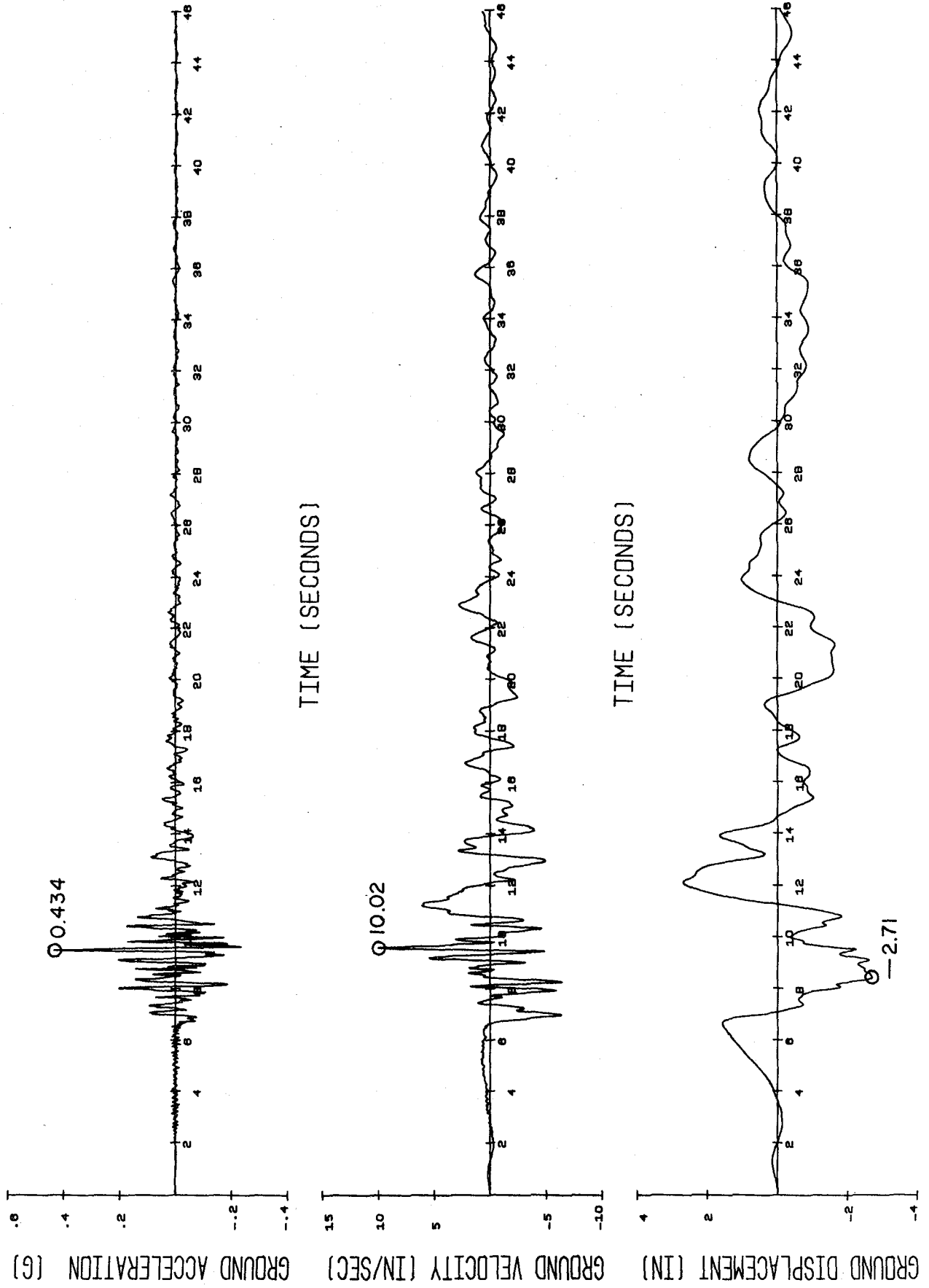
FIG. 3.5   GROUND MOTION FOR THE CHOLAME-STA. 5 RECORD OF JUNE 27, 1966.   N85E COMPONENT.
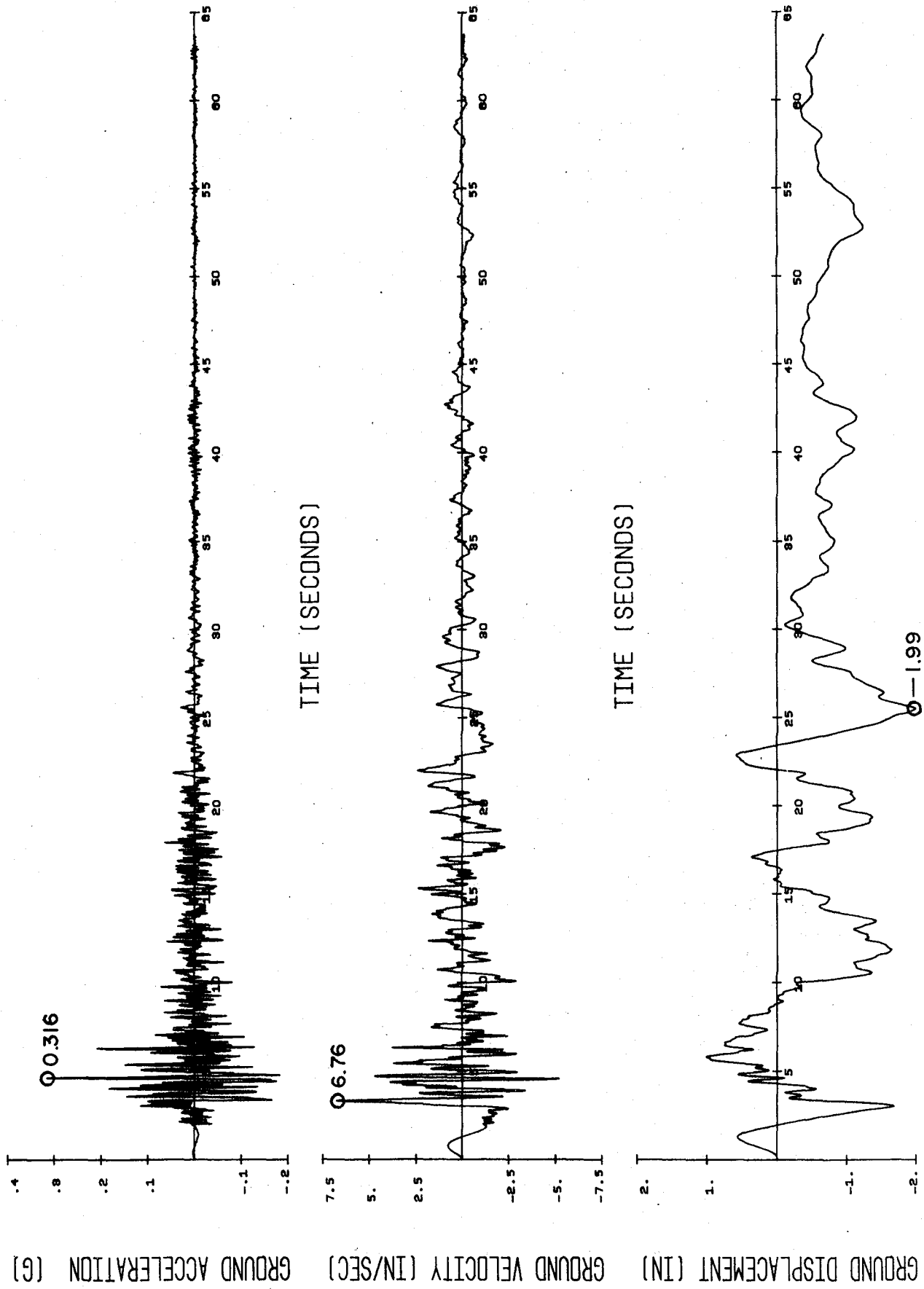
FIG. 3.6 GROUND MOTION FOR THE CASTAIC RECORD OF FEBRUARY 9, 1971. N21E COMPONENT.
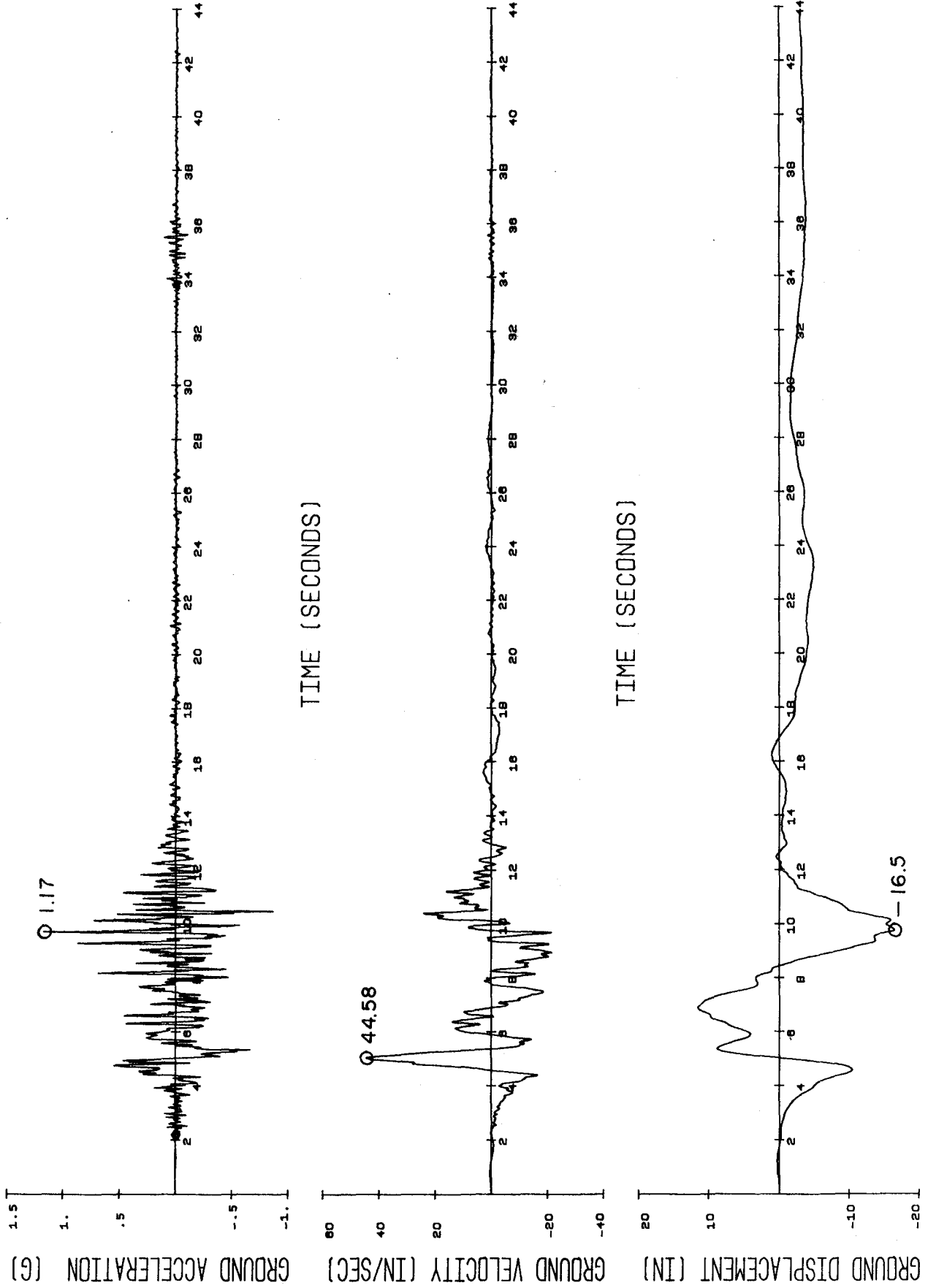
FIG. 3.7 GROUND MOTION FOR THE PACOIMA RECORD OF FEBRUARY 9, 1971. S16E COMPONENT.
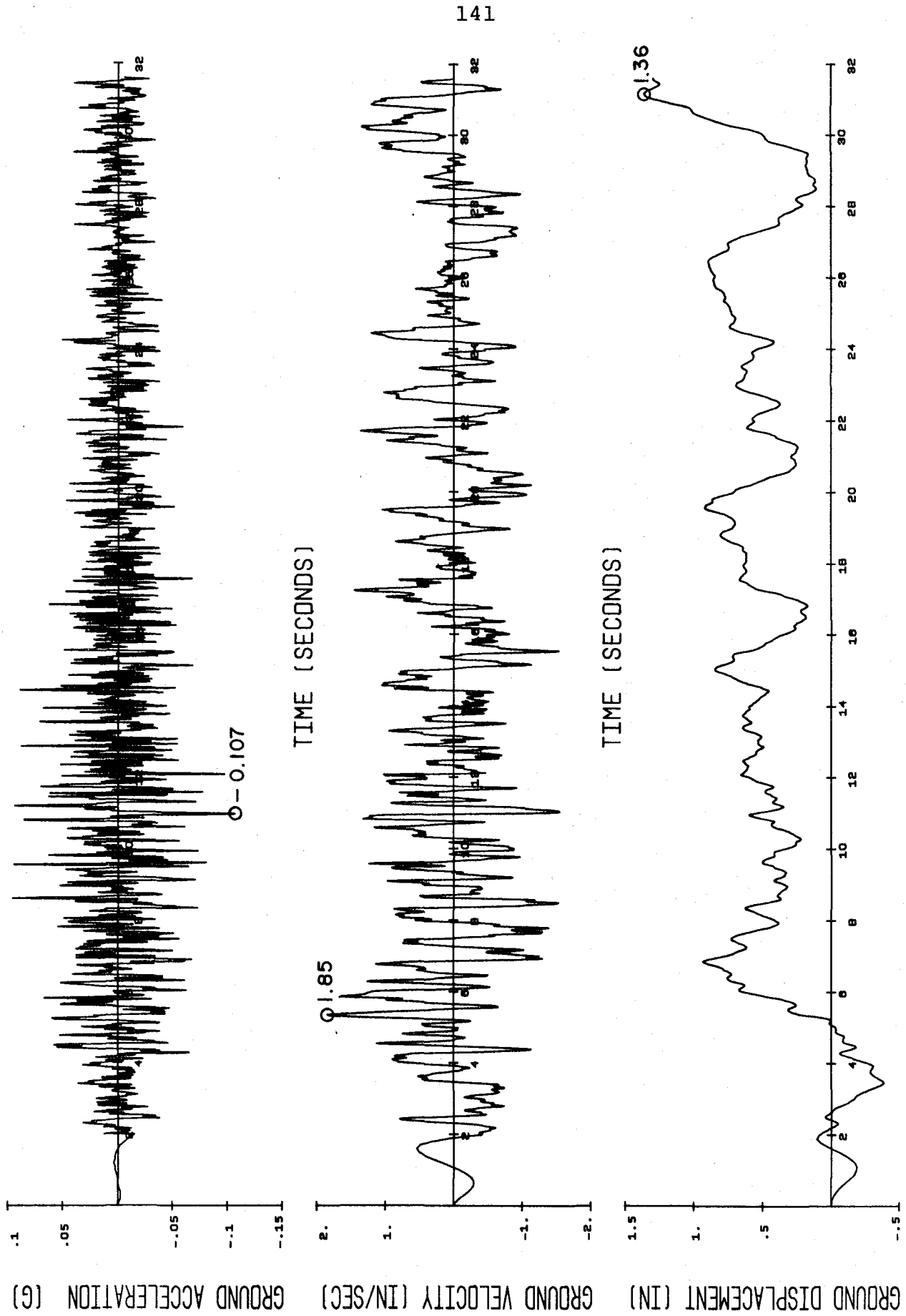
FIG. 3.8 GROUND MOTION FOR THE LIMA RECORD OF MAY 31, 1970. N82W COMPONENT.
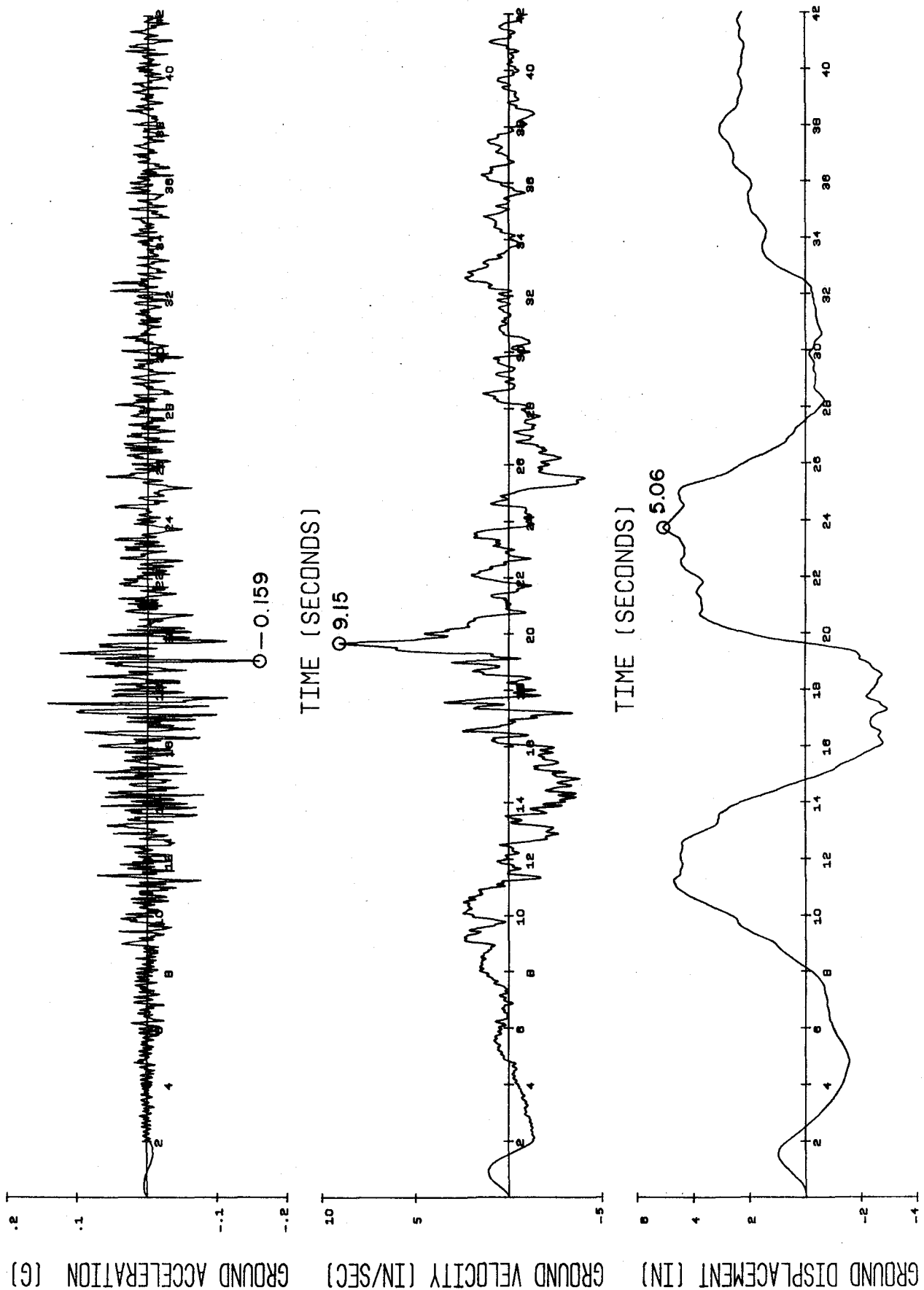
FIG. 3.9 GROUND MOTION FOR THE SANTIAGO RECORD OF JULY 8, 1971. N10W COMPONENT.
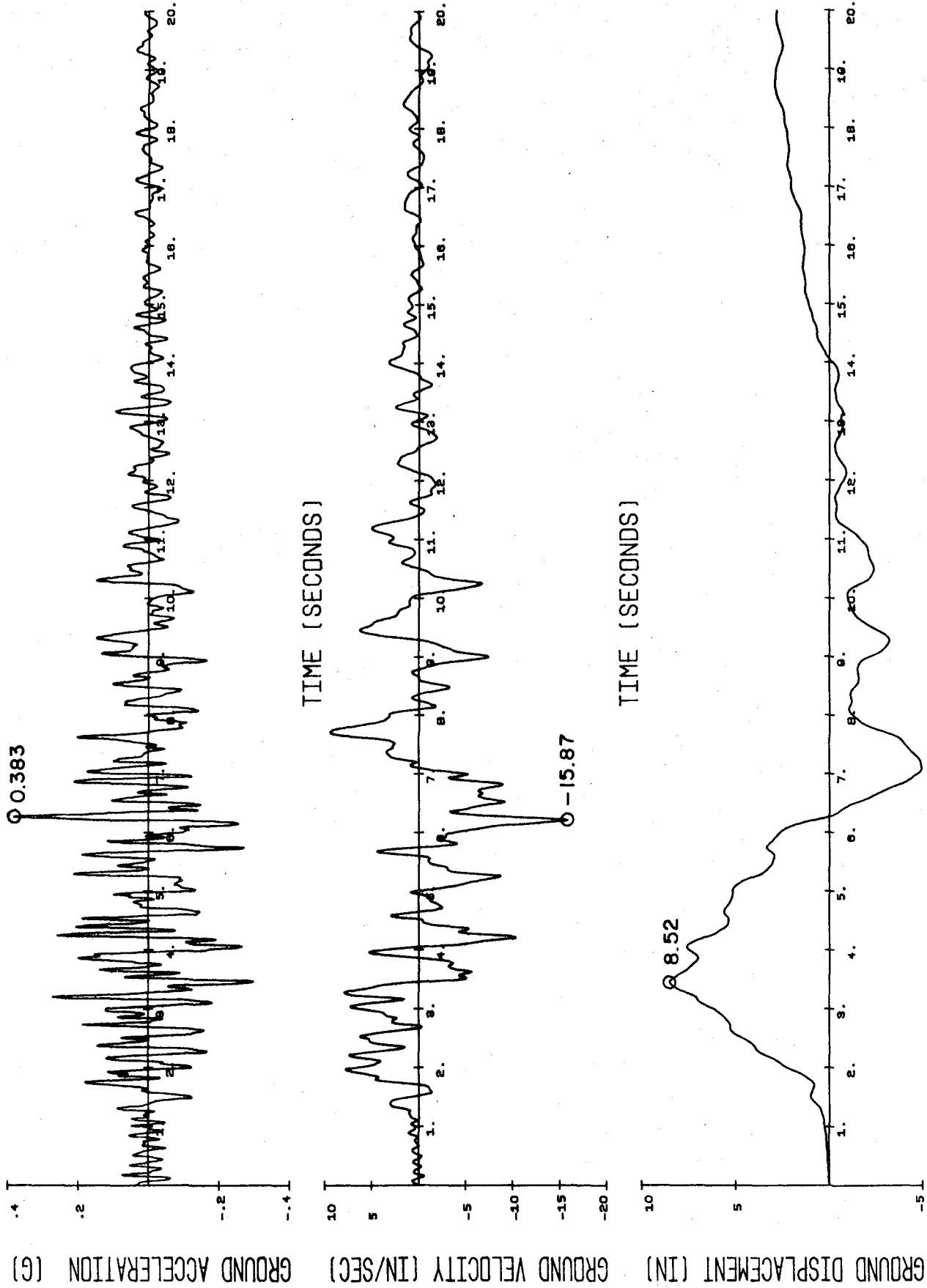
FIG. 3.10 GROUND MOTION FOR THE MANAGUA RECORD OF DECEMBER 23, 1972. E-W COMPONENT.
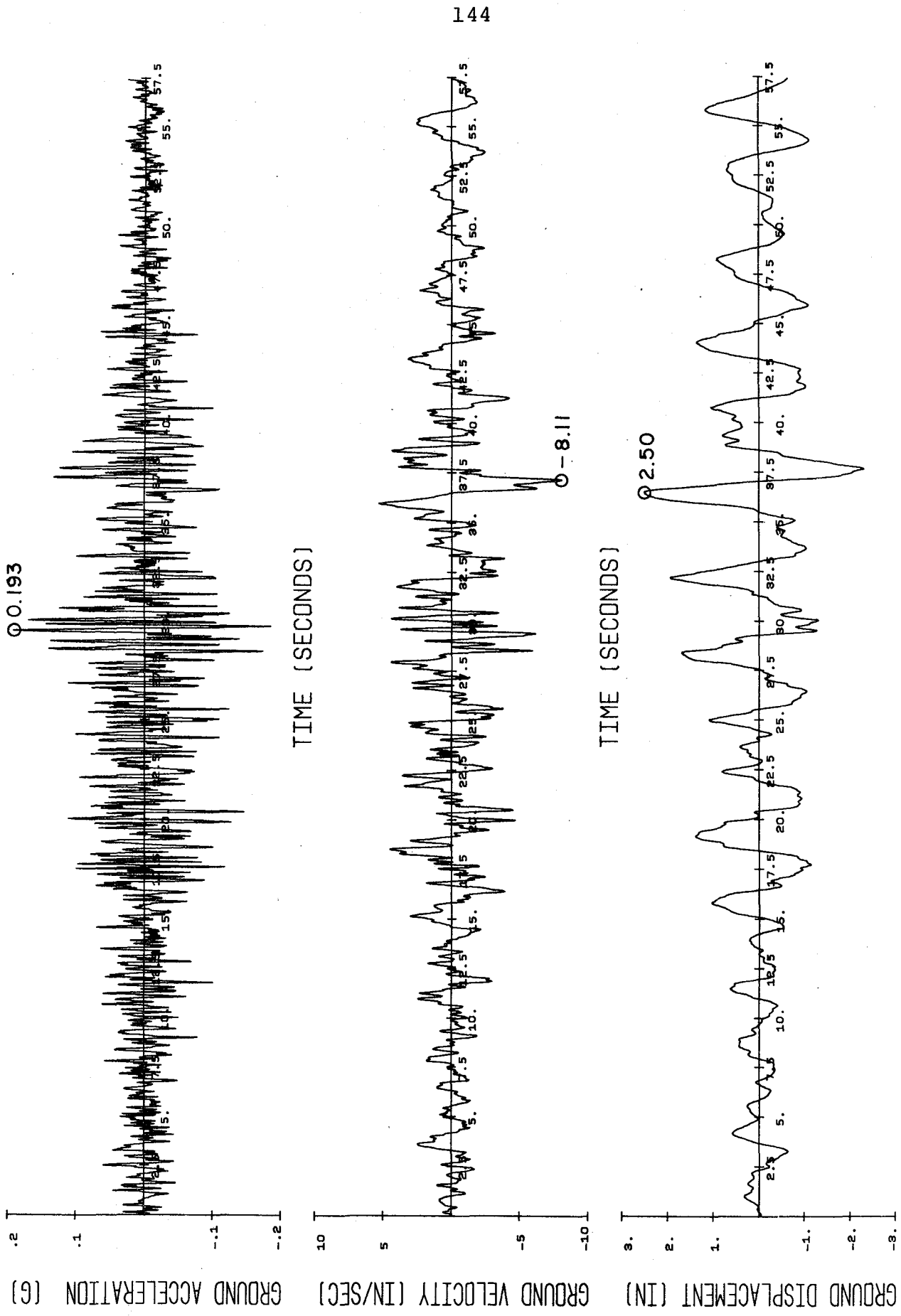
FIG. 3.11 GROUND MOTION FOR THE SAN JUAN RECORD OF NOVEMBER 23, 1977. E-W COMPONENT.
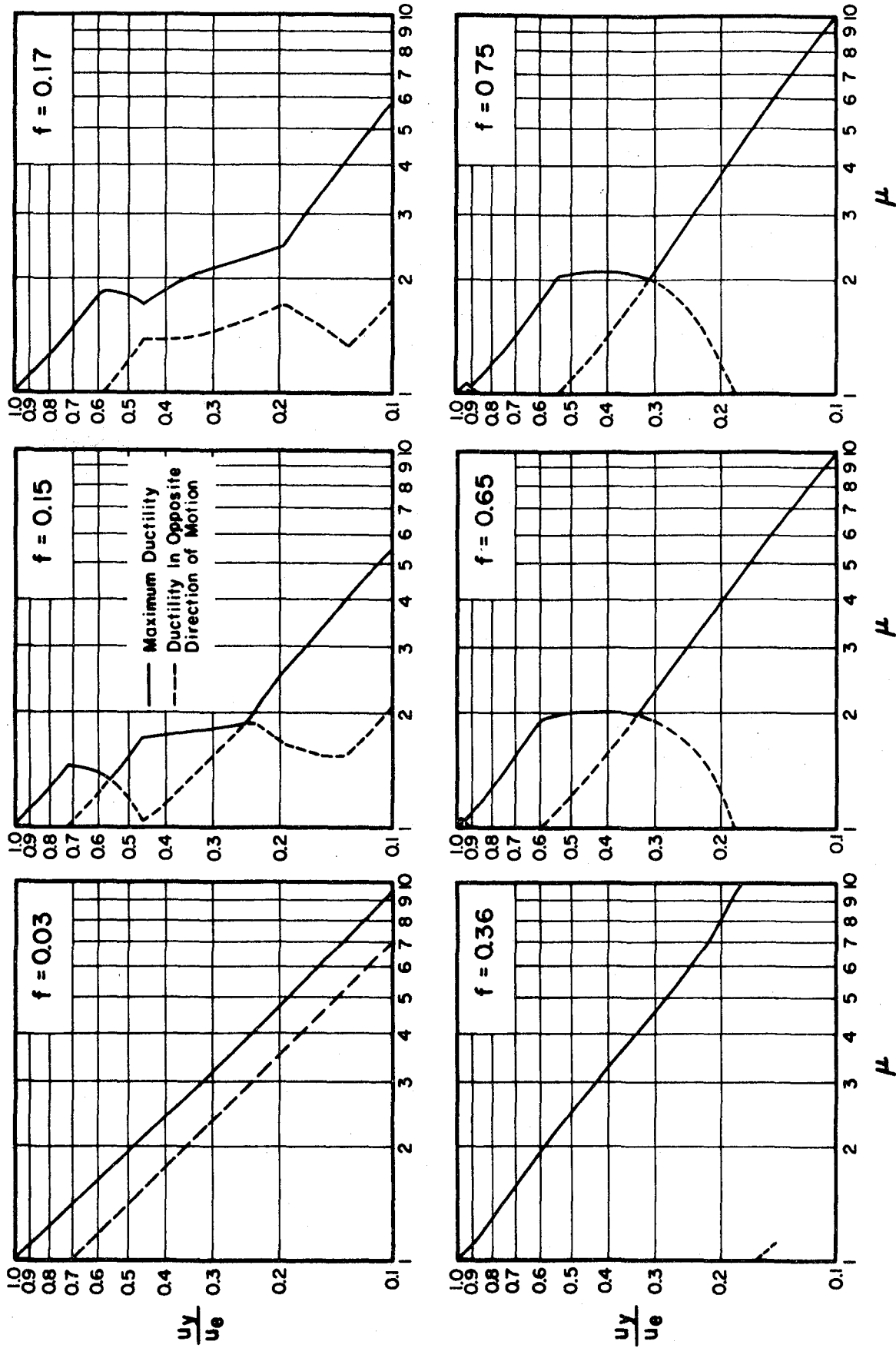
FIG. 3.12 DUCTILITY FACTOR VS. YIELD LEVEL CURVES FOR ELASTOPLASTIC SYSTEMS WITH 5% DAMPING SUBJECTED TO THE PACOIMA S16E RECORD. FREQUENCIES BETWEEN 0.03 AND 0.75 CPS.

146
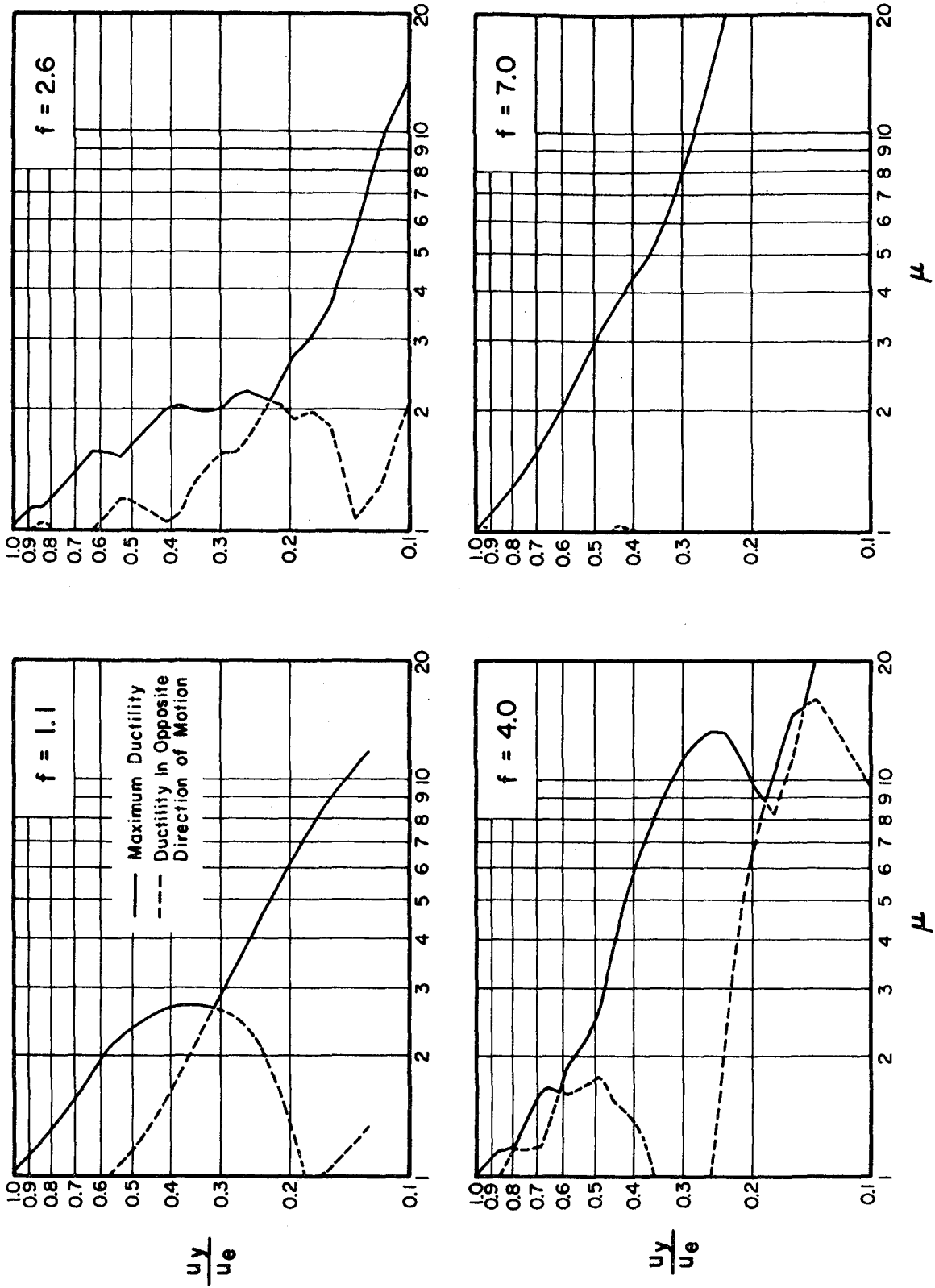
FIG. 3.13 DUCTILITY VS. YIELD LEVEL CURVES FOR ELASTOPLASTIC SYSTEMS WITH 5% DAMPING SUBJECTED TO THE PACOIMA S16E RECORD. FREQUENCIES BETWEEN 1.1 AND 7 CPS.

147
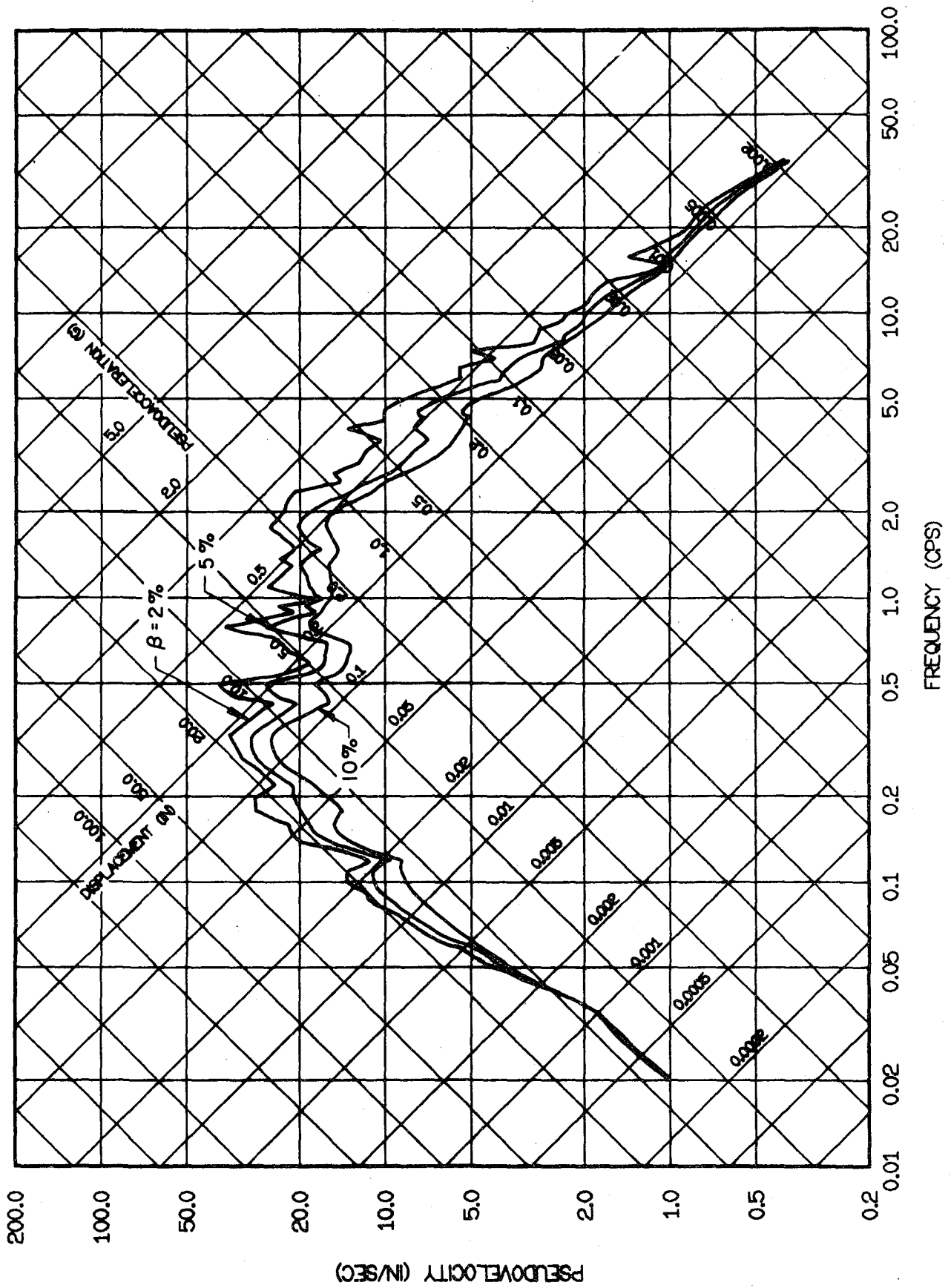
FIG. 3.14 ELASTIC RESPONSE SPECTRA FOR EL CENTRO, MAY 18, 1940. E-W COMPONENT.
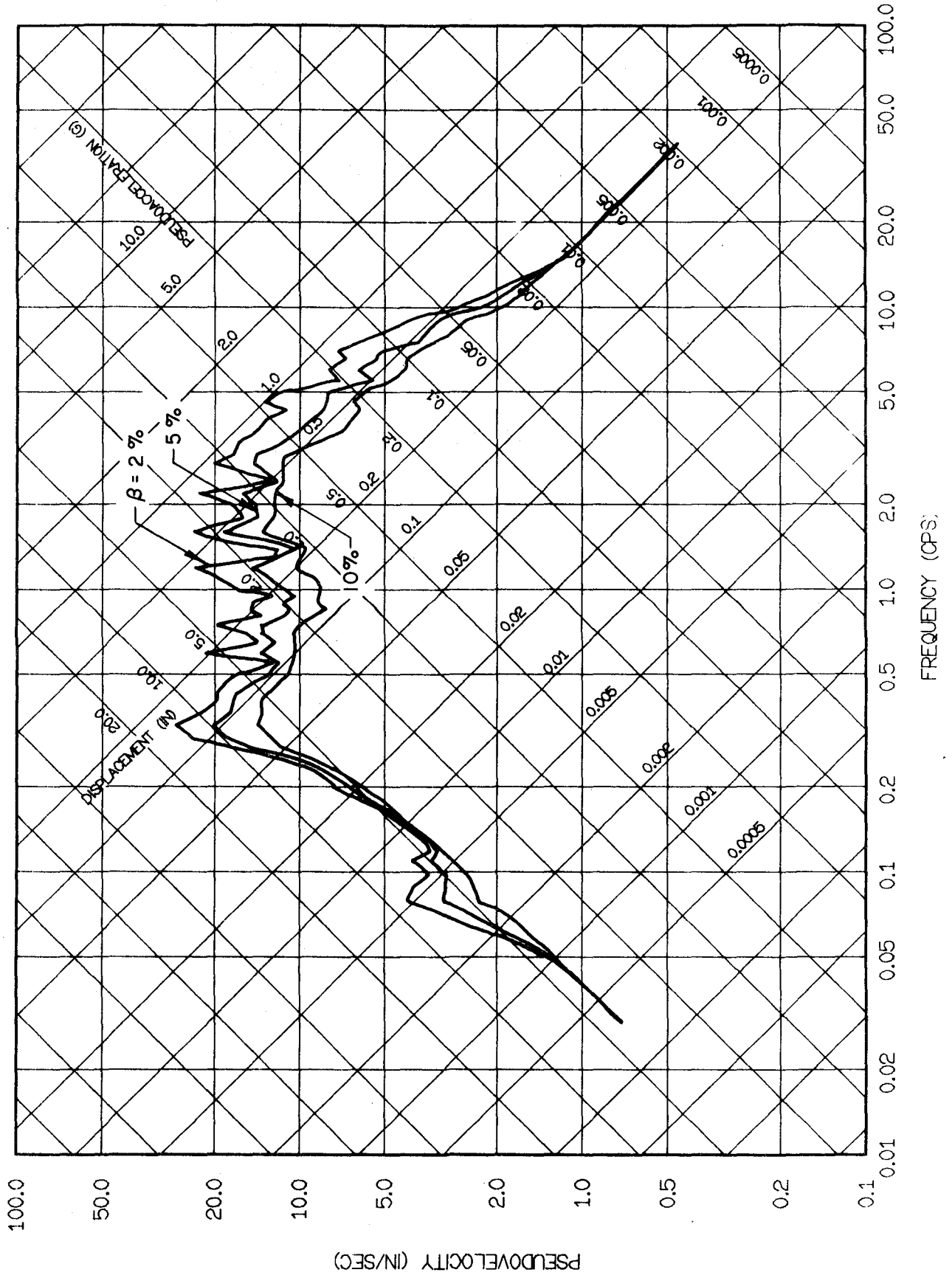
FIG. 3.15 ELASTIC RESPONSE SPECTRA FOR OLYMPIA, APRIL 13, 1949. N86E COMPONENT.
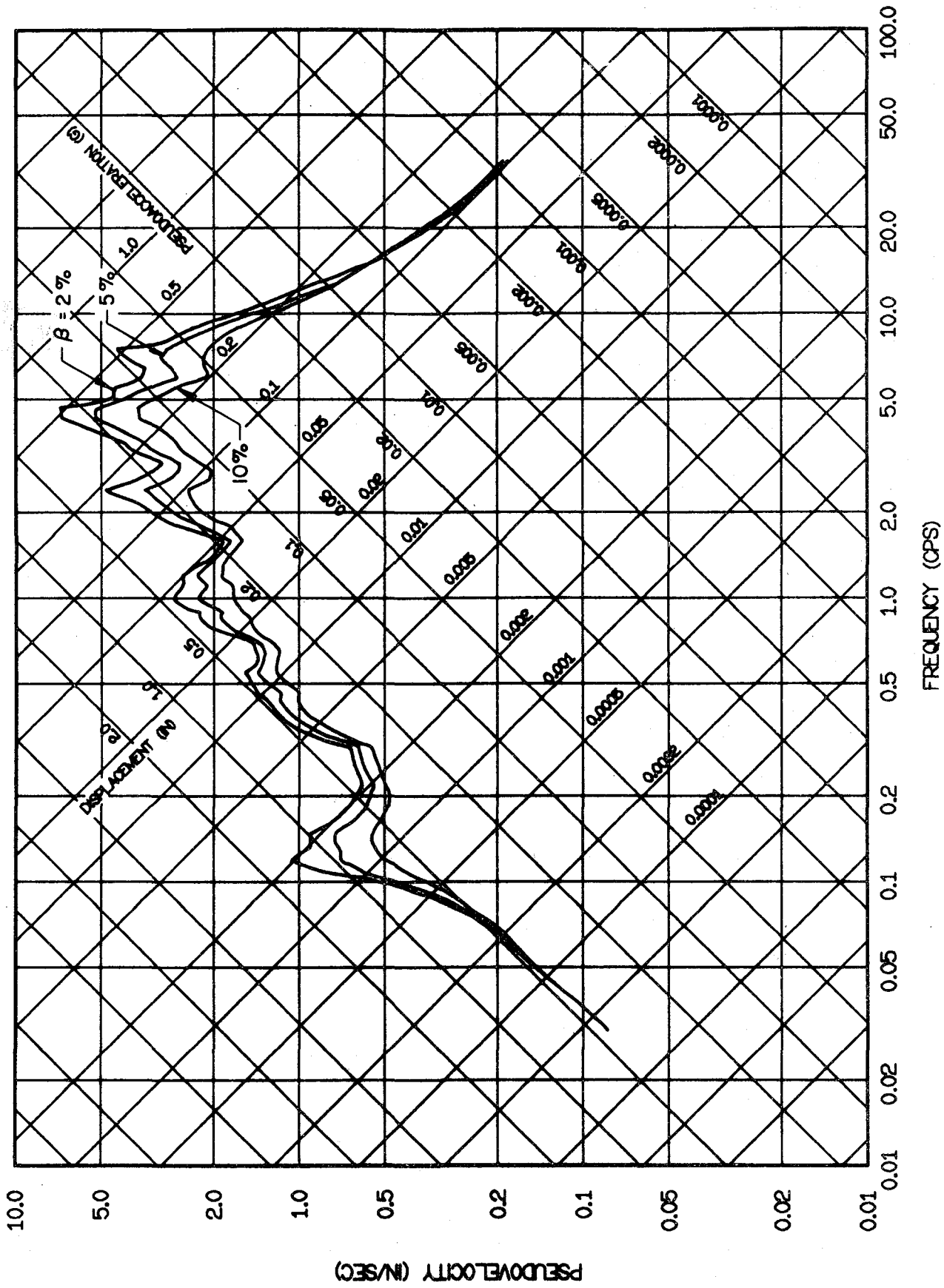
FIG. 3.16 ELASTIC RESPONSE SPECTRA FOR GOLDEN GATE PARK, MARCH 22, 1957. S80E COMPONENT.
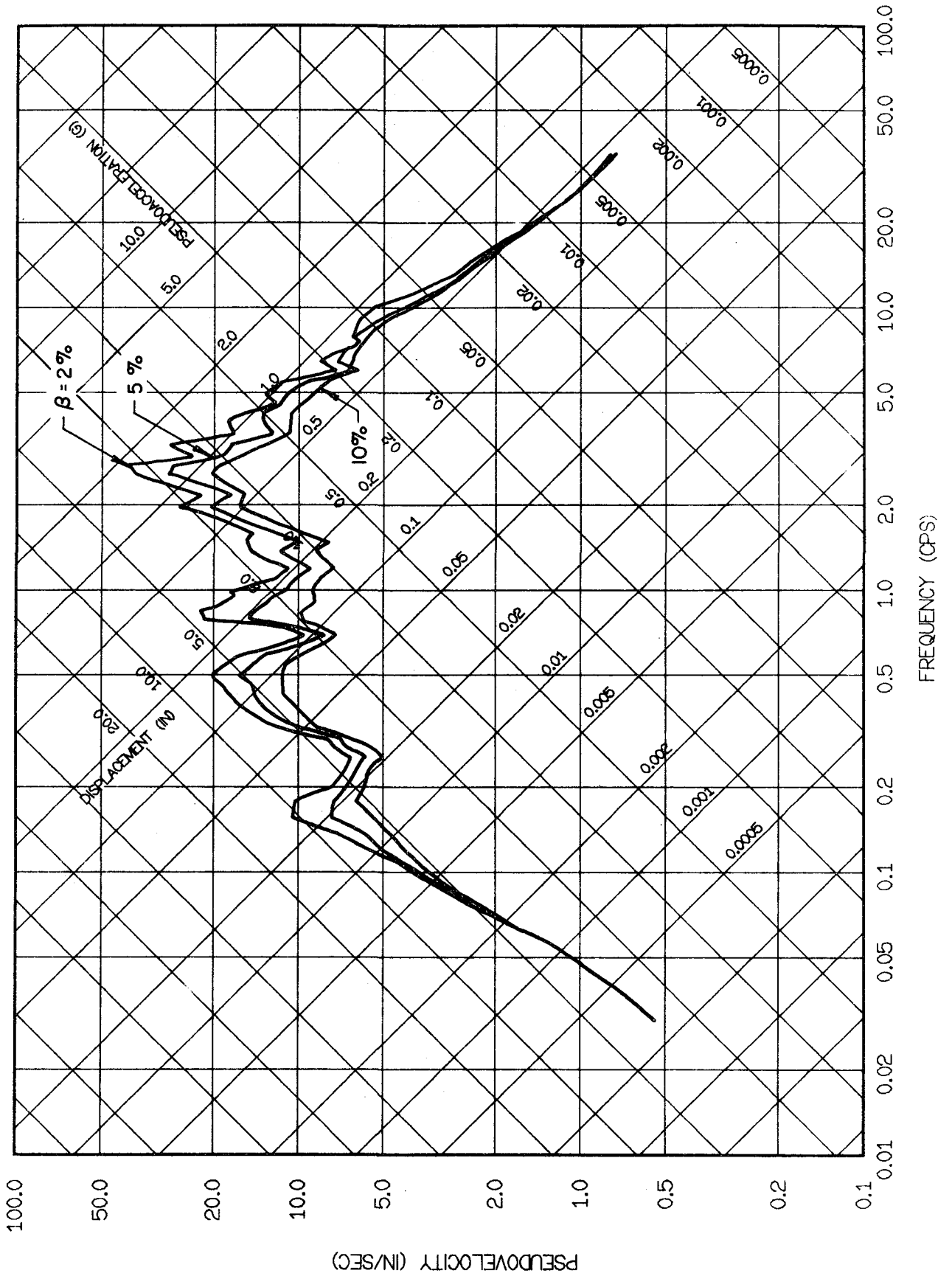
FIG. 3.17 ELASTIC RESPONSE SPECTRA FOR CHOLAME, STA. 5, JUNE 27, 1966. N85E COMPONENT.
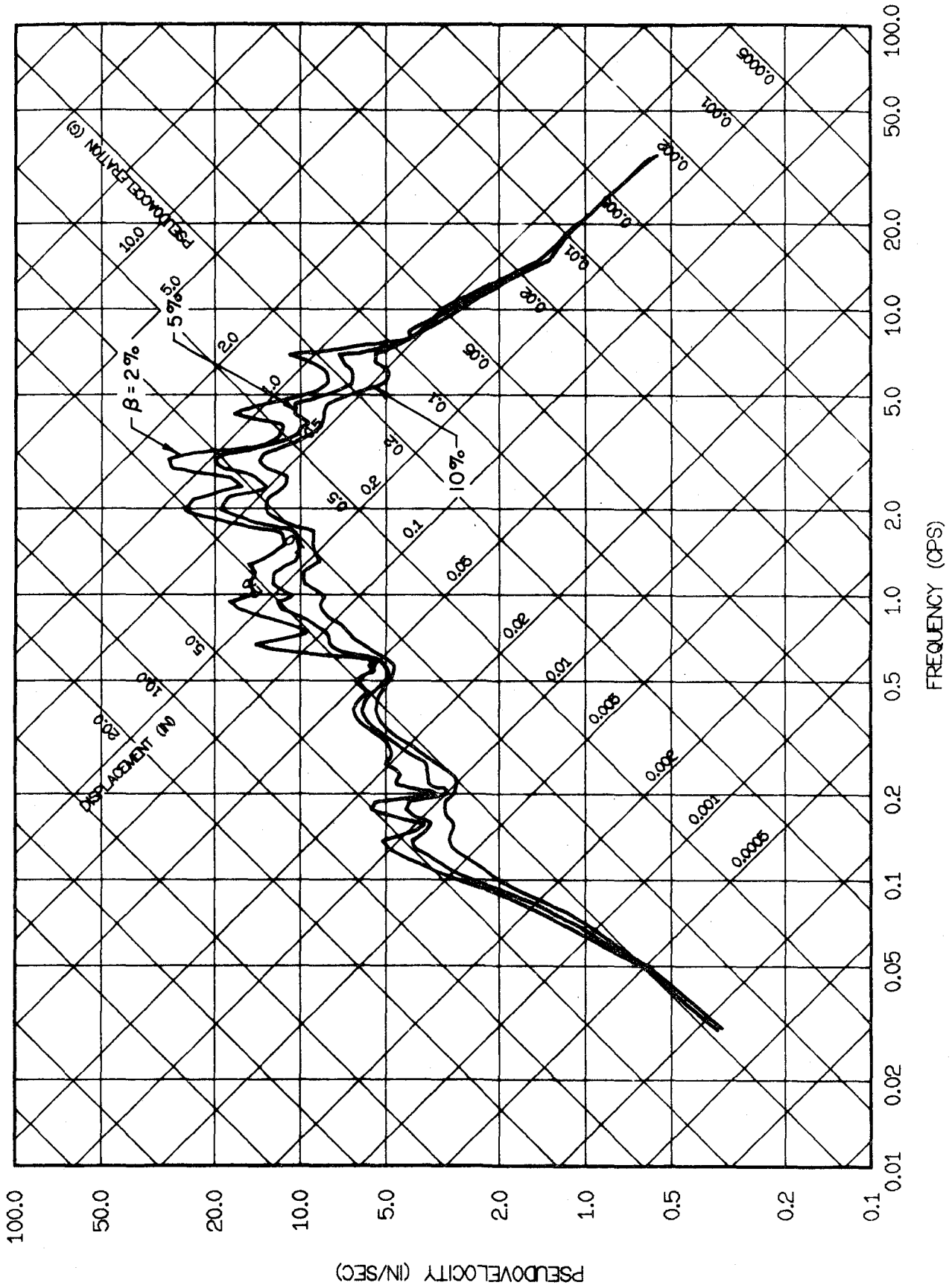
FIG. 3.18 ELASTIC RESPONSE SPECTRA FOR CASTAIC, FEBRUARY 9, 1971. N21E COMPONENT.
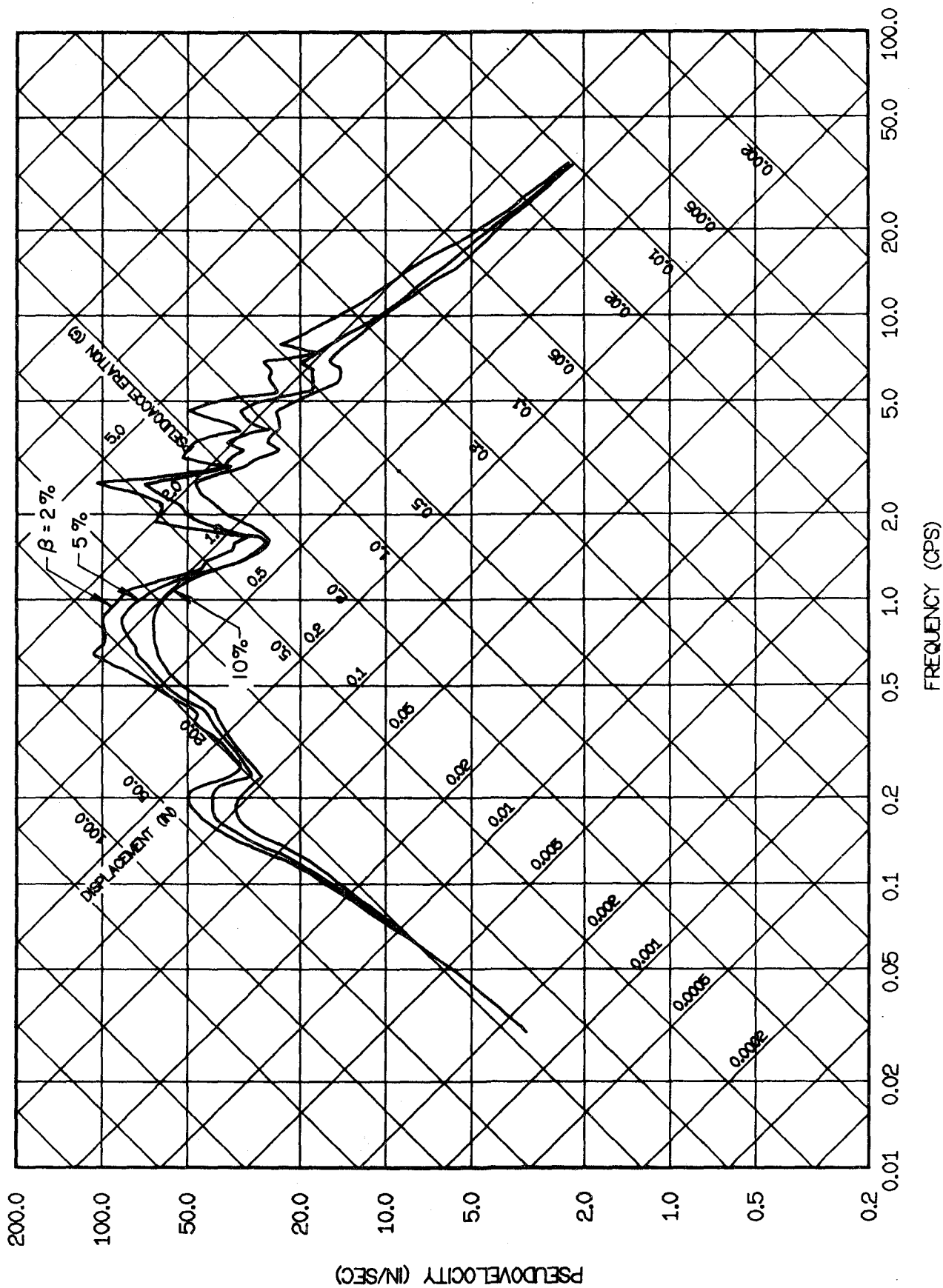
FIG. 3.19 ELASTIC RESPONSE SPECTRA FOR PACOIMA, FEBRUARY 9, 1971. S16E COMPONENT.
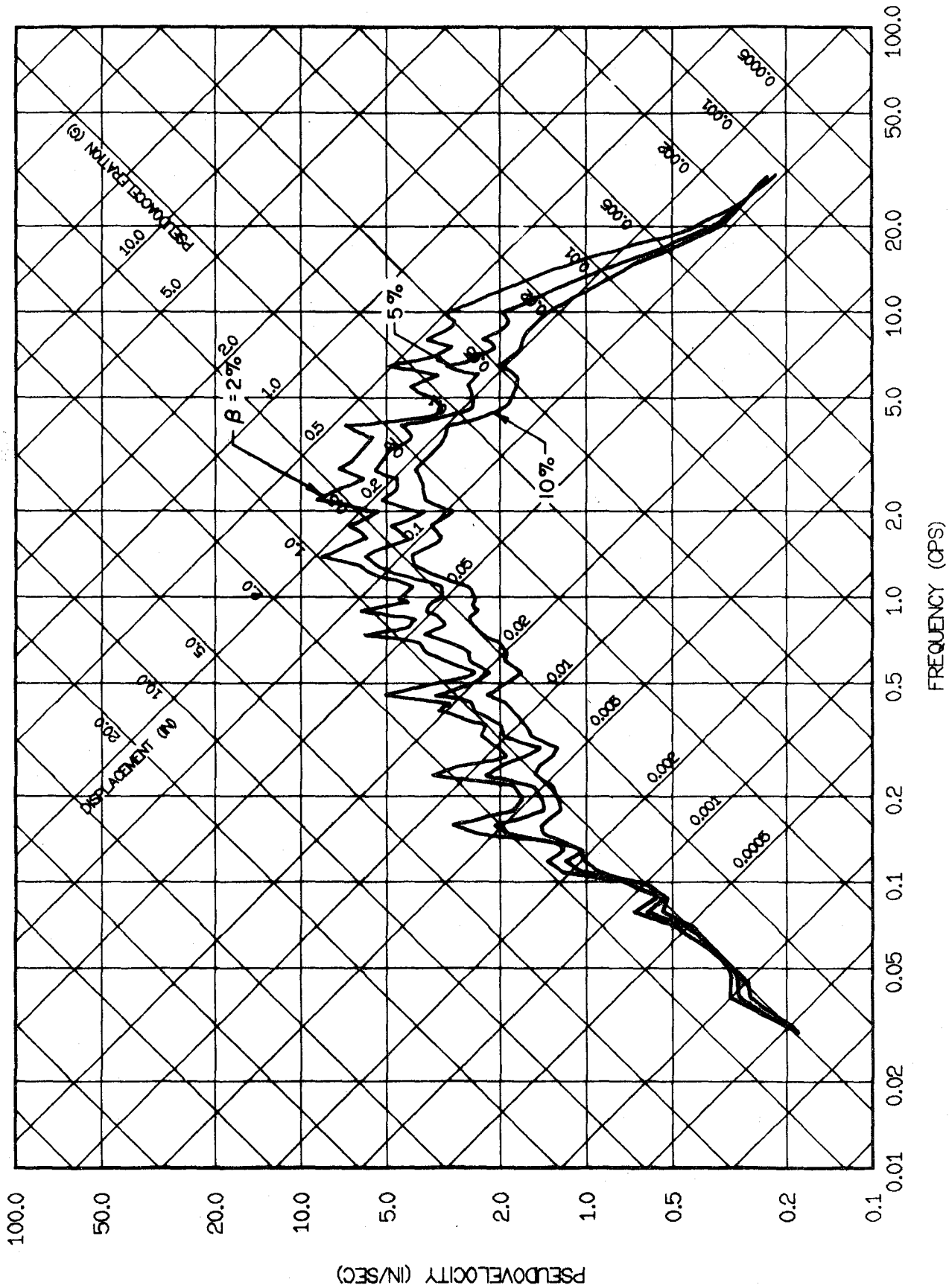
FIG. 3.20 ELASTIC RESPONSE SPECTRA FOR LIMA, MAY 31, 1970. N82W COMPONENT.
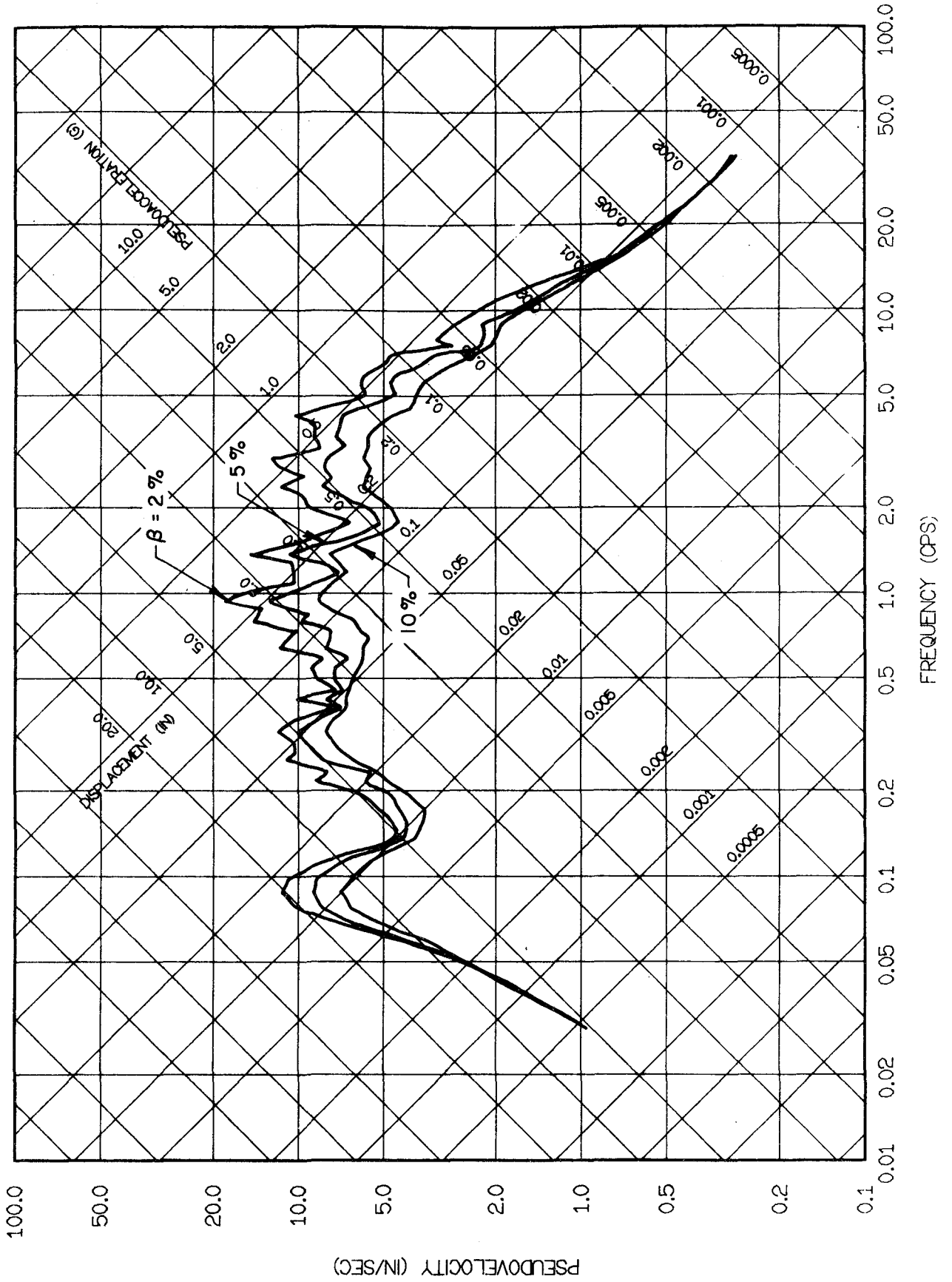
FIG. 3.21 ELASTIC RESPONSE SPECTRA FOR SANTIAGO, JULY 8, 1971. N10W COMPONENT.
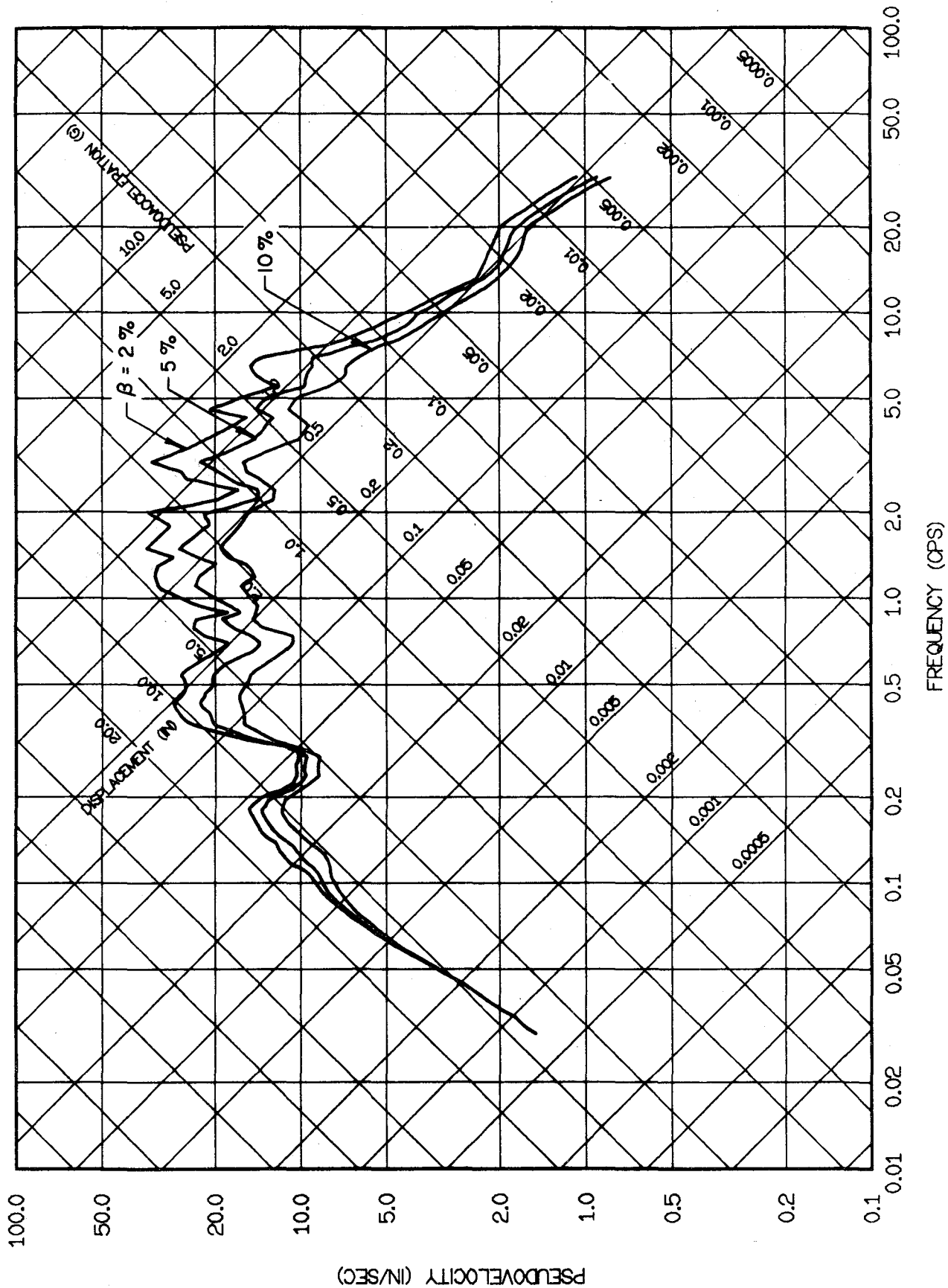
FIG. 3.22 ELASTIC RESPONSE SPECTRA FOR MANAGUA, DECEMBER 23, 1972. E-W COMPONENT.
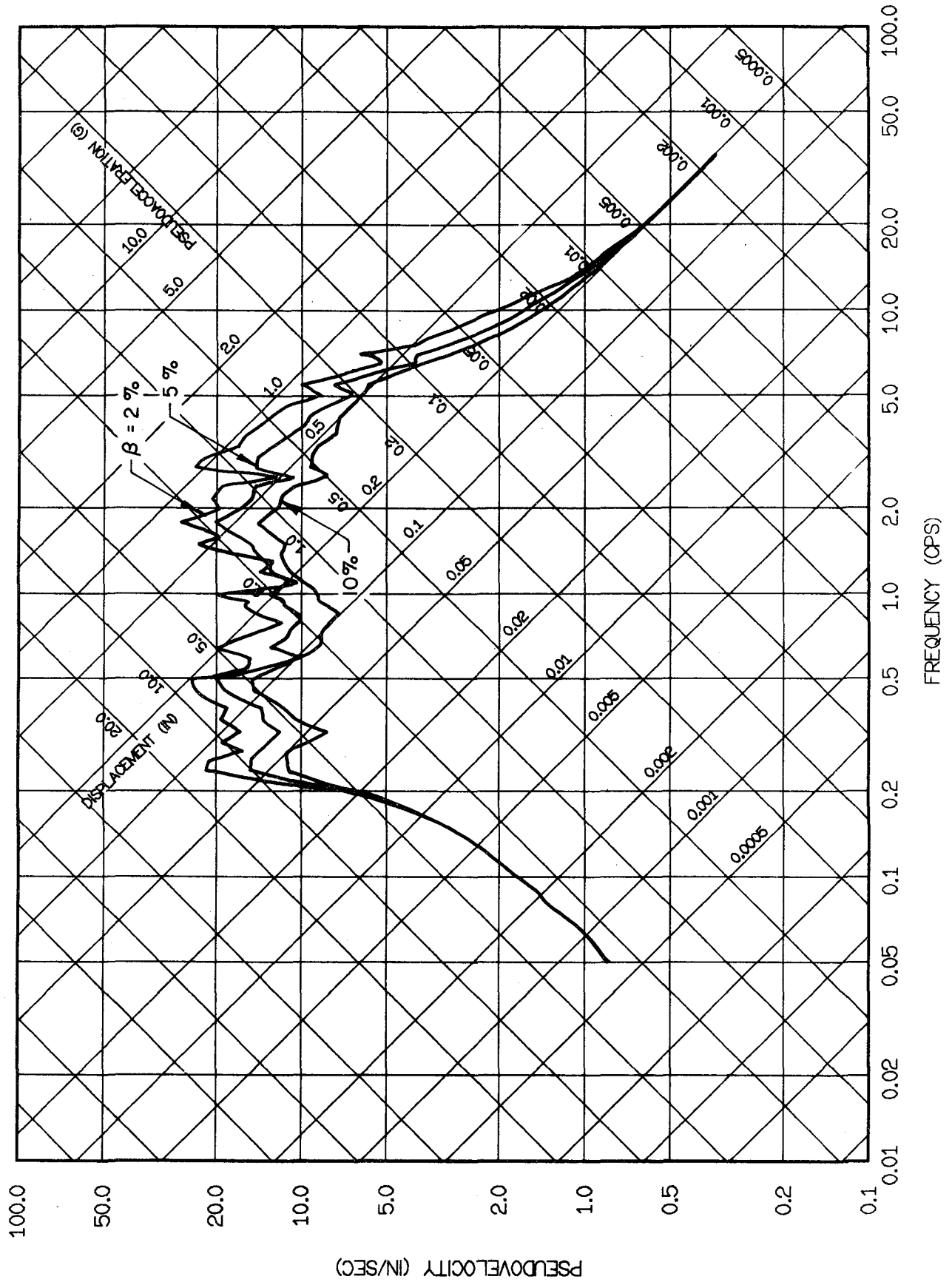
FIG. 3.23 ELASTIC RESPONSE SPECTRA FOR SAN JUAN, NOVEMBER 23, 1977. E–W COMPONENT.
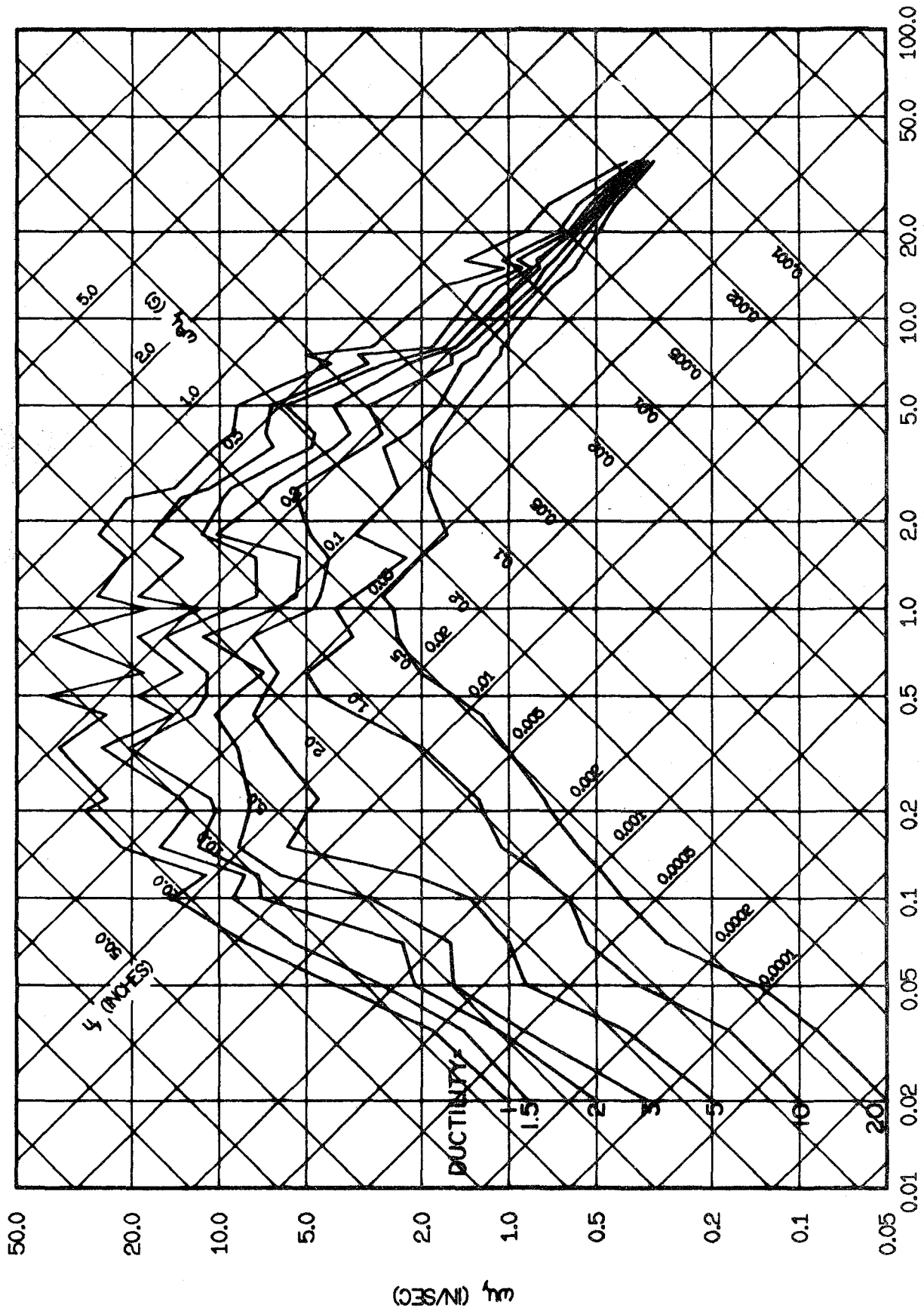
FIG. 3.24 INELASTIC YIELD SPECTRA FOR EL CENTRO, MAY 18, 1940, E-W. ELASTOPLASTIC SYSTEMS WITH 2% DAMPING.
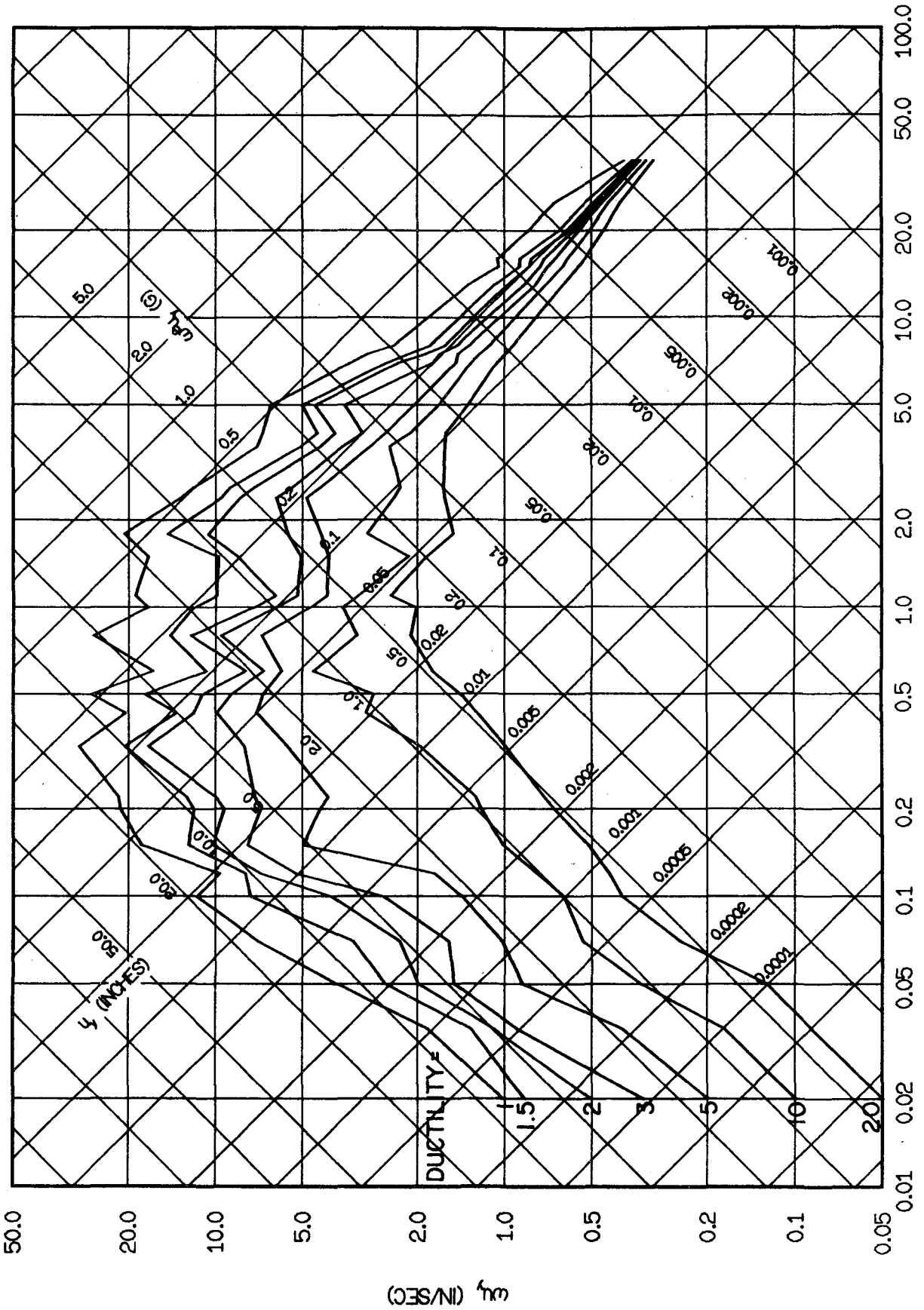
FIG. 3.25   INELASTIC YIELD SPECTRA FOR EL CENTRO, MAY 18, 1940, E-W.   ELASTOPLASTIC
SYSTEMS WITH 5% DAMPING.
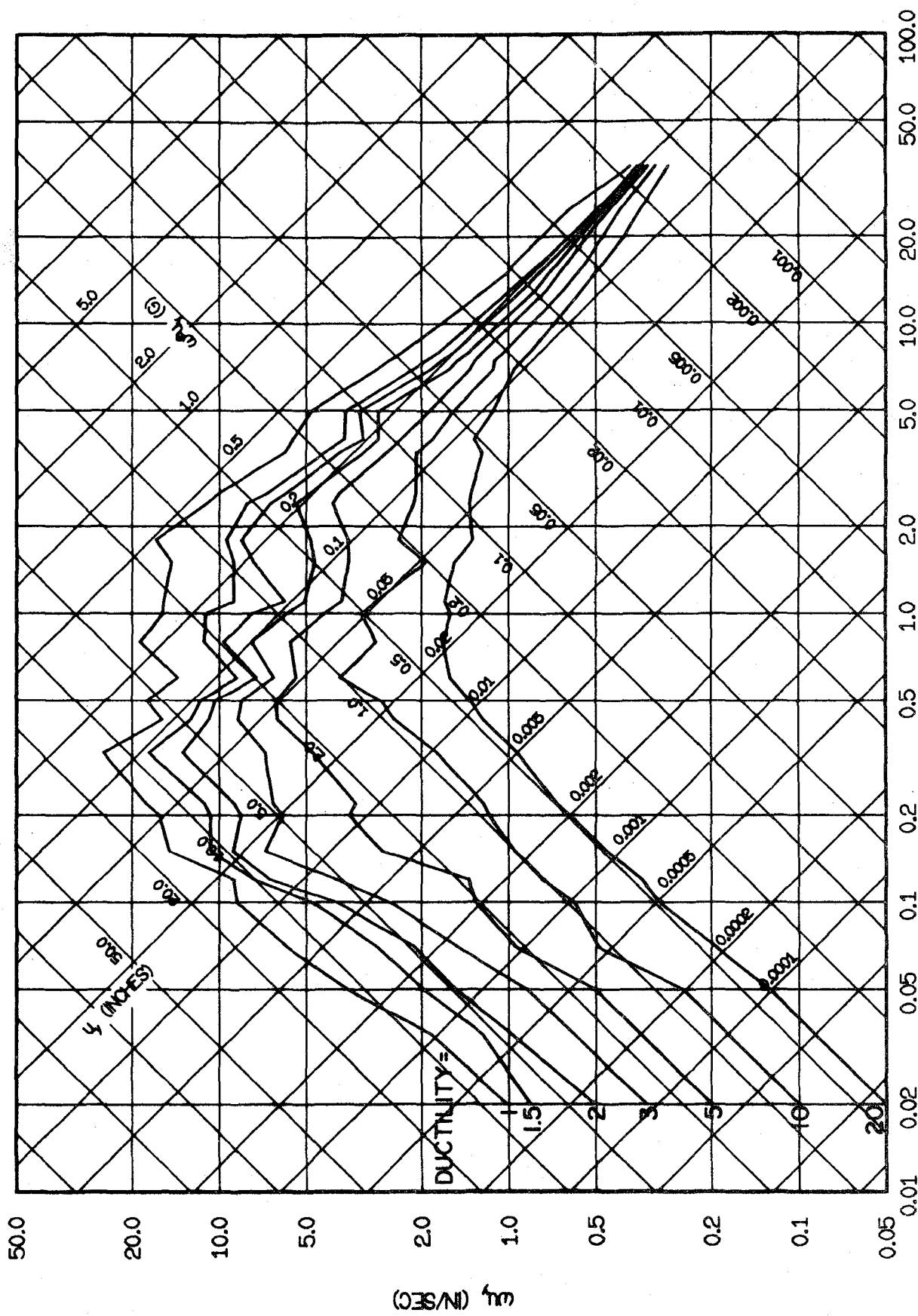
FIG. 3.26   INELASTIC YIELD SPECTRA FOR EL CENTRO, MAY 18, 1940, E-W.   ELASTOPLASTIC
SYSTEMS WITH 10% DAMPING.
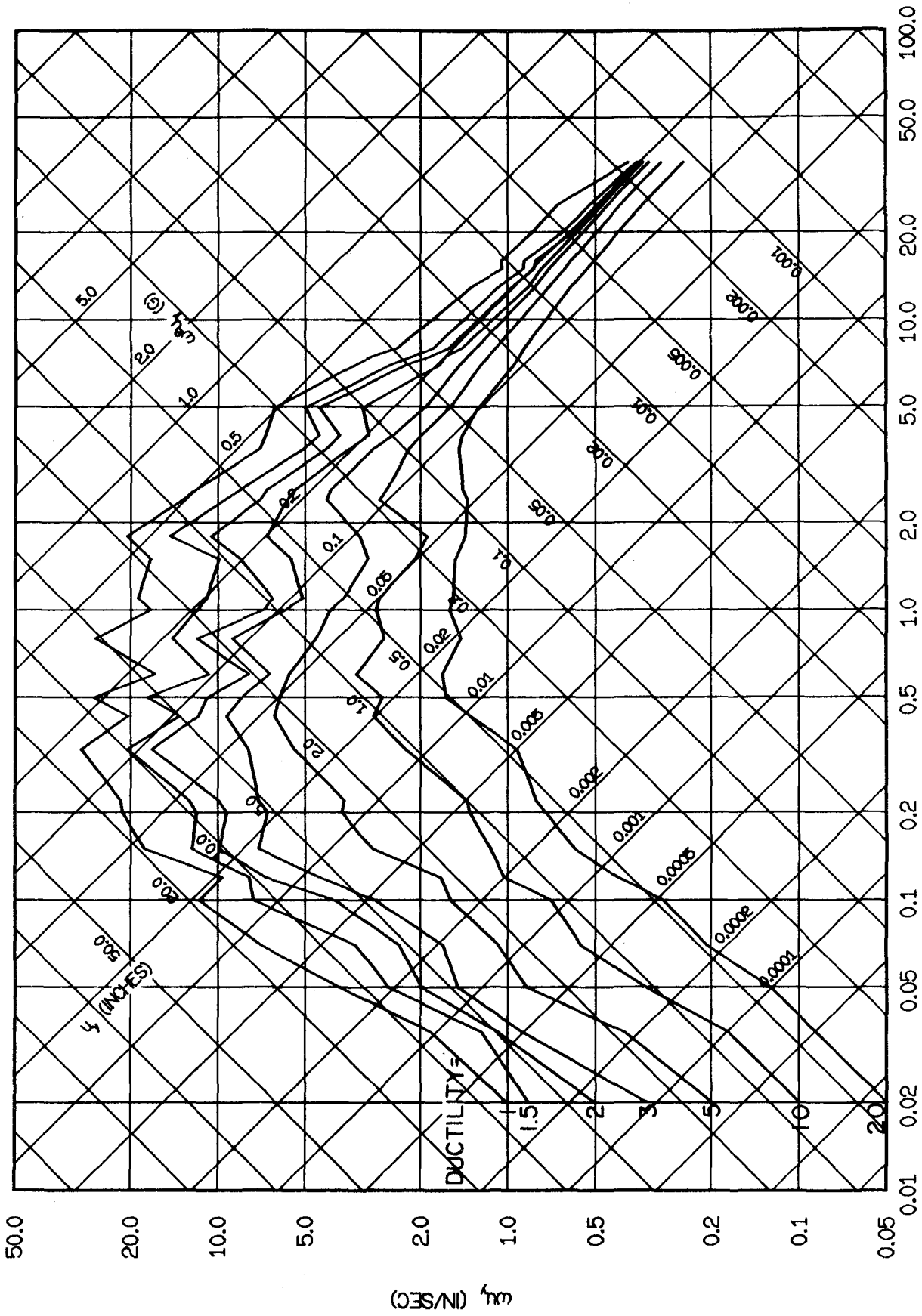
FIG. 3.27   INELASTIC YIELD SPECTRA FOR EL CENTRO, MAY 18, 1940, E-W.   BILINEAR
SYSTEMS WITH 5% DAMPING.

FREQUENCY (CPS)
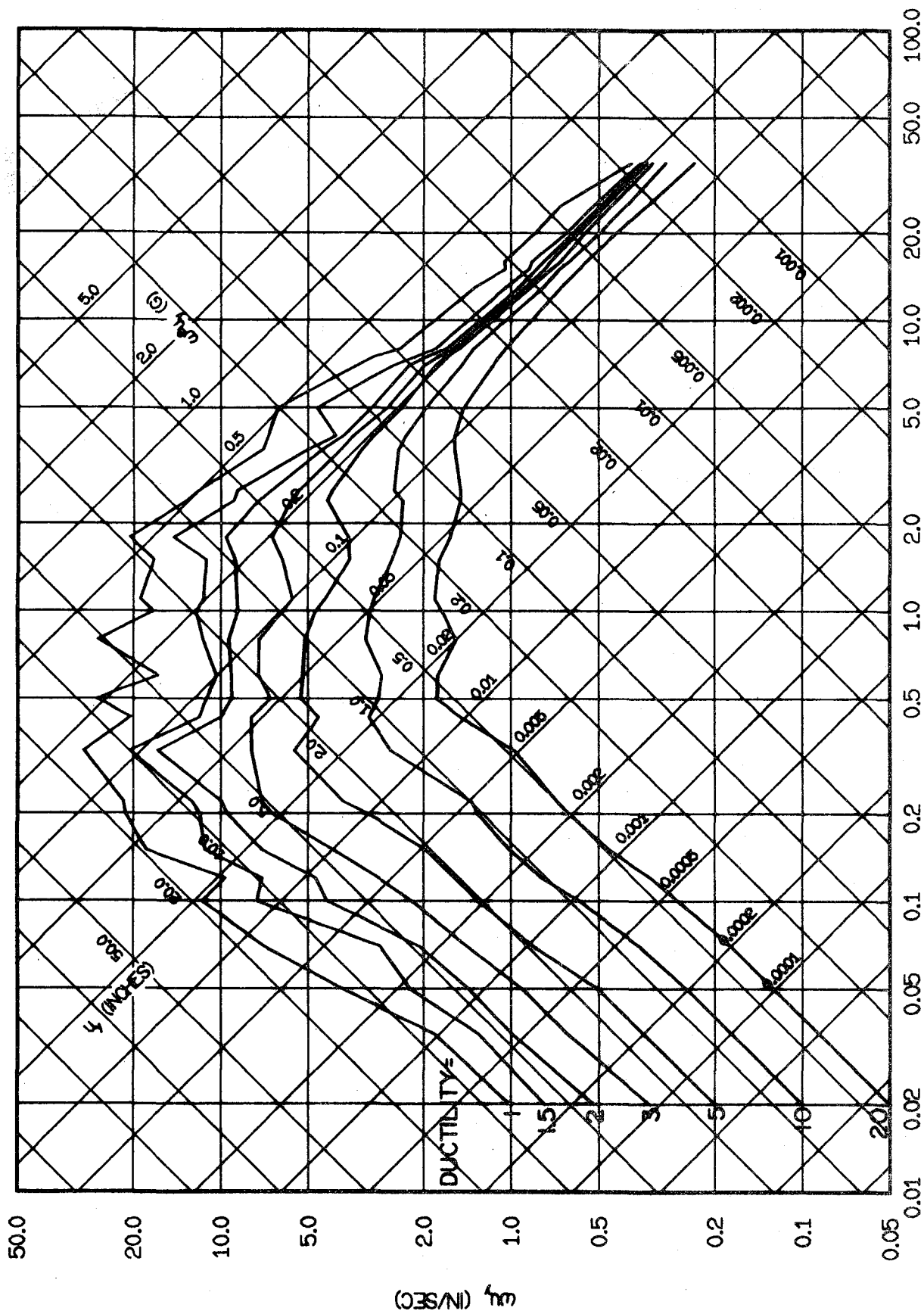
FIG. 3.28 INELASTIC YIELD SPECTRA FOR EL CENTRO, MAY 18, 1940, E-W. DEGRADING
SYSTEMS WITH 5% DAMPING.
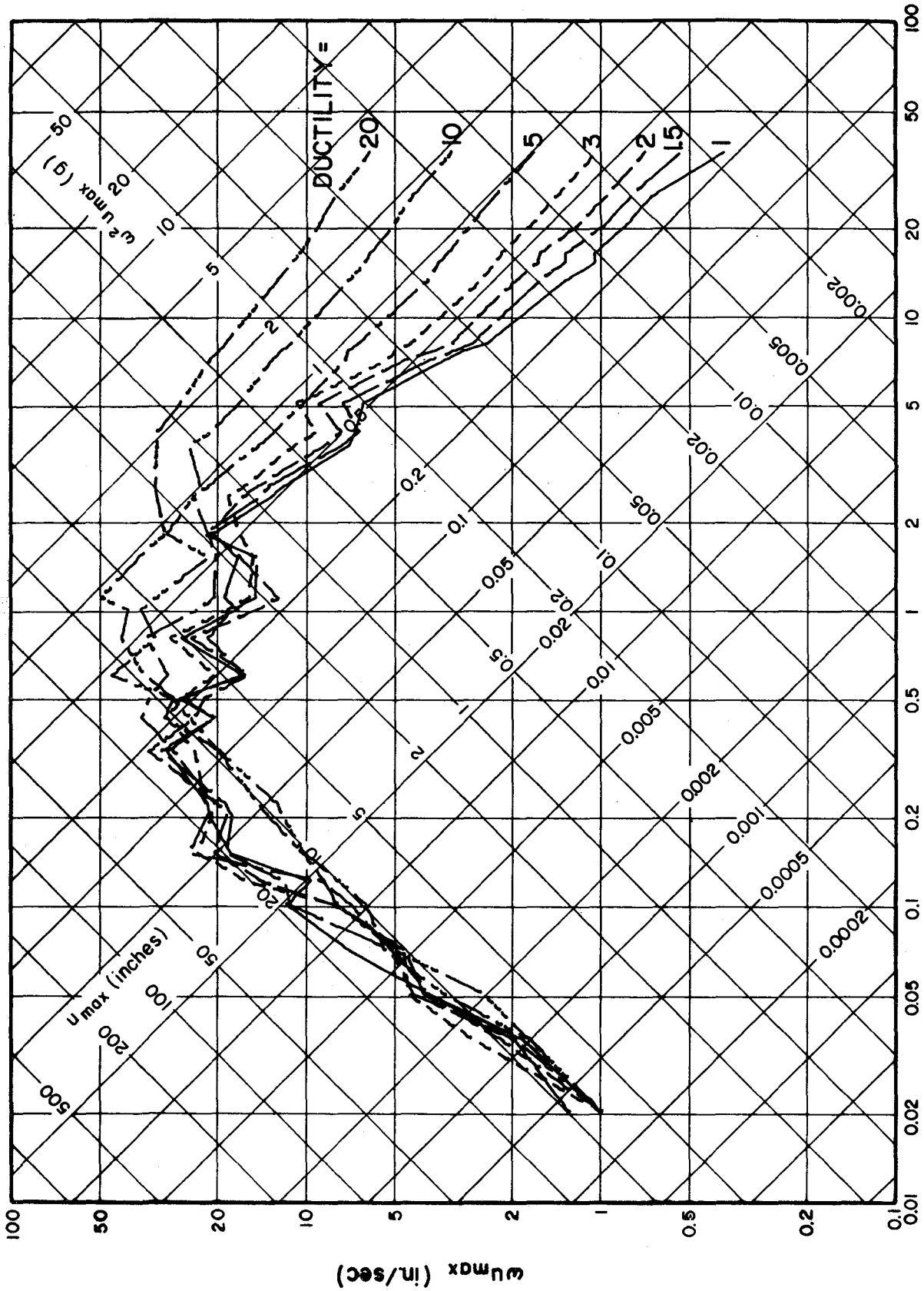
FIG. 3.29 TOTAL DEFORMATION SPECTRA FOR EL CENTRO, MAY 18, 1940, E-W. ELASTOPLASTIC SYSTEMS WITH 5% DAMPING.

FIG. 3.30   INELASTIC ACCELERATION SPECTRA FOR EL CENTRO, MAY 18, 1940, E-W.   BILINEAR
           SYSTEMS WITH 5% DAMPING.
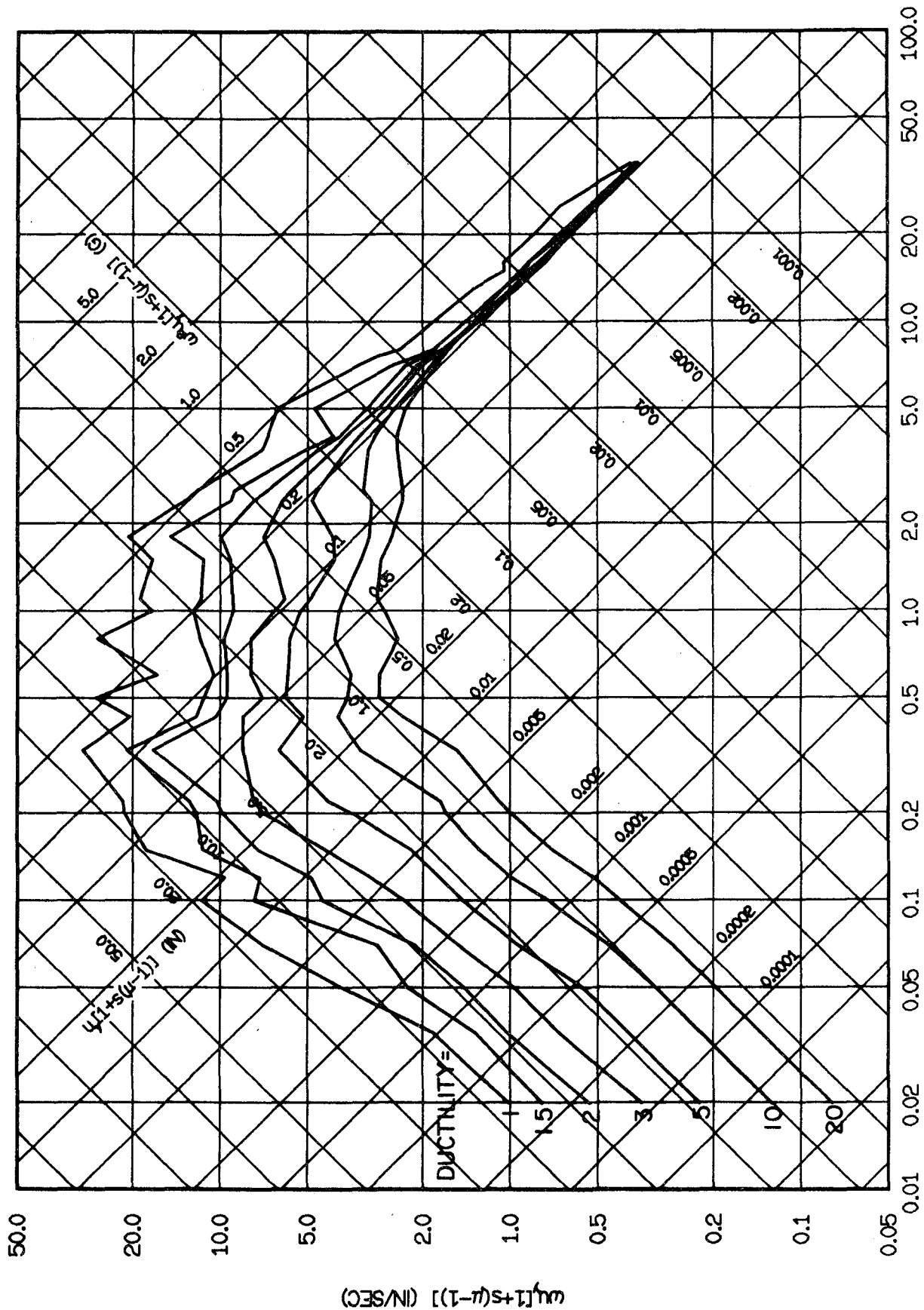
FIG. 3.31 INELASTIC ACCELERATION SPECTRA FOR EL CENTRO, MAY 18, 1940, E-W. DEGRADING SYSTEMS WITH 5% DAMPING.
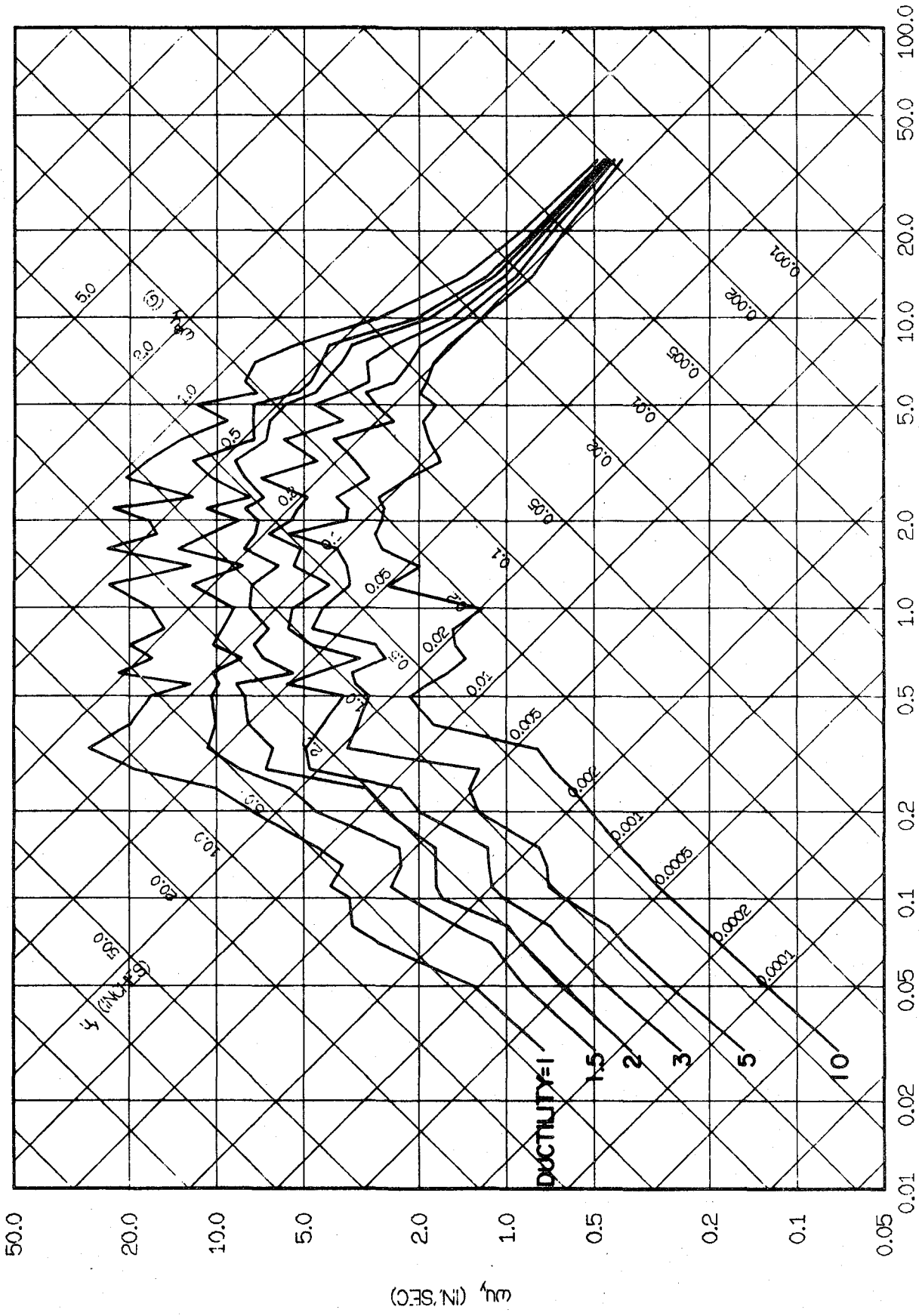
FIG. 3.32   INELASTIC YIELD SPECTRA FOR OLYMPIA, APRIL 13, 1949, N86E.   ELASTOPLASTIC
SYSTEMS WITH 2% DAMPING.

166
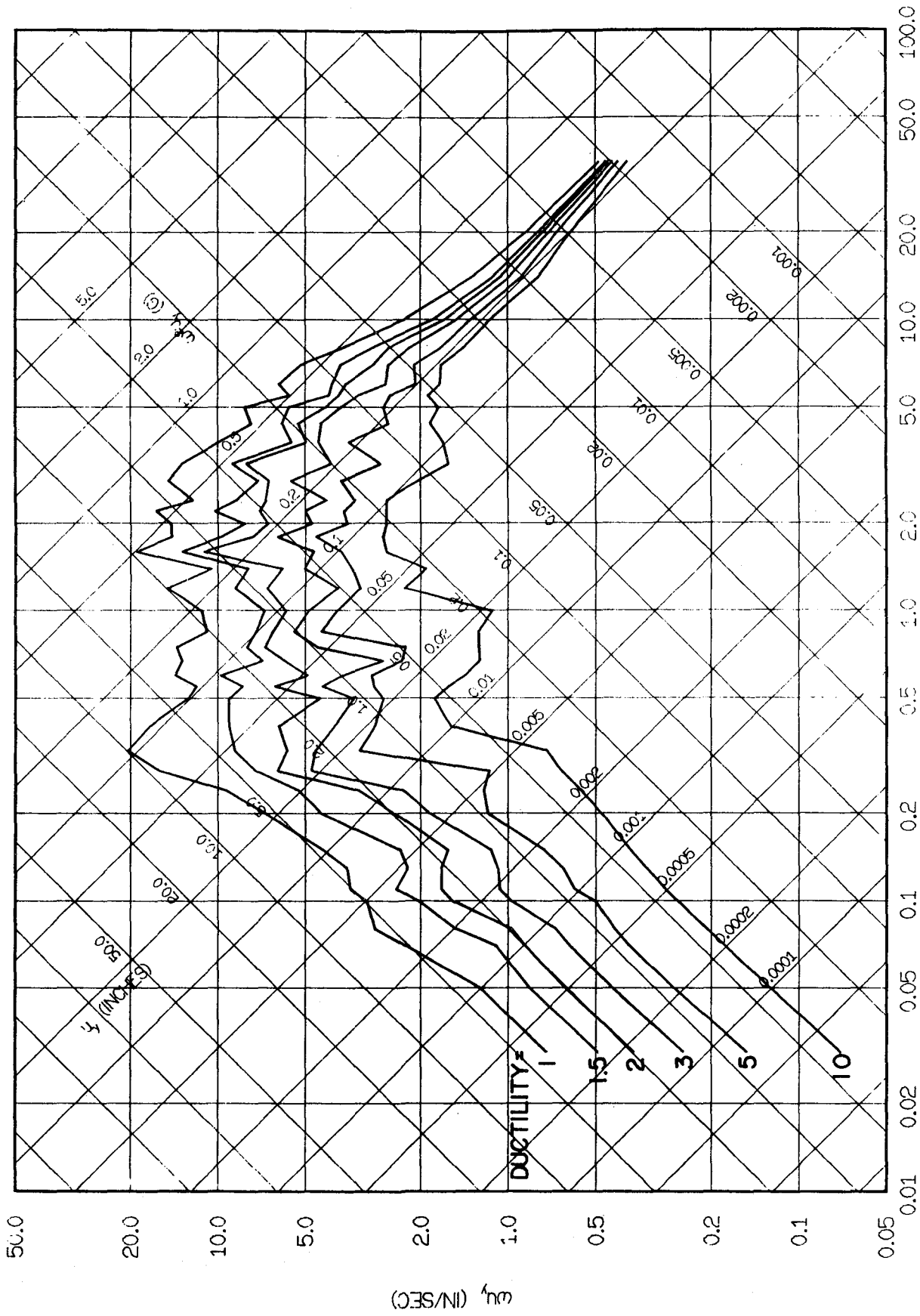
FIG. 3.33   INELASTIC YIELD SPECTRA FOR OLYMPIA, APRIL 13, 1949, N86E.   ELASTOPLASTIC SYSTEMS WITH 5% DAMPING.
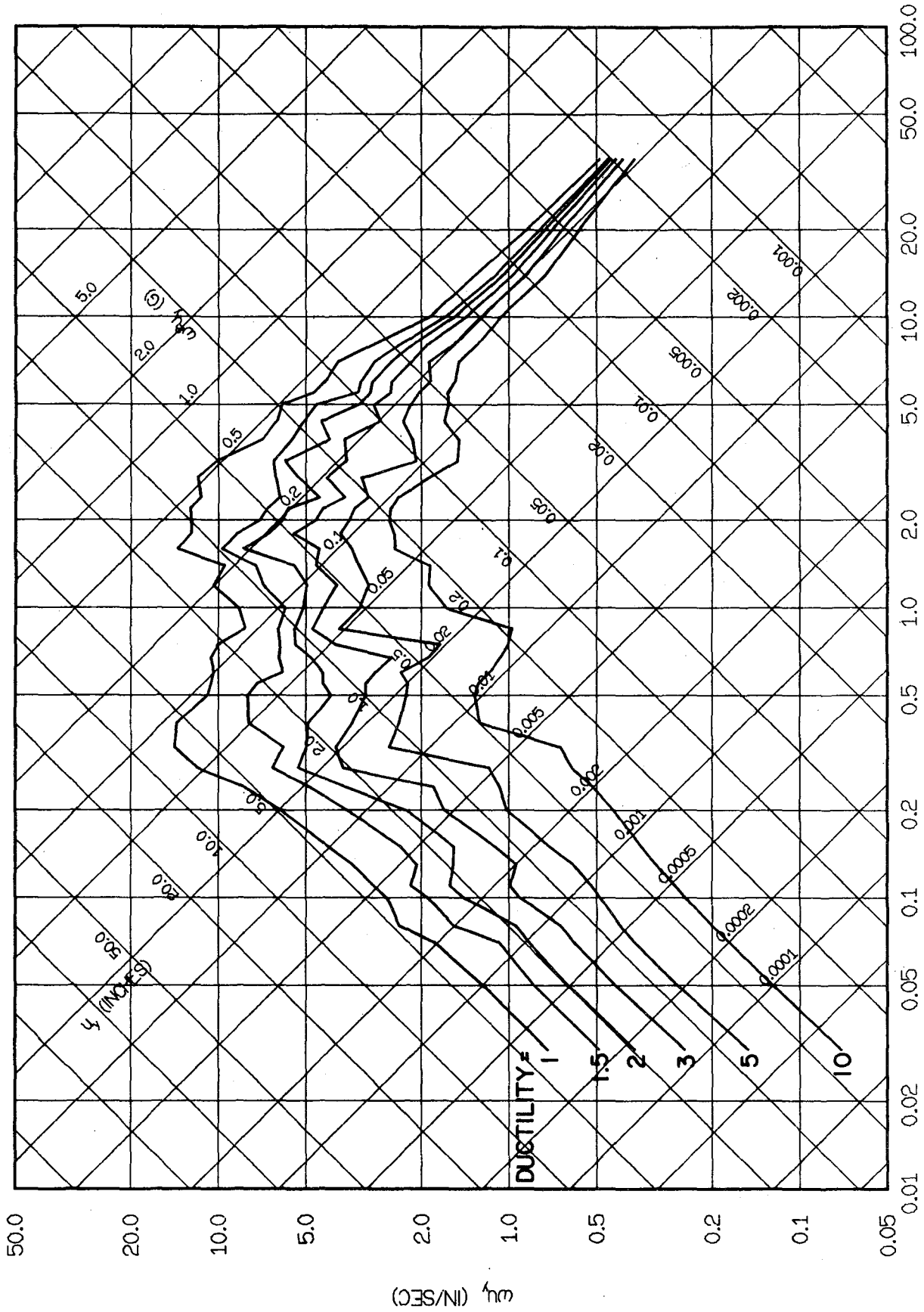
FIG. 3.34   INELASTIC YIELD SPECTRA FOR OLYMPIA, APRIL 13, 1949, N86E.   ELASTOPLASTIC SYSTEMS WITH 10% DAMPING.
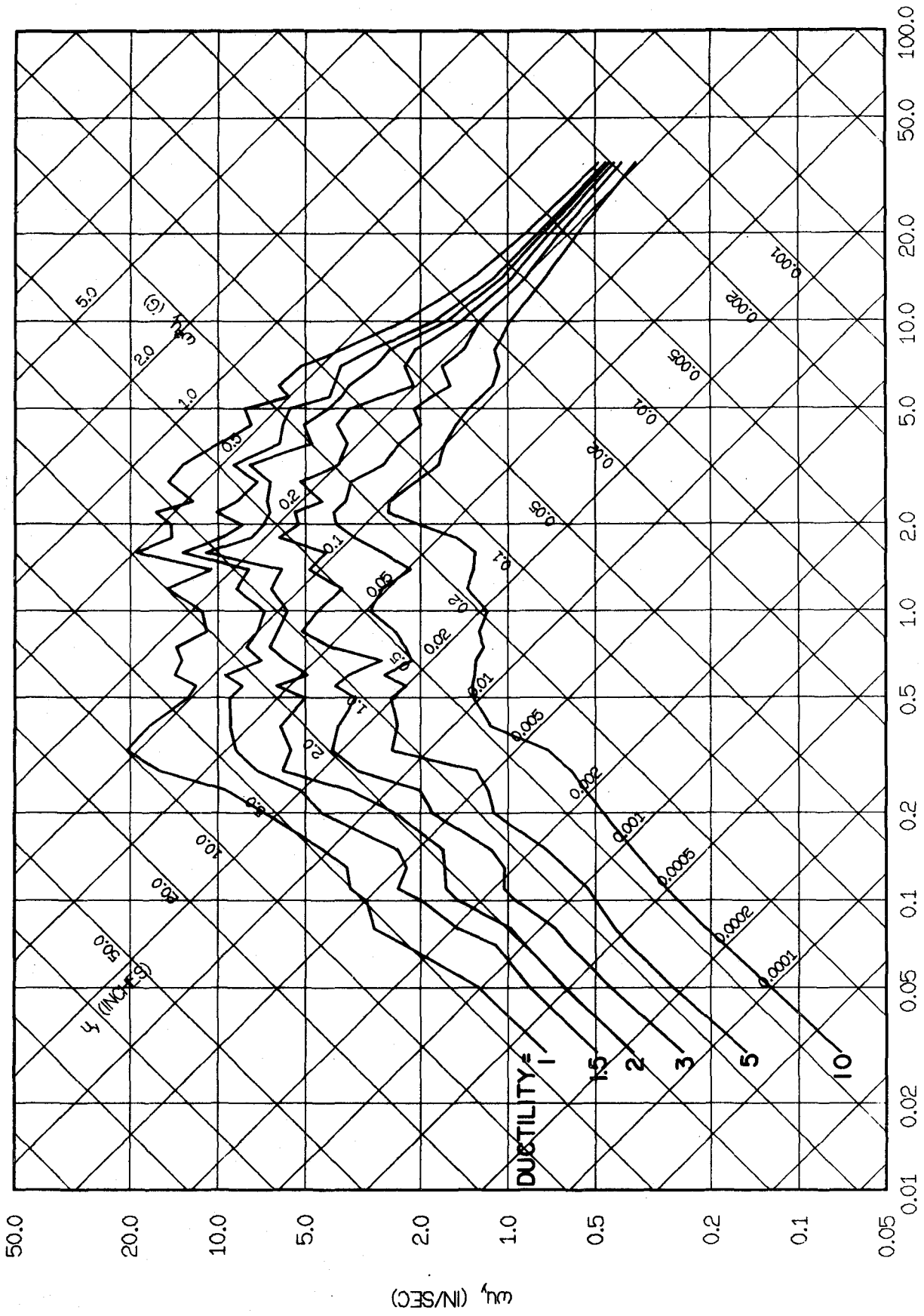
FIG. 3.35   INELASTIC YIELD SPECTRA FOR OLYMPIA, APRIL 13, 1949, N86E.   BILINEAR
SYSTEMS WITH 5% DAMPING.
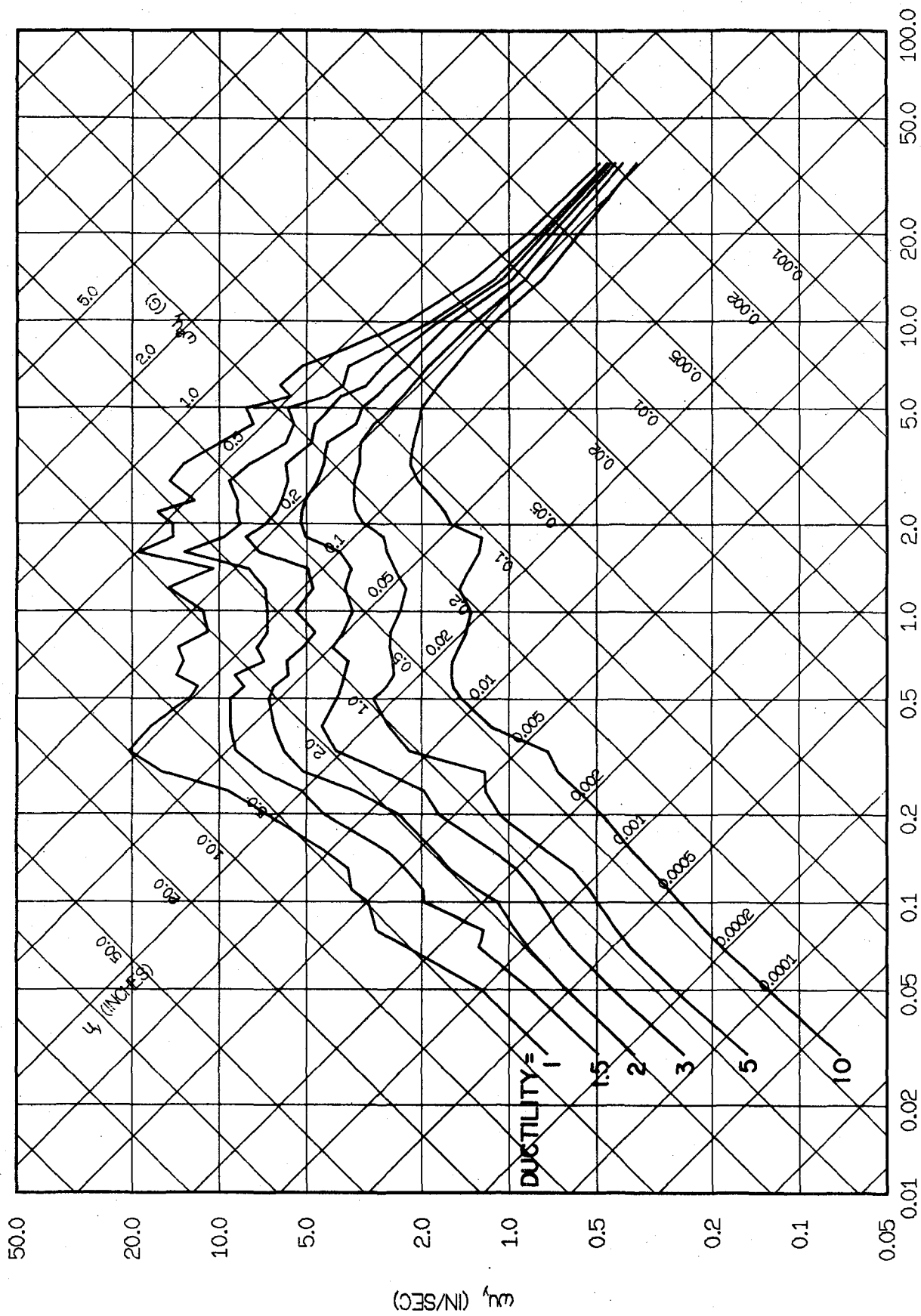
FIG. 3.36 INELASTIC YIELD SPECTRA FOR OLYMPIA, APRIL 13, 1949, N86E. DEGRADING SYSTEMS WITH 5% DAMPING.
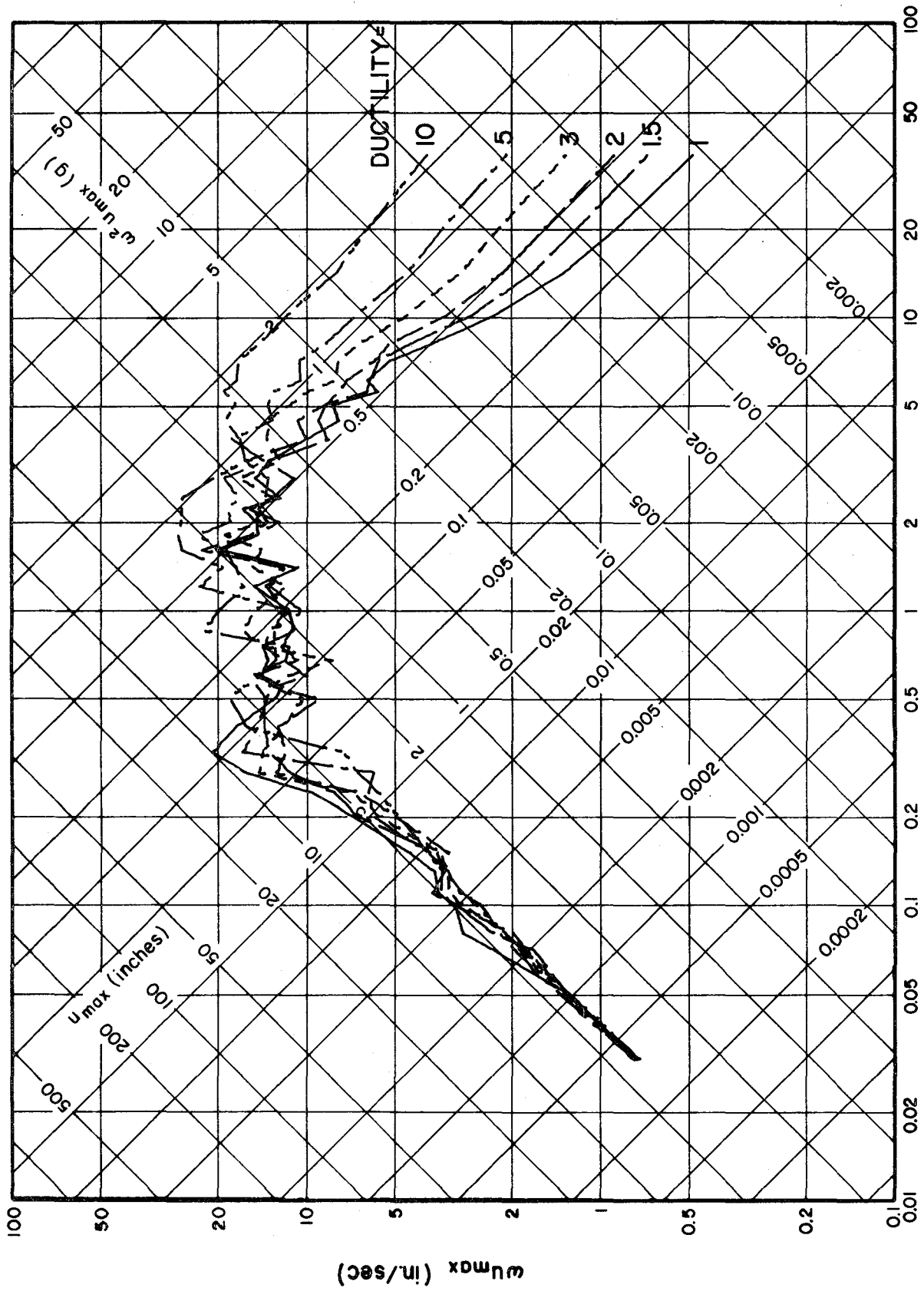
FIG. 3.37 TOTAL DEFORMATION SPECTRA FOR OLYMPIA, APRIL 13, 1949, N86E. ELASTOPLASTIC SYSTEMS WITH 5% DAMPING.
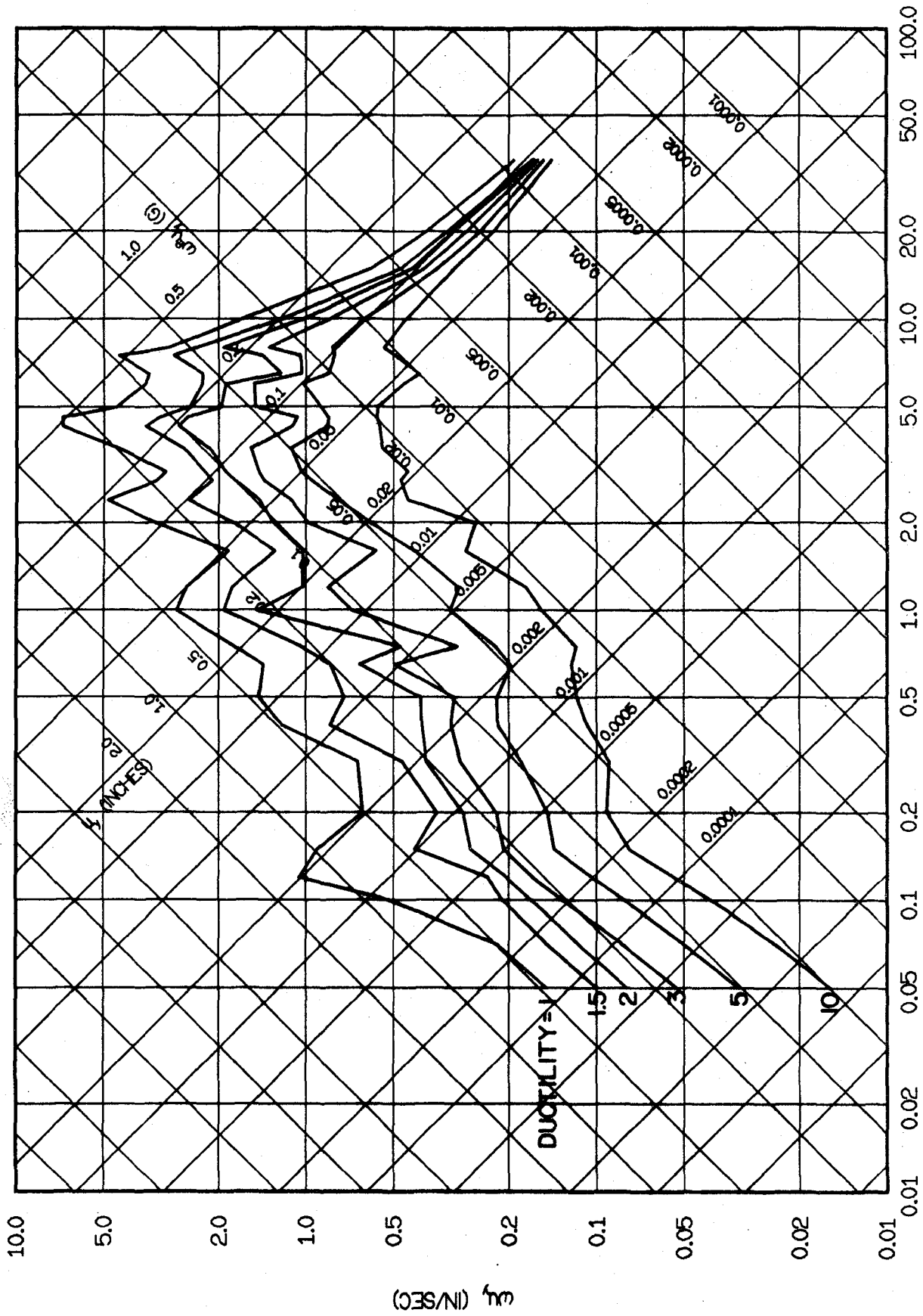
FIG. 3.38   INELASTIC YIELD SPECTRA FOR GOLDEN GATE PARK, MARCH 22, 1957, S80E.
ELASTOPLASTIC SYSTEMS WITH 2% DAMPING.
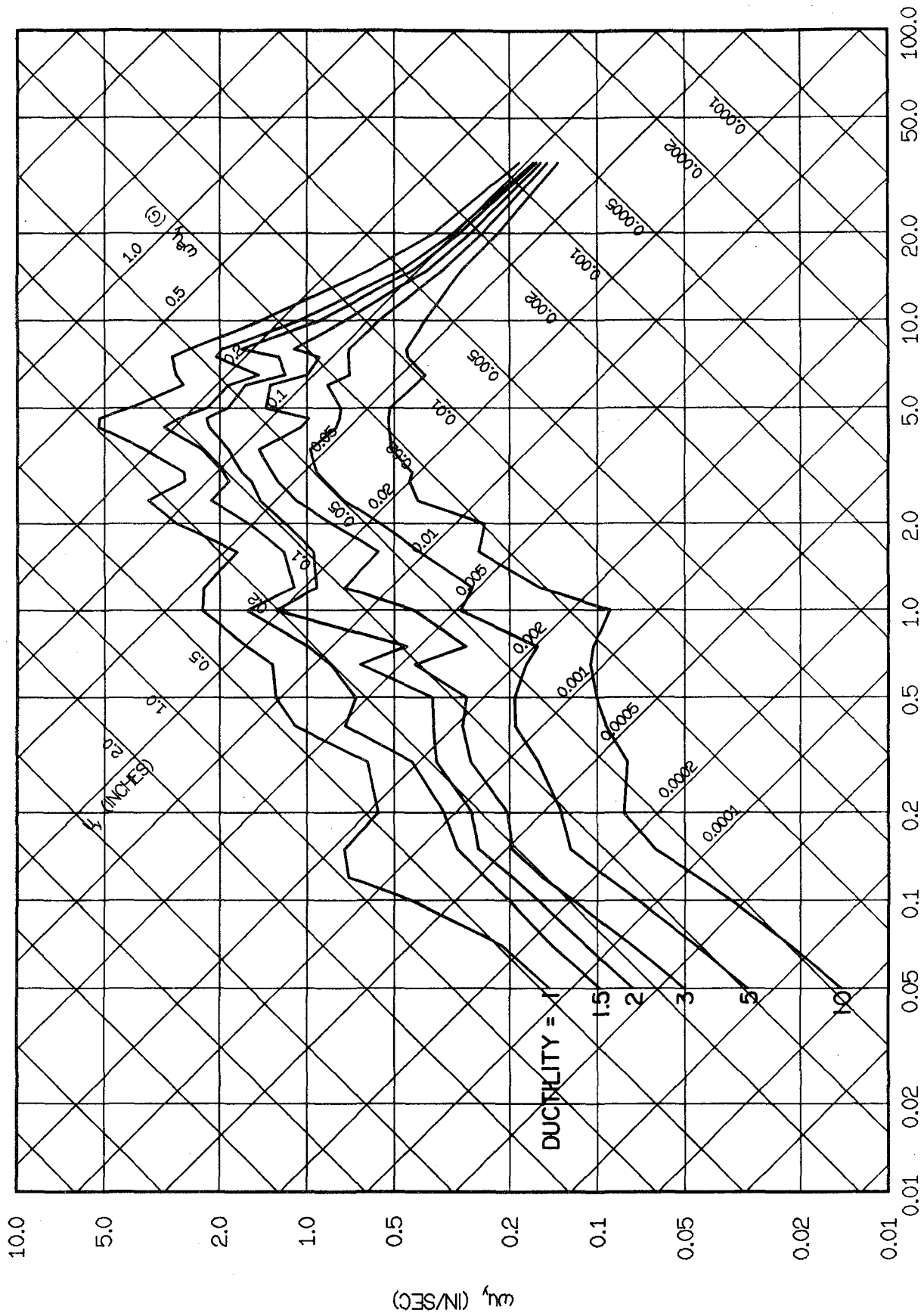
FIG. 3.39   INELASTIC YIELD SPECTRA FOR GOLDEN GATE PARK, MARCH 22, 1957, S80E.
ELASTOPLASTIC SYSTEMS WITH 5% DAMPING.
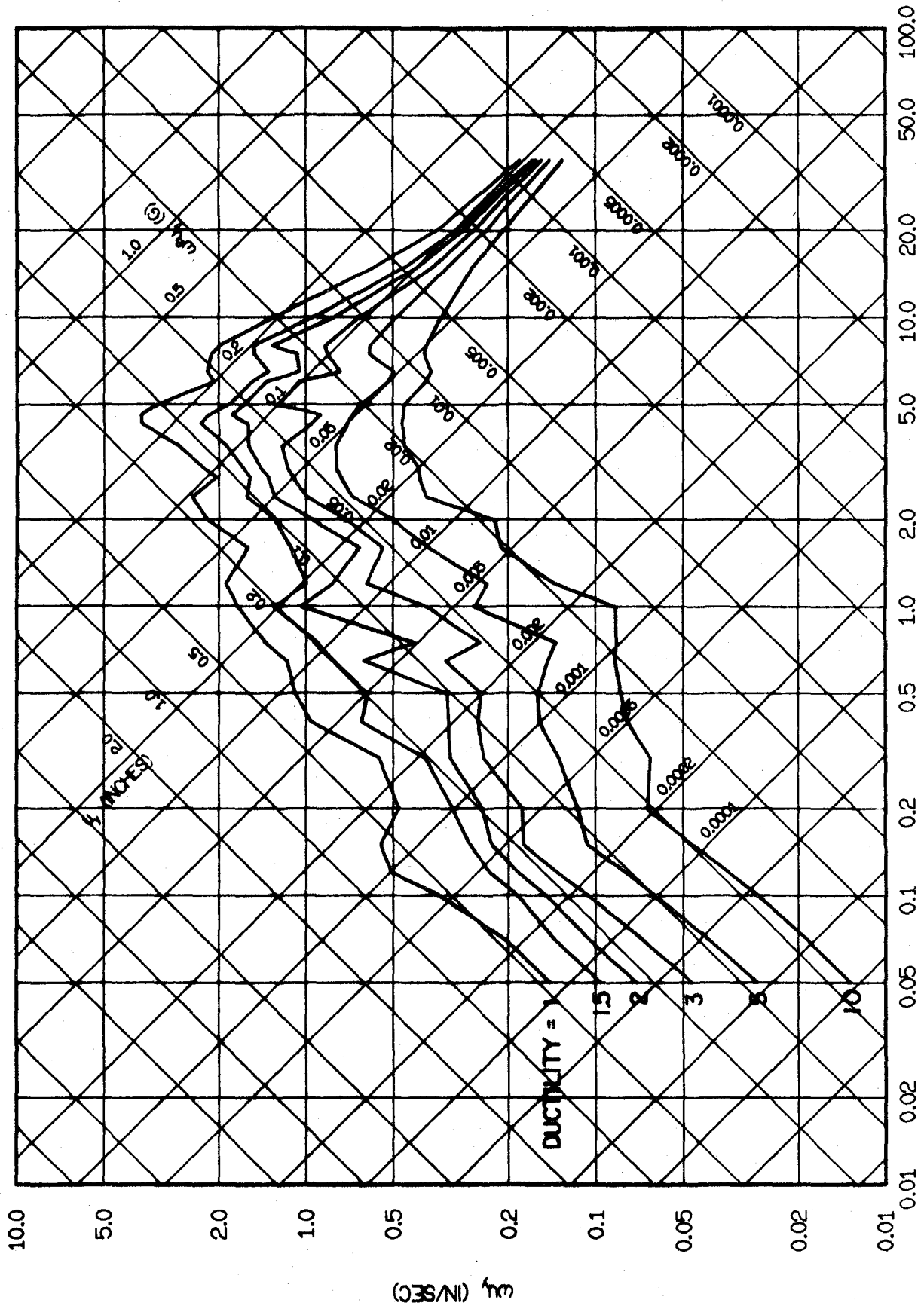
FIG. 3.40   INELASTIC YIELD SPECTRA FOR GOLDEN GATE PARK, MARCH 22, 1957, S80E.
ELASTOPLASTIC SYSTEMS WITH 10% DAMPING
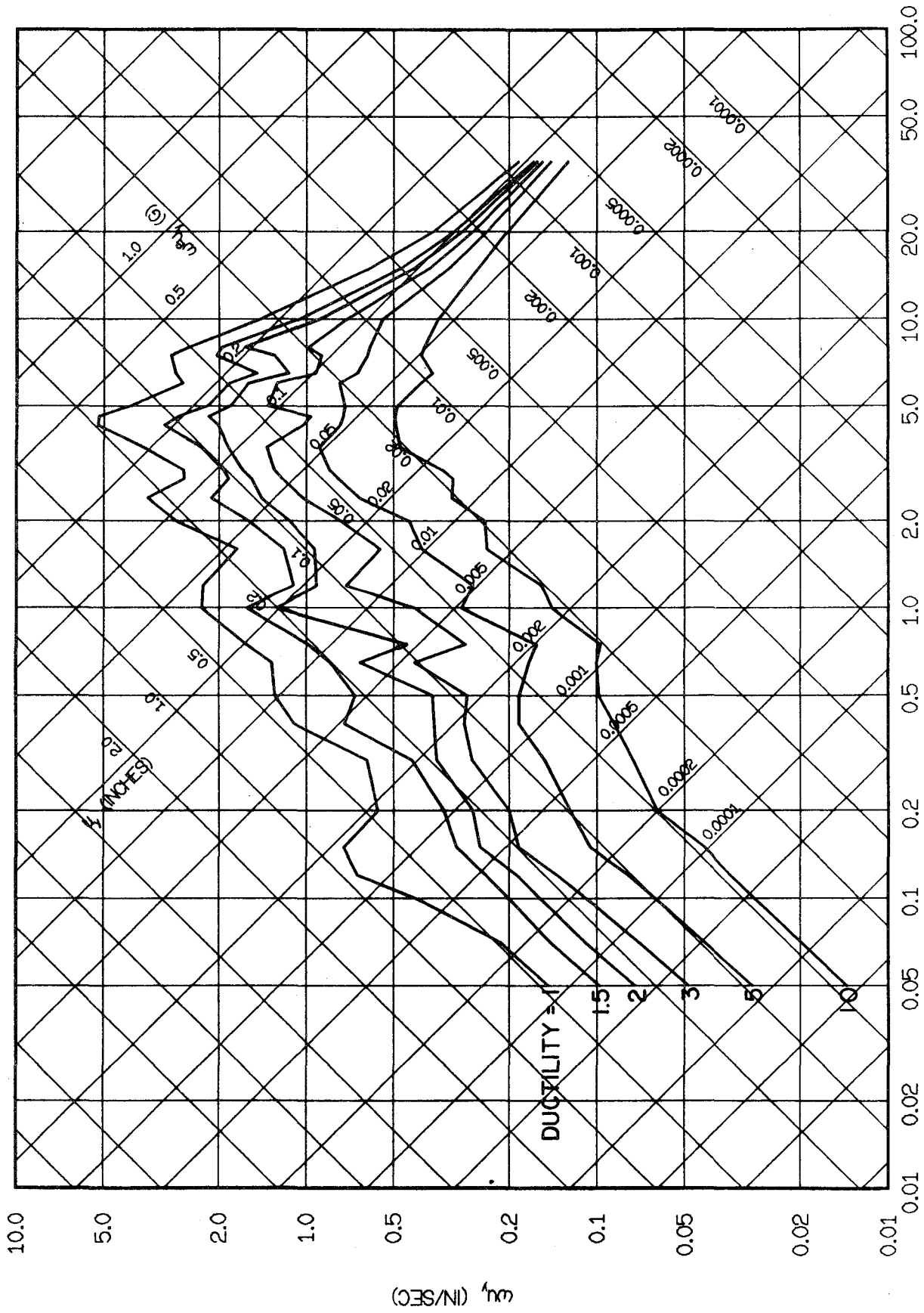
FIG. 3.41 INELASTIC YIELD SPECTRA FOR GOLDEN GATE PARK, MARCH 22, 1957 S80E
BILINEAR SYSTEMS WITH 5% DAMPING.
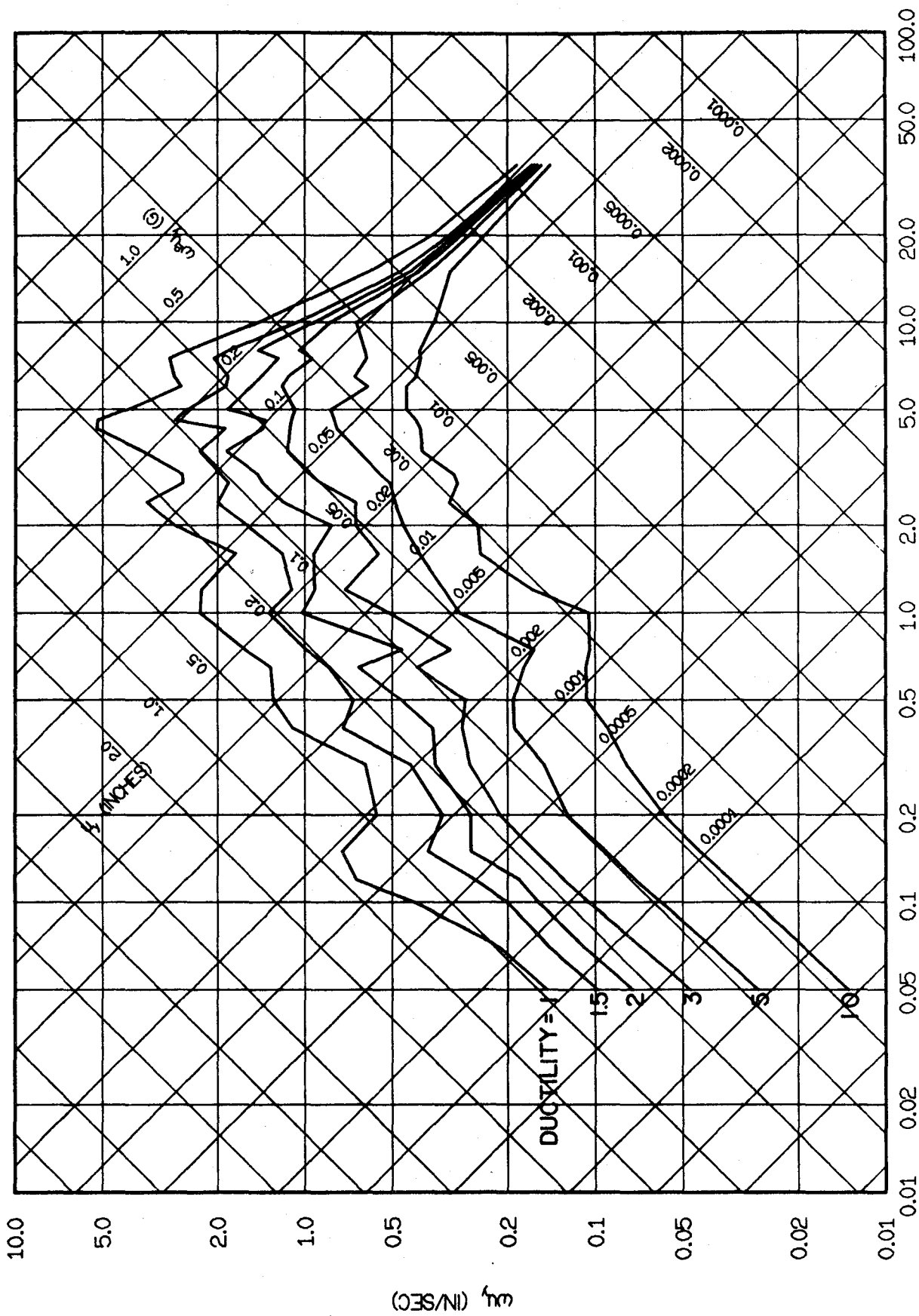
FIG. 3.42 INELASTIC YIELD SPECTRA FOR GOLDEN GATE PARK, MARCH 22, 1957, S80E.
DEGRADING SYSTEMS WITH 5% DAMPING.
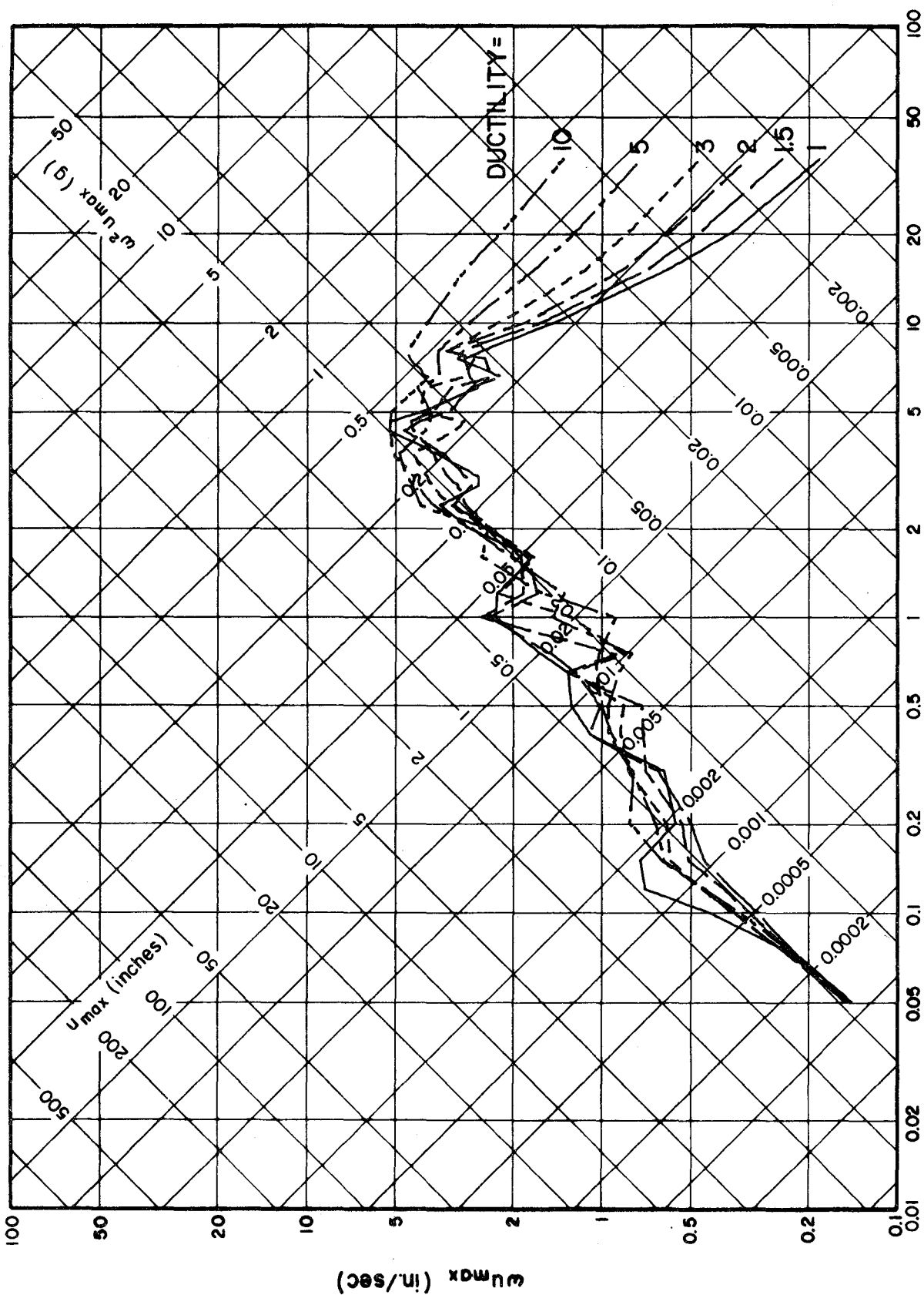
FIG. 3.43   TOTAL DEFORMATION SPECTRA FOR GOLDEN GATE PARK, MARCH 22, 1957, S80E.
ELASTOPLASTIC SYSTEMS WITH 5% DAMPING.

FREQUENCY (CPS)
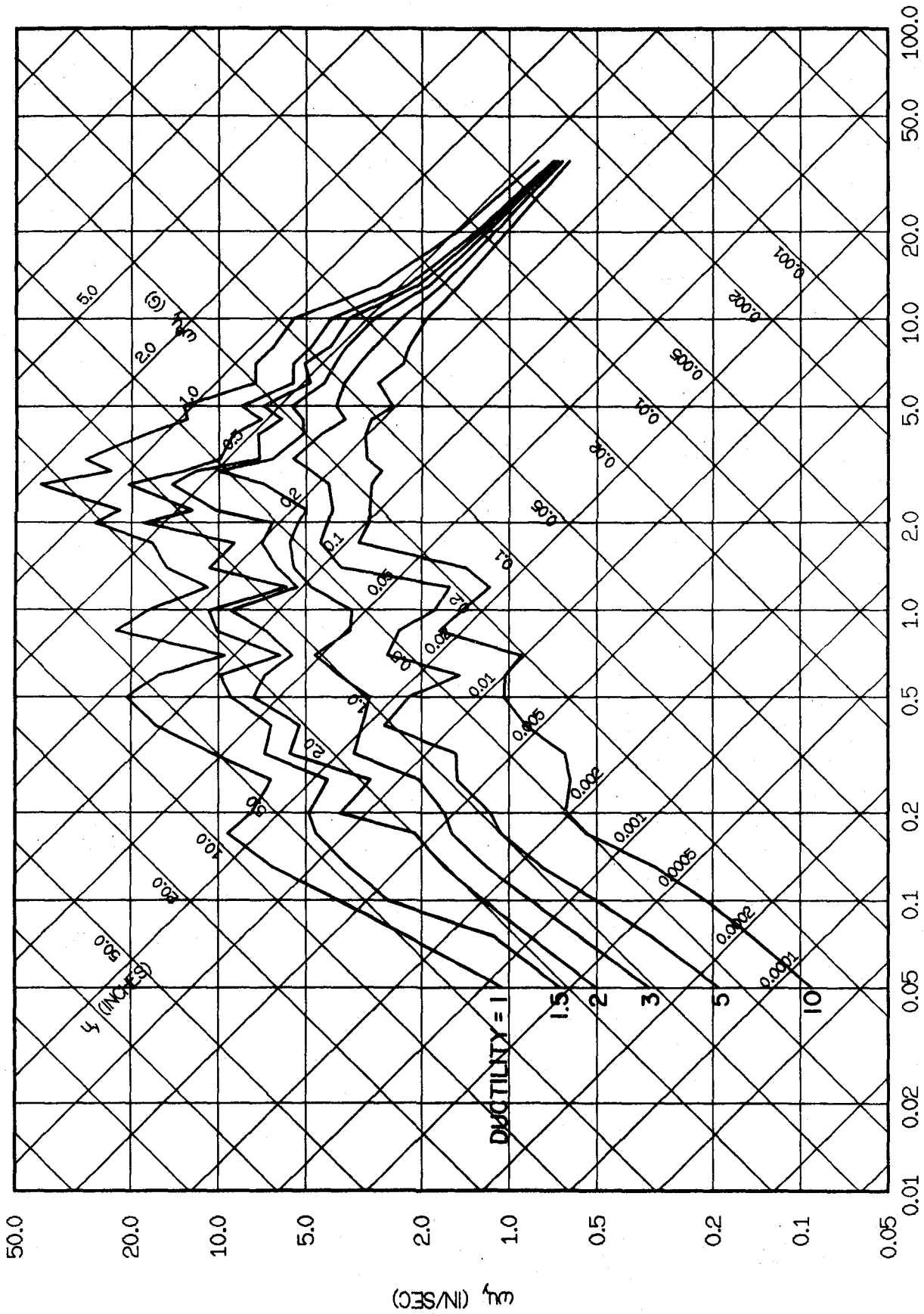
FIG. 3.44   INELASTIC YIELD SPECTRA FOR CHOLAME-STATION 5, JUNE 27, 1966, N85E.
ELASTOPLASTIC SYSTEMS WITH 2% DAMPING.
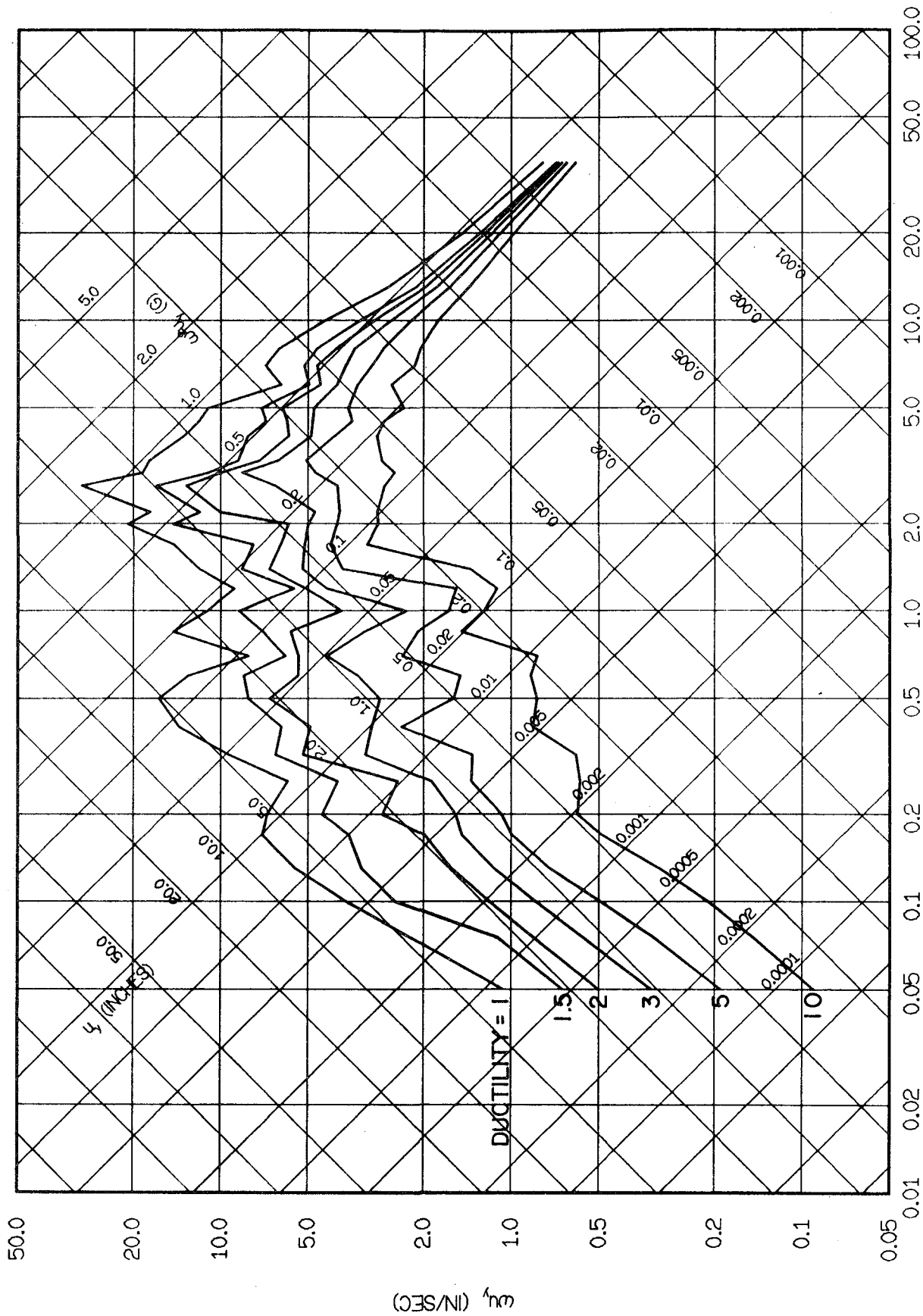
FIG. 3.45 INELASTIC YIELD SPECTRA FOR CHOLAME-STATION 5, JUNE 27, 1966, N85E.
ELASTOPLASTIC SYSTEMS WITH 5% DAMPING.
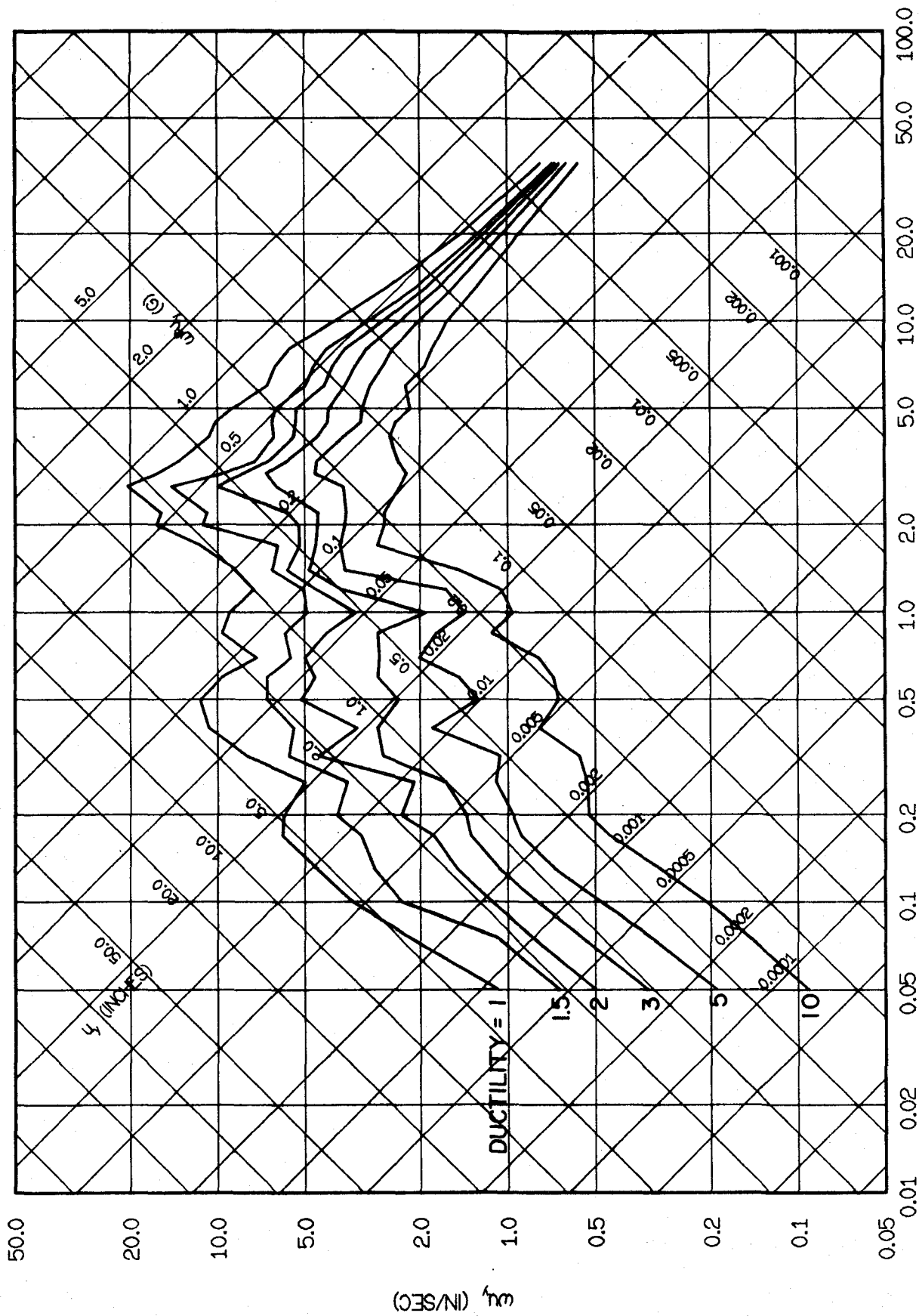
FIG. 3.46 INELASTIC YIELD SPECTRA FOR CHOLAME-STATION 5, JUNE 27, 1966, N85E. ELASTOPLASTIC SYSTEMS WITH 10% DAMPING.
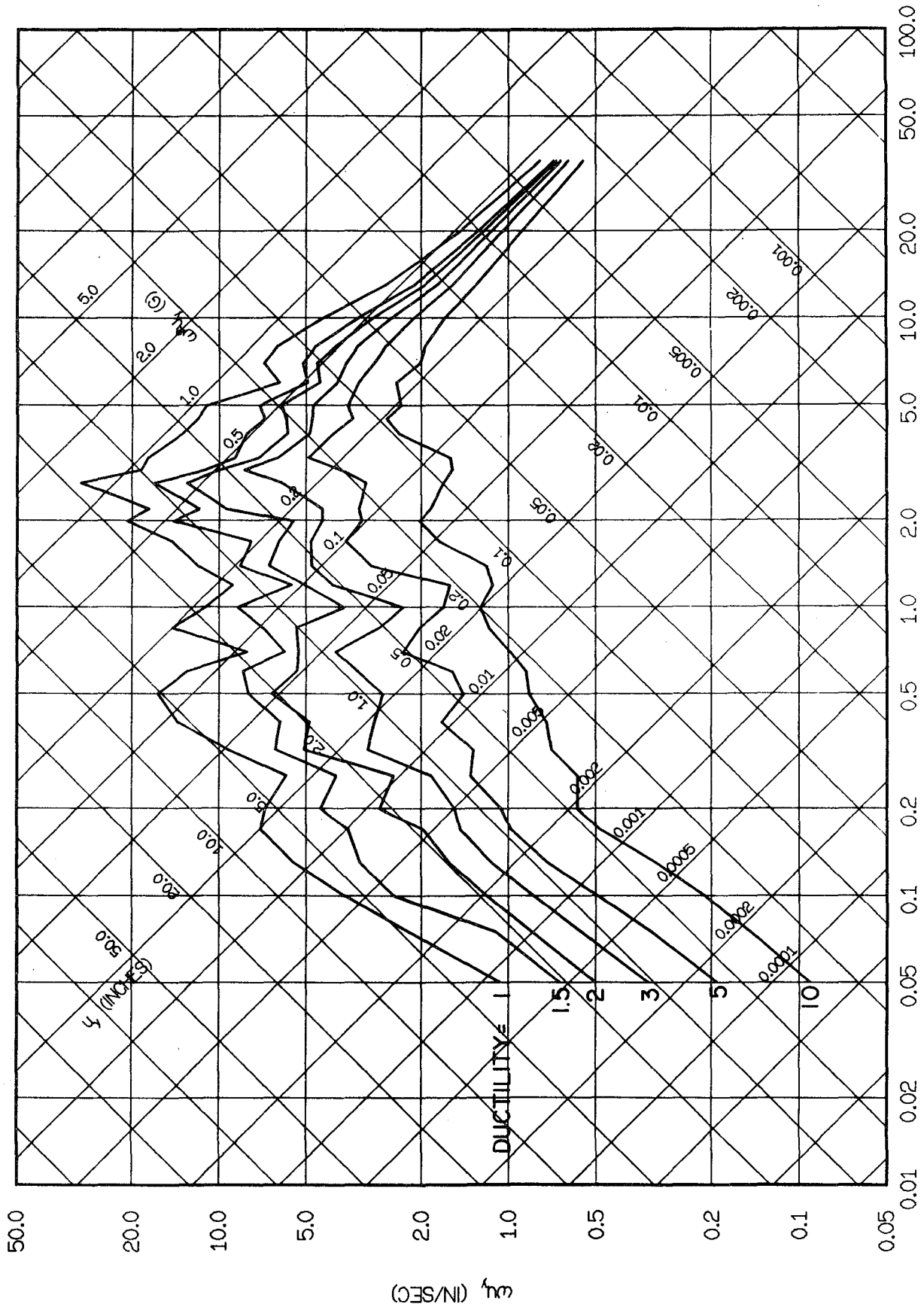
FIG. 3.47 INELASTIC YIELD SPECTRA FOR CHOLAME-STATION 5, JUNE 27, 1966, N85E.
BILINEAR SYSTEMS WITH 5% DAMPING

FREQUENCY (CPS)
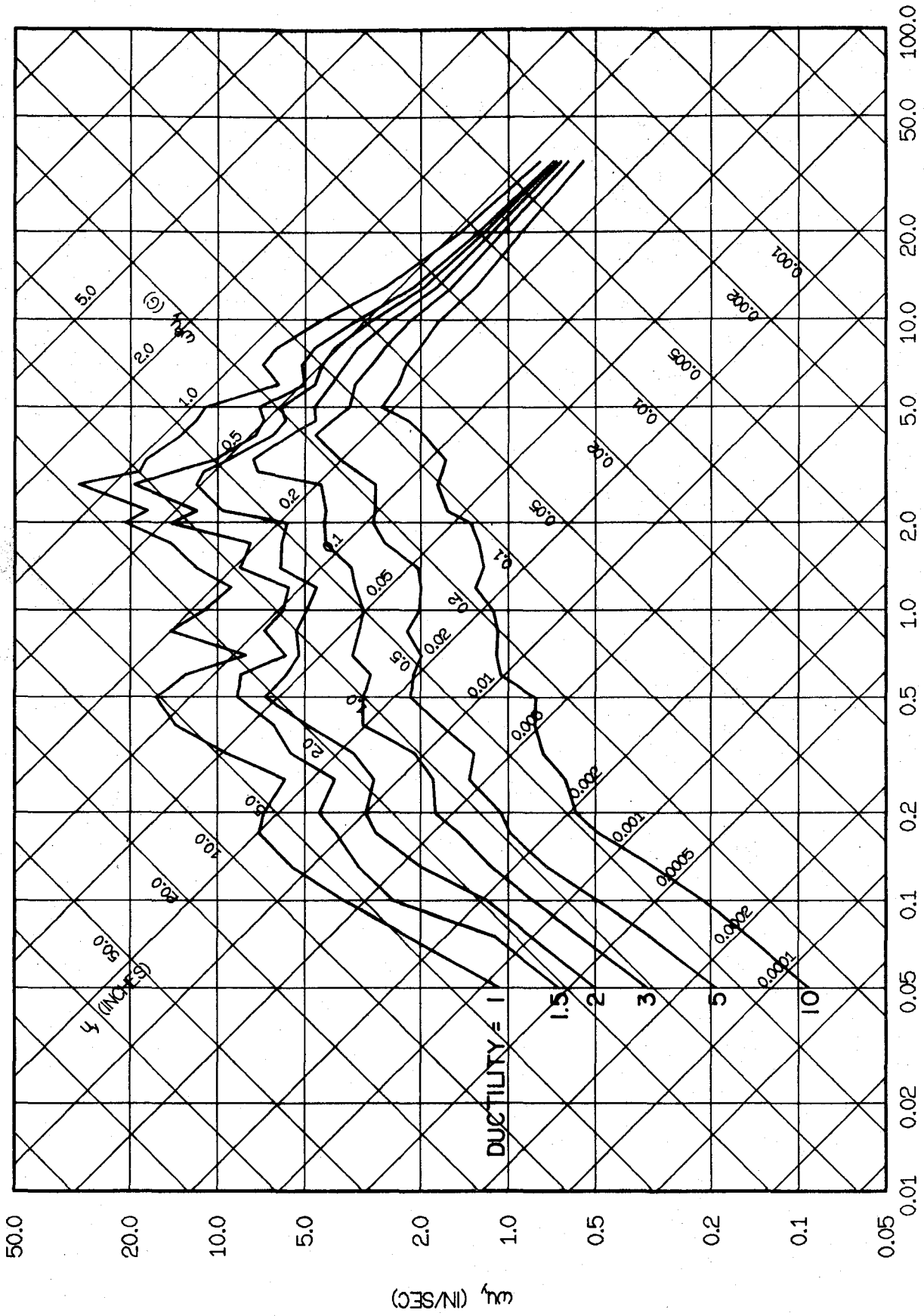
FIG. 3.48   INELASTIC YIELD SPECTRA FOR CHOLAME-STATION 5, JUNE 27, 1966, N85E
DEGRADING SYSTEMS WITH 5% DAMPING.

Frequency (cps)
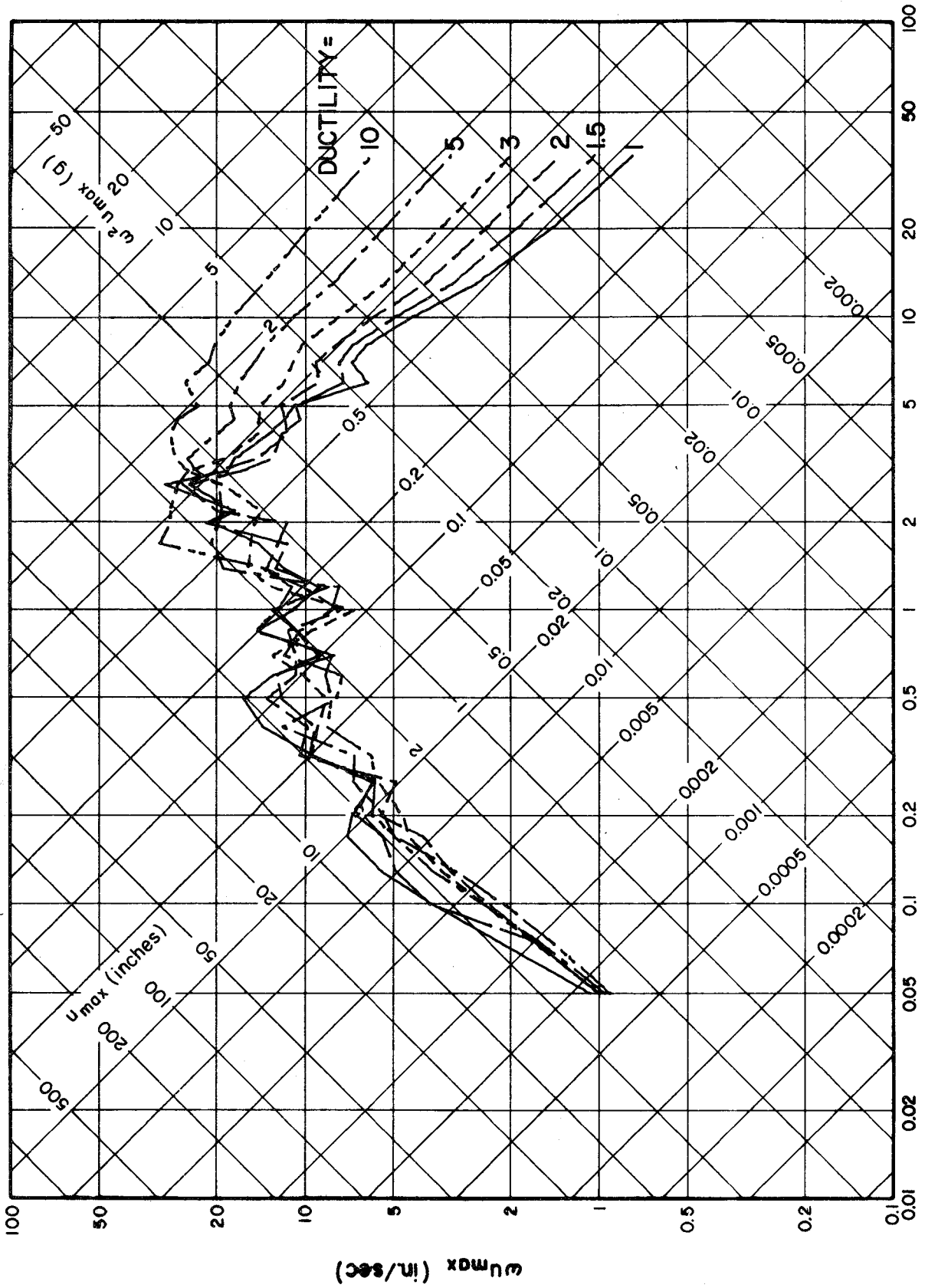
FIG. 3.49   TOTAL DEFORMATION SPECTRA FOR CHOLAME-STATION 5, JUNE 27, 1966, N85E.
ELASTOPLASTIC SYSTEMS WITH 5% DAMPING.
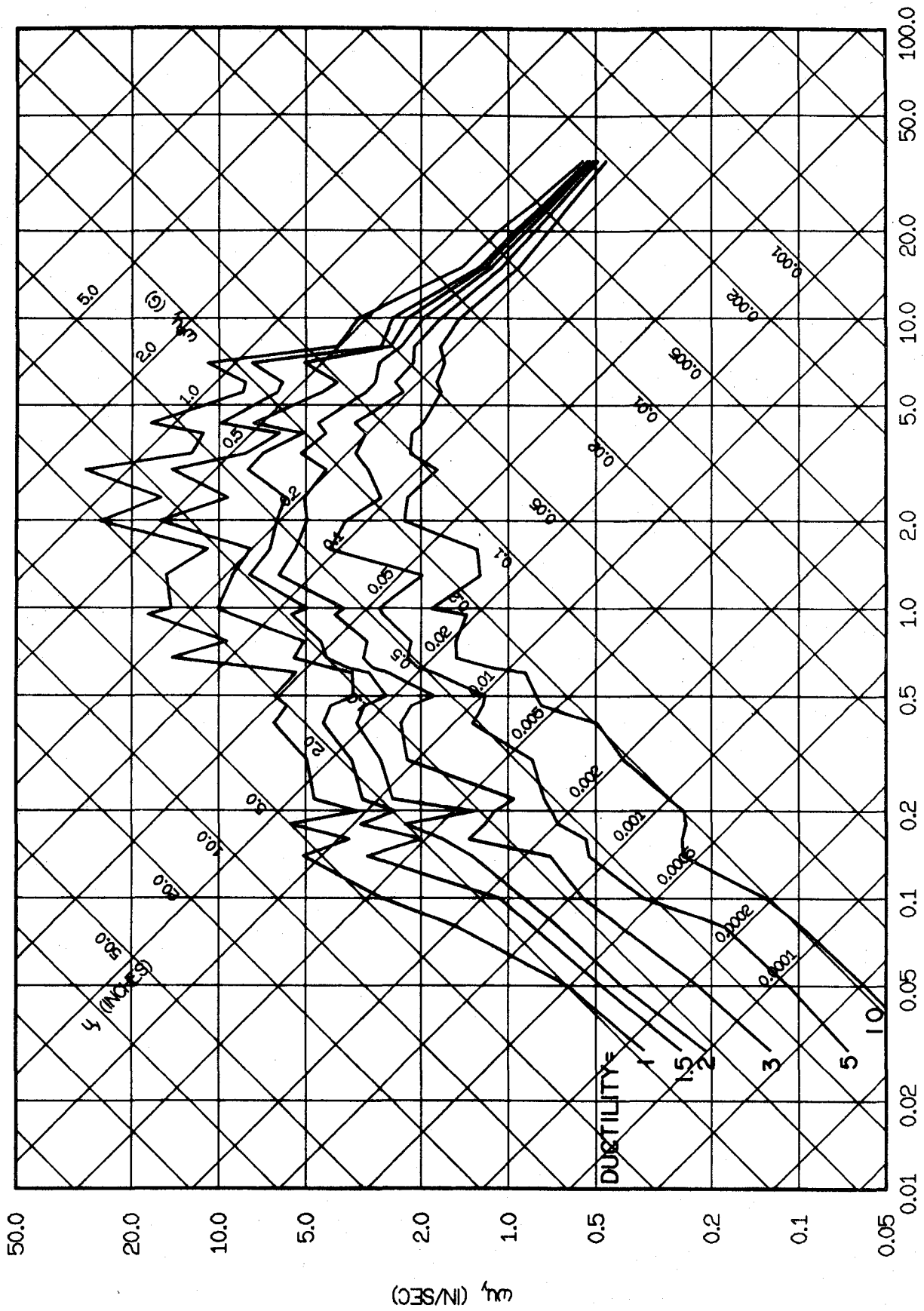
FIG. 3.50 INELASTIC YIELD SPECTRA FOR CASTAIC, FEBRUARY 9, 1971, N21E. ELASTOPLASTIC SYSTEMS WITH 2% DAMPING.
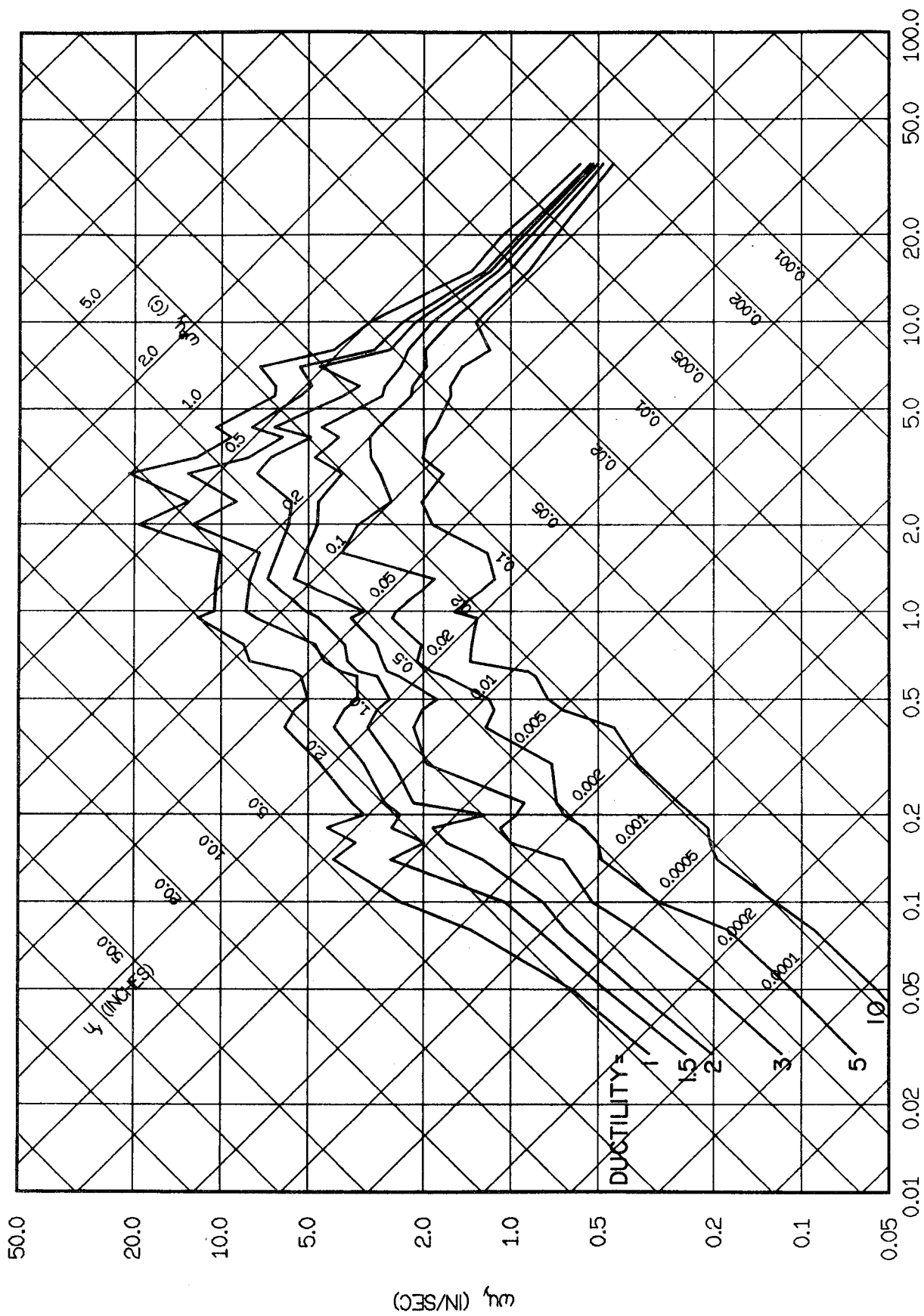
FIG. 3.51 INELASTIC YIELD SPECTRA FOR CASTAIC, FEBRUARY 9, 1971, N21E. ELASTOPLASTIC SYSTEMS WITH 5% DAMPING.
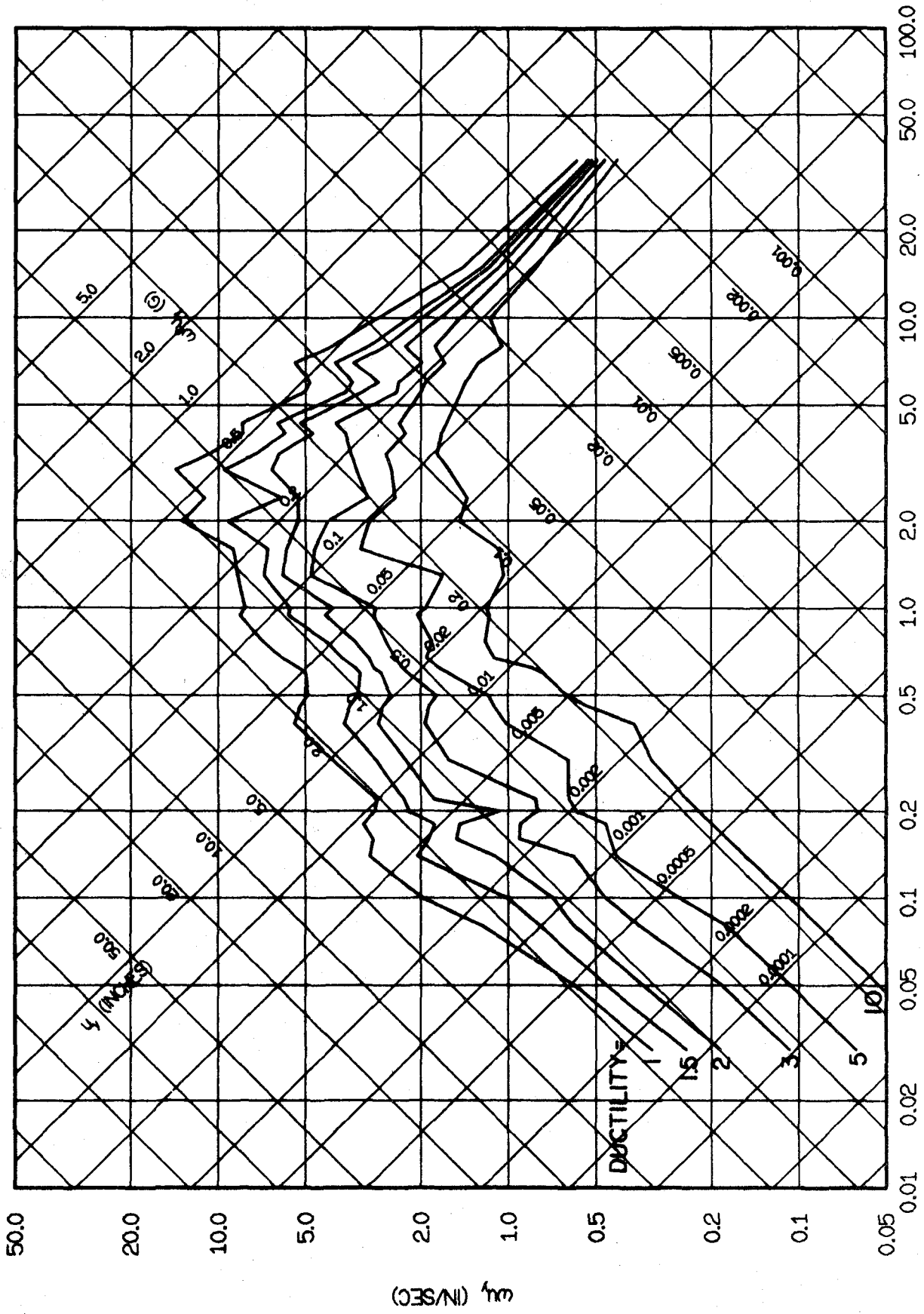
FIG. 3.52 INELASTIC YIELD SPECTRA FOR CASTAIC, FEBRUARY 9, 1971, N21E. ELASTOPLASTIC SYSTEMS WITH 10% DAMPING.

FREQUENCY (CPS)
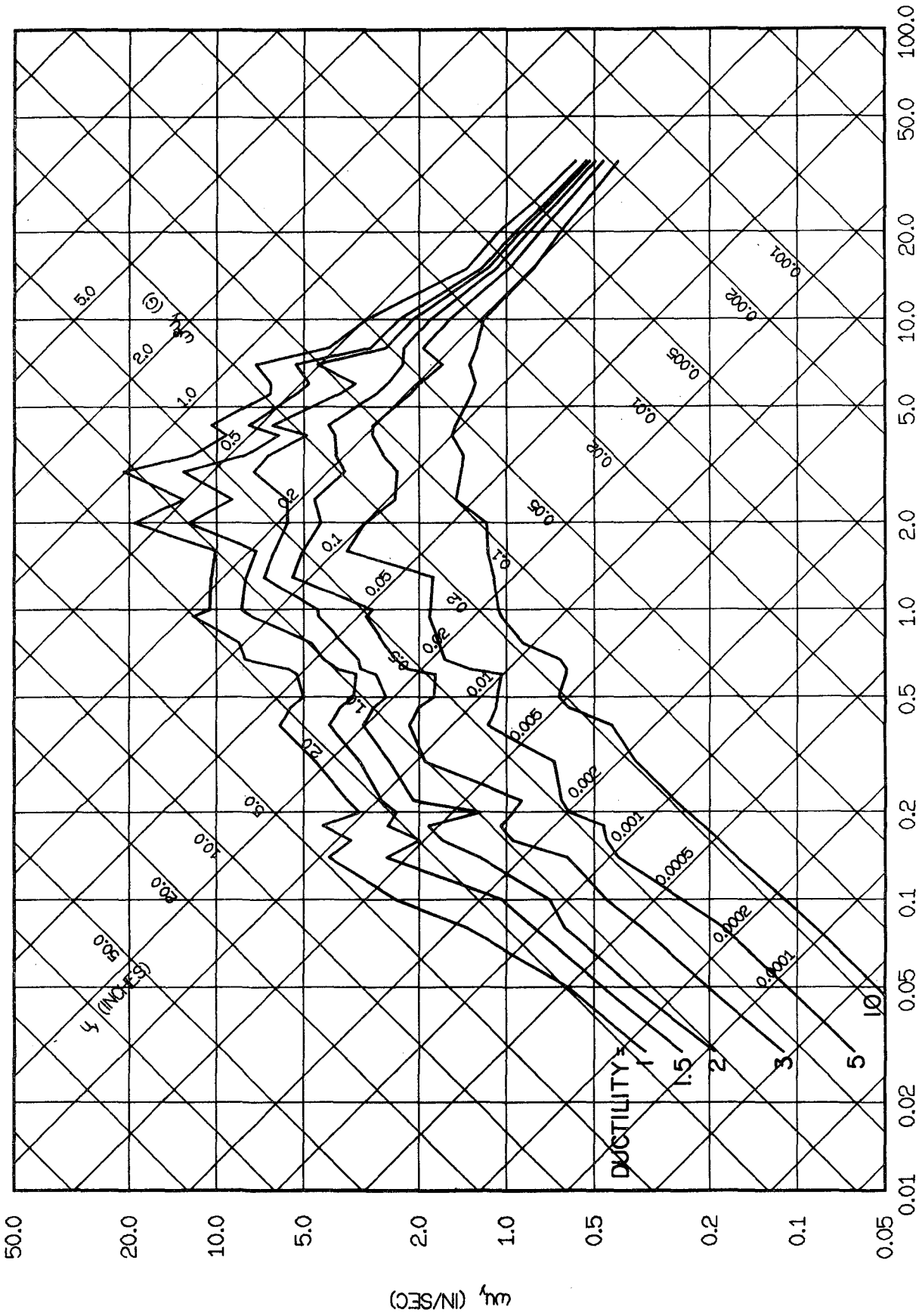
FIG. 3.53   INELASTIC YIELD SPECTRA FOR CASTAIC, FEBRUARY 9, 1971, N21E.
BILINEAR SYSTEMS WITH 5% DAMPING.

FREQUENCY (CPS)
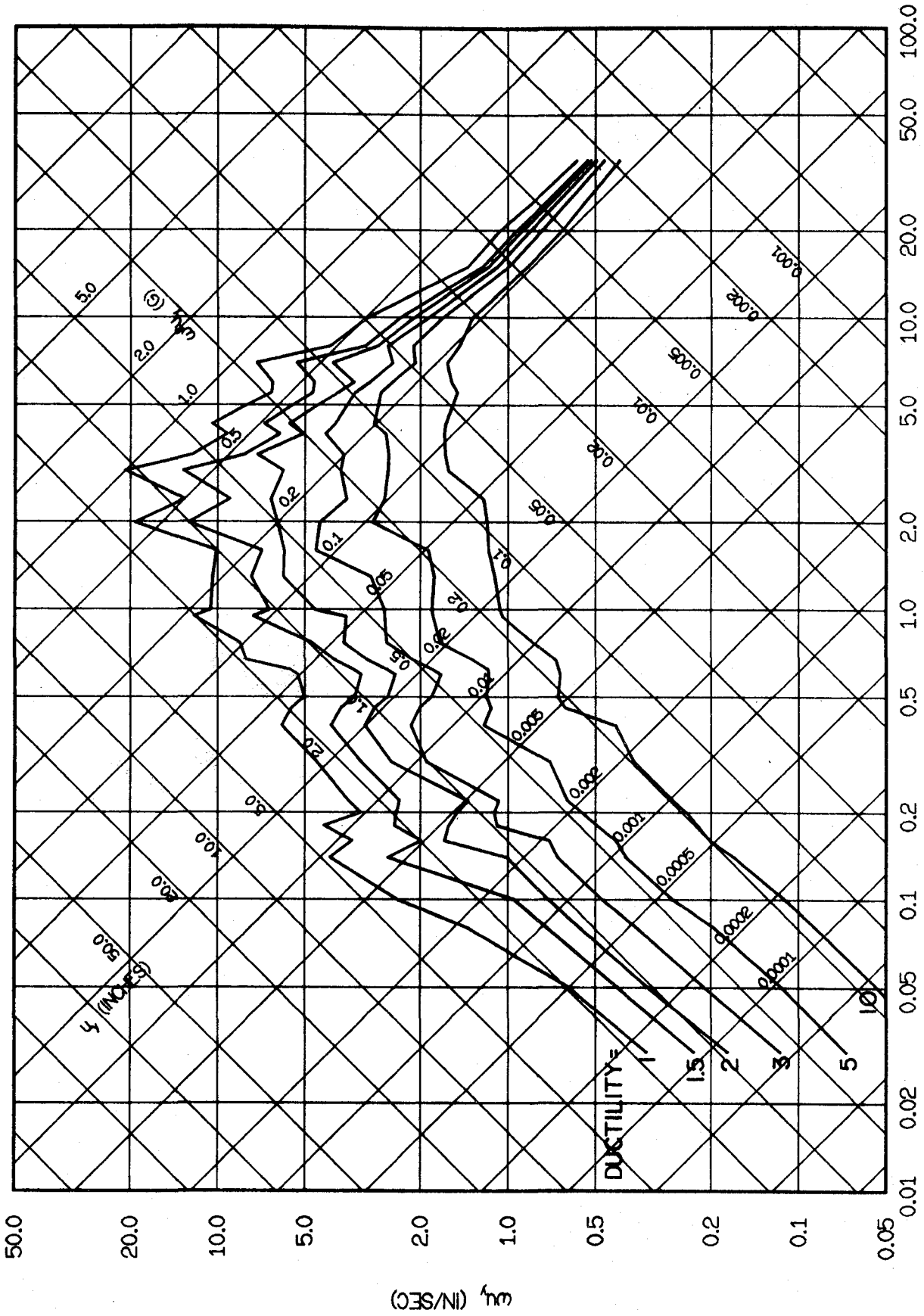
FIG. 3.54   INELASTIC YIELD SPECTRA FOR CASTAIC, FEBRUARY 9, 1971, N21E.
DEGRADING SYSTEMS WITH 5% DAMPING.
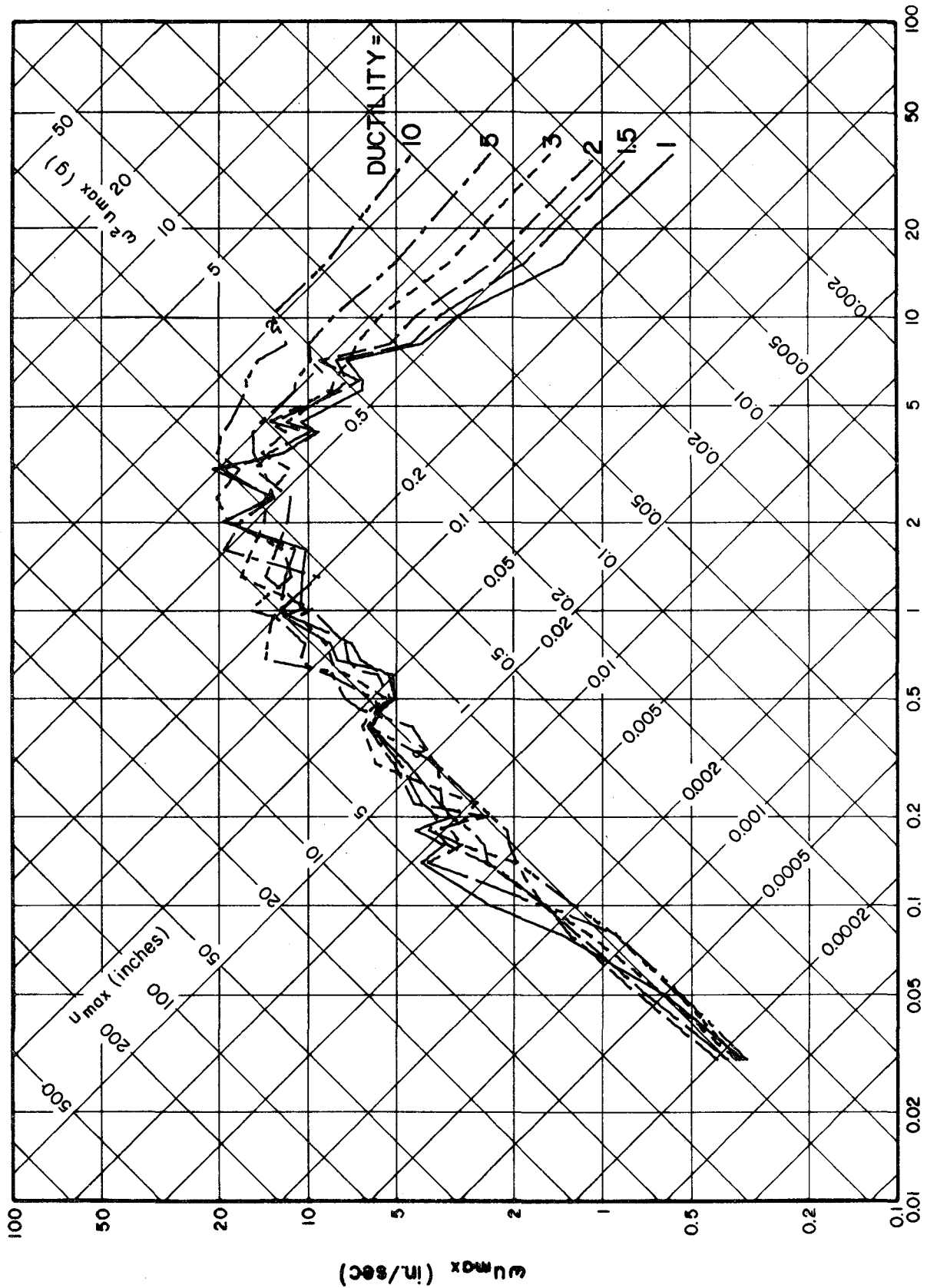
FIG. 3.55   TOTAL DEFORMATION SPECTRA FOR CASTAIC, FEBRUARY 9, 1971, N21E ELASTOPLASTIC SYSTEMS WITH 5% DAMPING.
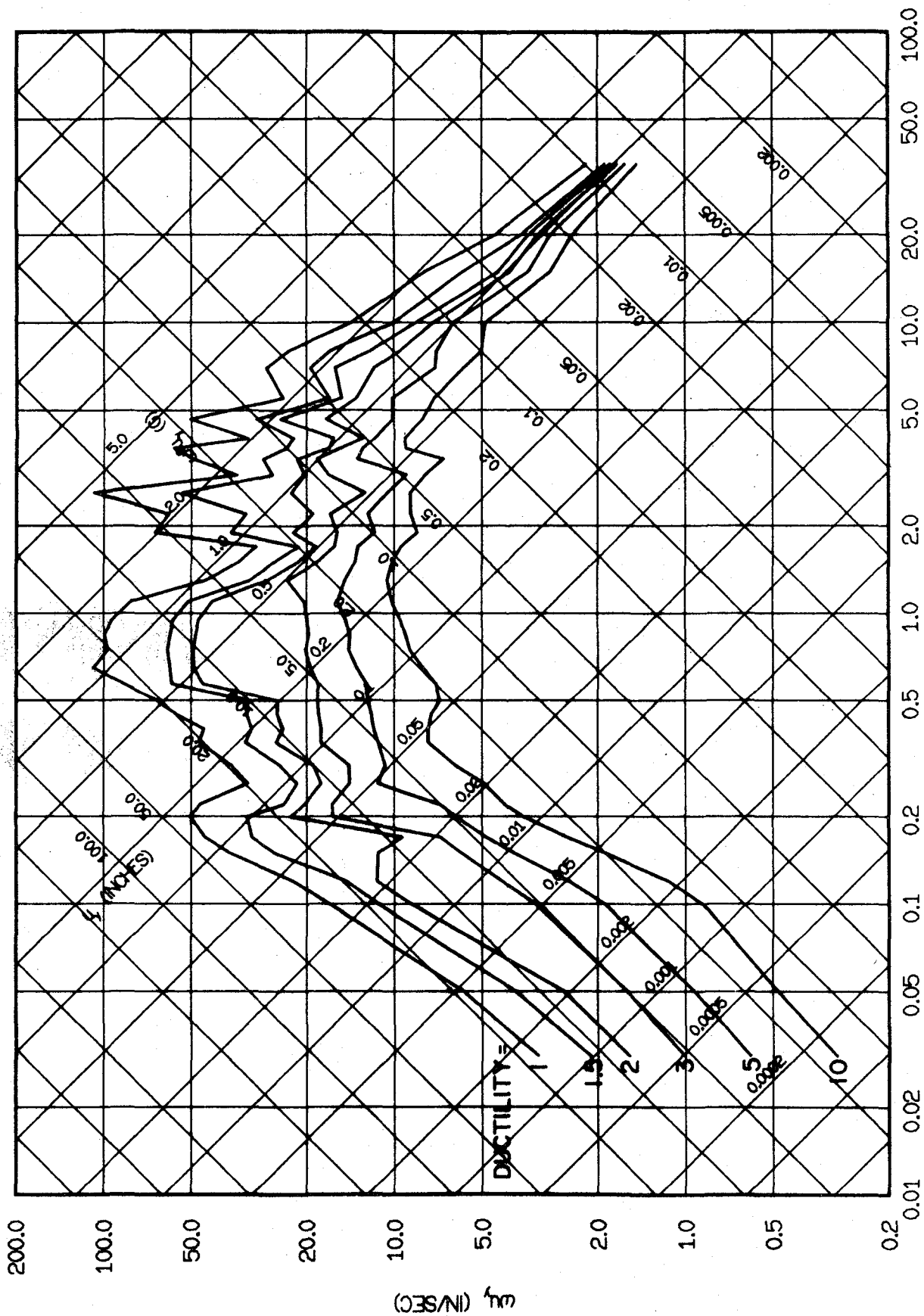
FIG. 3.56 INELASTIC YIELD SPECTRA FOR PACOIMA, FEBRUARY 9, 1971, S16E. ELASTOPLASTIC SYSTEMS WITH 2% DAMPING.

190

FIG. 3.57 INELASTIC YIELD SPECTRA FOR PACOIMA, FEBRUARY 9, 1971, S16E. ELASTOPLASTIC SYSTEMS WITH 5% DAMPING.
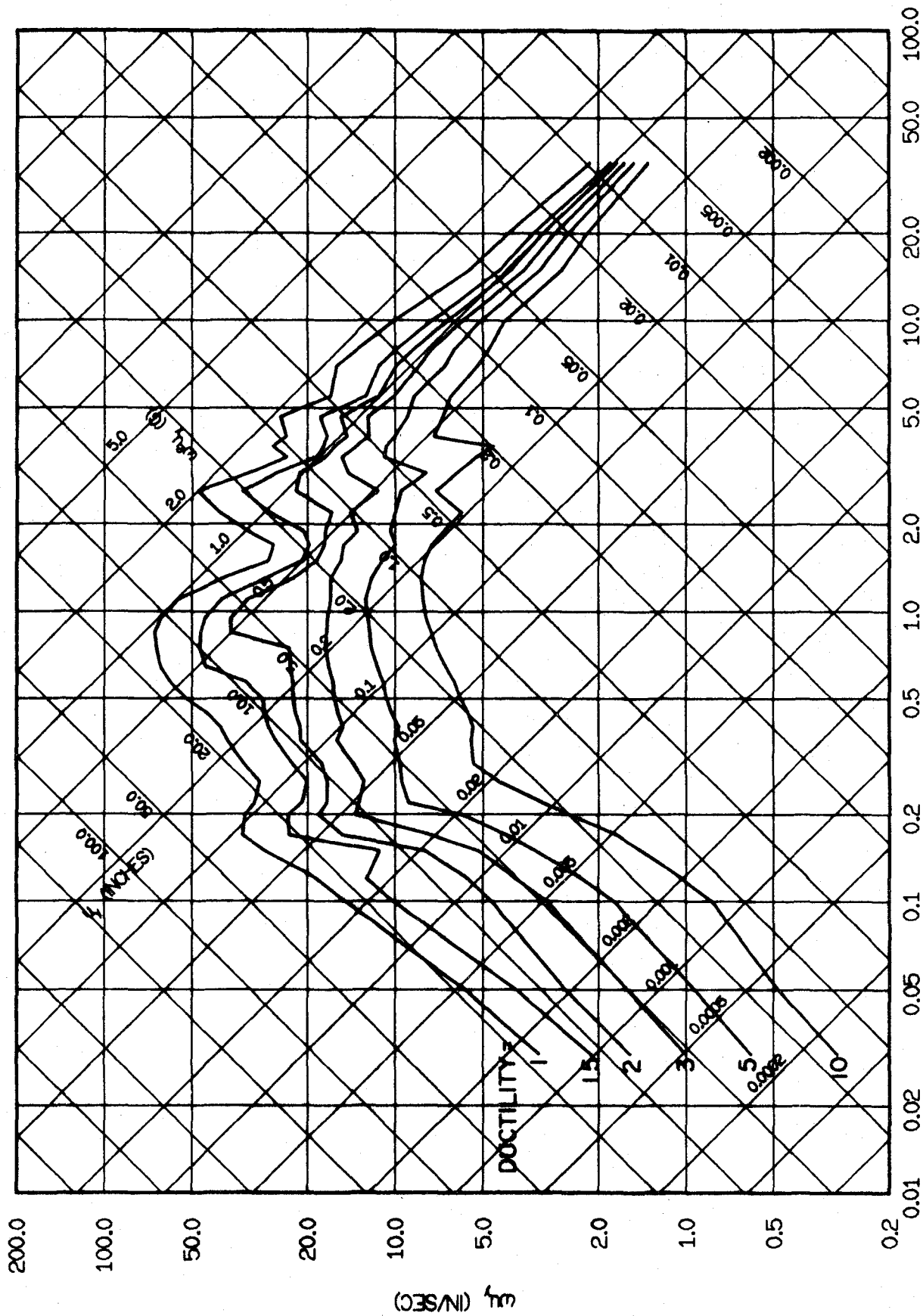
FIG. 3.58   INELASTIC YIELD SPECTRA FOR PACOIMA, FEBRUARY 9, 1971, S16E.   ELASTOPLASTIC
SYSTEMS WITH 10% DAMPING.
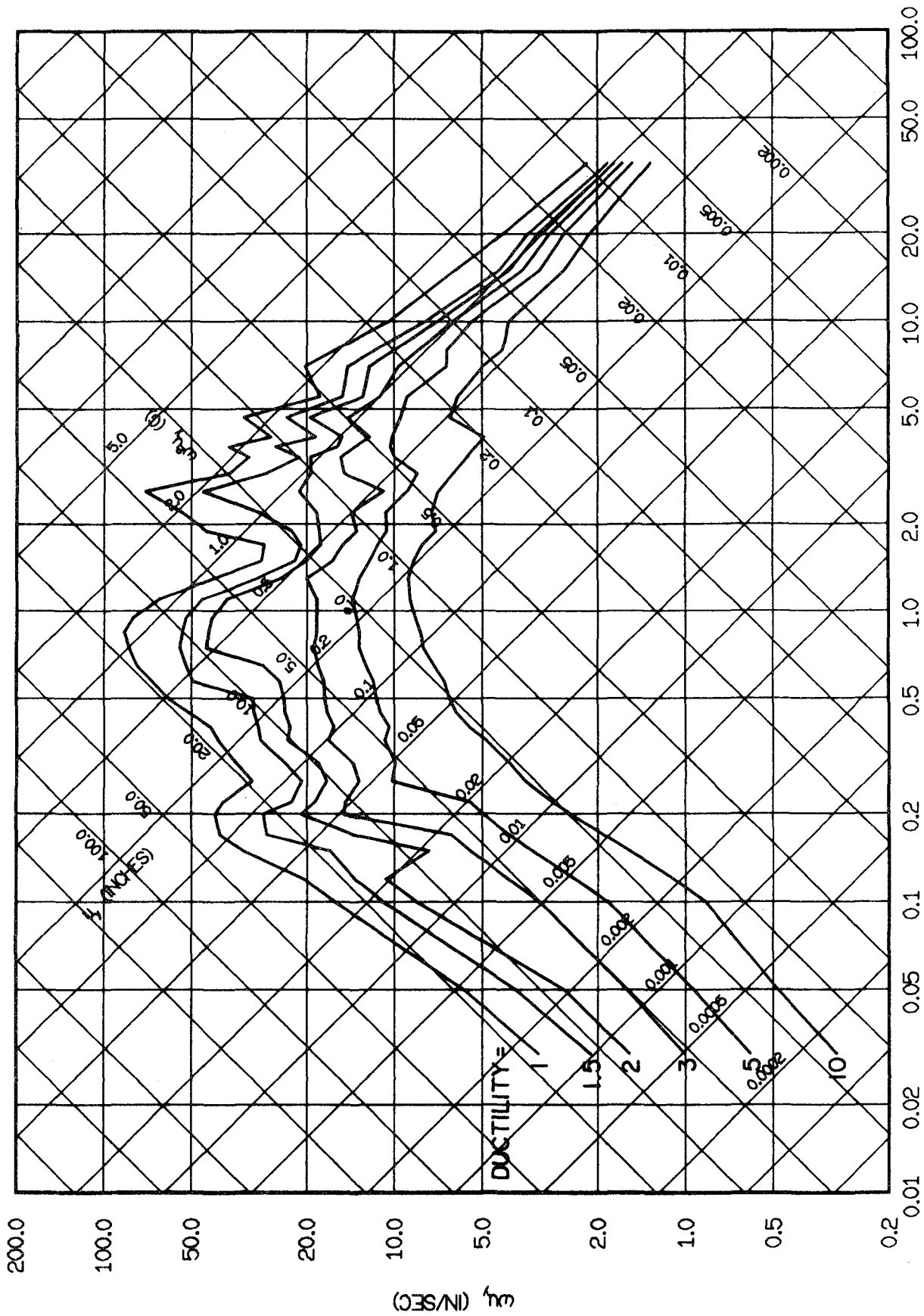
FIG. 3.59   INELASTIC YIELD SPECTRA FOR PACOIMA, FEBRUARY 9, 1971, S16E.   BILINEAR
SYSTEMS WITH 5% DAMPING.
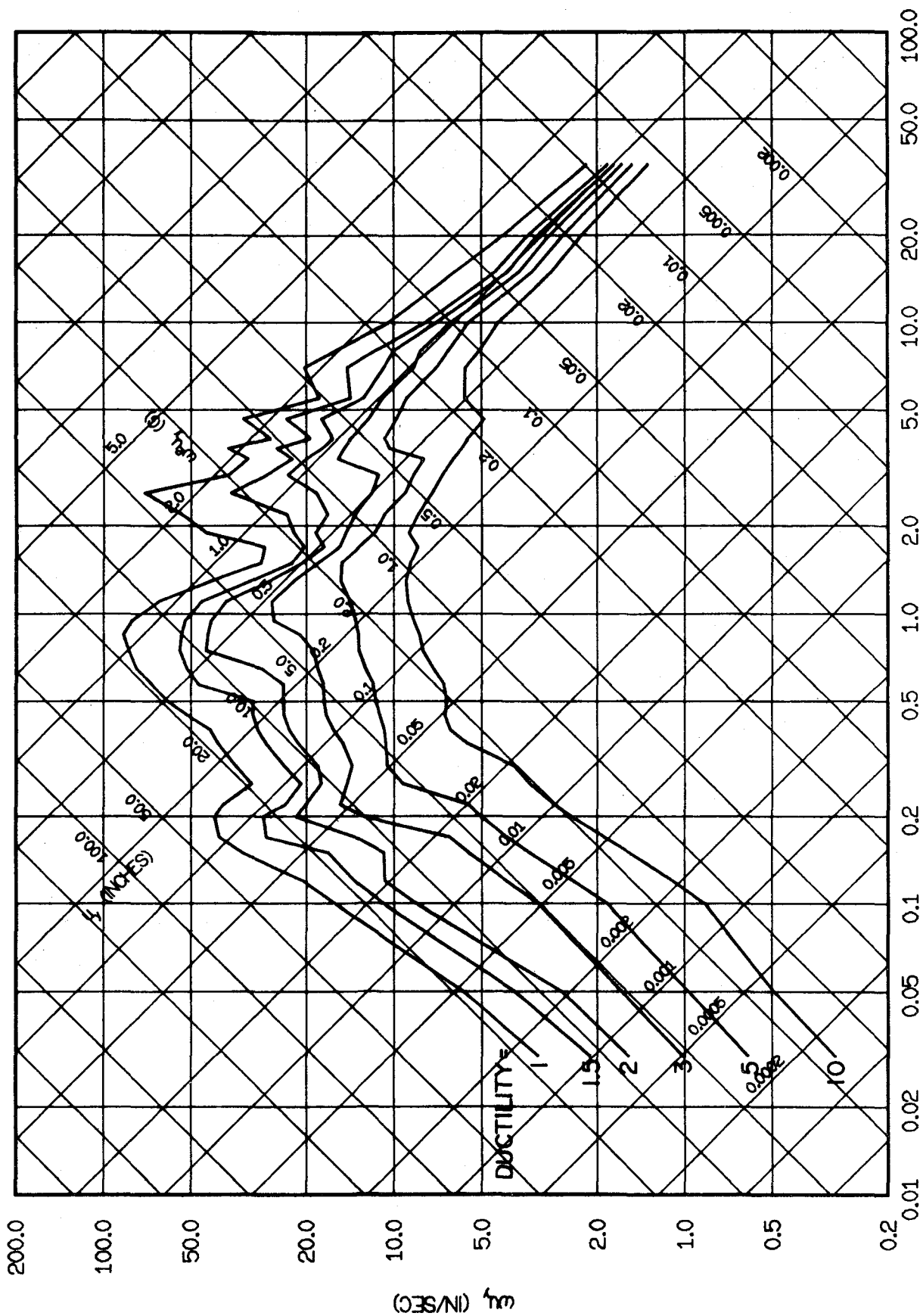
FIG. 3.60   INELASTIC YIELD SPECTRA FOR PACOIMA, FEBRUARY 9, 1971, S16E.   DEGRADING SYSTEMS WITH 5% DAMPING.
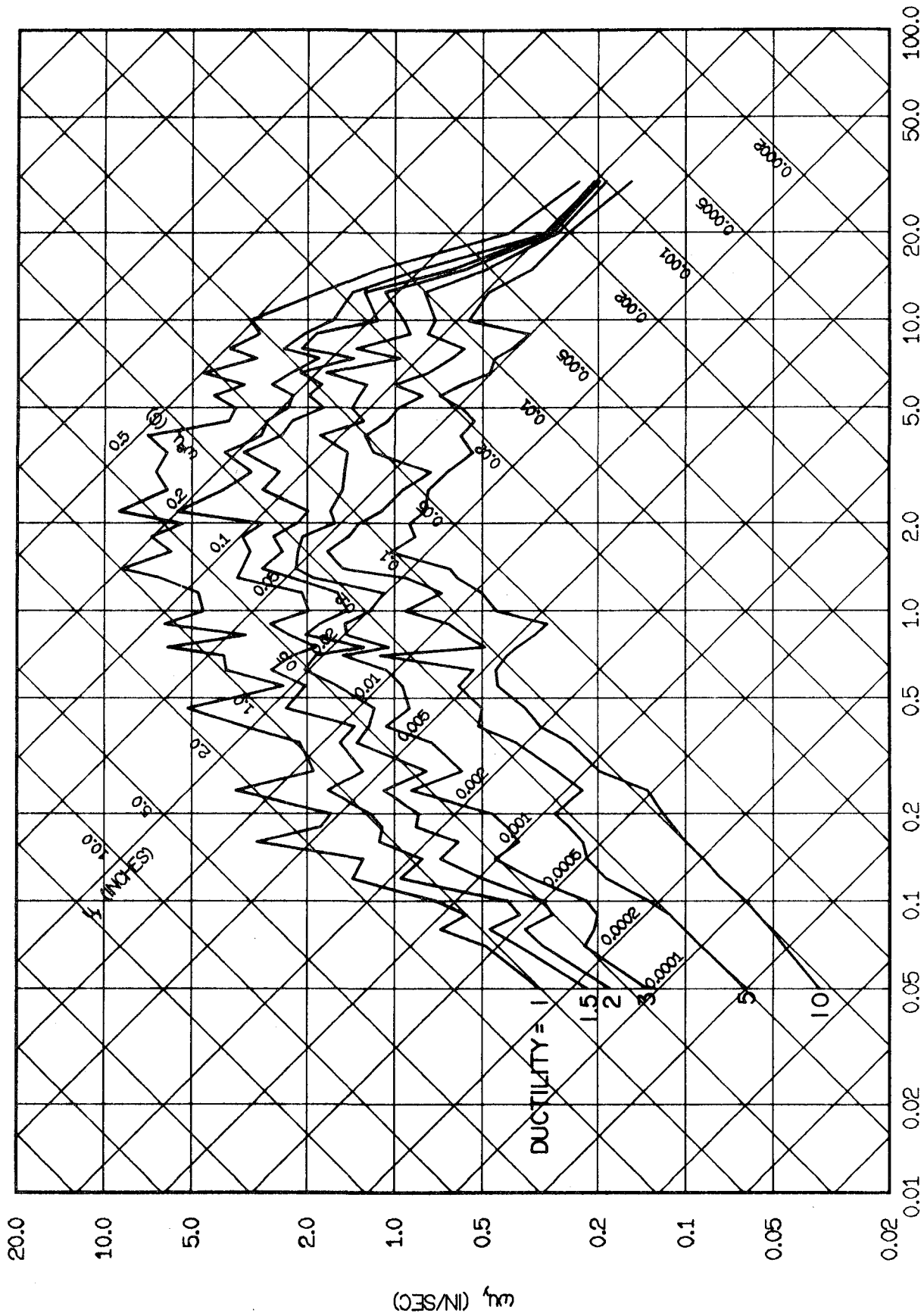
FIG. 3.61   INELASTIC YIELD SPECTRA FOR LIMA, MAY 31, 1970, N82W. ELASTOPLASTIC
SYSTEMS WITH 2% DAMPING.

FIG. 3.62 INELASTIC YIELD SPECTRA FOR LIMA, MAY 31, 1970, N82W. ELASTOPLASTIC SYSTEMS WITH 5% DAMPING.
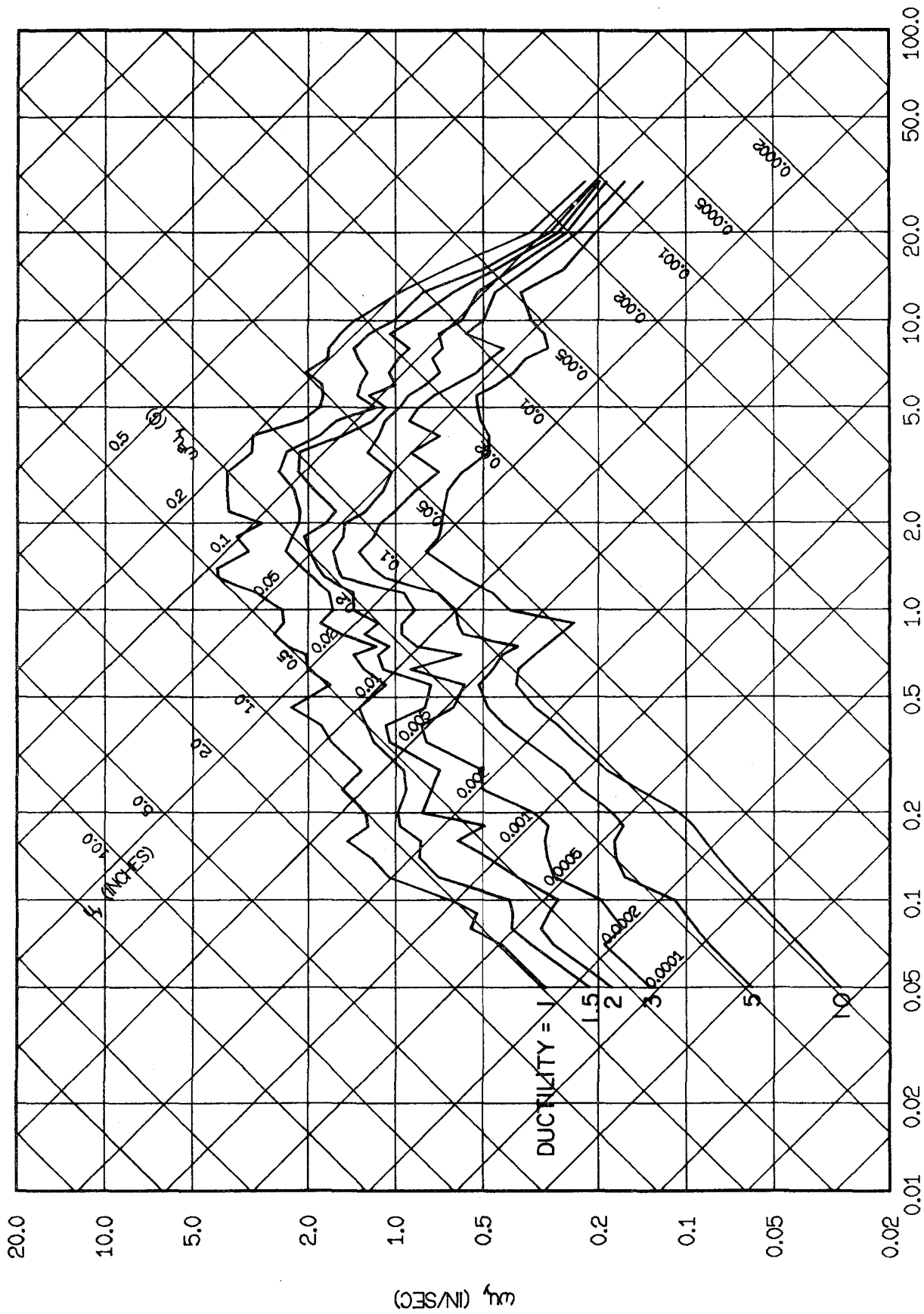
FIG. 3.63   INELASTIC YIELD SPECTRA FOR LIMA, MAY 31, 1970, N82W.   ELASTOPLASTIC SYSTEMS WITH 10% DAMPING.
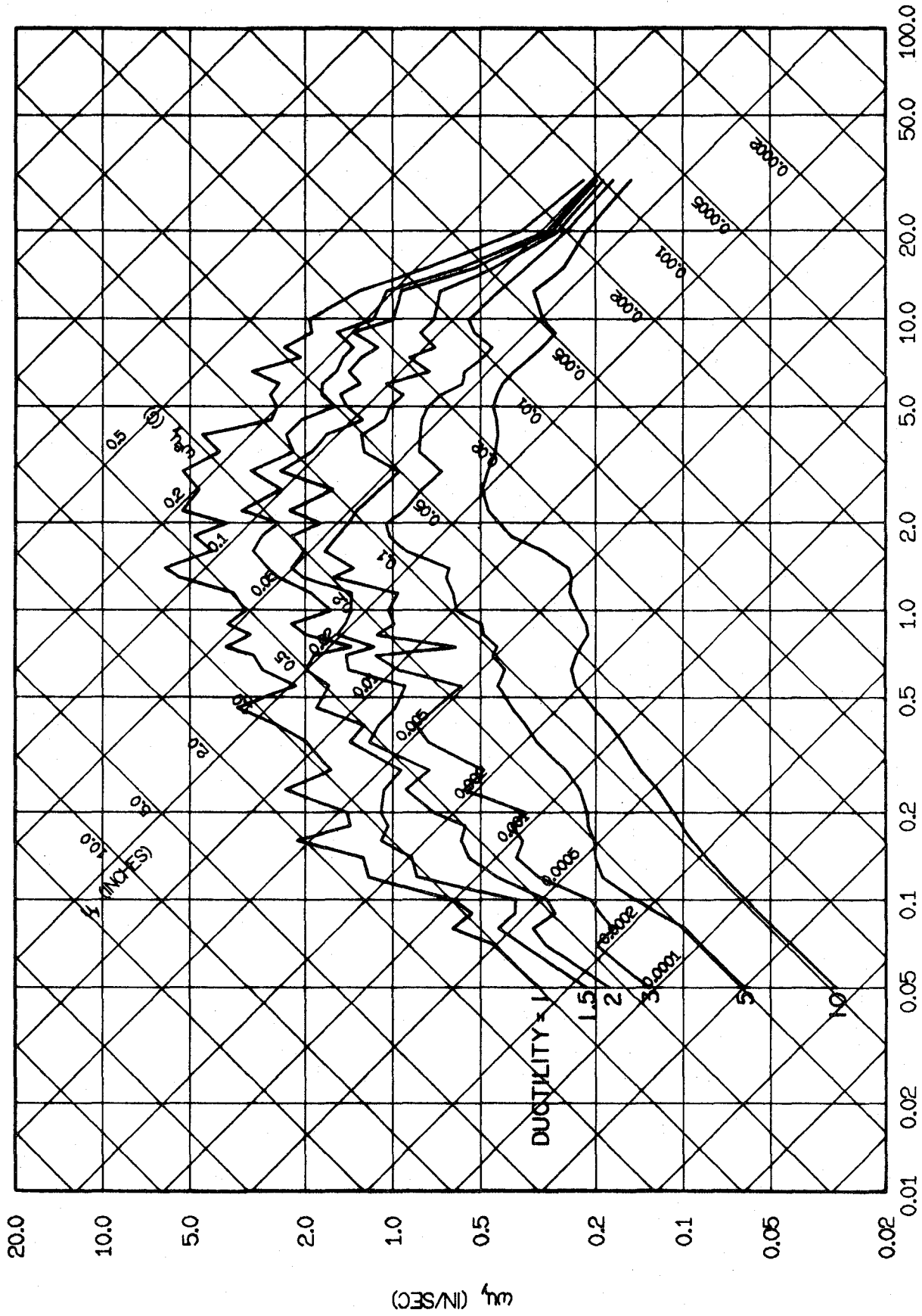
FIG. 3.64 INELASTIC YIELD SPECTRA FOR LIMA, MAY 31, 1970, N82W. BILINEAR
SYSTEMS WITH 5% DAMPING.
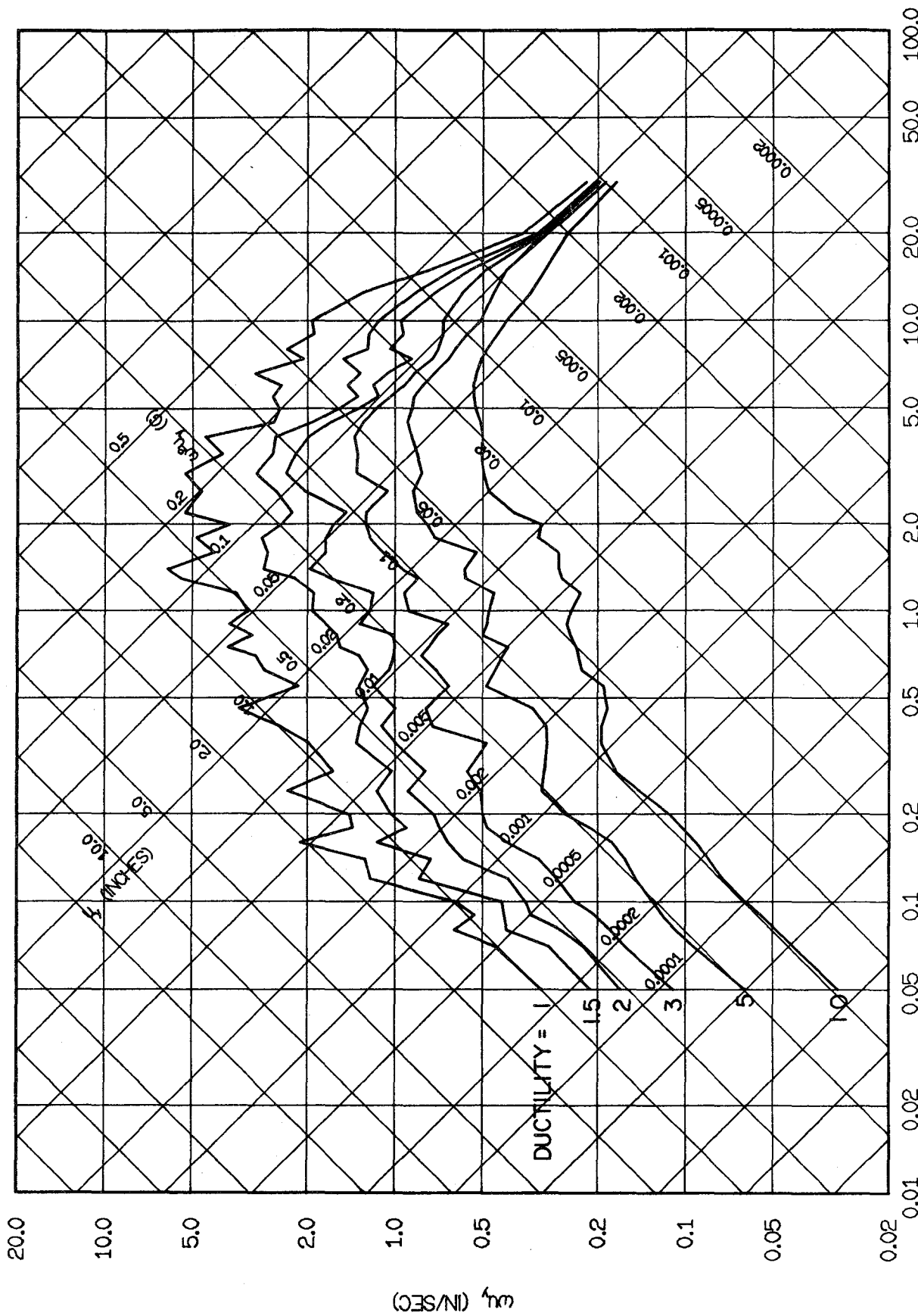
FIG. 3.65   INELASTIC YIELD SPECTRA FOR LIMA, MAY 31, 1970, N82W.   DEGRADING SYSTEMS WITH 5% DAMPING.
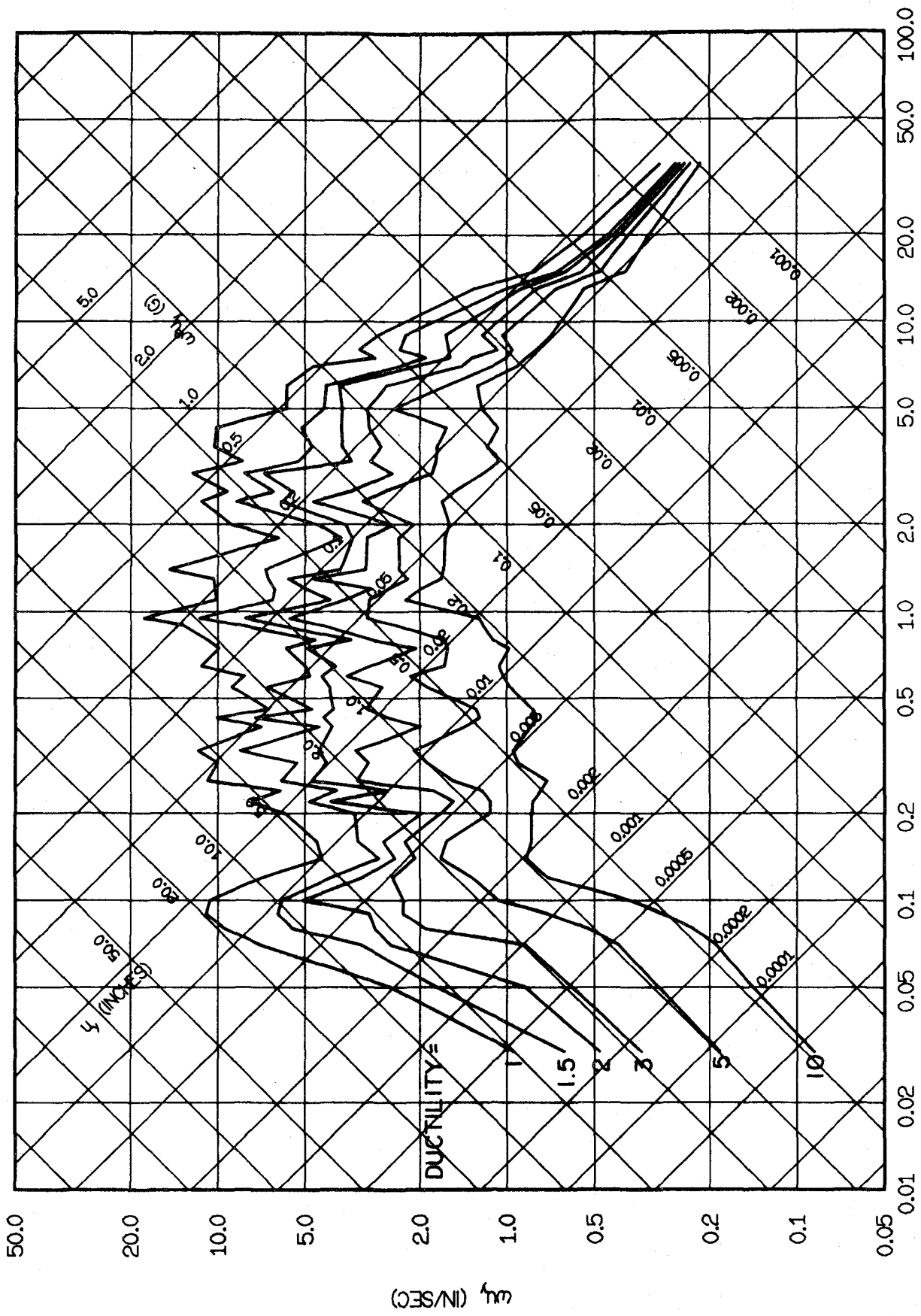
FIG. 3.66 INELASTIC YIELD SPECTRA FOR SANTIAGO, JULY 8, 1971, N10W. ELASTOPLASTIC SYSTEMS WITH 2% DAMPING.
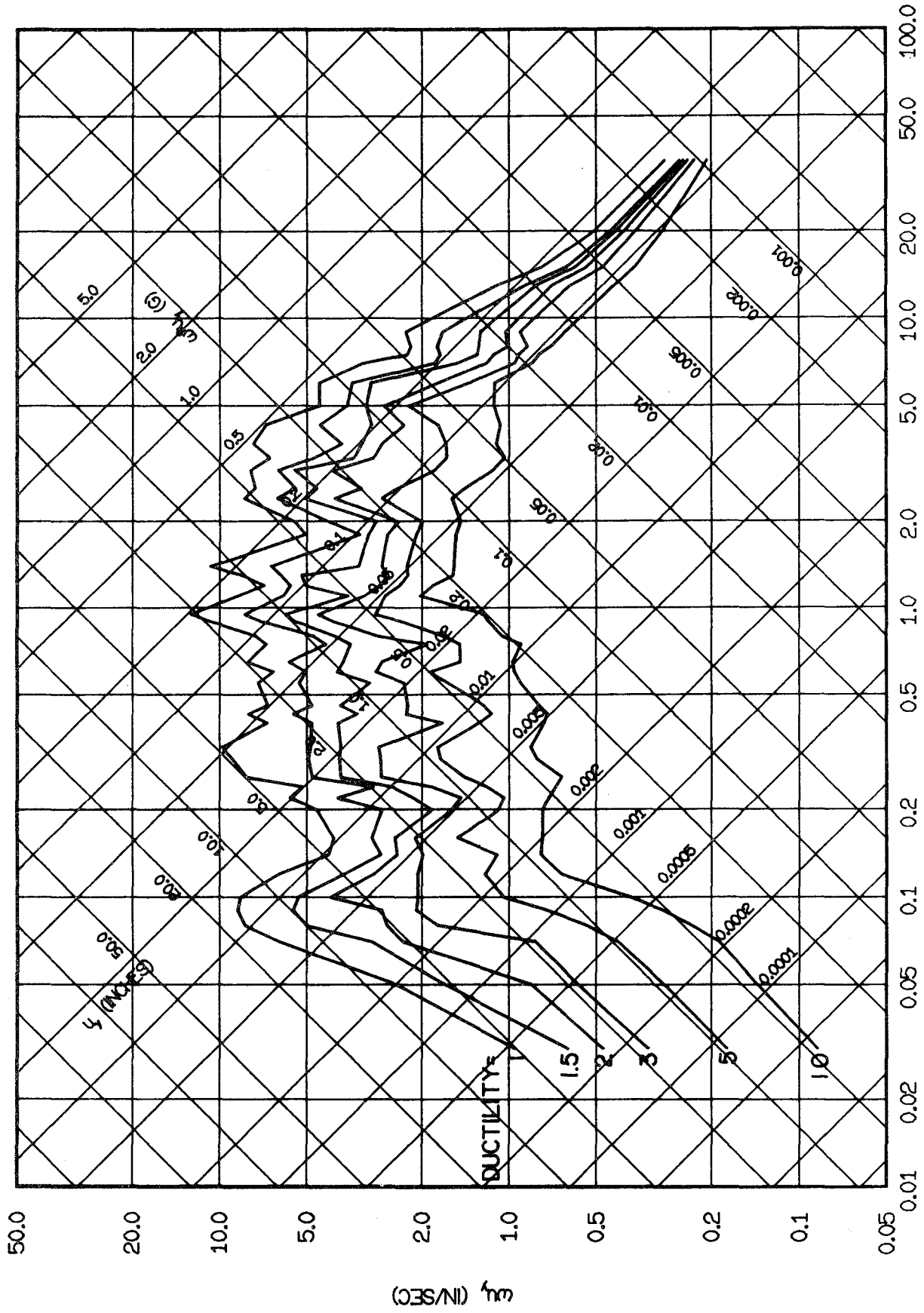
FIG. 3.67 INELASTIC YIELD SPECTRA FOR SANTIAGO, JULY 8, 1971, N10W. ELASTOPLASTIC SYSTEMS WITH 5% DAMPING.
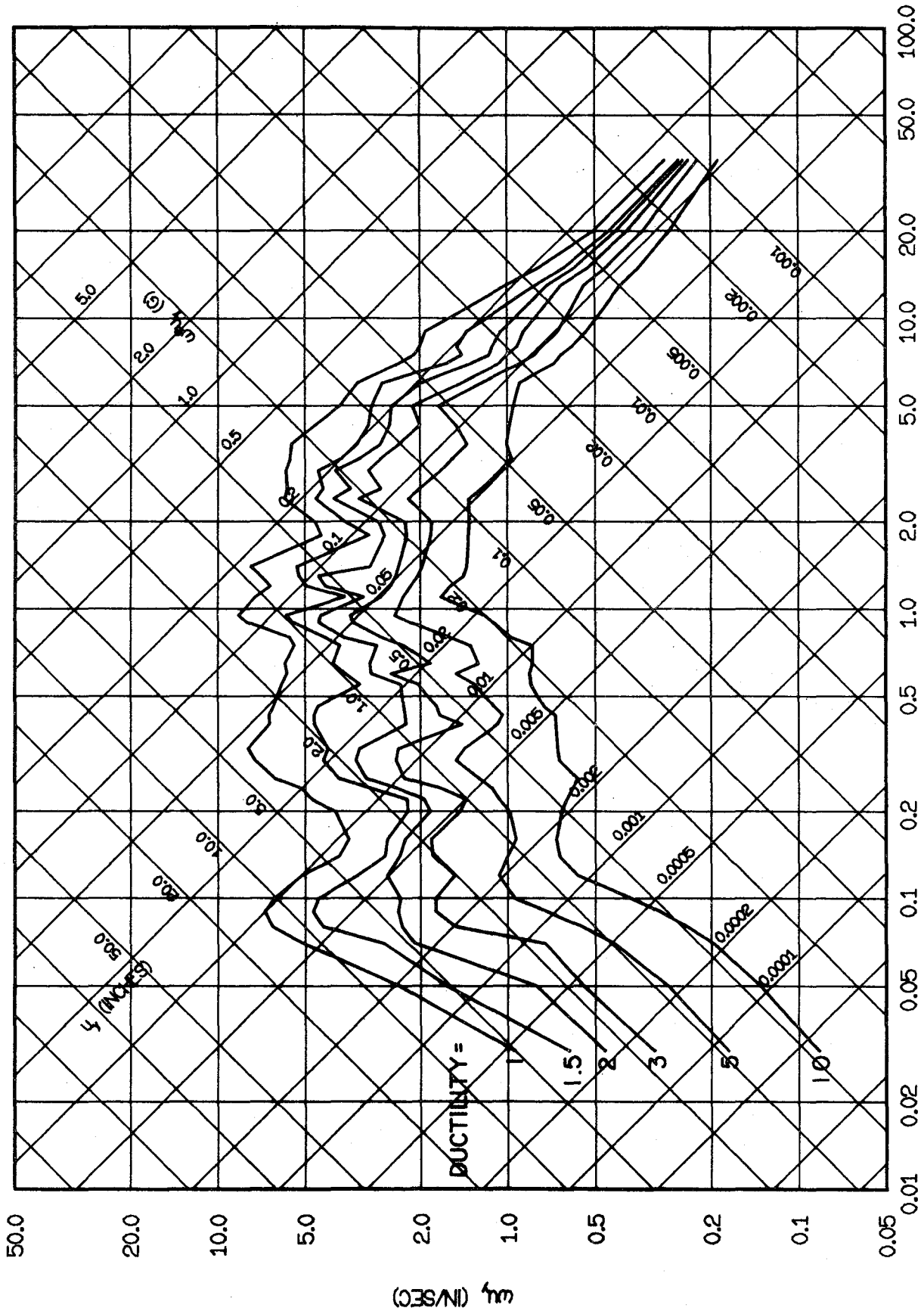
FIG. 3.68   INELASTIC YIELD SPECTRA FOR SANTIAGO, JULY 8, 1971, N10W.   ELASTOPLASTIC
SYSTEMS WITH 10% DAMPING.
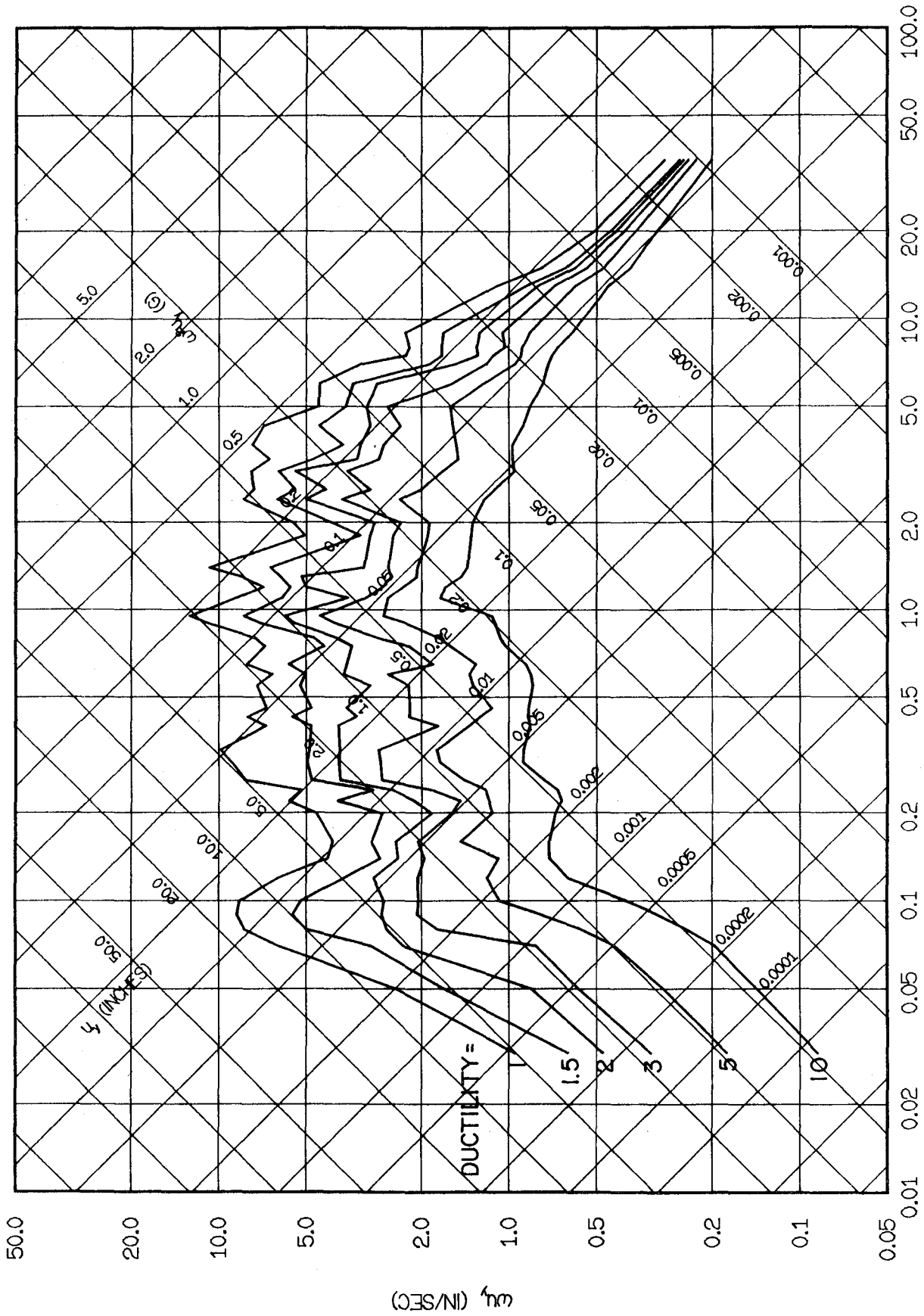
FIG. 3.69   INELASTIC YIELD SPECTRA FOR SANTIAGO, JULY 8, 1971, N10W.   BILINEAR
SYSTEMS WITH 5% DAMPING.
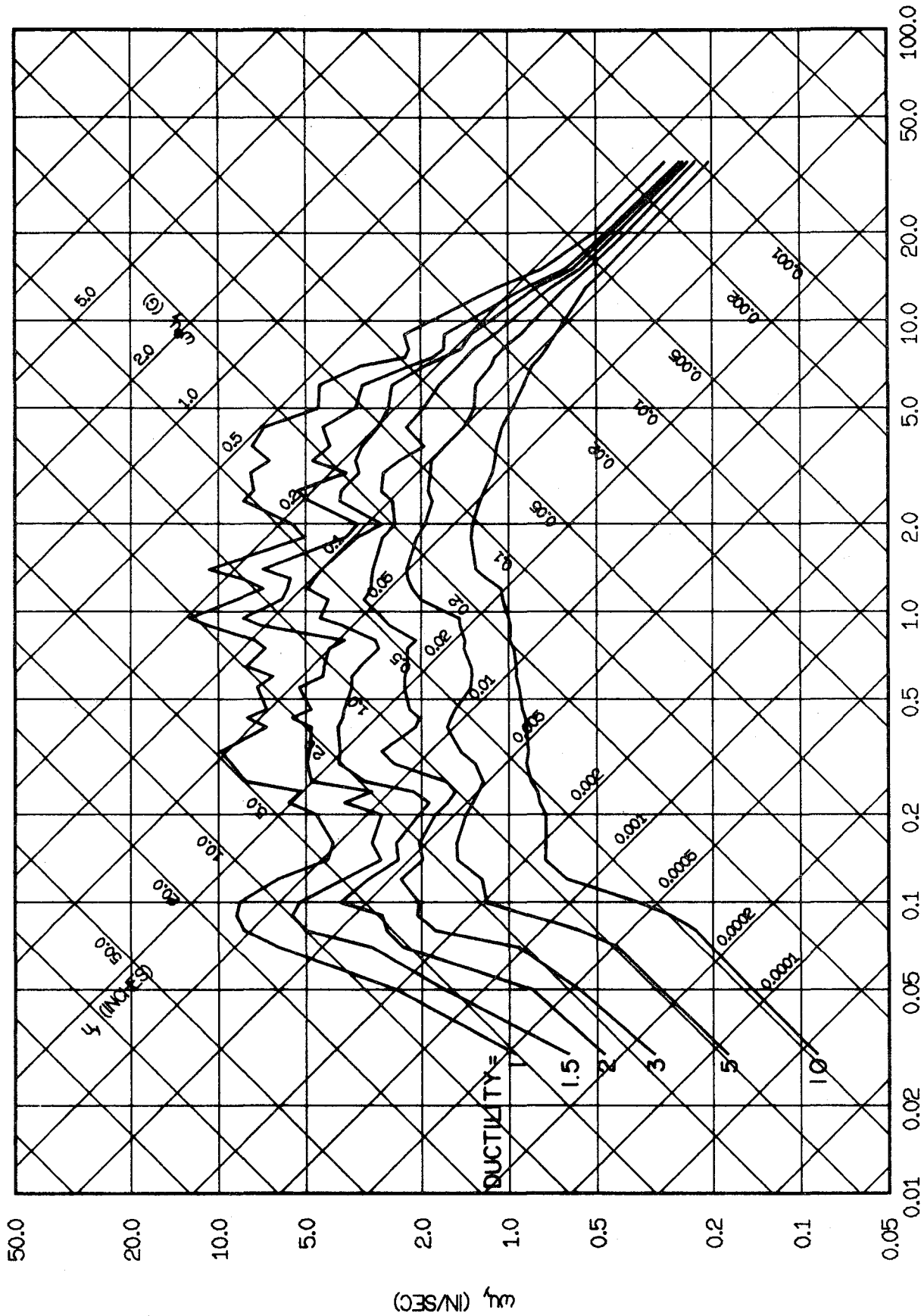
FIG. 3.70 INELASTIC YIELD SPECTRA FOR SANTIAGO, JULY 8, 1971, N10W. DEGRADING
SYSTEMS WITH 5% DAMPING.
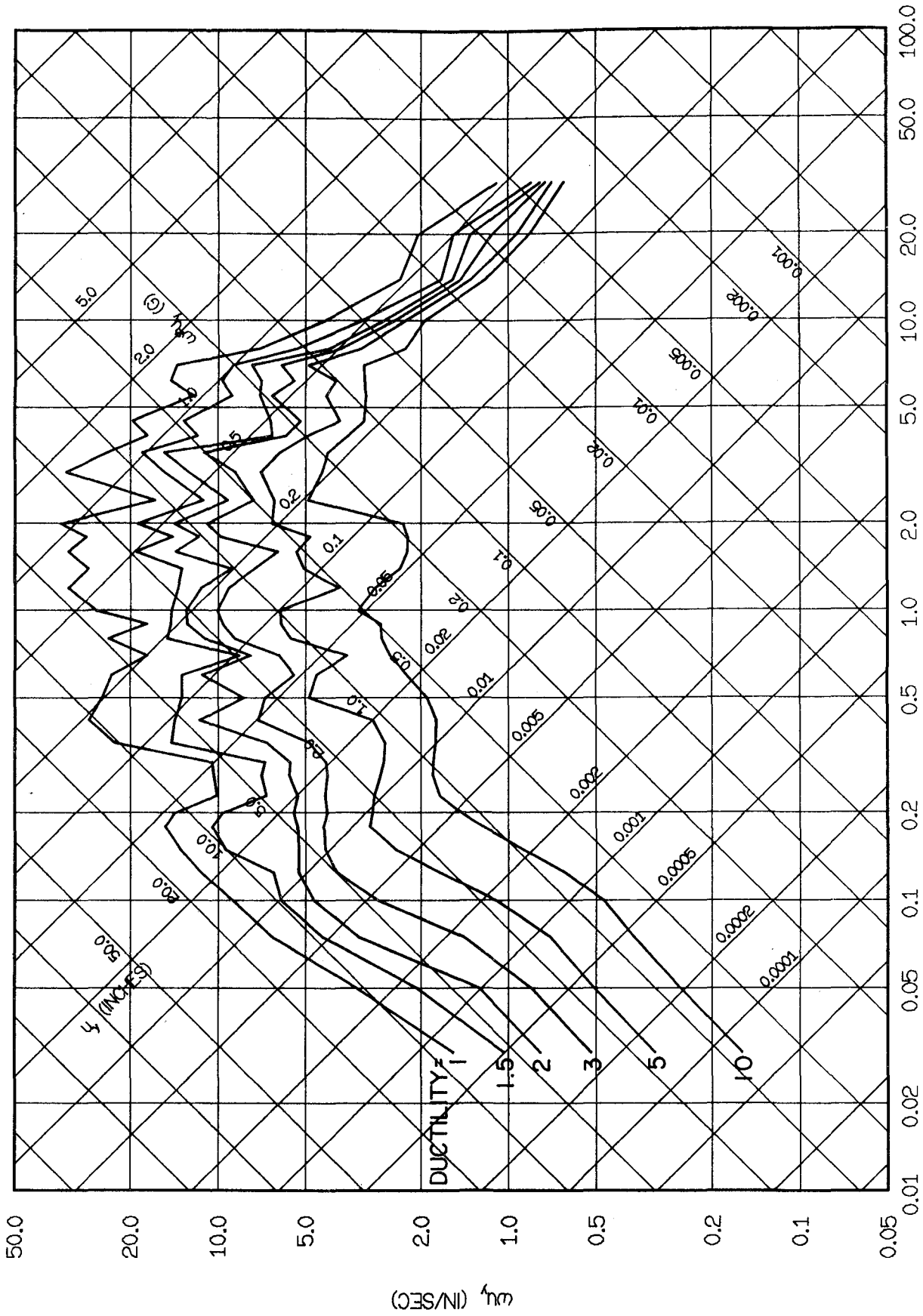
FIG. 3.71 INELASTIC YIELD SPECTRA FOR MANAGUA, DECEMBER 23, 1972, E-W. ELASTOPLASTIC SYSTEMS WITH 2% DAMPING.

205
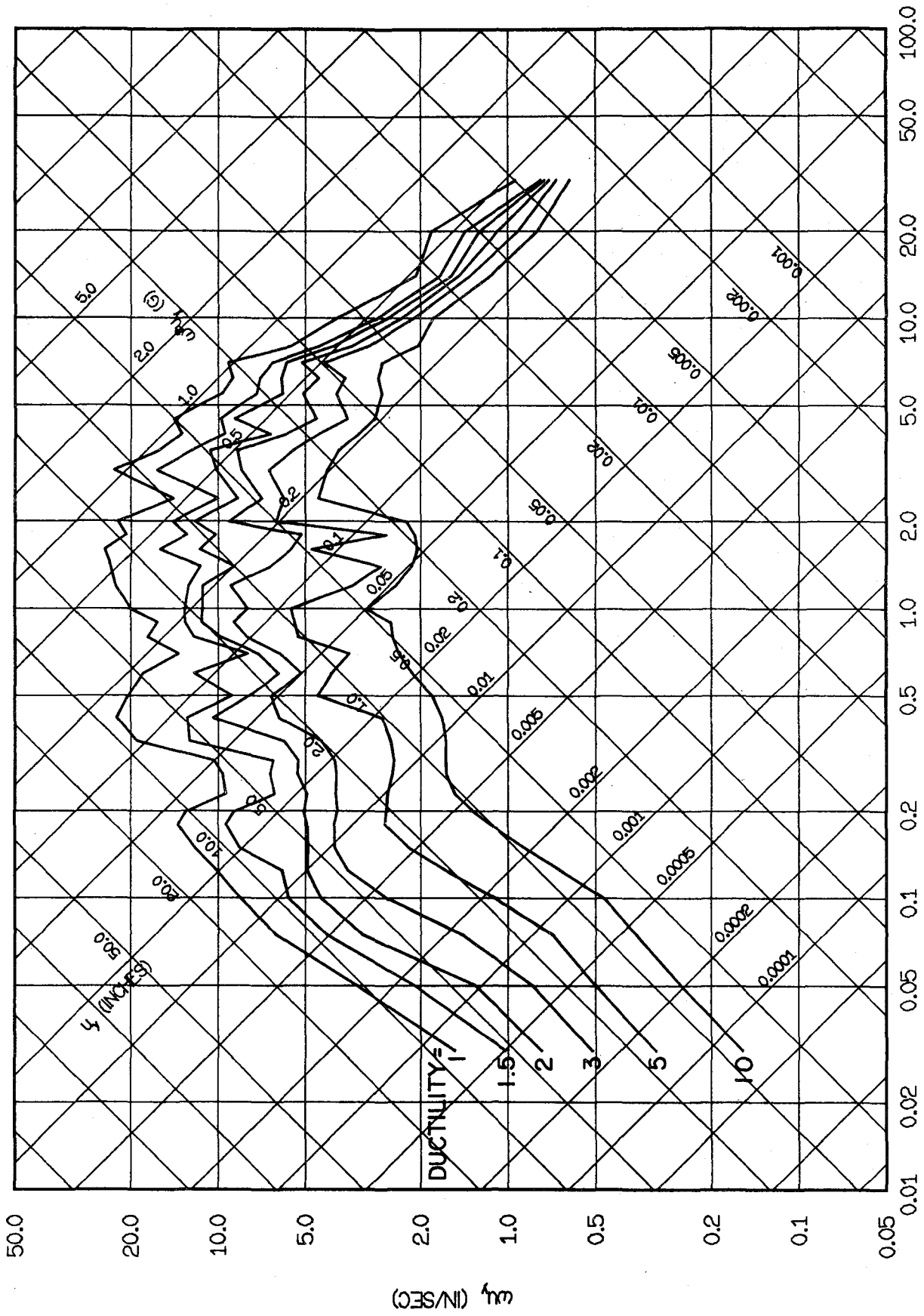
FIG. 3.72 INELASTIC YIELD SPECTRA FOR MANAGUA, DECEMBER 23, 1972, E-W. ELASTOPLASTIC SYSTEMS WITH 5% DAMPING.
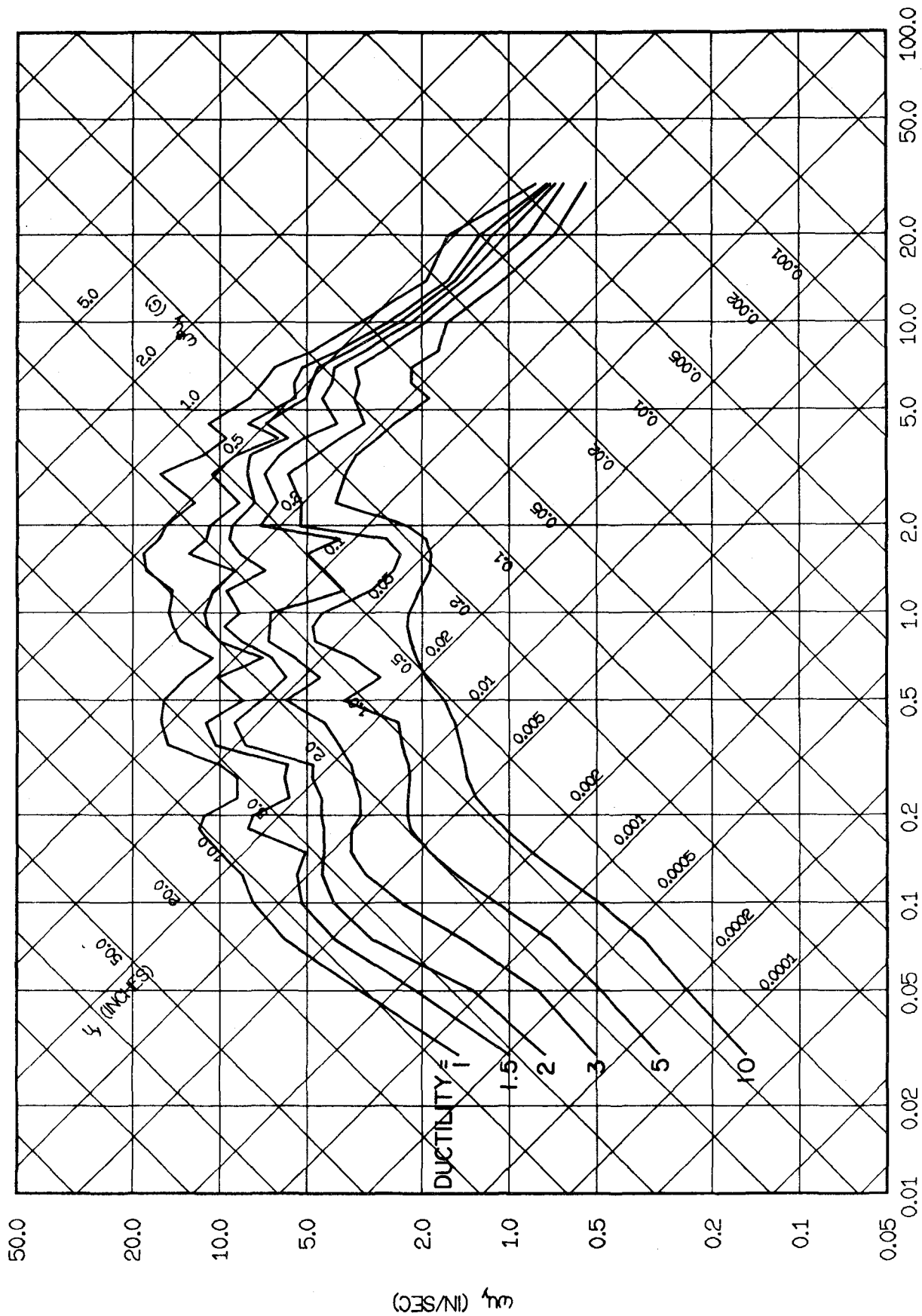
FIG. 3.73 INELASTIC YIELD SPECTRA FOR MANAGUA, DECEMBER 23, 1972, E-W. ELASTOPLASTIC SYSTEMS WITH 10% DAMPING.
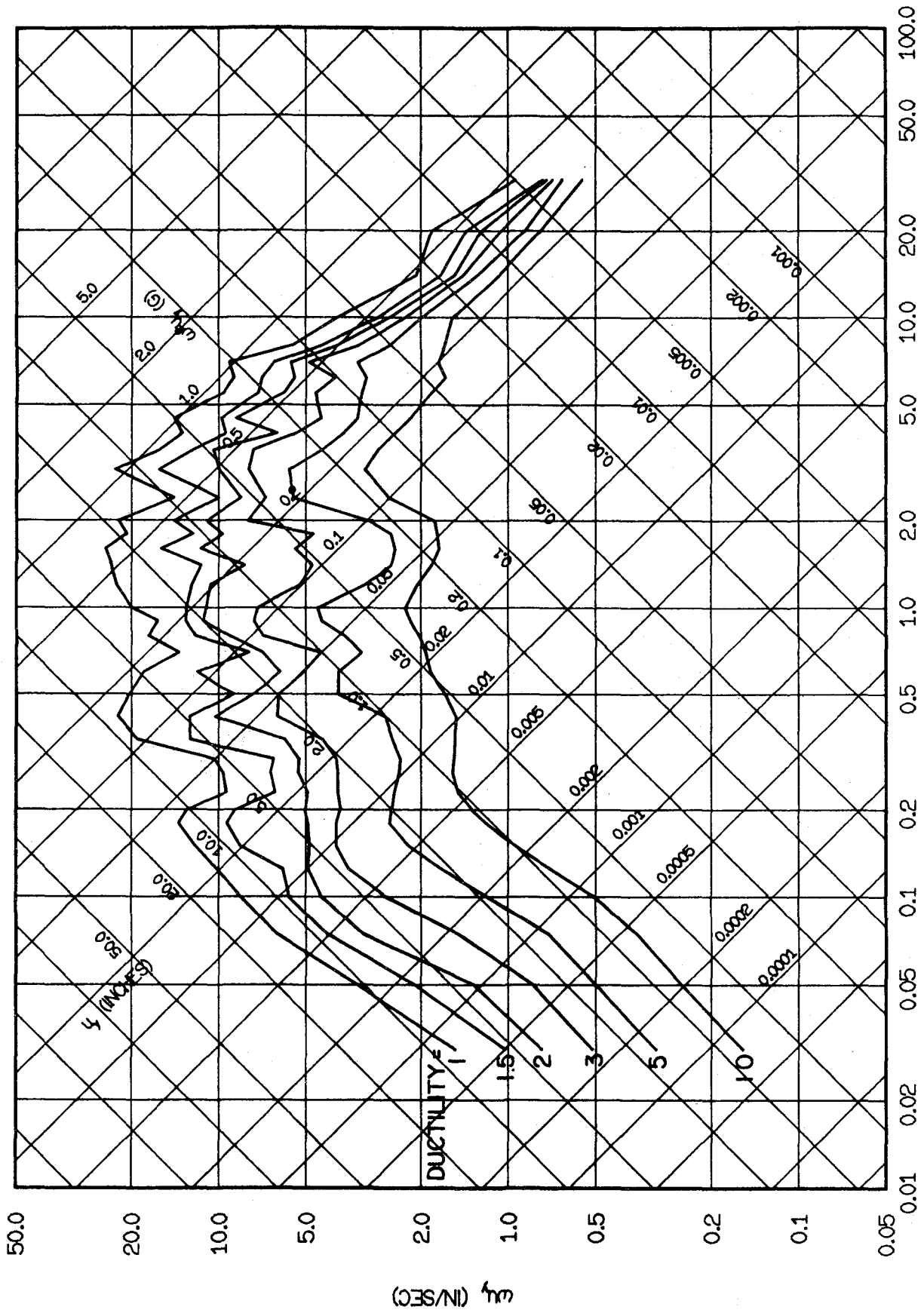
FIG. 3.74 INELASTIC YIELD SPECTRA FOR MANAGUA, DECEMBER 23, 1972, E-W. BILINEAR SYSTEMS WITH 5% DAMPING.
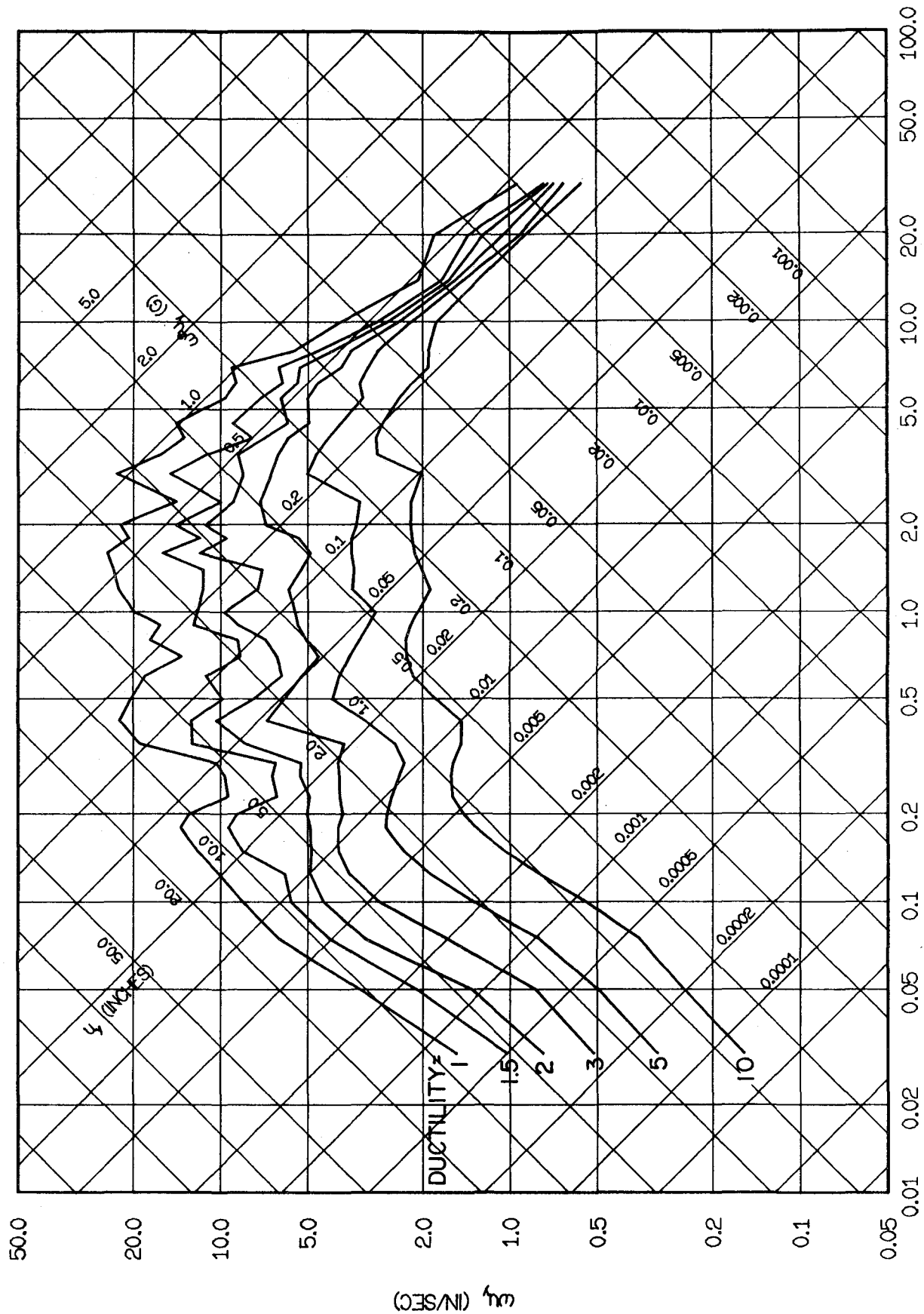
FIG. 3.75   INELASTIC YIELD SPECTRA FOR MANAGUA, DECEMBER 23, 1972, E-W.   DEGRADING SYSTEMS WITH 5% DAMPING.
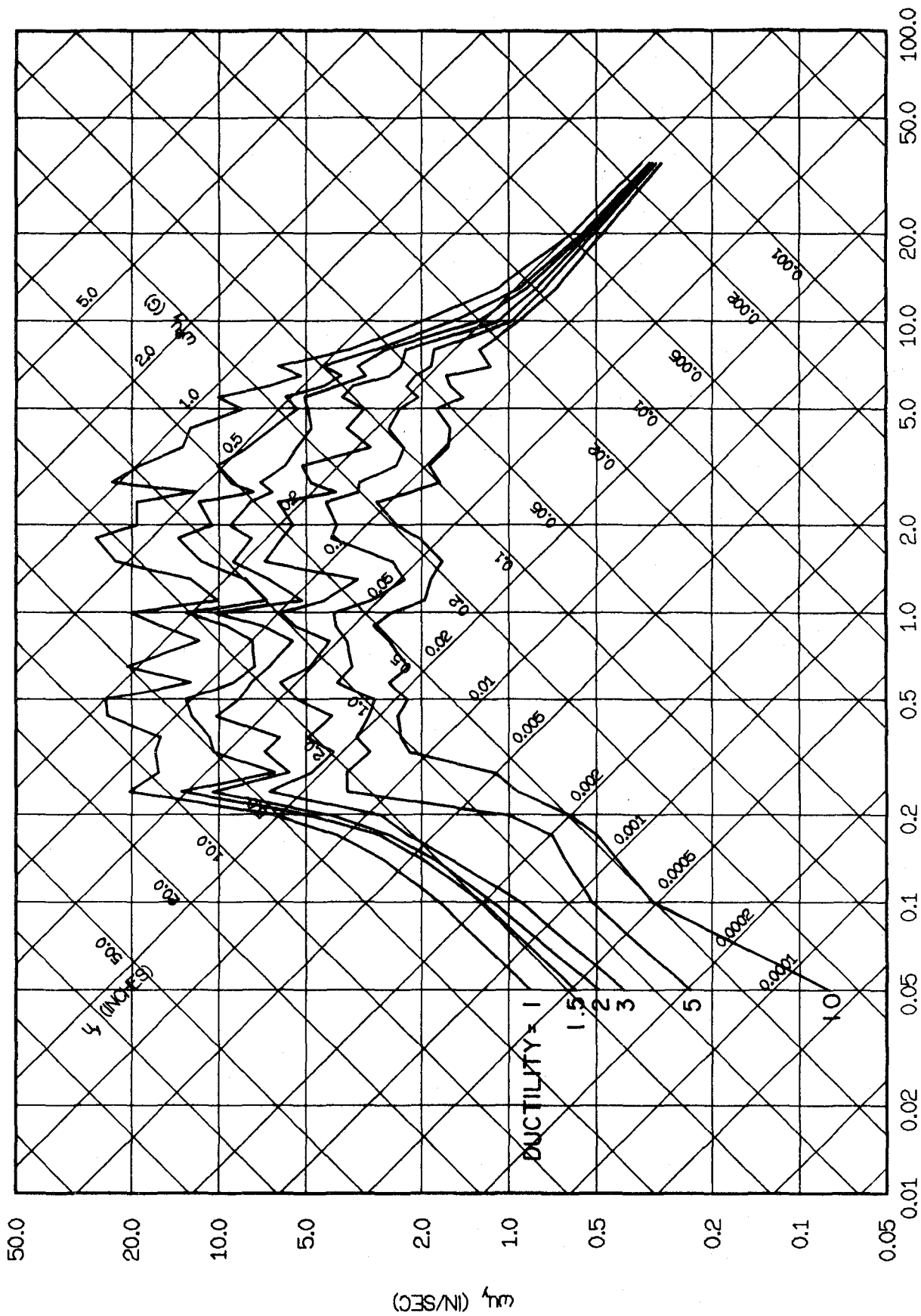
FIG. 3.76 INELASTIC YIELD SPECTRA FOR SAN JUAN, NOVEMBER 23, 1977, E-W. ELASTOPLASTIC SYSTEMS WITH 2% DAMPING.
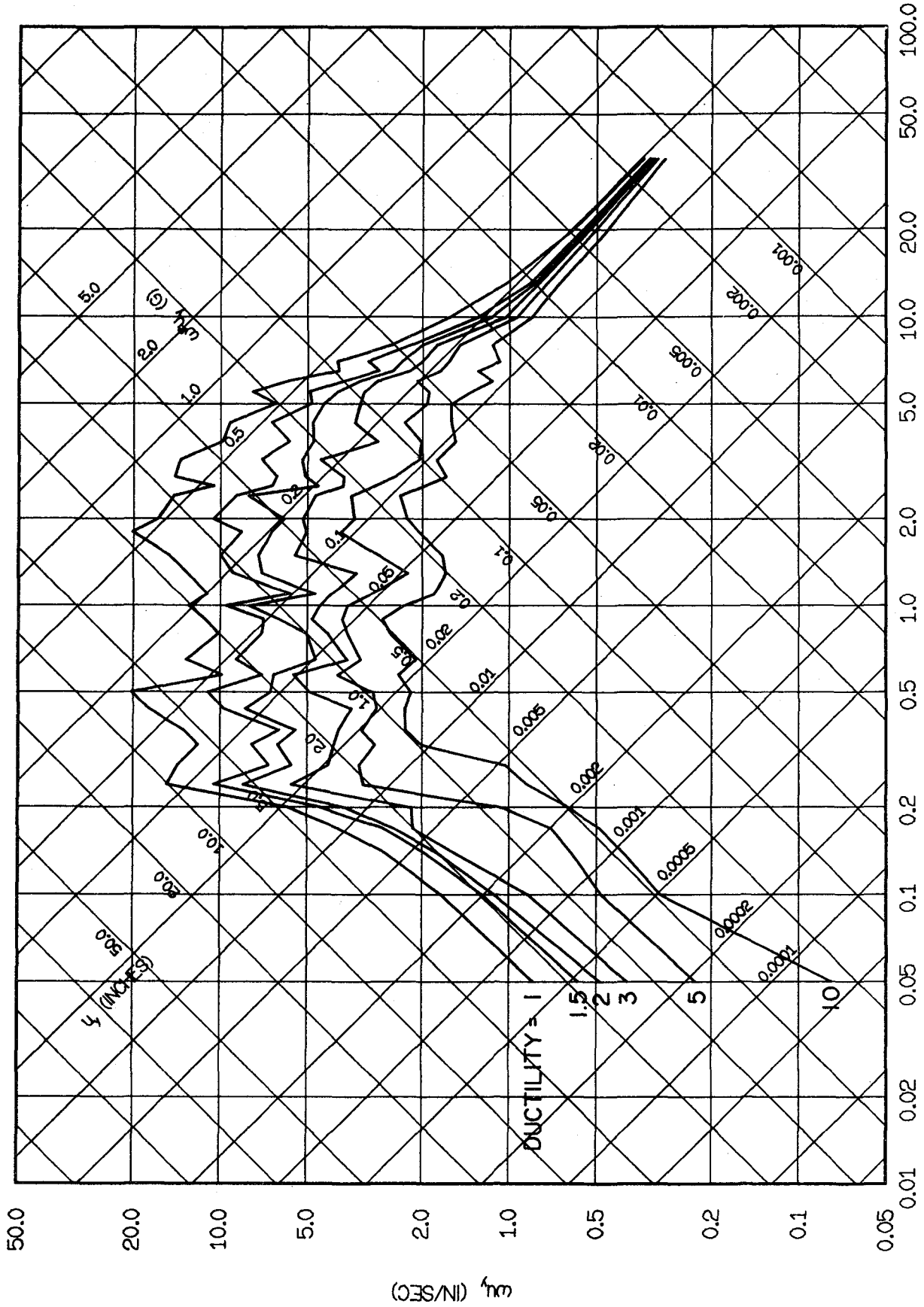
FIG. 3.77 INELASTIC YIELD SPECTRA FOR SAN JUAN, NOVEMBER 23, 1977, E-W. ELASTOPLASTIC SYSTEMS WITH 5% DAMPING.
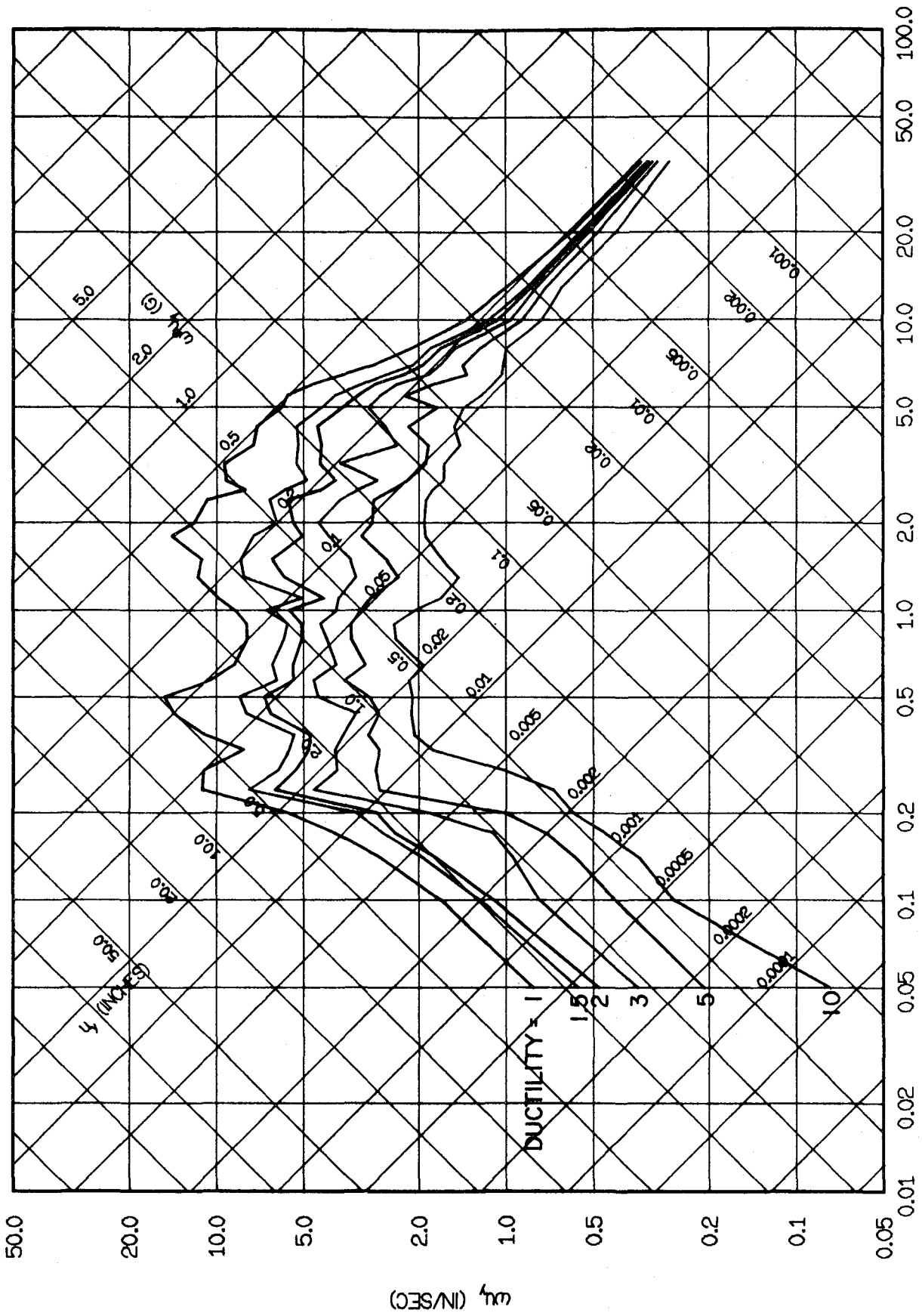
FIG. 3.78   INELASTIC YIELD SPECTRA FOR SAN JUAN, NOVEMBER 23, 1977, E-W.   ELASTOPLASTIC SYSTEMS WITH 10% DAMPING.
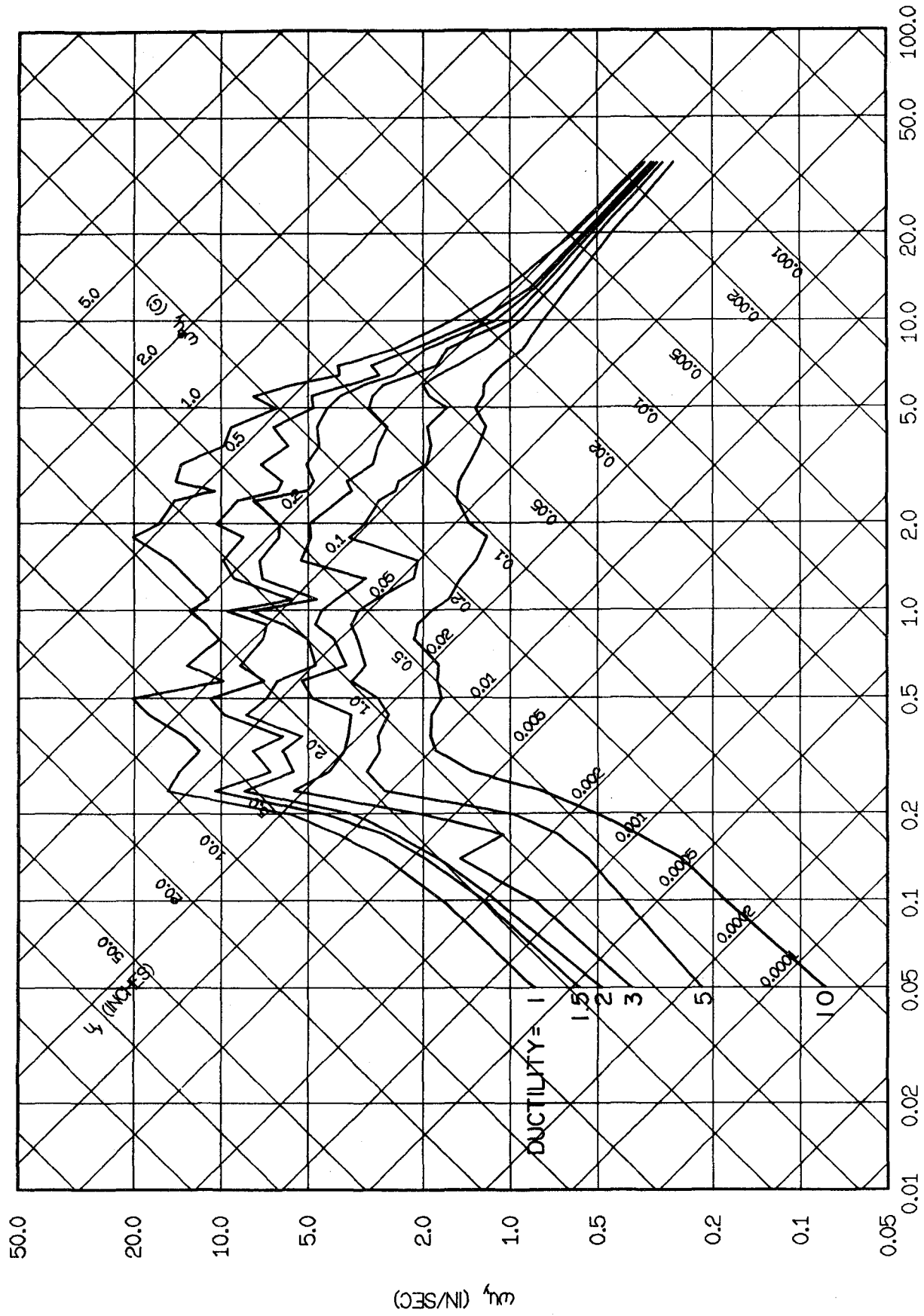
FIG. 3.79 INELASTIC YIELD SPECTRA FOR SAN JUAN, NOVEMBER 23, 1977, E-W. BILINEAR SYSTEMS WITH 5% DAMPING.
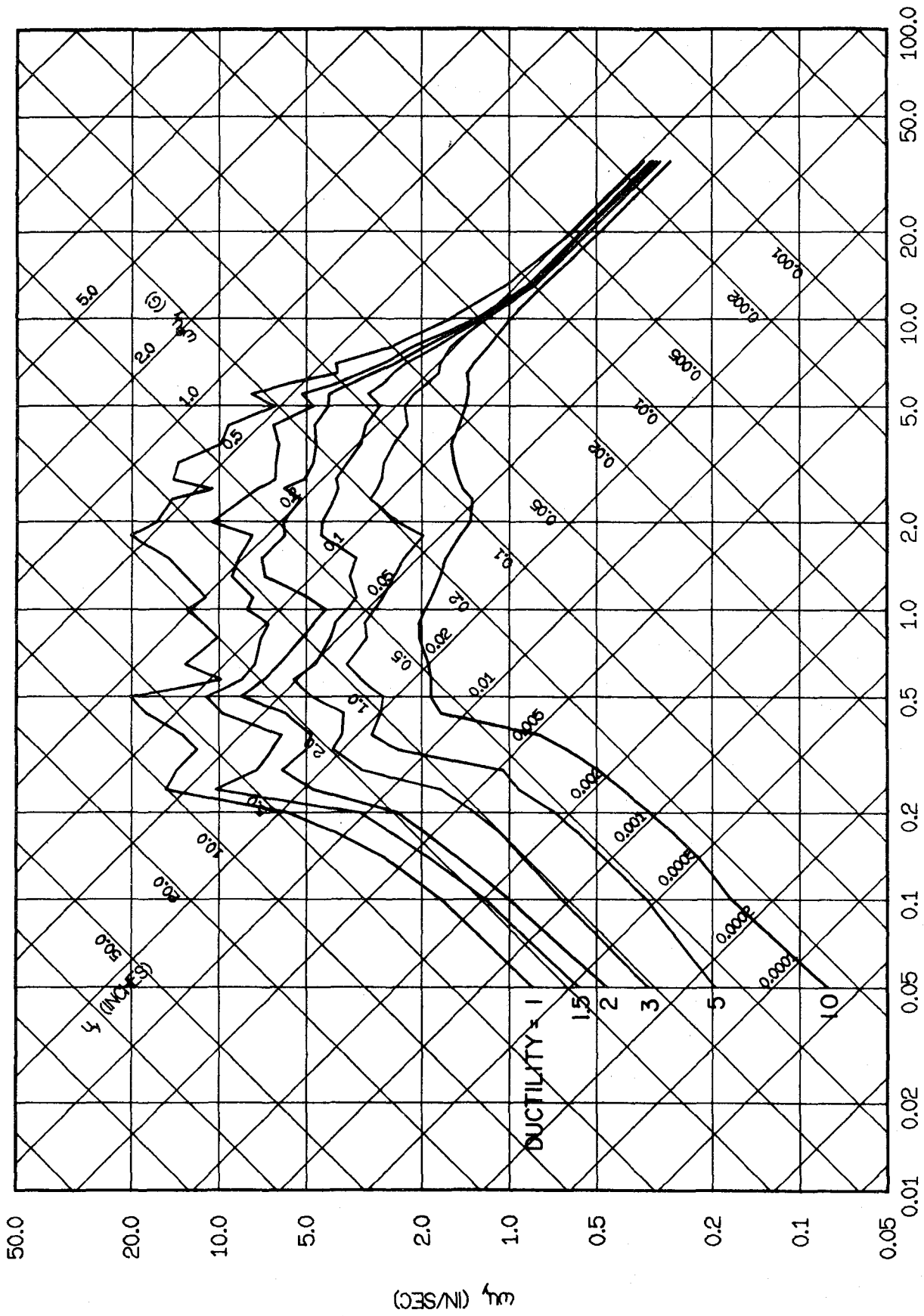
FIG. 3.80   INELASTIC YIELD SPECTRA FOR SAN JUAN, NOVEMBER 23, 1977, E-W.   DEGRADING
SYSTEMS WITH 5% DAMPING.
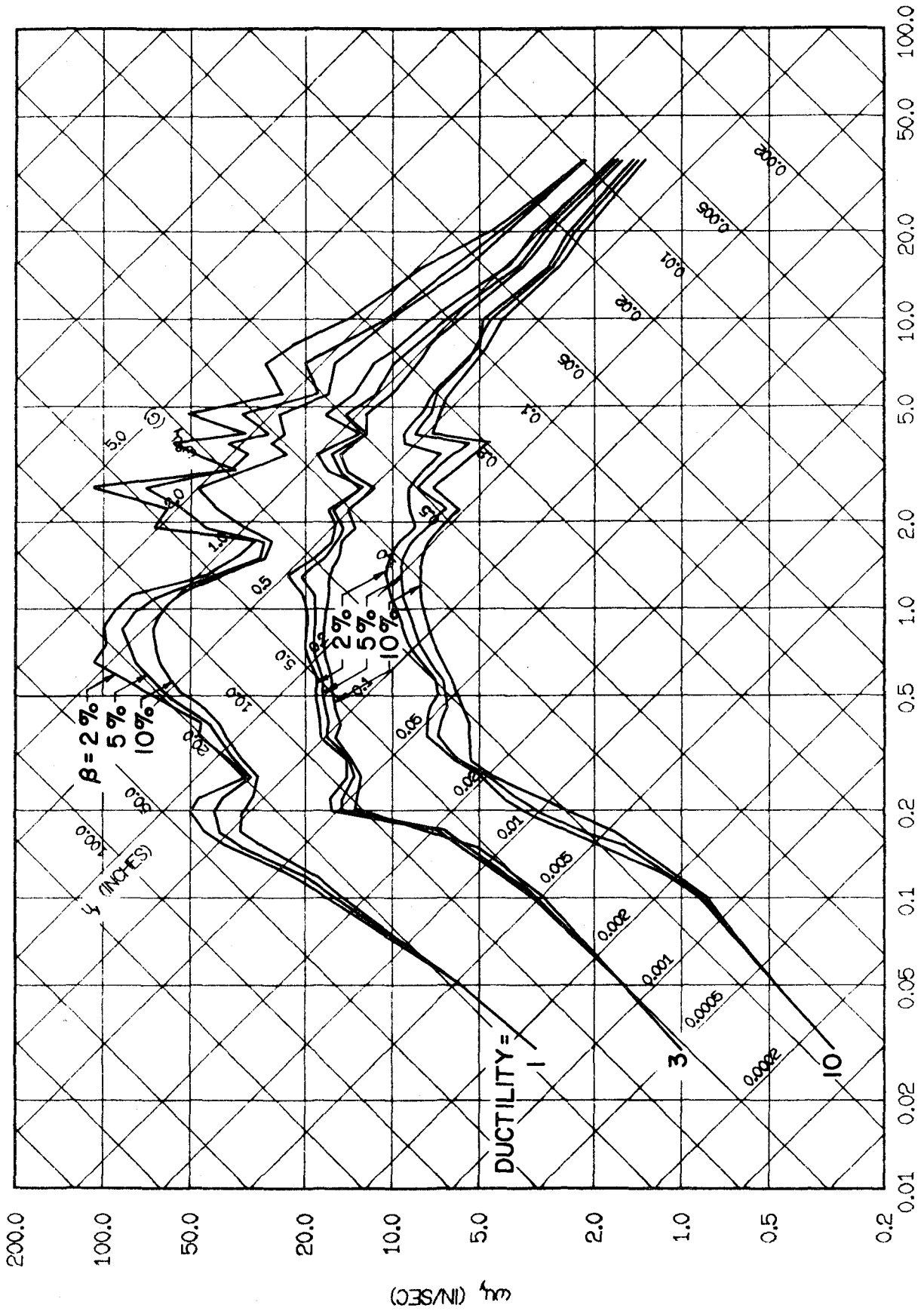
FIG. 3.81 COMPARISON OF INELASTIC SPECTRA FOR ELASTOPLASTIC SYSTEMS WITH 2, 5, AND 10% DAMPING, SUBJECTED TO PACOIMA, FEB. 9, 1971, S16E COMPONENT.
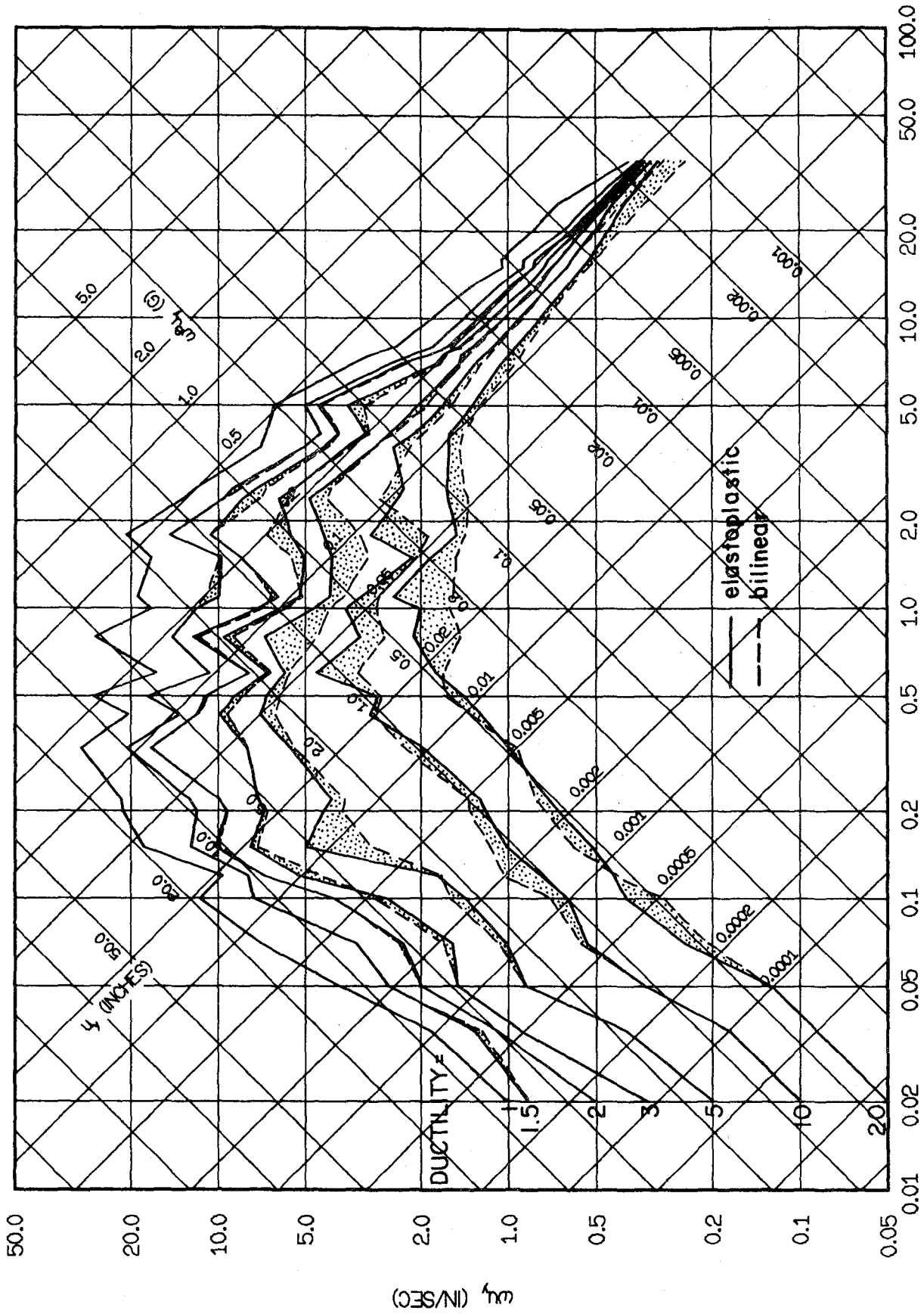
FIG. 3.82   COMPARISON OF INELASTIC SPECTRA FOR ELASTOPLASTIC AND BILINEAR SYSTEMS
WITH 5% DAMPING, SUBJECTED TO EL CENTRO, MAY 18, 1940, E-W COMPONENT.
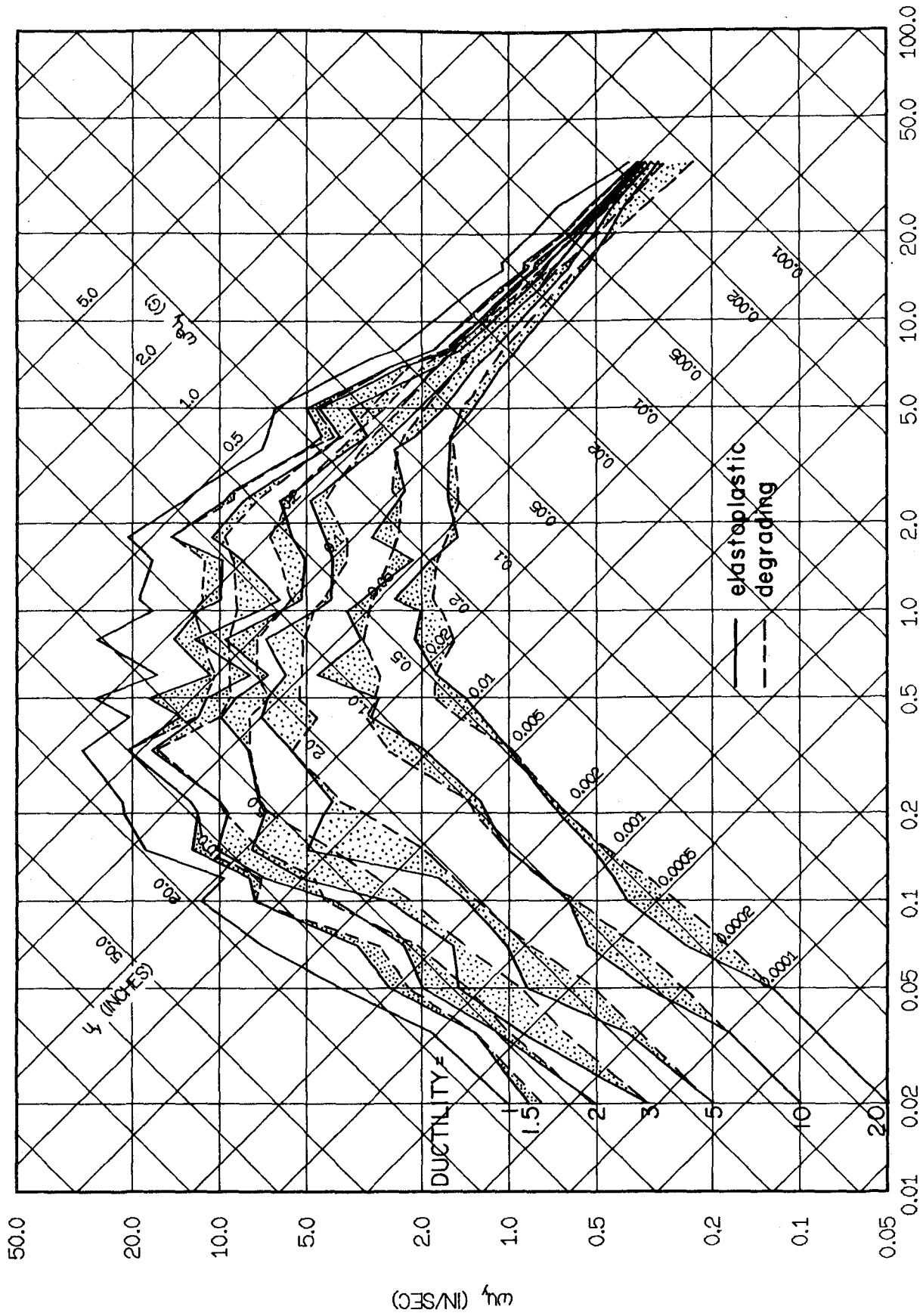
FIG. 3.83 COMPARISON OF INELASTIC SPECTRA FOR ELASTOPLASTIC AND DEGRADING SYSTEMS
WITH 5% DAMPING, SUBJECTED TO EL CENTRO, MAY 18, 1940, E-W COMPONENT.

FREQUENCY (CPS)
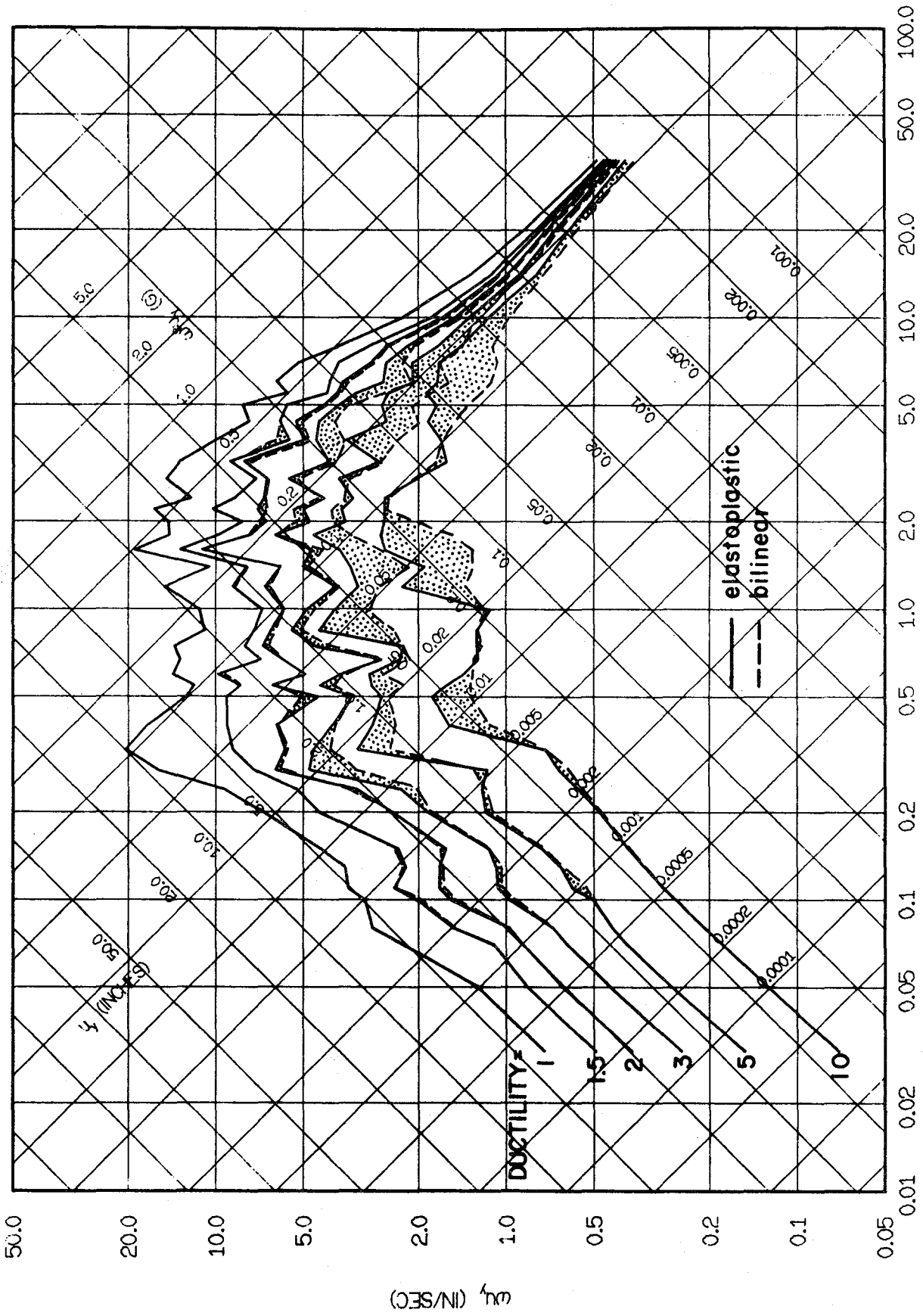
FIG. 3.84 COMPARISON OF INELASTIC SPECTRA FOR ELASTOPLASTIC AND BILINEAR SYSTEMS WITH 5% DAMPING, SUBJECTED TO OLYMPIA, APRIL 13, 1949, N86E COMPONENT.
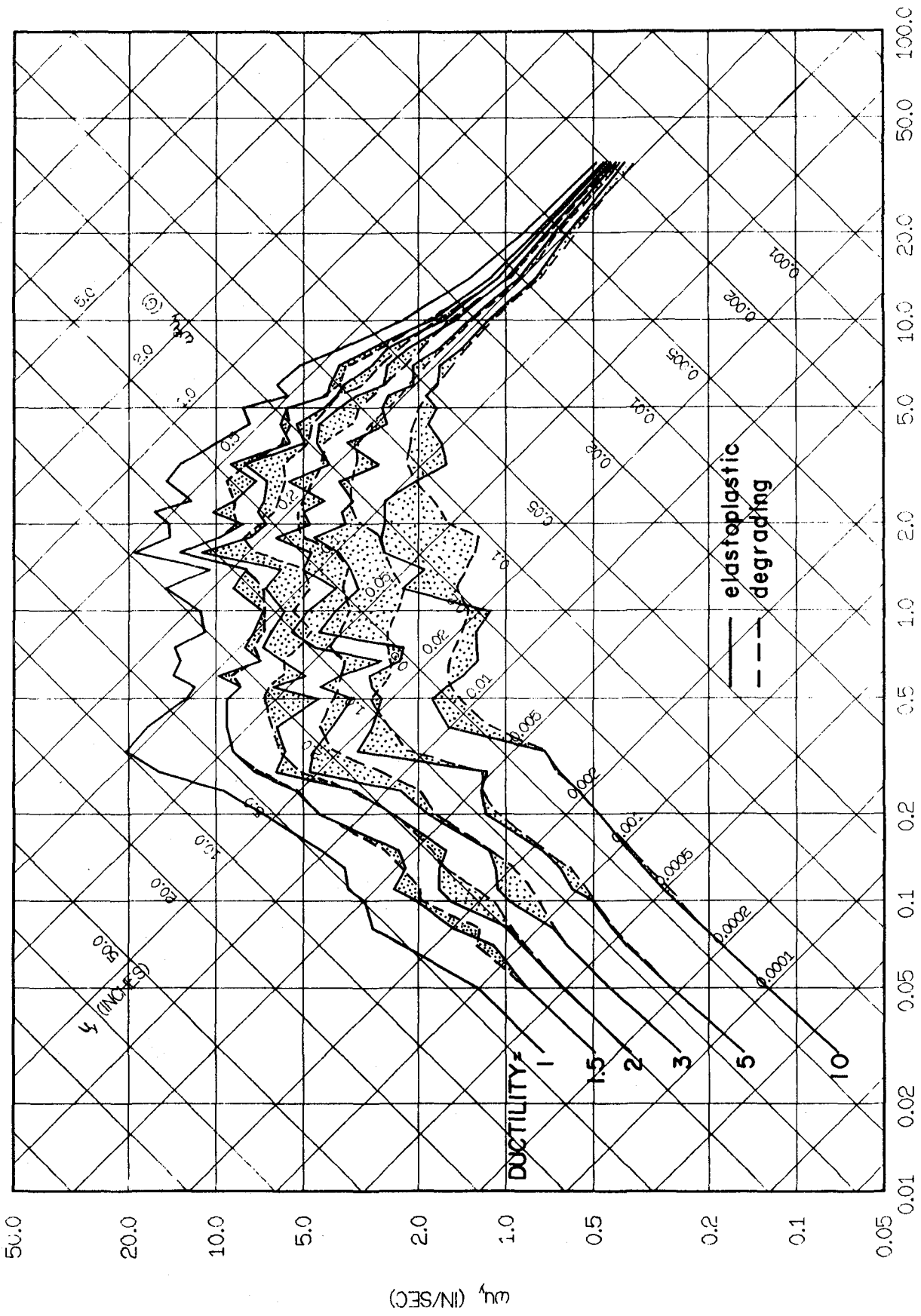
FIG. 3.85 COMPARISON OF INELASTIC SPECTRA FOR ELASTOPLASTIC AND DEGRADING SYSTEMS WITH 5% DAMPING, SUBJECTED TO OLYMPIA, APRIL 13, 1949, N86E COMPONENT.
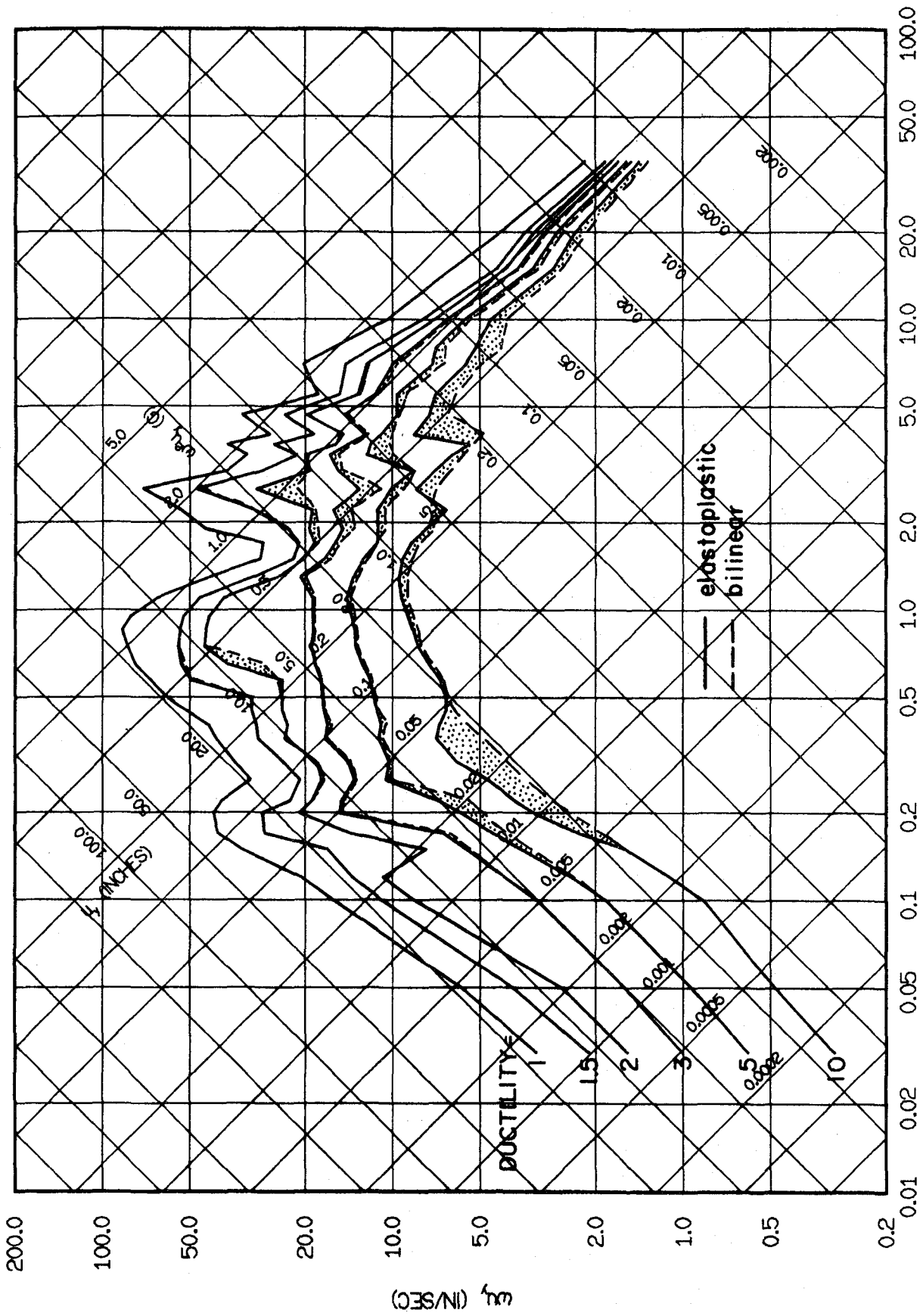
FIG. 3.86   COMPARISON OF INELASTIC SPECTRA FOR ELASTOPLASTIC AND BILINEAR SYSTEMS WITH 5% DAMPING, SUBJECTED TO PACOIMA, FEB. 9, 1971, S16E COMPONENT.
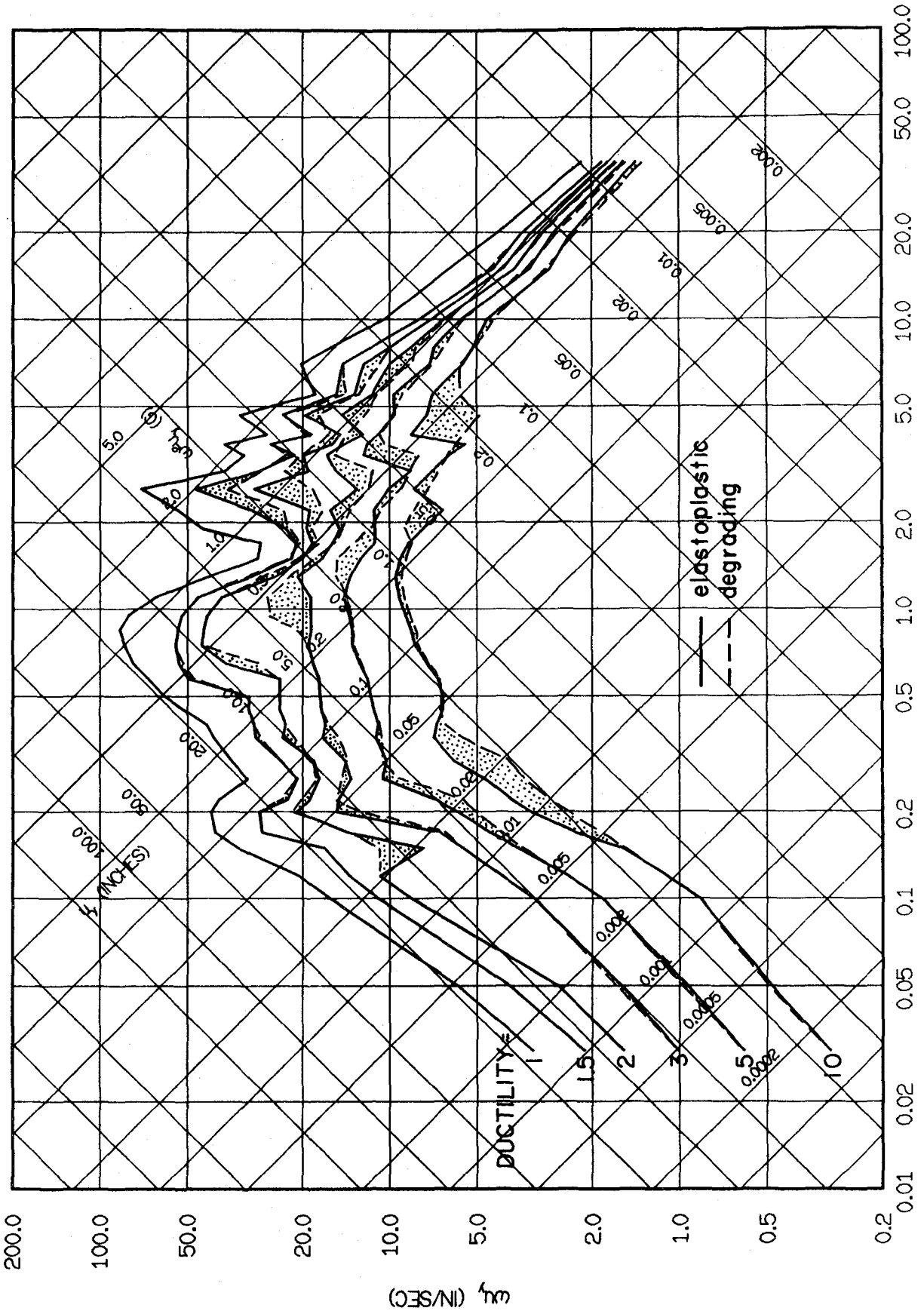
FIG. 3.87 COMPARISON OF INELASTIC SPECTRA FOR ELASTOPLASTIC AND DEGRADING SYSTEMS WITH 5% DAMPING, SUBJECTED TO PACOIMA, FEB. 9, 1971, S16E COMPONENT.
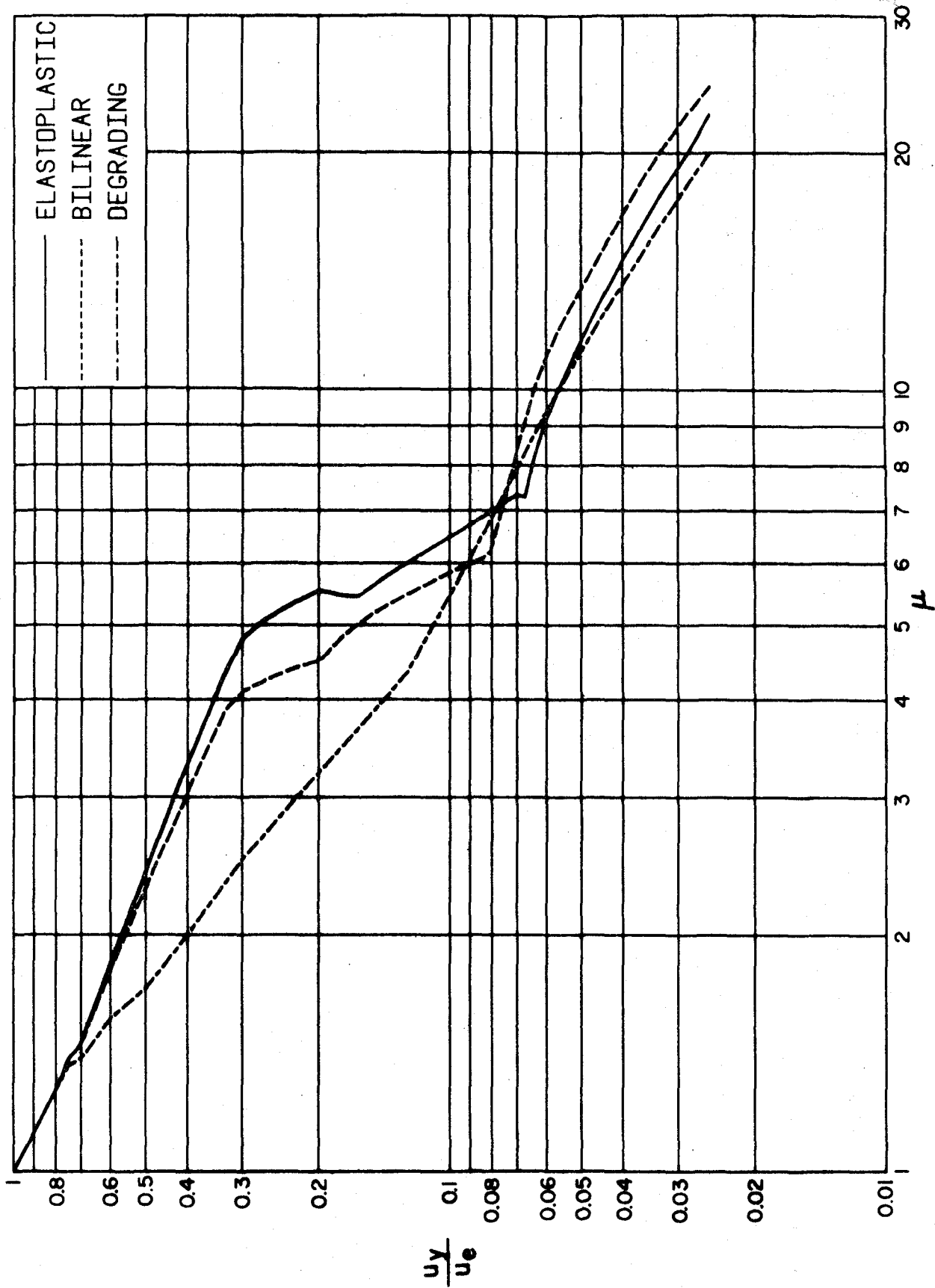
FIG. 3.88 VARIATION OF DUCTILITY WITH YIELD LEVEL FOR SYSTEMS WITH f = 0.15 HERTZ
AND 5% DAMPING, SUBJECTED TO EL CENTRO, MAY 18, 1940, E-W COMPONENT.
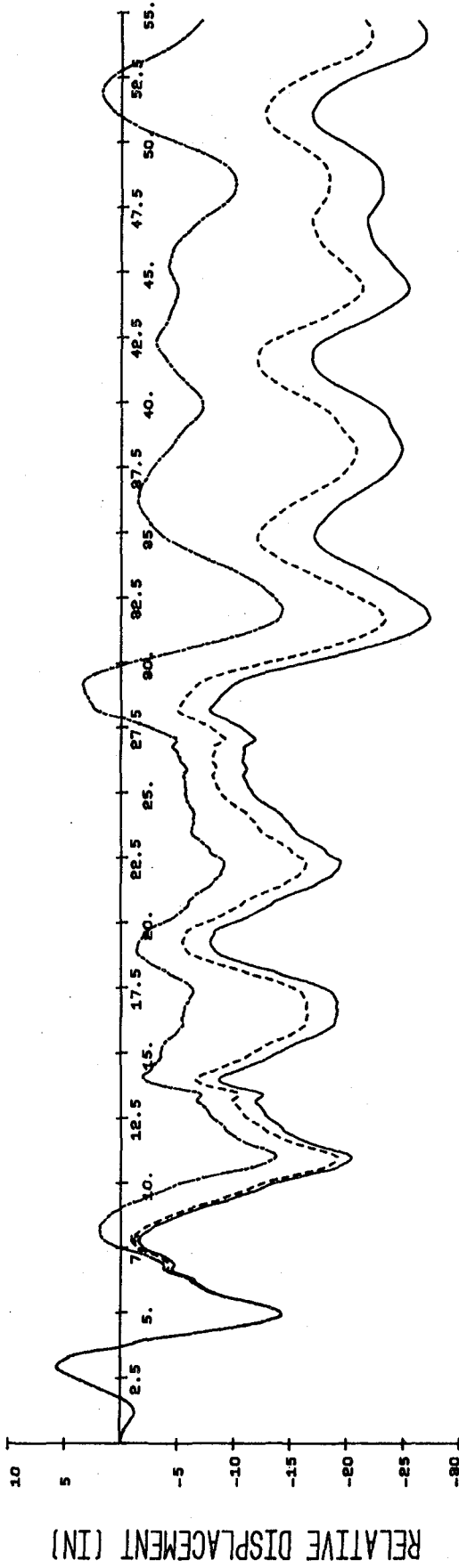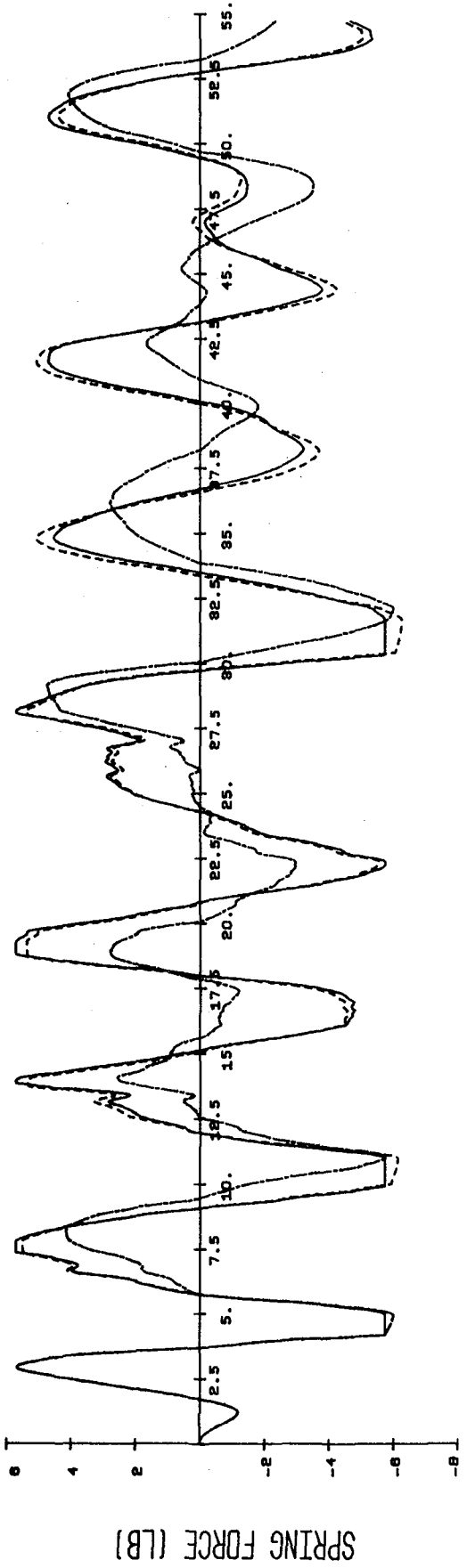
FIG. 3.89 RESPONSE TO EL CENTRO. SYSTEMS WITH f = 0.15 CPS, u_y = 5.73 INCHES, AND 5% DAMPING.

RELATIVE DISPLACEMENT. INCHES
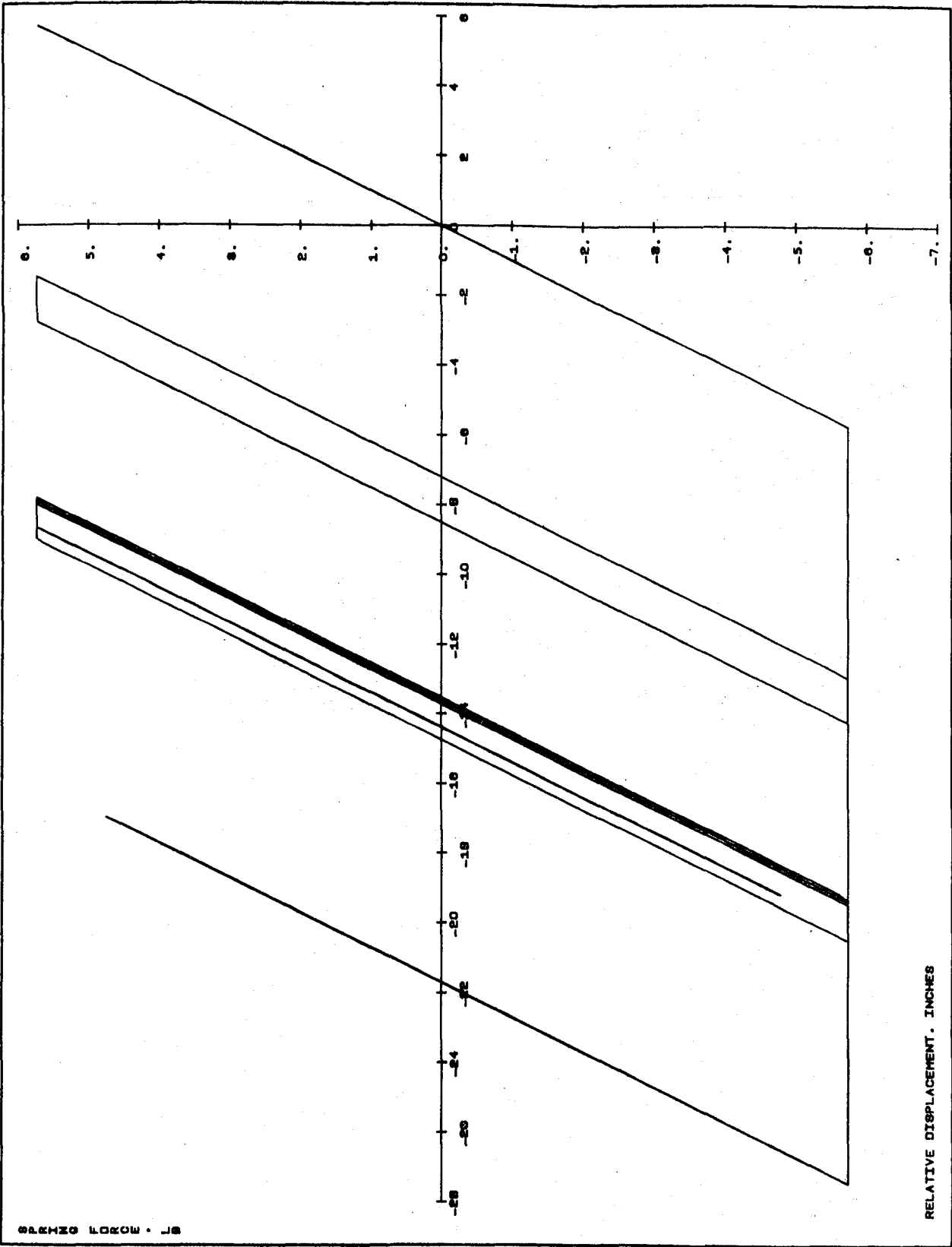
FIG. 3.90.a INTERNAL FORCE VS. DEFORMATION FOR THE ELASTOPLASTIC SYSTEM OF FIG. 3.89.

RELATIVE DISPLACEMENT, INCHES

FIG. 3.90.b INTERNAL FORCE VS. DEFORMATION FOR THE BILINEAR SYSTEM OF FIG. 3.89.

RELATIVE DISPLACEMENT. INCHES
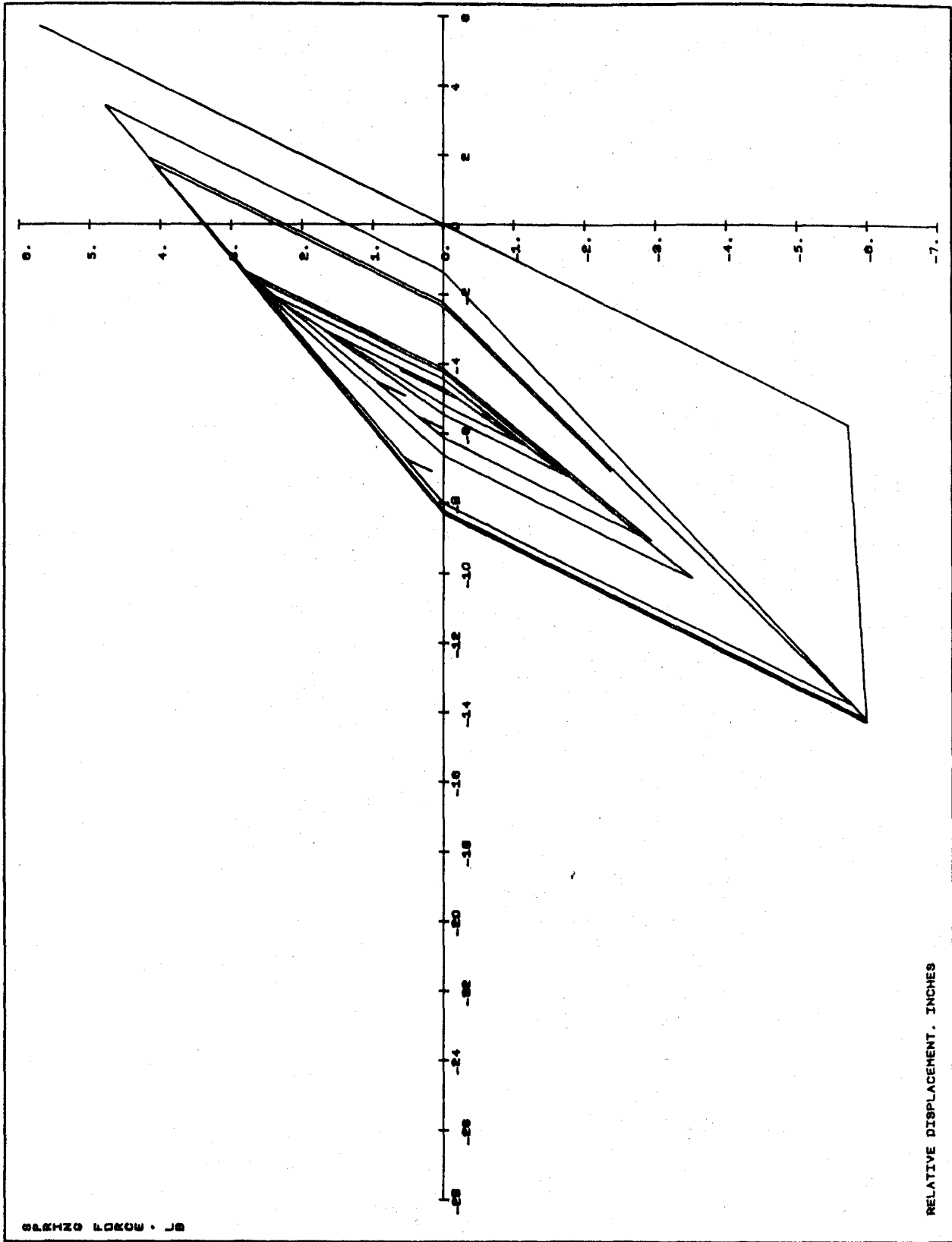
FIG. 3.90.c INTERNAL FORCE VS. DEFORMATION FOR THE DEGRADING SYSTEM OF FIG. 3.89.
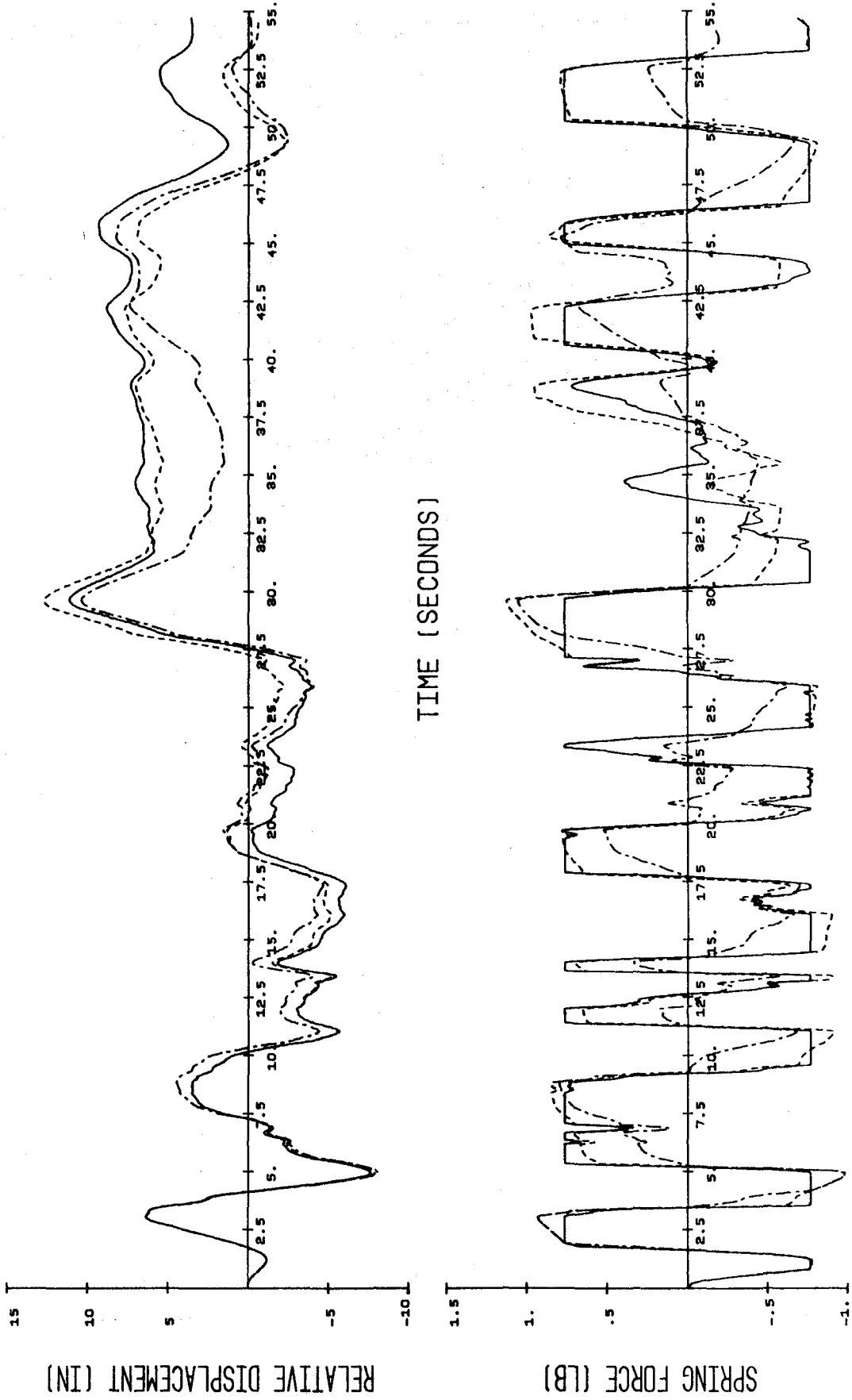
FIG. 3.91   RESPONSE TO EL CENTRO.   SYSTEMS WITH f = 0.15 CPS, u_y = .764 INCHES AND 5% DAMPING.

227
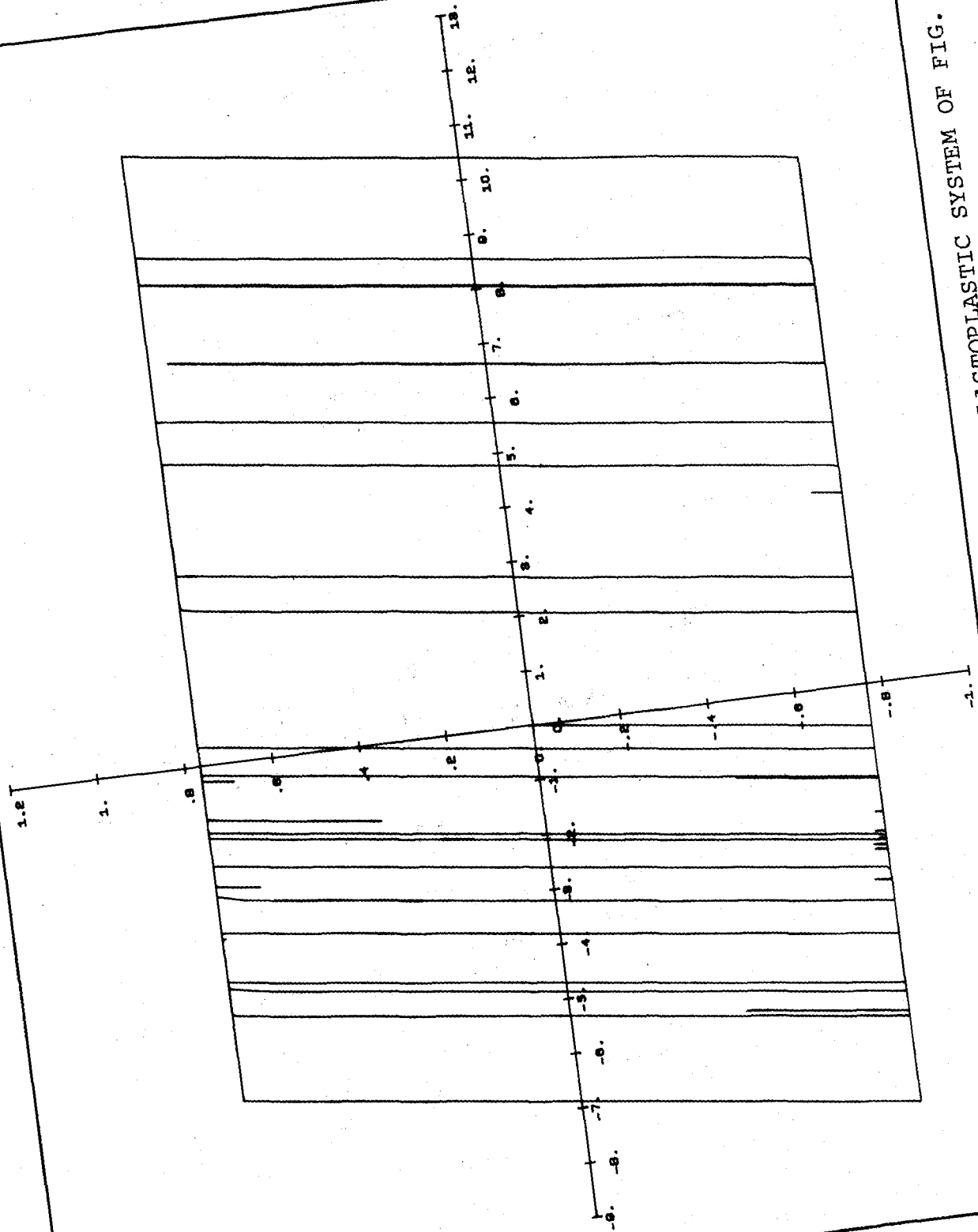
RELATIVE DISPLACEMENT, INCHES

FIG. 3.92.a   INTERNAL FORCE VS. DEFORMATION FOR THE ELASTOPLASTIC SYSTEM OF FIG. 3.91.
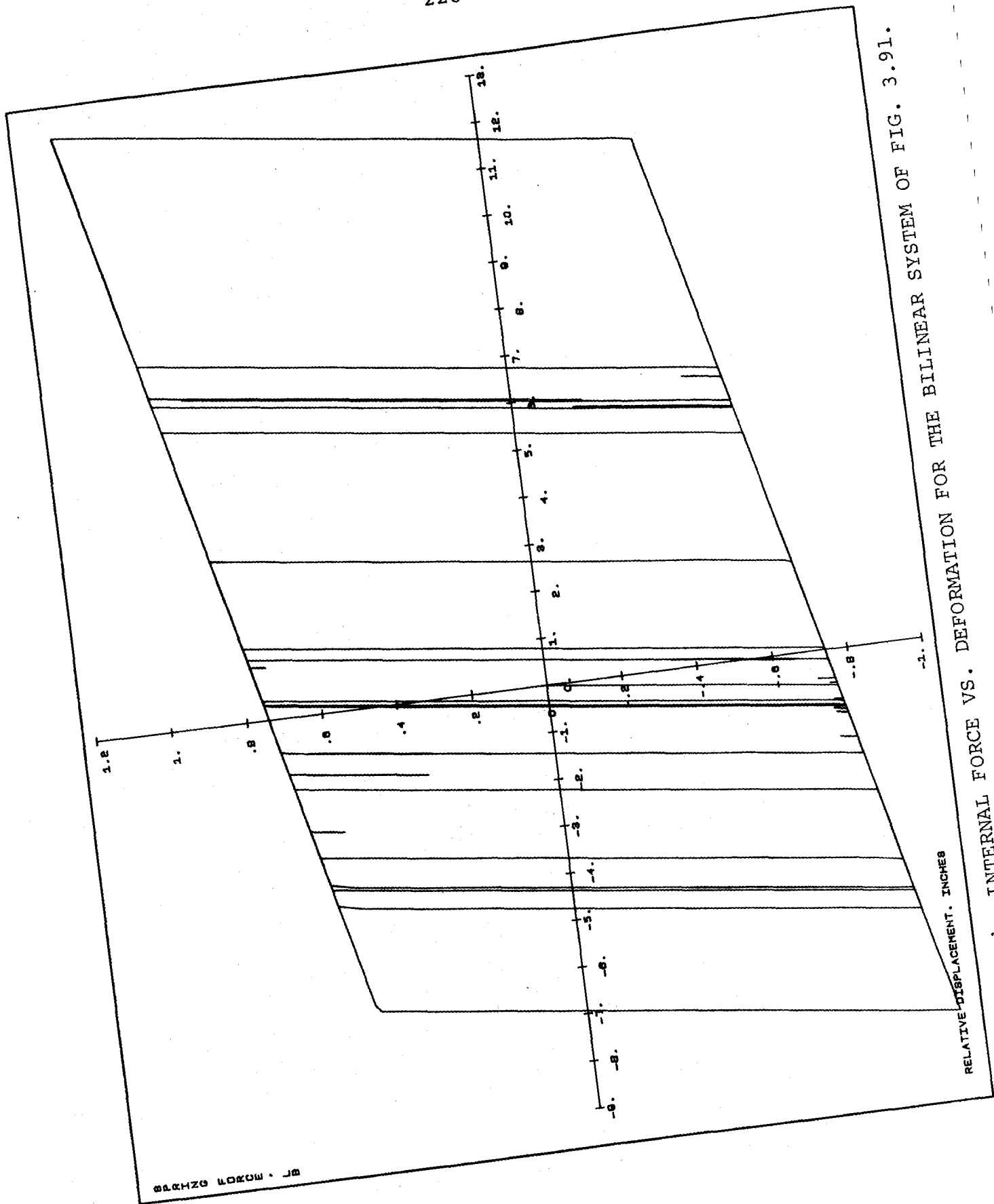
RELATIVE DISPLACEMENT. INCHES

FIG. 3.92.b INTERNAL FORCE VS. DEFORMATION FOR THE BILINEAR SYSTEM OF FIG. 3.91.
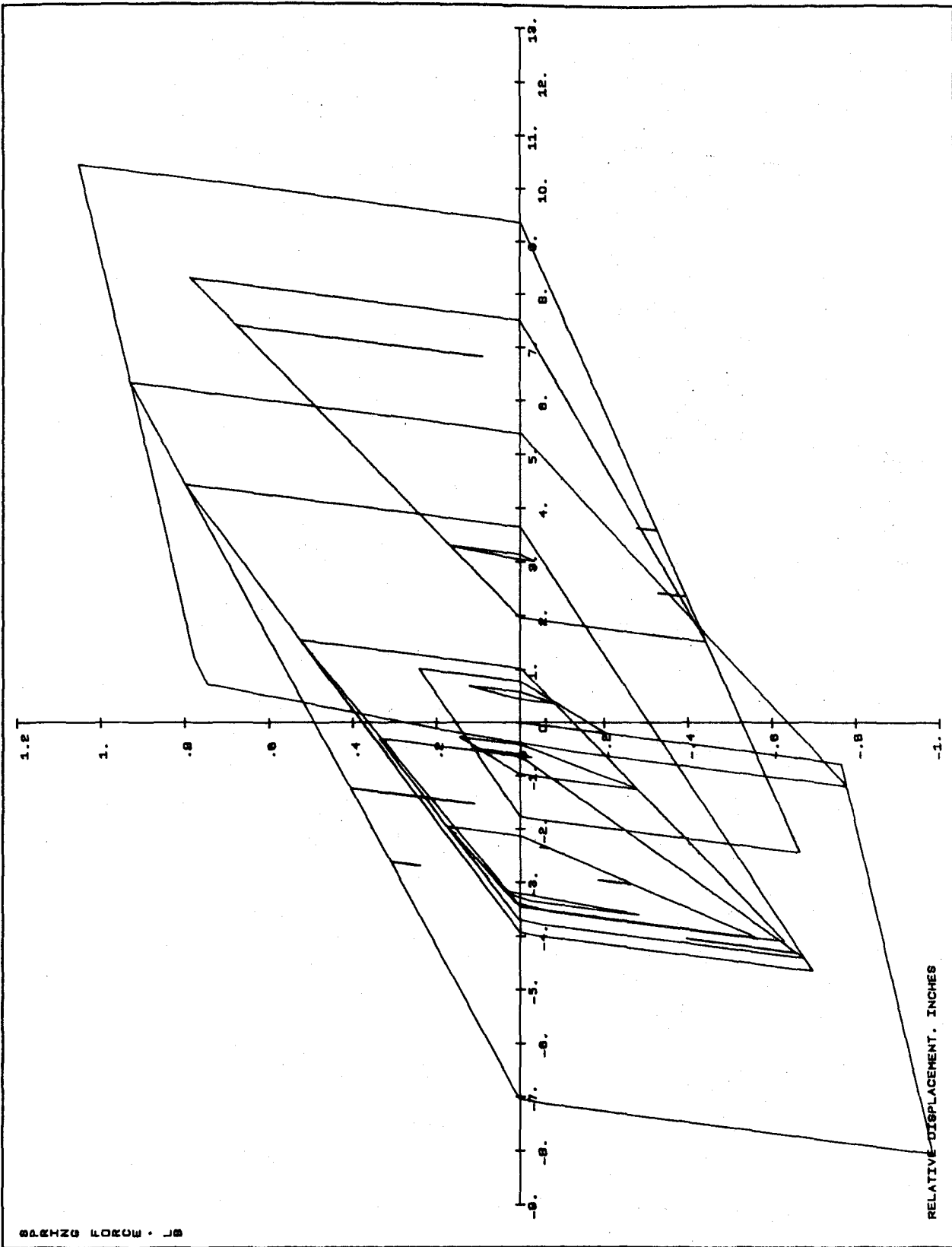
FIG. 3.92.c   INTERNAL FORCE VS. DEFORMATION FOR THE DEGRADING SYSTEM OF FIG. 3.91.
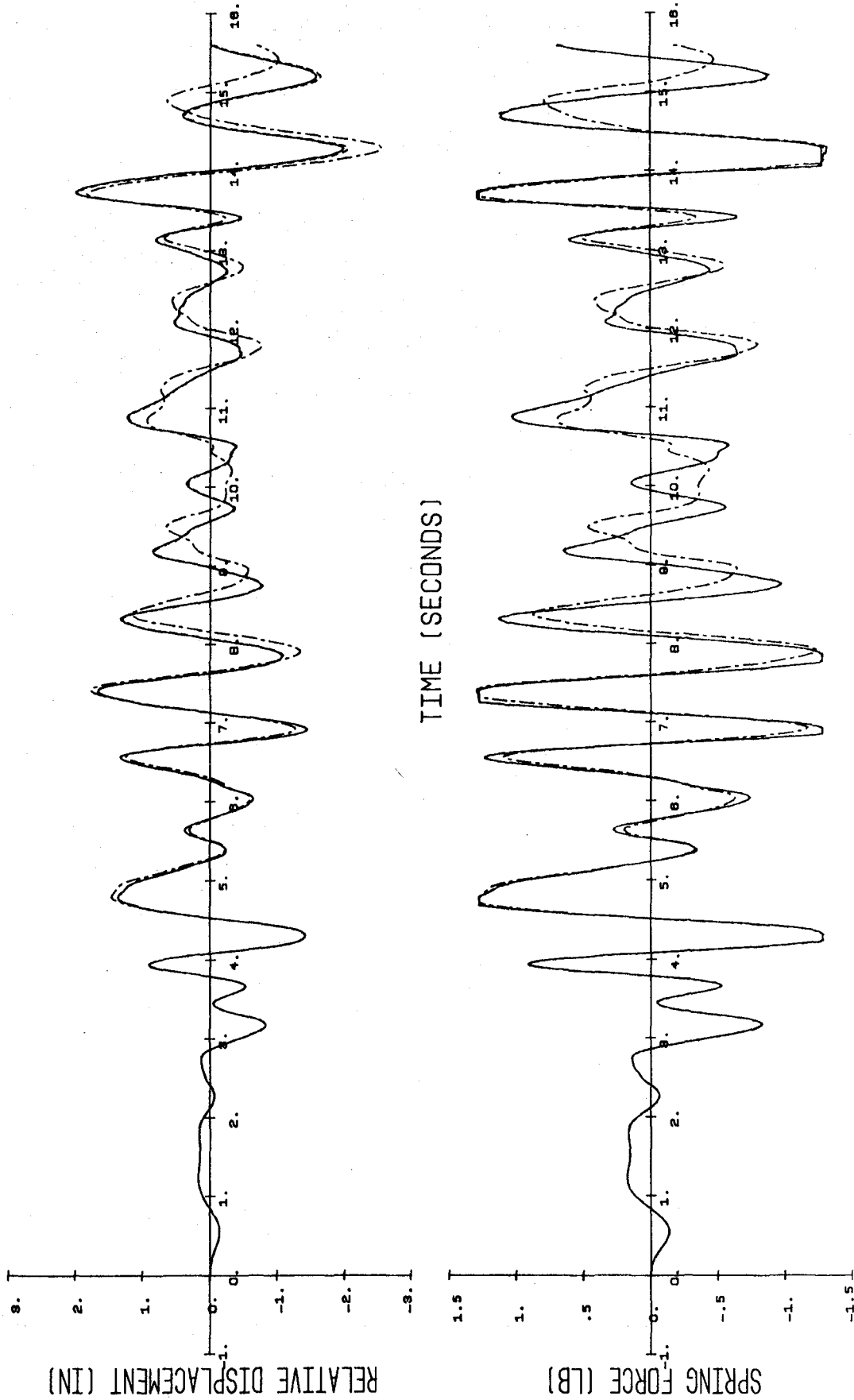
FIG. 3.93   RESPONSE TO EL CENTRO.   SYSTEMS WITH f = 1.1 CPS, u_y = 1.28 INCHES, AND 5% DAMPING.

RELATIVE DISPLACEMENT, INCHES
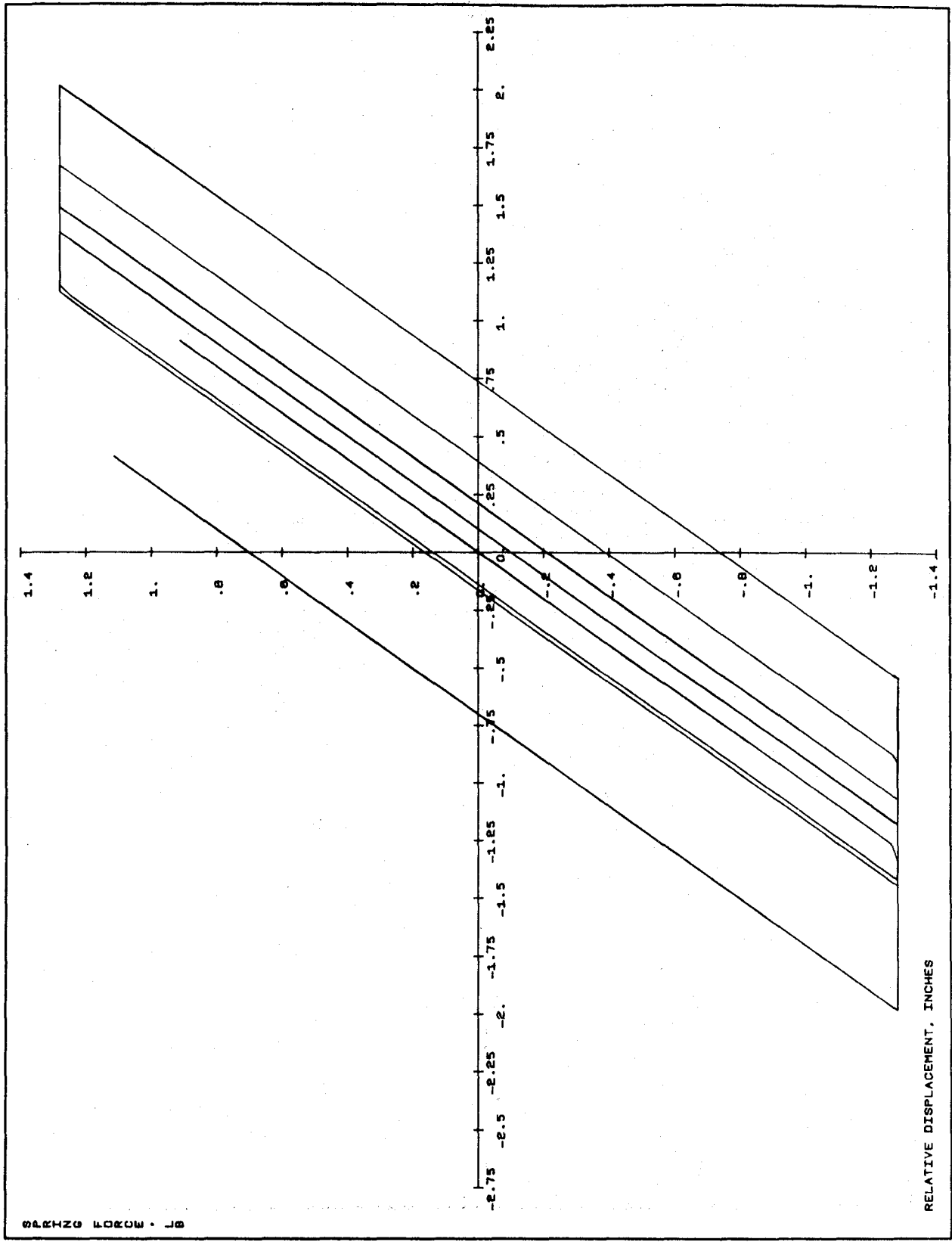
FIG. 3.94.a INTERNAL FORCE VS. DEFORMATION FOR THE ELASTOPLASTIC SYSTEM OF FIG. 3.93.

RELATIVE DISPLACEMENT, INCHES
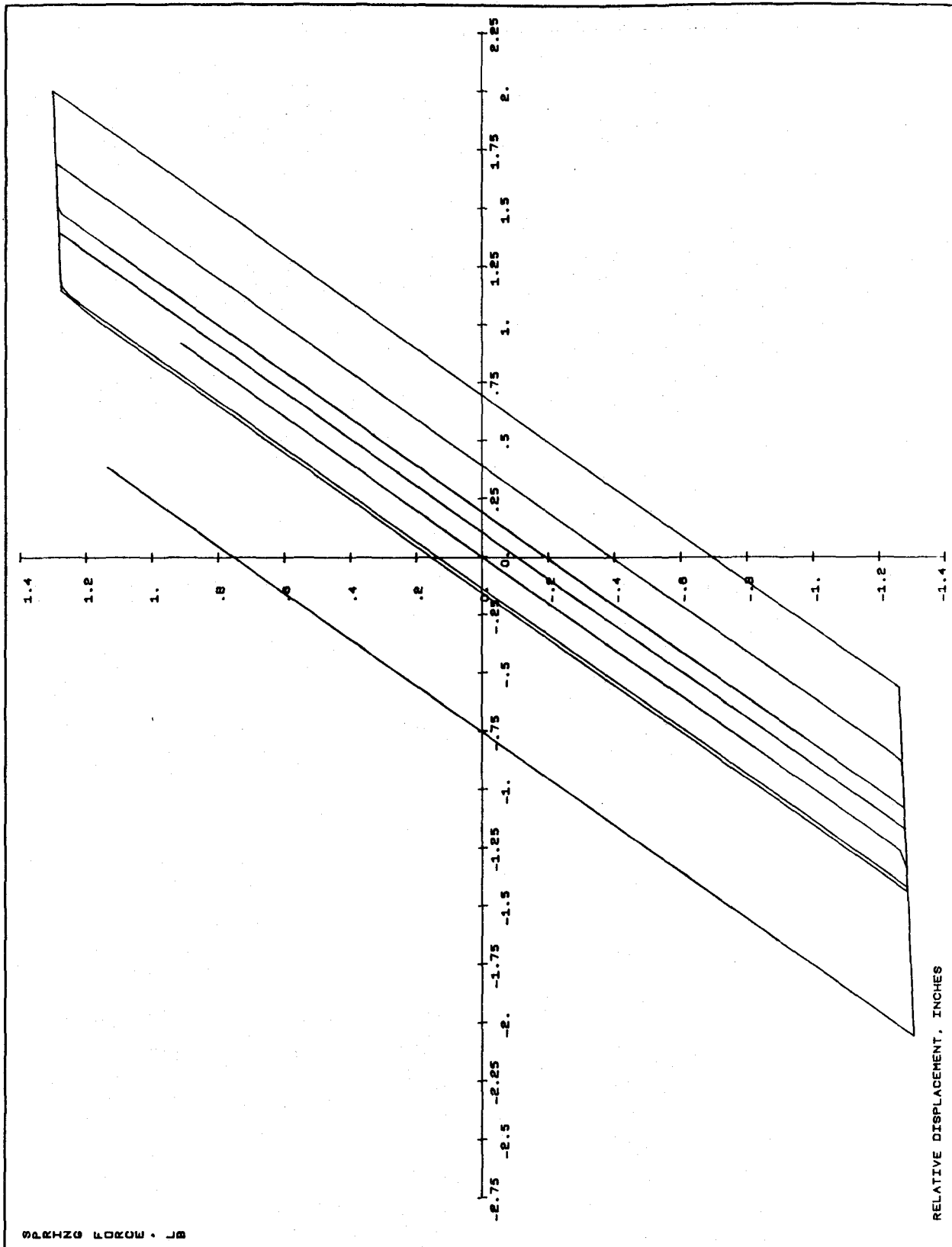
FIG. 3.94.b INTERNAL FORCE VS. DEFORMATION FOR THE BILINEAR SYSTEM OF FIG. 3.93.
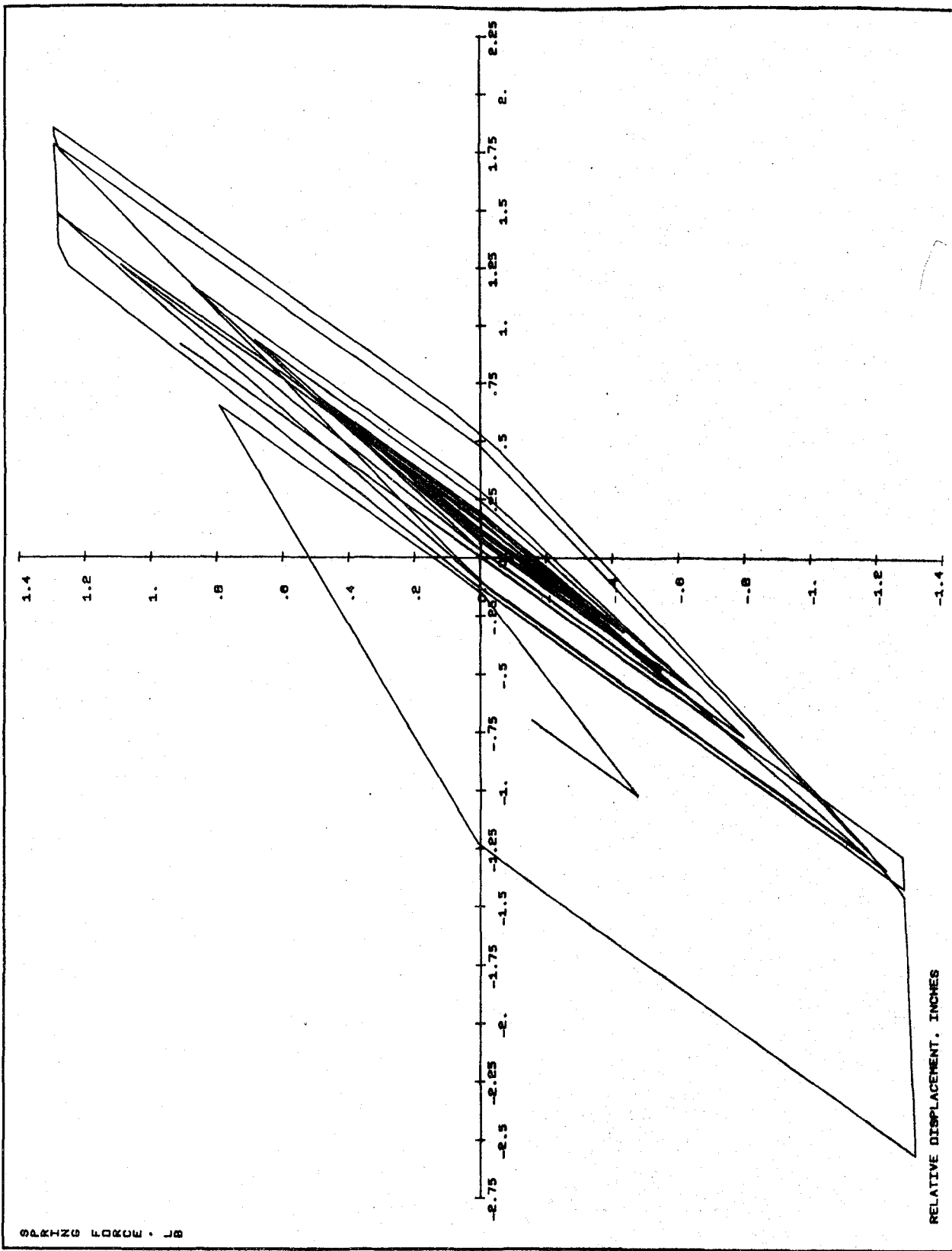
FIG. 3.94.c INTERNAL FORCE VS. DEFORMATION FOR THE DEGRADING SYSTEM OF FIG. 3.93.

234
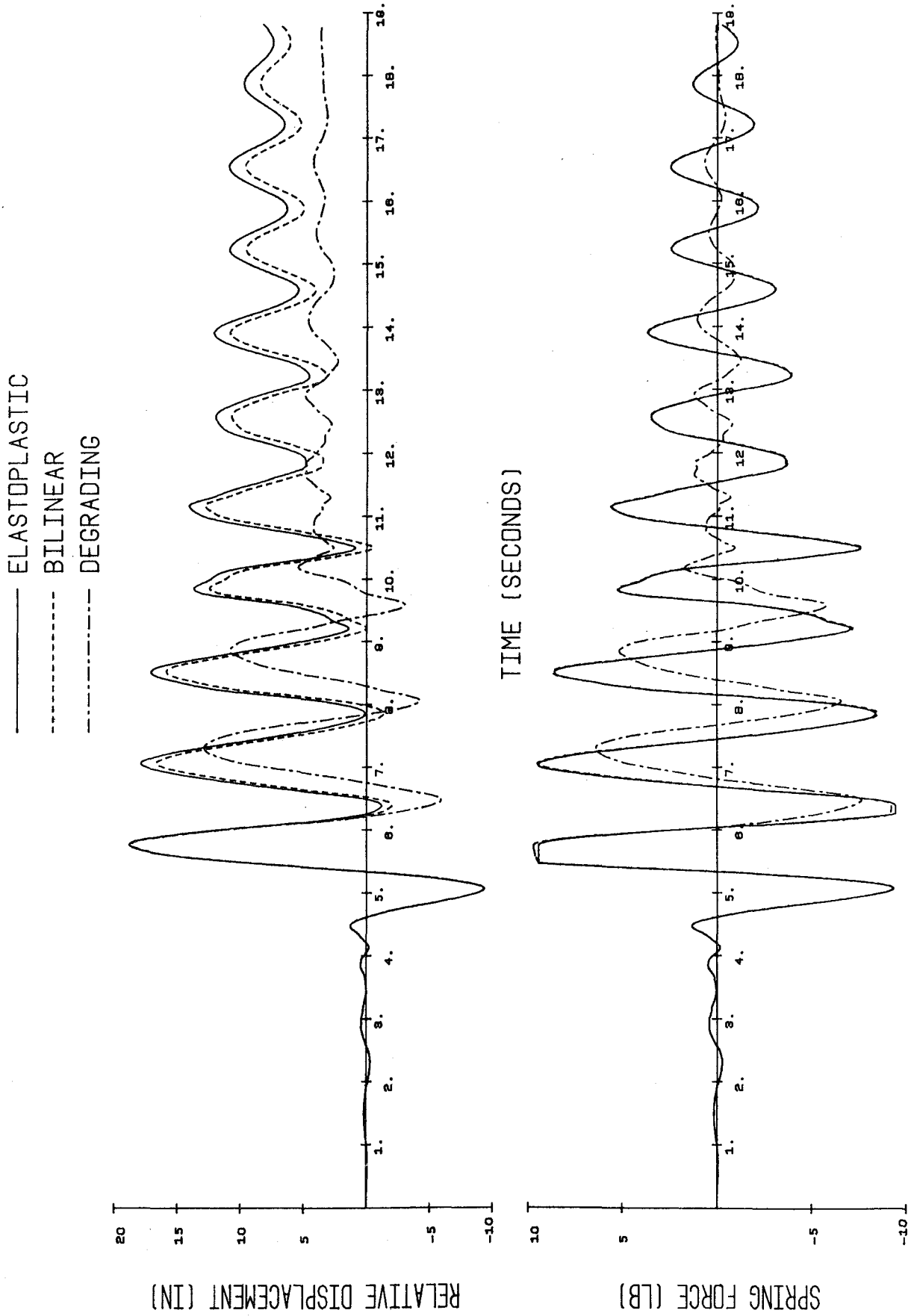
FIG. 3.95   RESPONSE TO PACOIMA.   SYSTEMS WITH f = 0.75 CPS, u_y = 9.44 INCHES, AND 5% DAMPING.

235
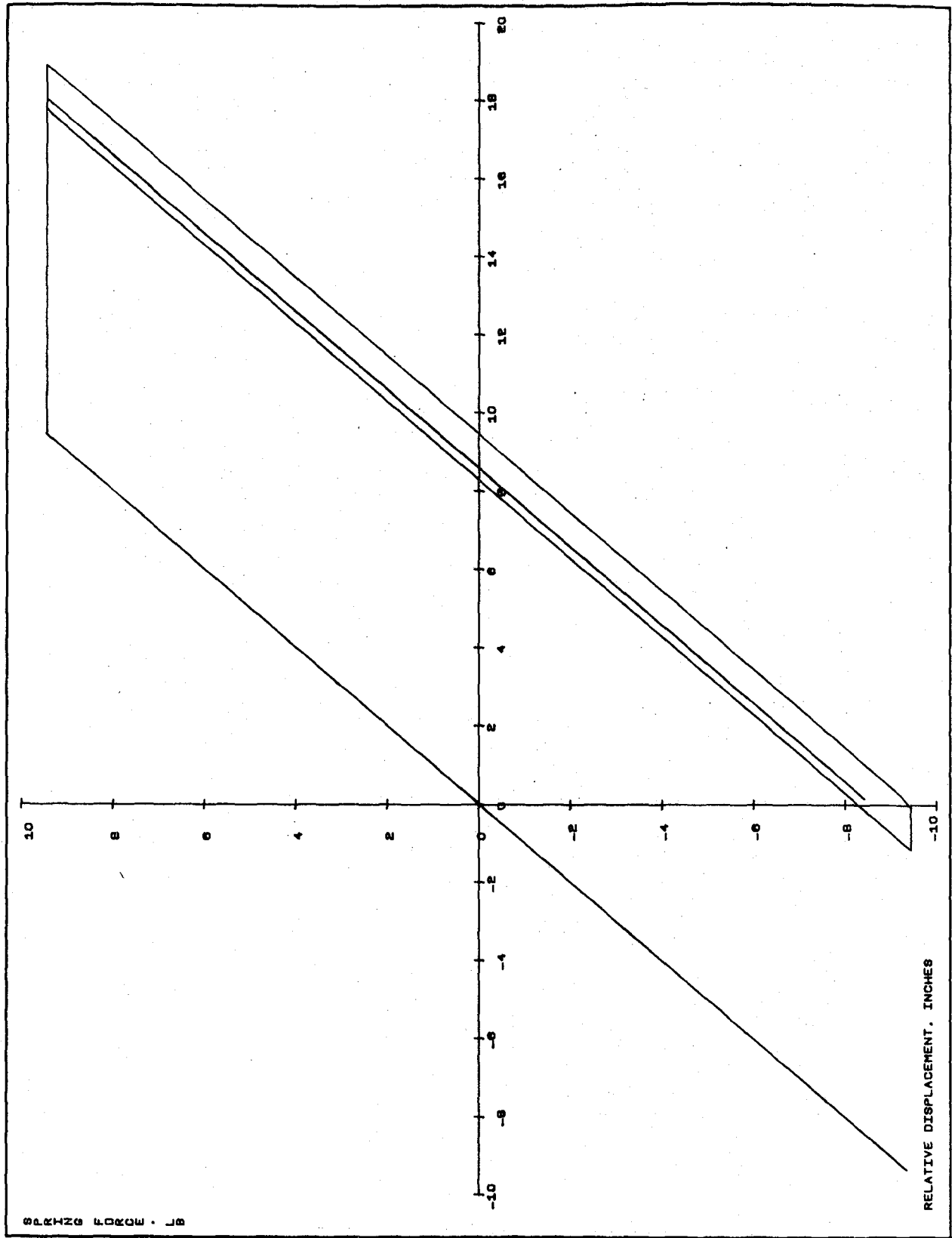
FIG. 3.96.a INTERNAL FORCE VS. DEFORMATION FOR THE ELASTOPLASTIC SYSTEM OF FIG. 3.95.
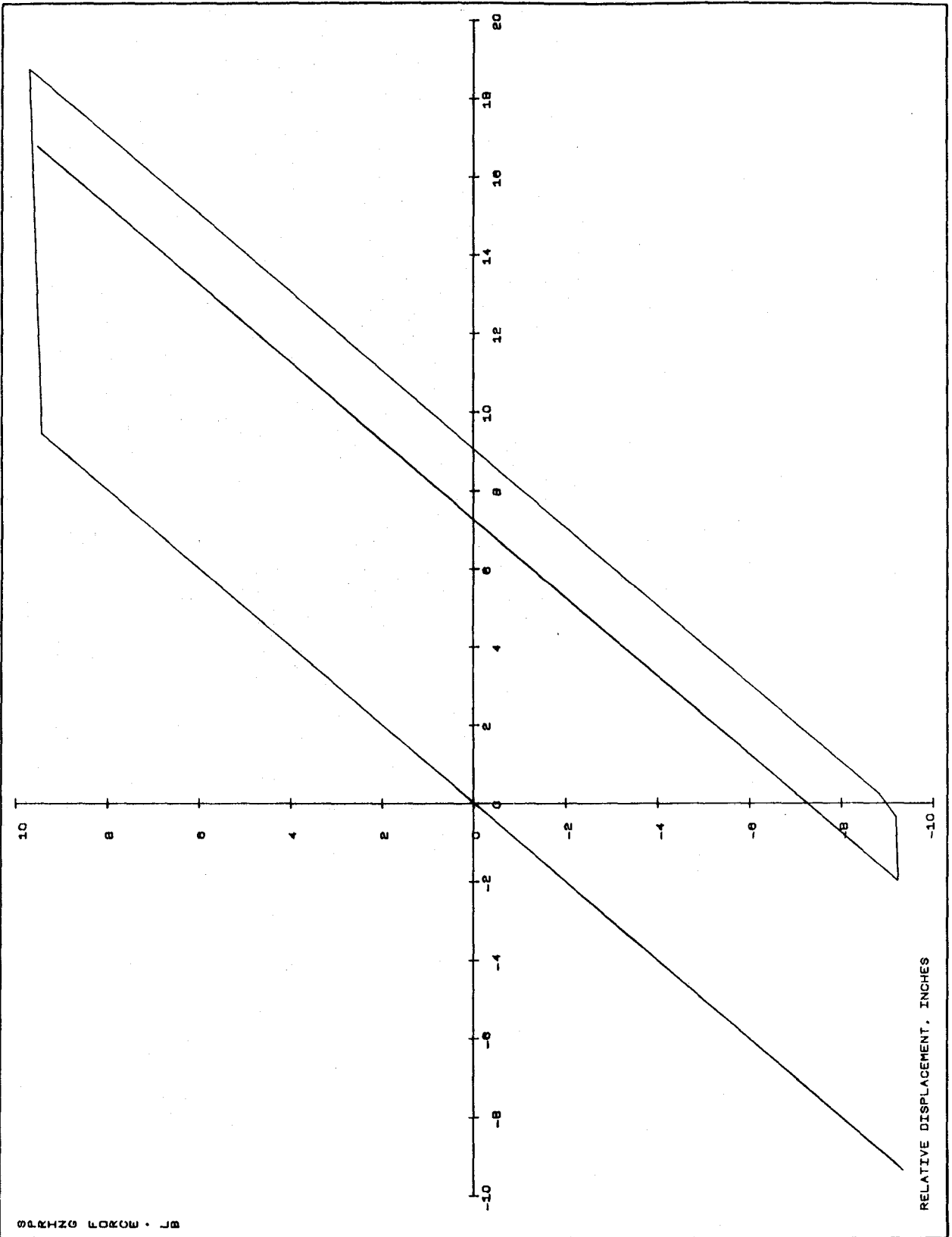
FIG. 3.96.b INTERNAL FORCE VS. DEFORMATION FOR THE BILINEAR SYSTEM OF FIG. 3.95.
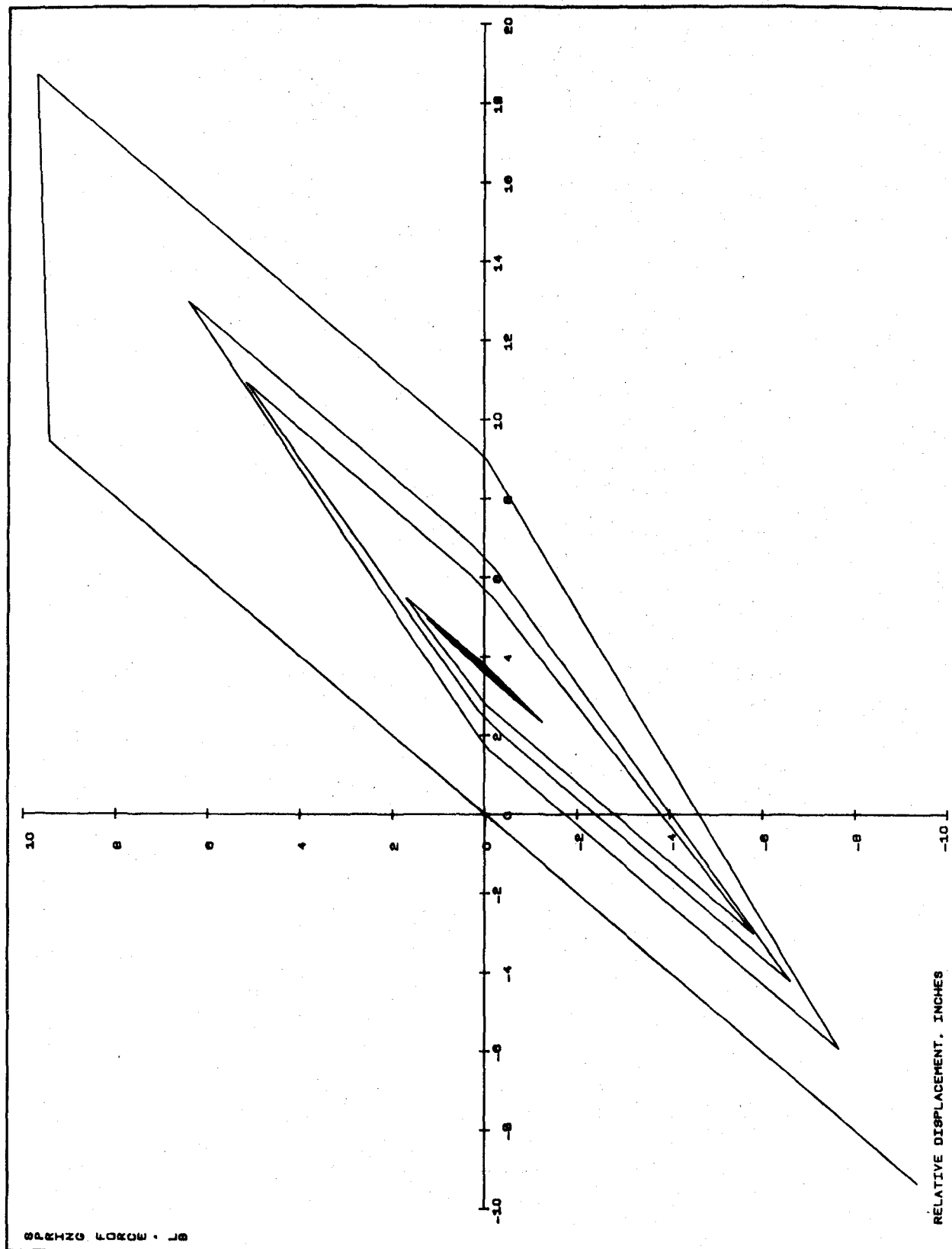
FIG. 3.96.c INTERNAL FORCE VS. DEFORMATION FOR THE DEGRADING SYSTEM OF FIG. 3.95.

238
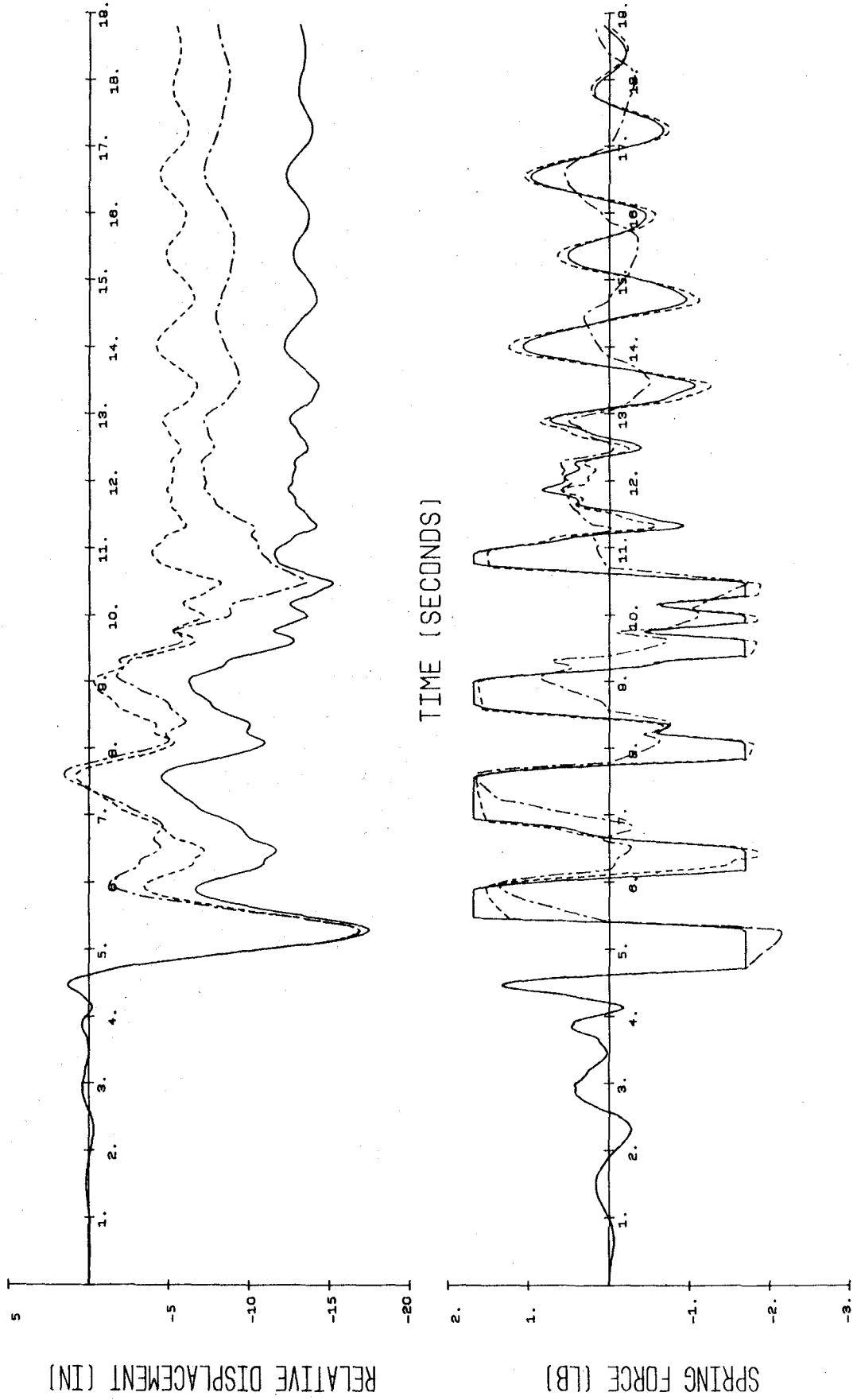
FIG. 3.97 RESPONSE TO PACOIMA. SYSTEMS WITH f = 0.75 CPS, u_y = 1.685 INCHES, AND 5% DAMPING.

RELATIVE DISPLACEMENT, INCHES
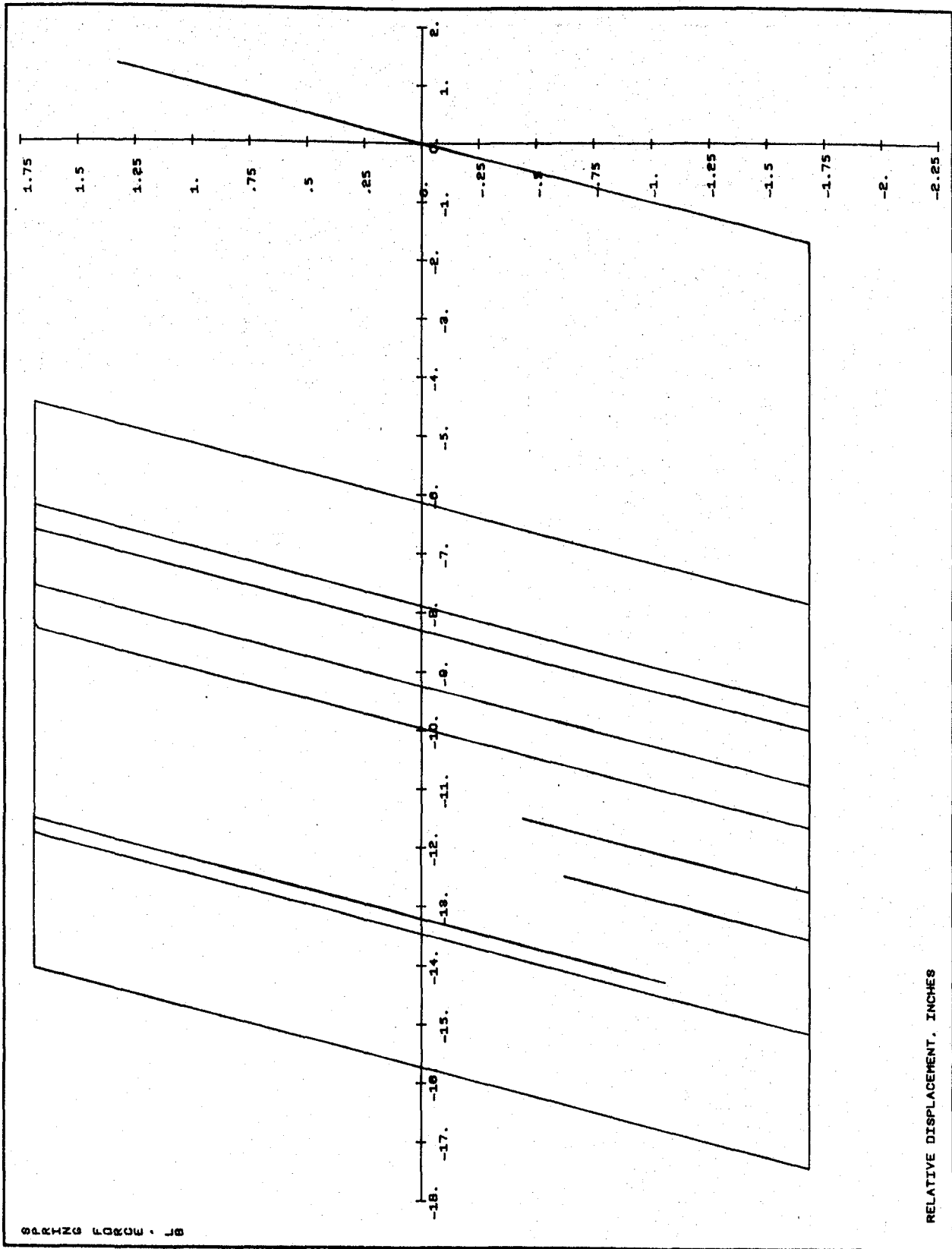
FIG. 3.98.a   INTERNAL FORCE VS. DEFORMATION FOR THE ELASTOPLASTIC SYSTEM OF FIG. 3.97.
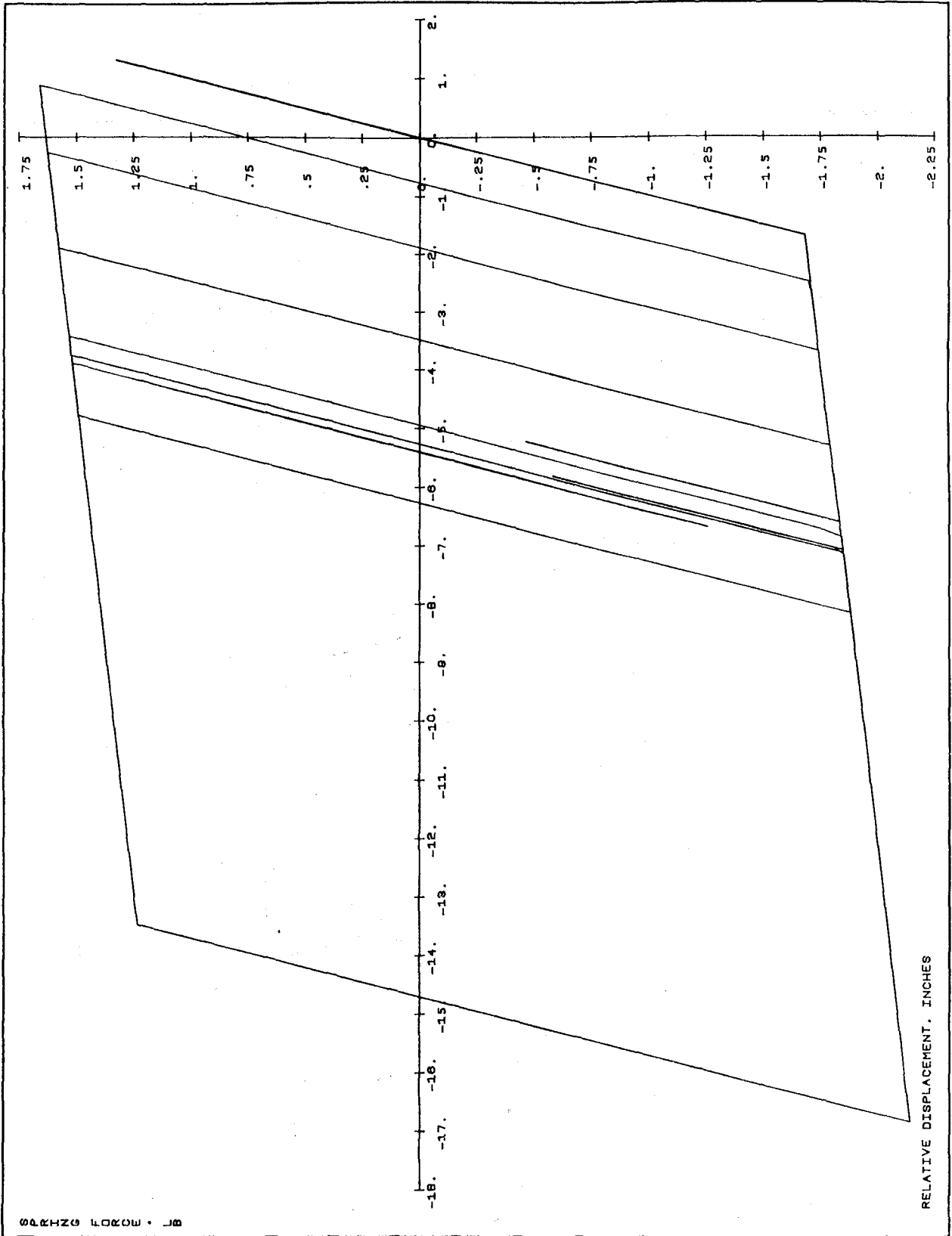
FIG. 3.98.b   INTERNAL FORCE VS. DEFORMATION FOR THE BILINEAR SYSTEM OF FIG. 3.97.
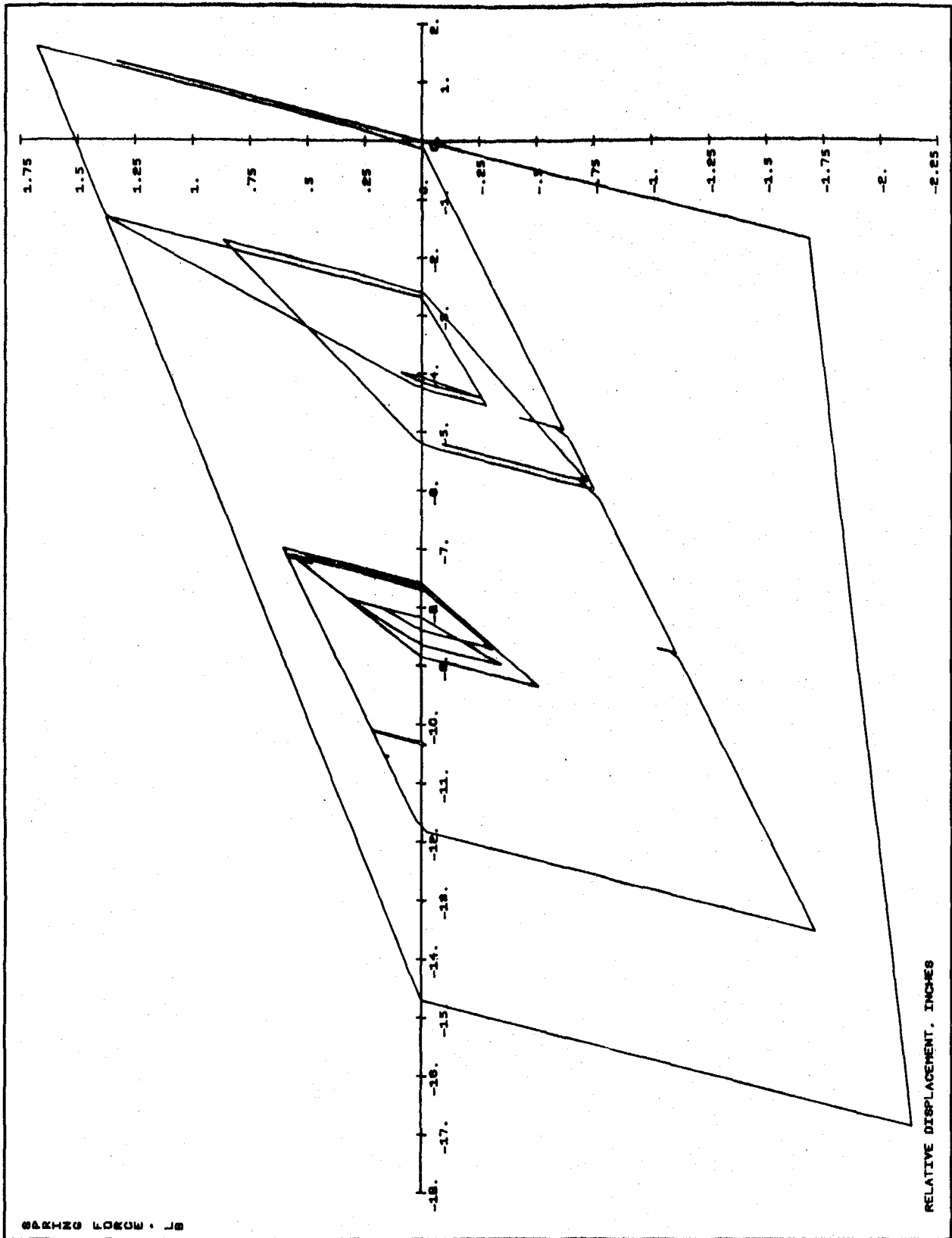
FIG. 3.98.c INTERNAL FORCE VS. DEFORMATION FOR THE DEGRADING SYSTEM OF FIG. 3.97.
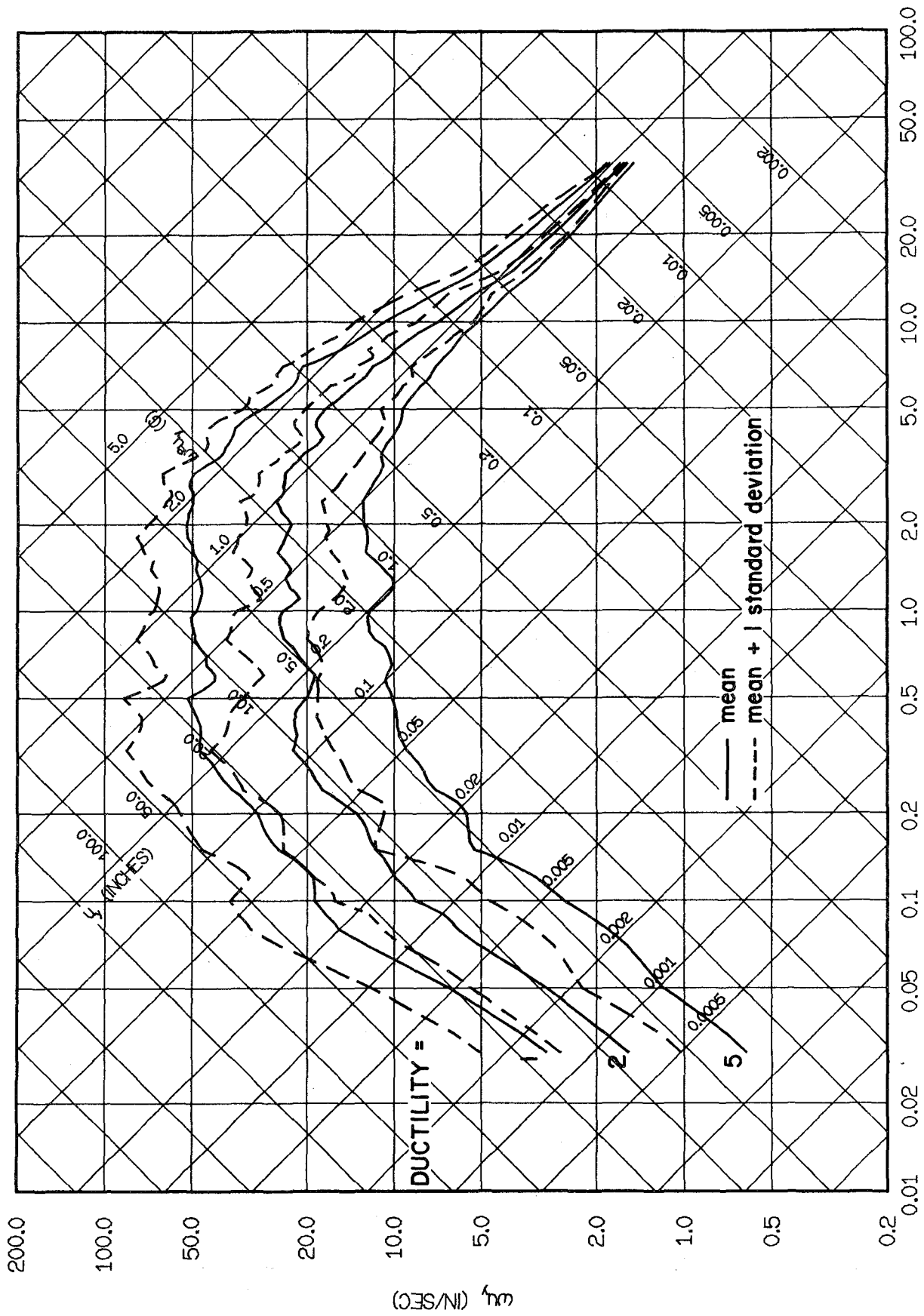
FIG. 4.1.a   MEAN AND MEAN + 1σ OF SPECTRA NORMALIZED TO GROUND ACCELERATION.   ELASTOPLASTIC SYSTEMS WITH 5% DAMPING.   DUCTILITY FACTORS: 1, 2, AND 5.

243
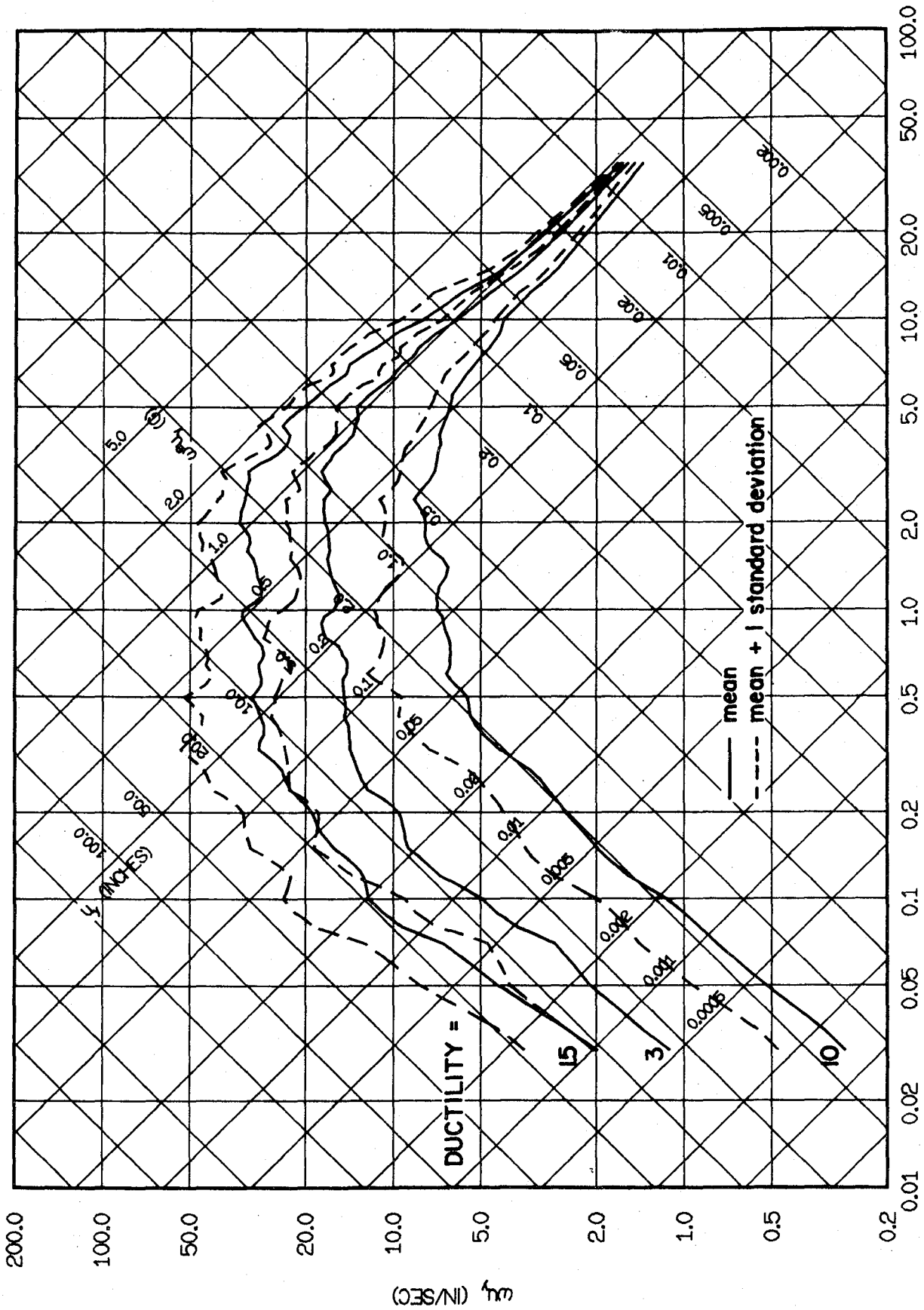
FIG. 4.1.b MEAN AND MEAN + 1σ OF SPECTRA NORMALIZED TO GROUND ACCELERATION. ELASTOPLASTIC SYSTEMS WITH 5% DAMPING. DUCTILITY FACTORS: 1.5, 3, AND 10.

FREQUENCY (CPS)
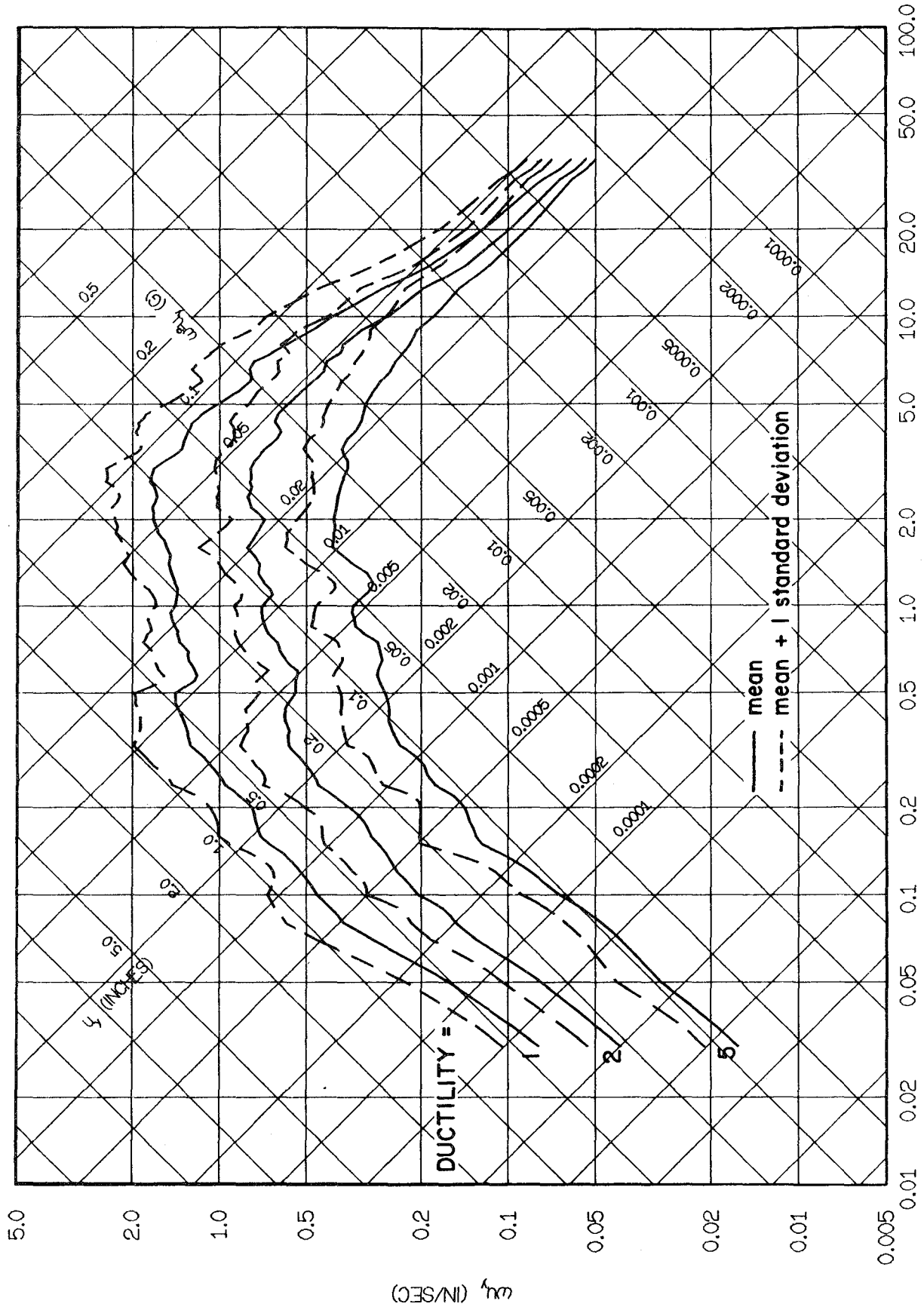
FIG. 4.2.a   MEAN AND MEAN + 1σ OF SPECTRA NORMALIZED TO GROUND VELOCITY.   ELASTOPLASTIC
SYSTEMS WITH 5% DAMPING.   DUCTILITY FACTORS: 1, 2, AND 5.
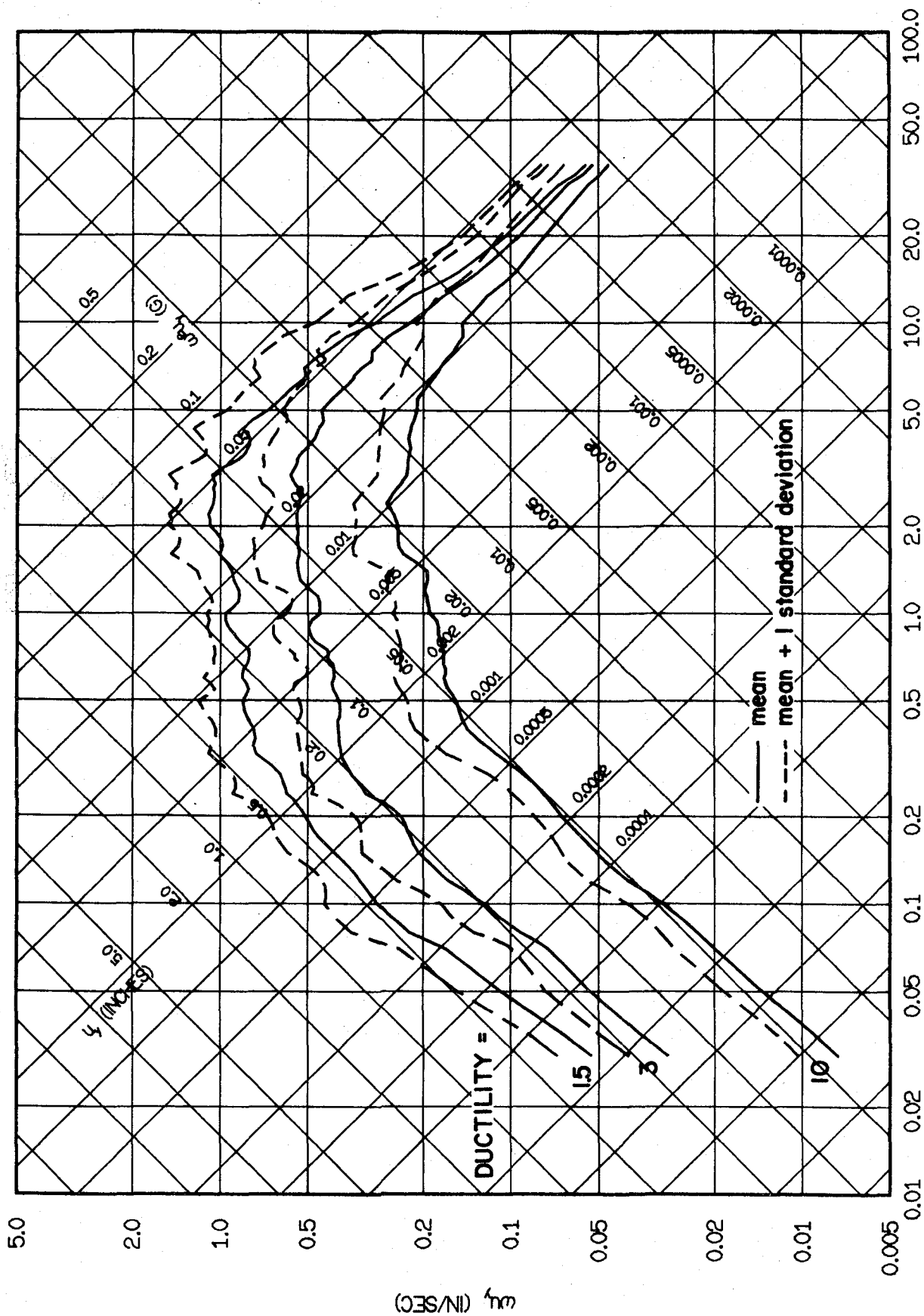
FIG. 4.2.b   MEAN AND MEAN + 1σ OF SPECTRA NORMALIZED TO GROUND VELOCITY.   ELASTOPLASTIC
SYSTEMS WITH 5% DAMPING.   DUCTILITY FACTORS: 1.5, 3, AND 10.
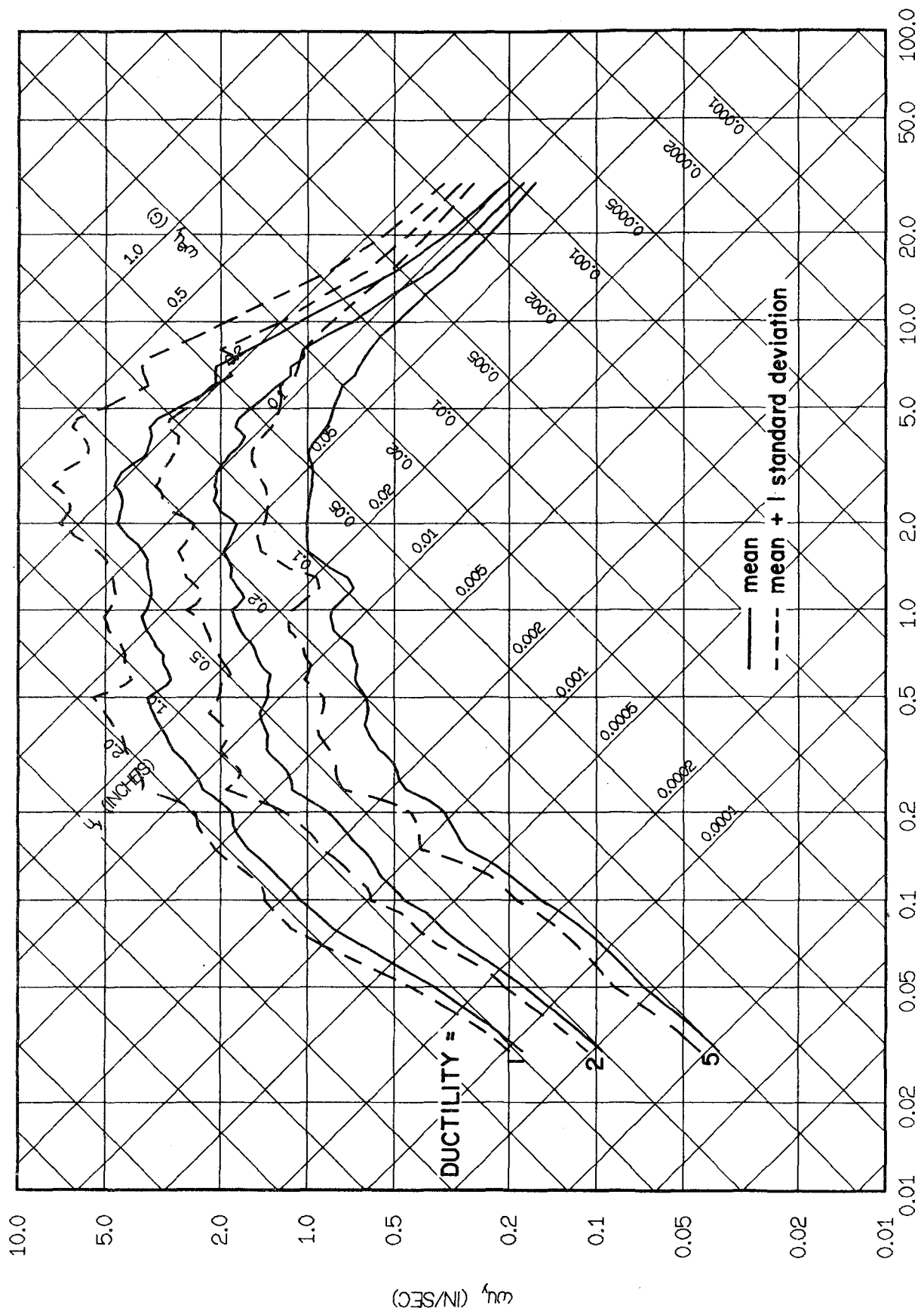
FIG. 4.3.a   MEAN AND MEAN + 1σ OF SPECTRA NORMALIZED TO GROUND DISPLACEMENT. ELASTOPLASTIC
SYSTEMS WITH 5% DAMPING. DUCTILITY FACTORS: 1, 2, AND 5.

247
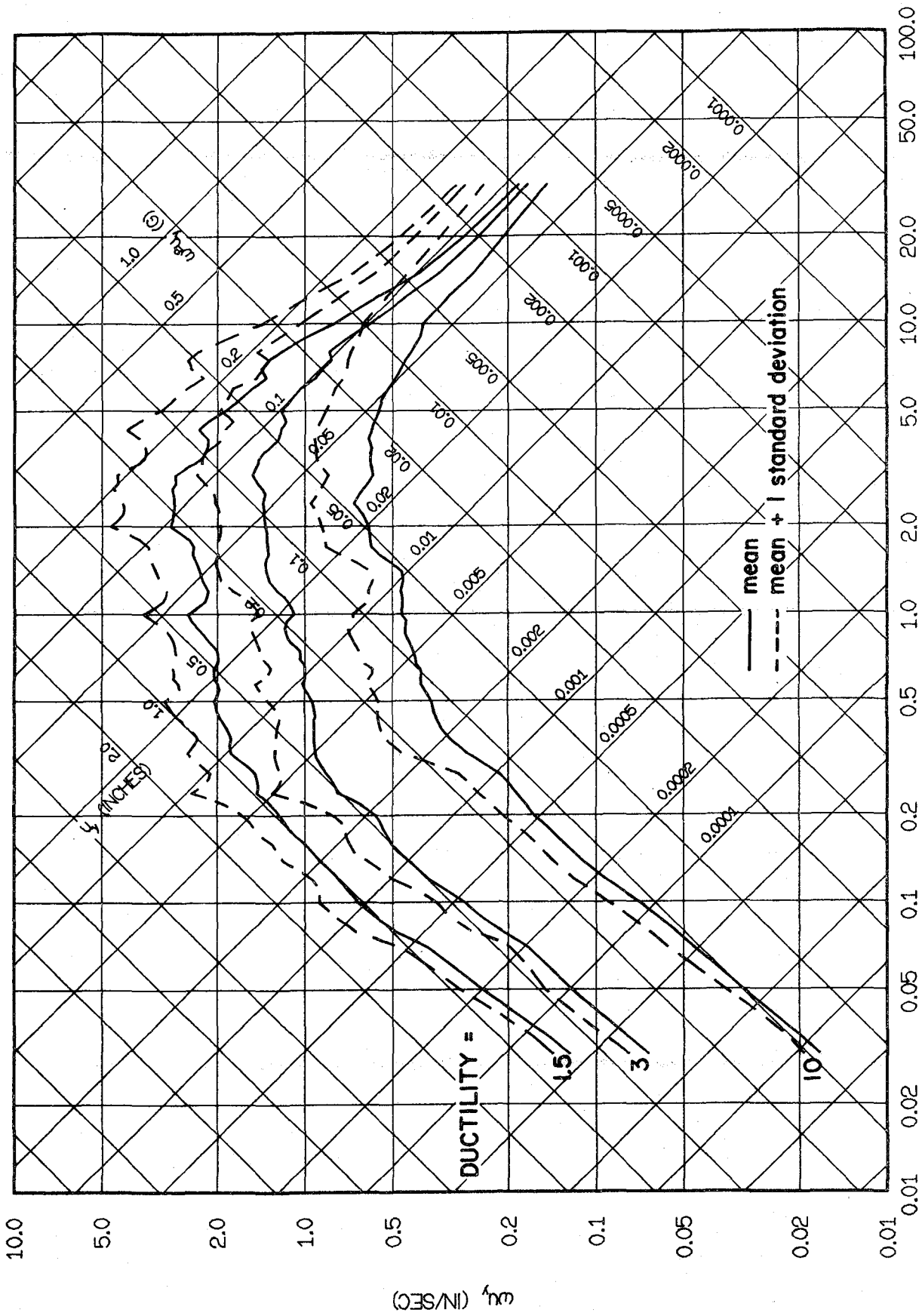
FIG. 4.3.b   MEAN AND MEAN + 1σ OF SPECTRA NORMALIZED TO GROUND DISPLACEMENT. ELASTOPLASTIC
SYSTEMS WITH 5% DAMPING. DUCTILITY FACTORS: 1.5, 3, AND 10.

248
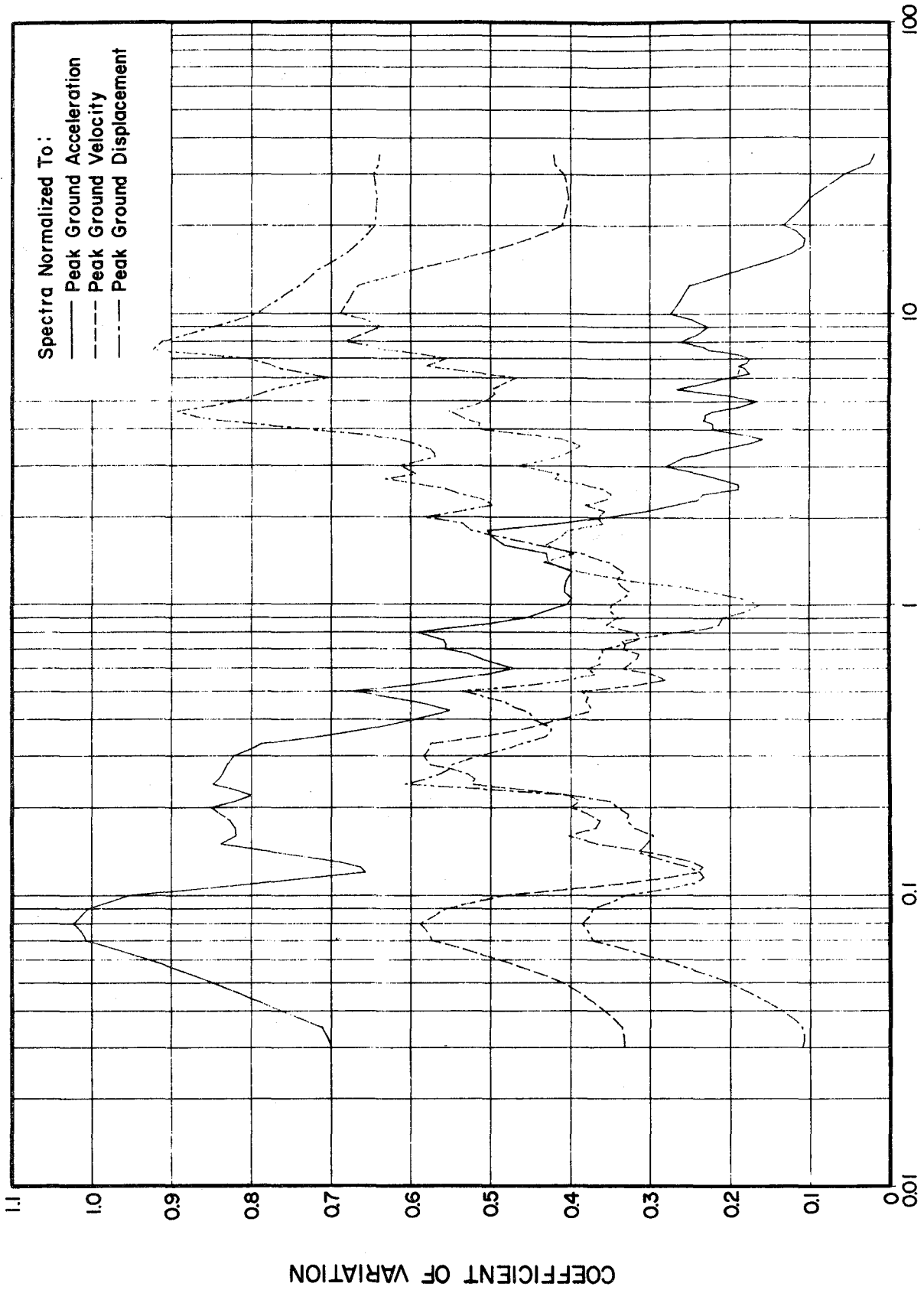
FIG. 4.4 COEFFICIENT OF VARIATION OF ELASTIC SPECTRA FOR SYSTEMS WITH 5% DAMPING
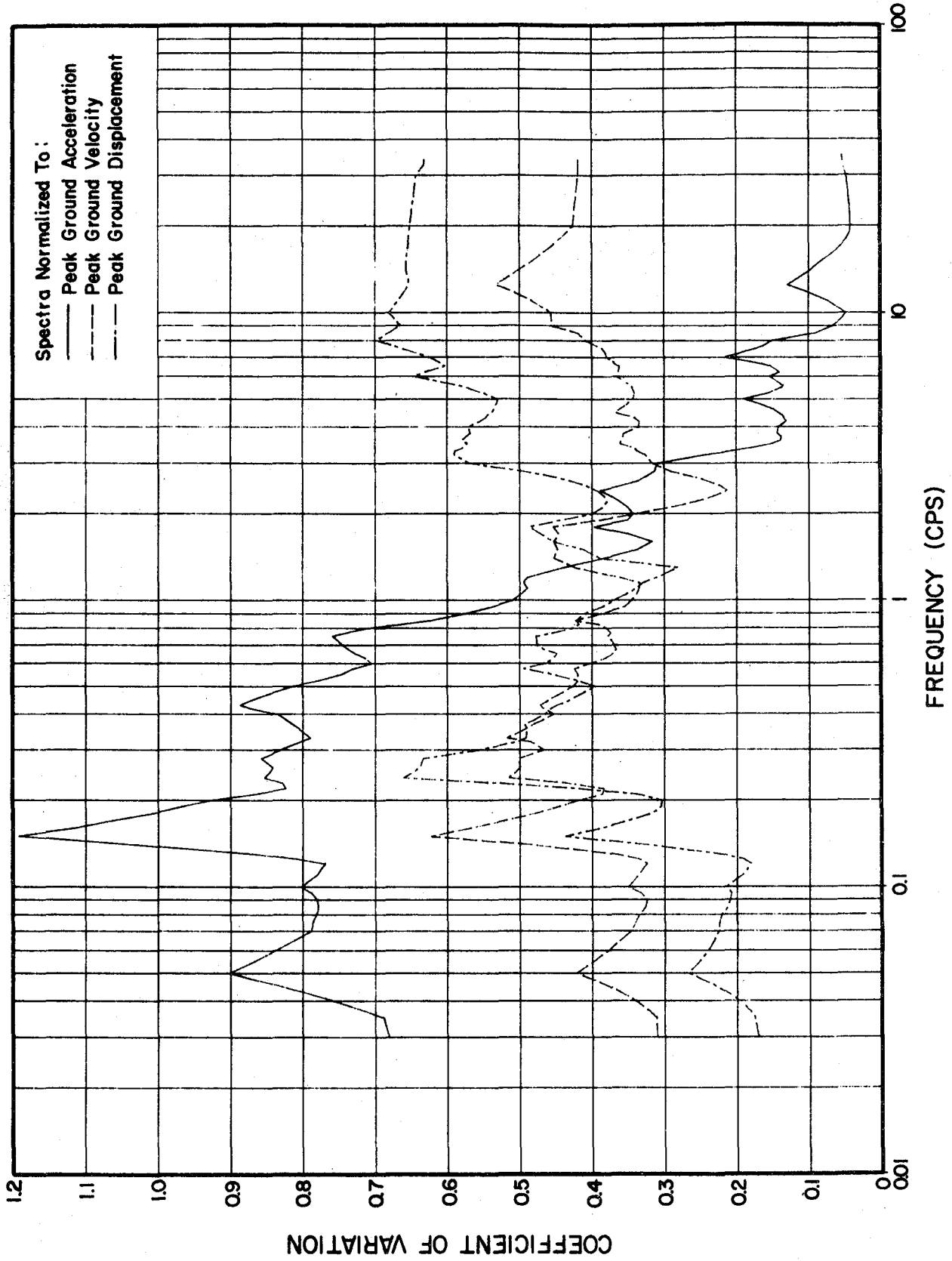
FIG. 4.5 COV OF SPECTRA FOR ELASTOPLASTIC SYSTEMS WITH 5% DAMPING AND DUCTILITY = 5
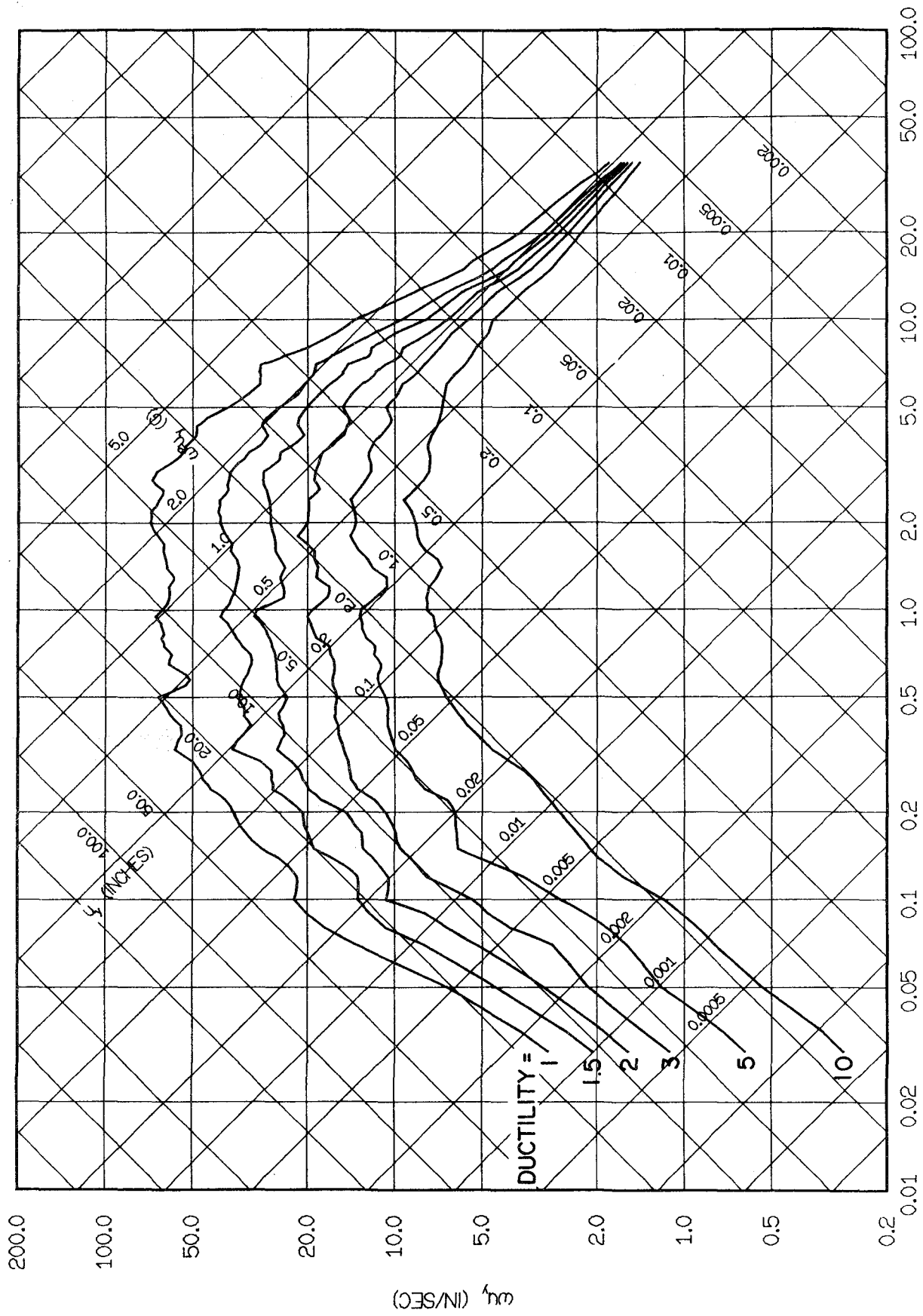
FIG. 4.6 MEAN OF SPECTRA NORMALIZED TO GROUND ACCELERATION. ELASTOPLASTIC SYSTEMS WITH 2% DAMPING.
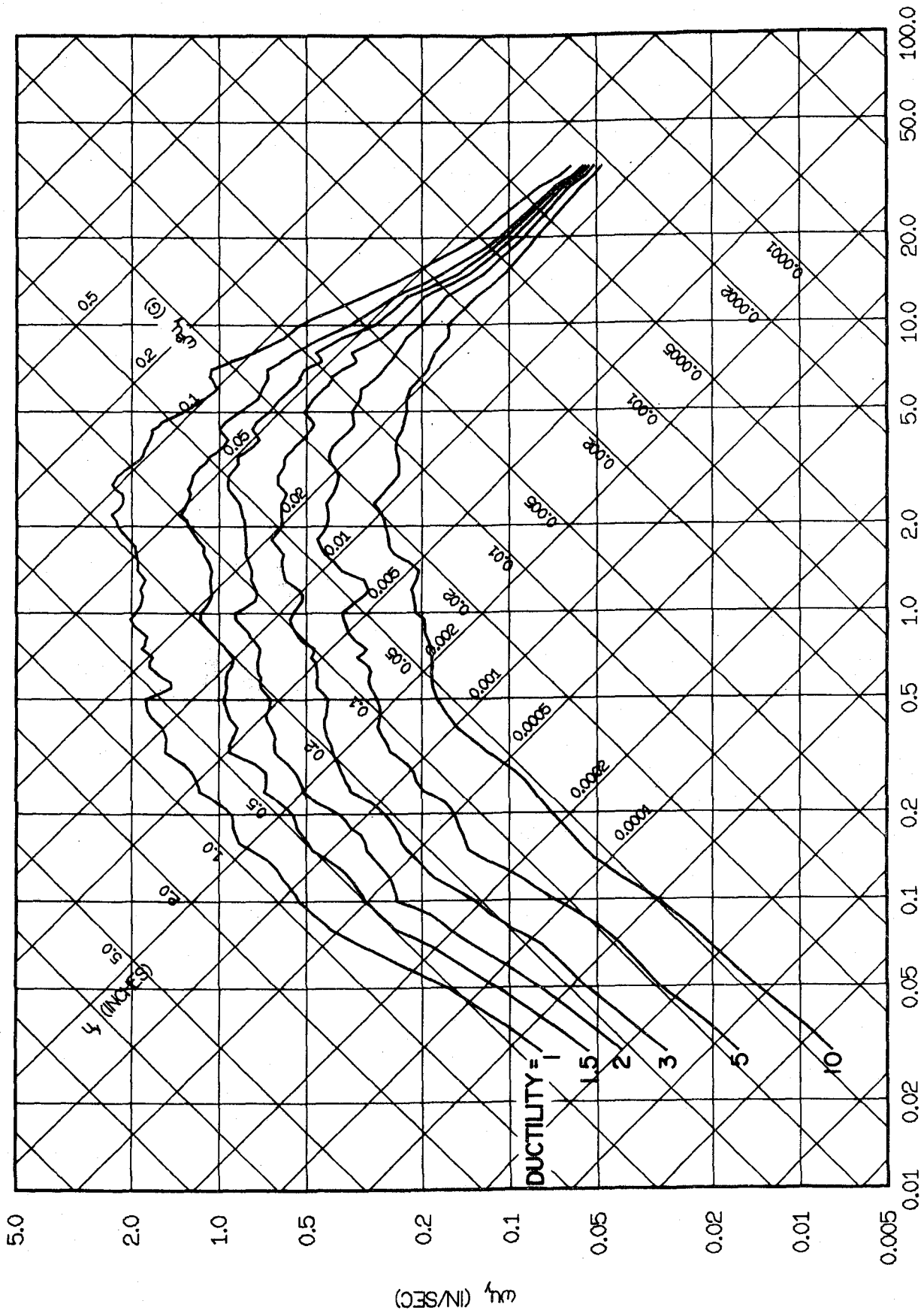
FIG. 4.7 MEAN OF SPECTRA NORMALIZED TO GROUND VELOCITY. ELASTOPLASTIC SYSTEMS WITH 2% DAMPING.
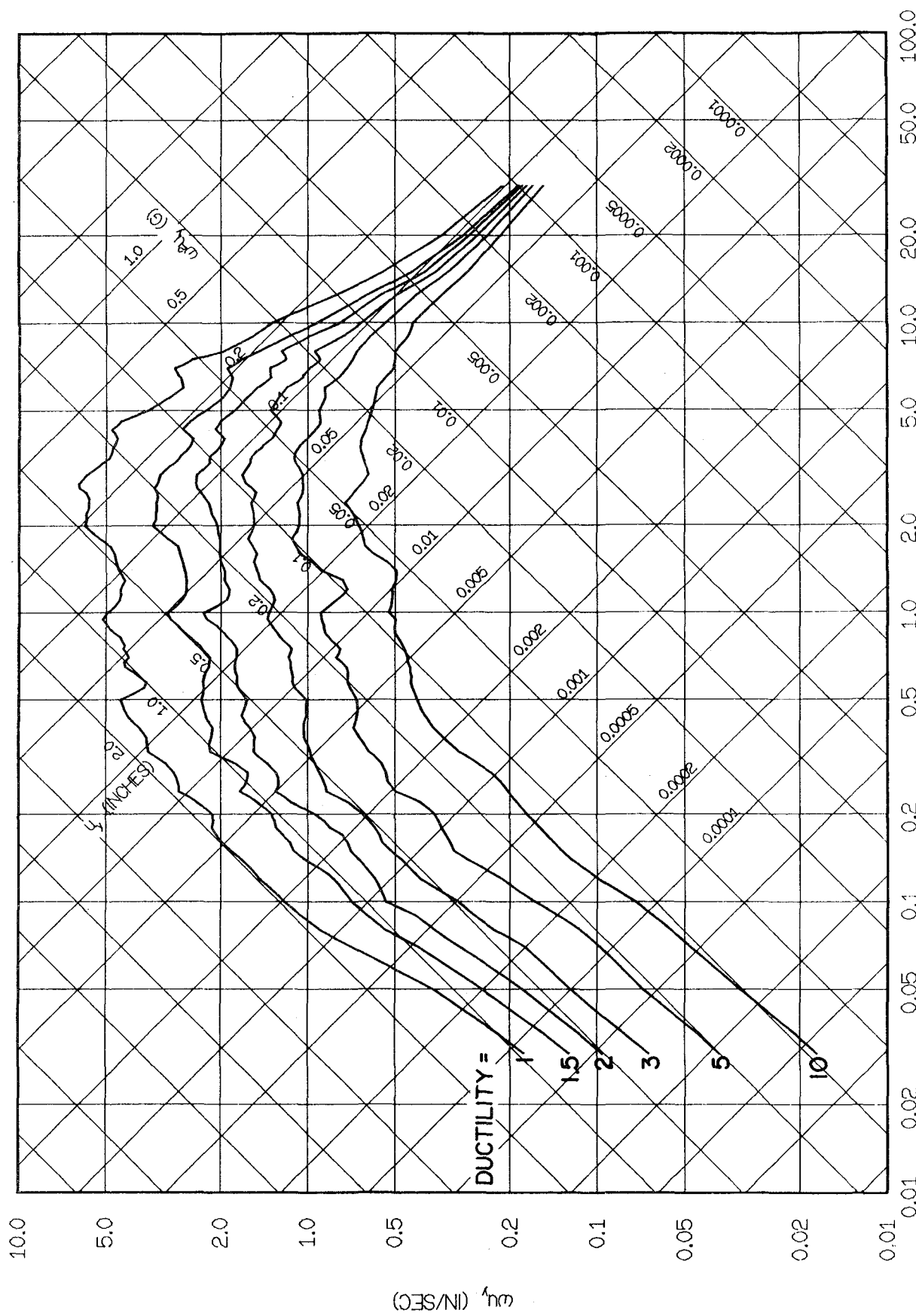
FIG. 4.8   MEAN OF SPECTRA NORMALIZED TO GROUND DISPLACEMENT.   ELASTOPLASTIC SYSTEMS
WITH 2% DAMPING.
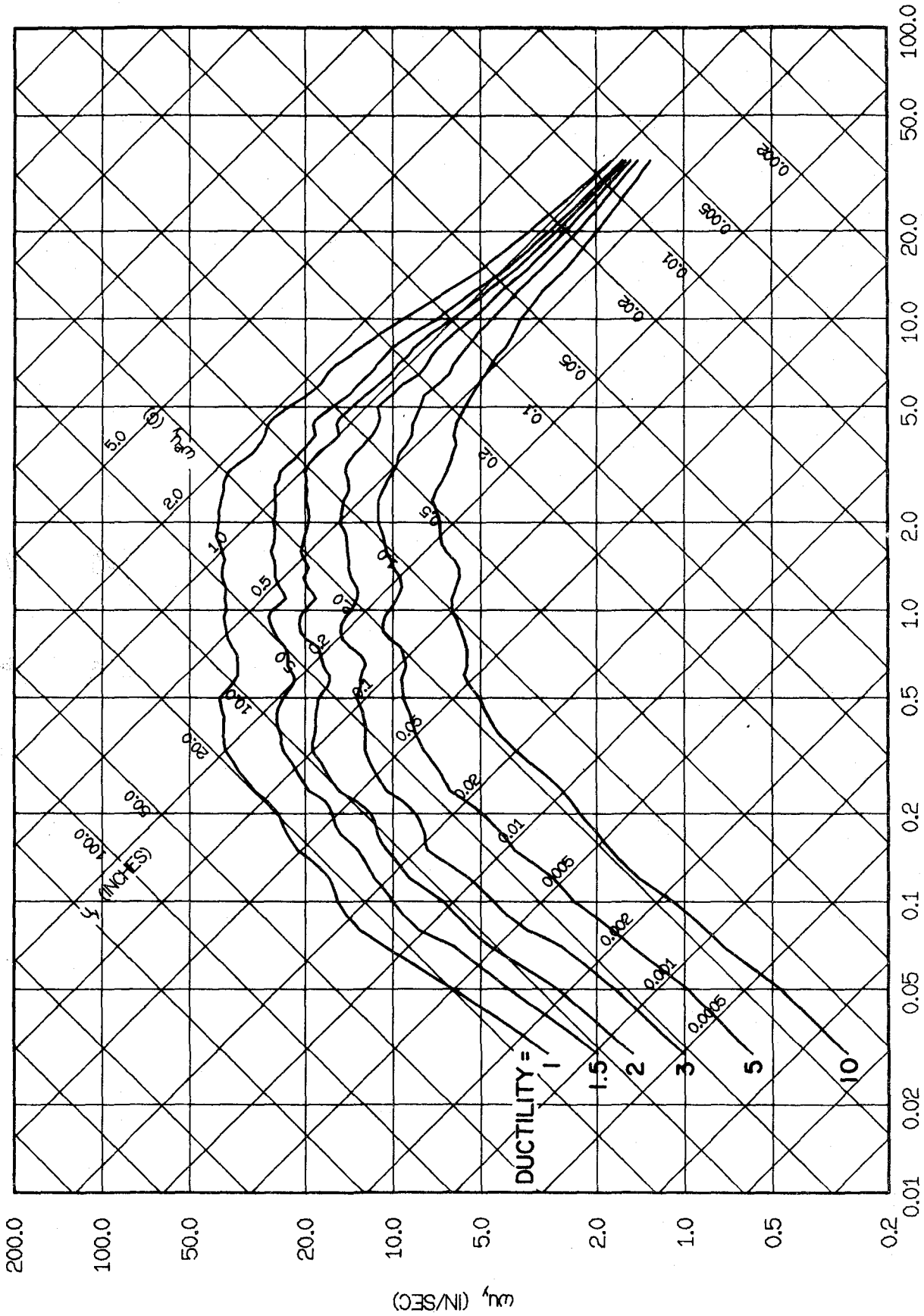
FIG. 4.9 MEAN OF SPECTRA NORMALIZED TO GROUND ACCELERATION. ELASTOPLASTIC SYSTEMS WITH 10% DAMPING.
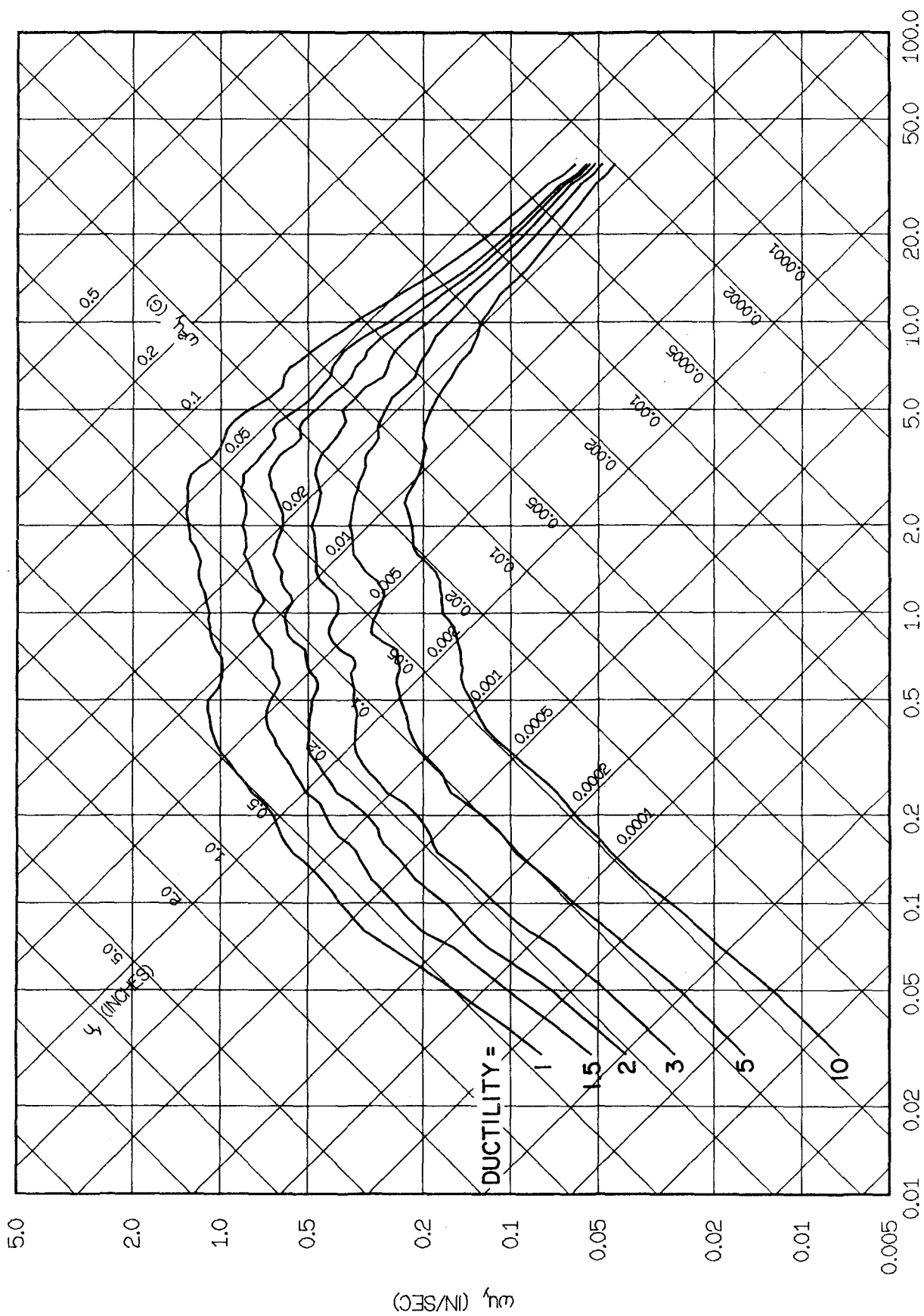
FIG. 4.10   MEAN OF SPECTRA NORMALIZED TO GROUND VELOCITY.   ELASTOPLASTIC SYSTEMS
WITH 10% DAMPING.
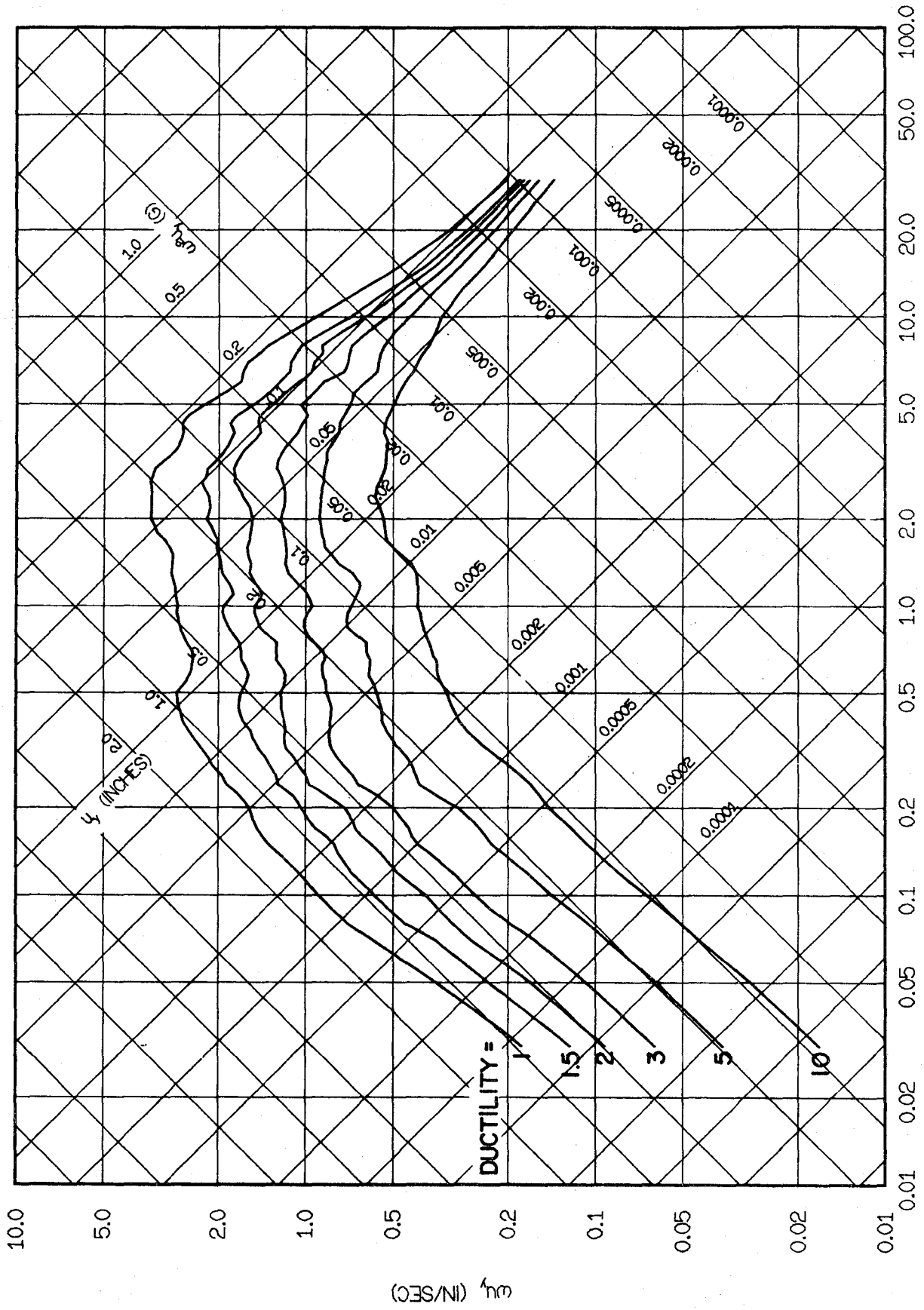
FIG. 4.11 MEAN OF SPECTRA NORMALIZED TO GROUND DISPLACEMENT. ELASTOPLASTIC SYSTEMS WITH 10% DAMPING.
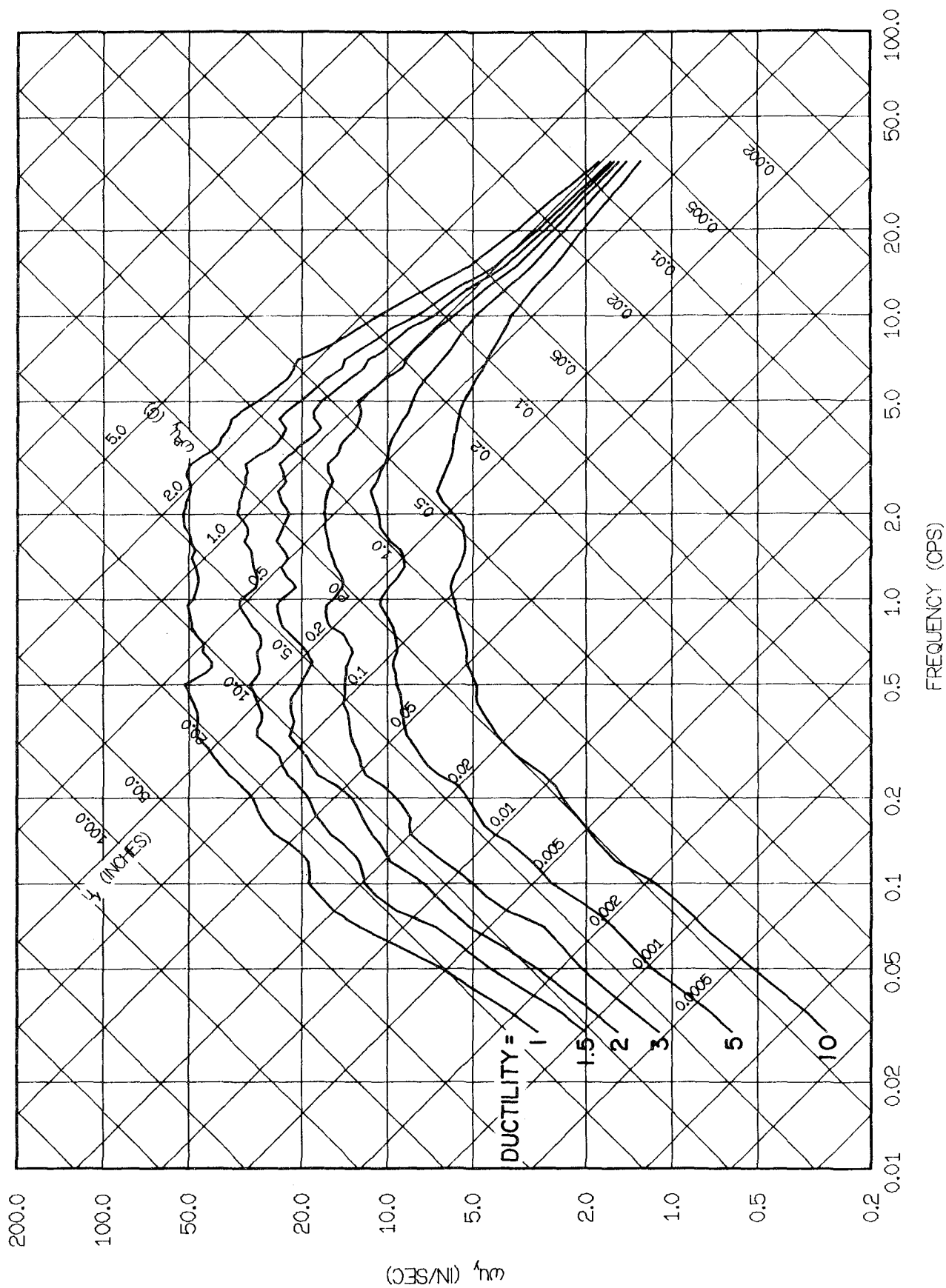
FIG. 4.12 MEAN OF YIELD SPECTRA NORMALIZED TO GROUND ACCELERATION. BILINEAR SYSTEMS.
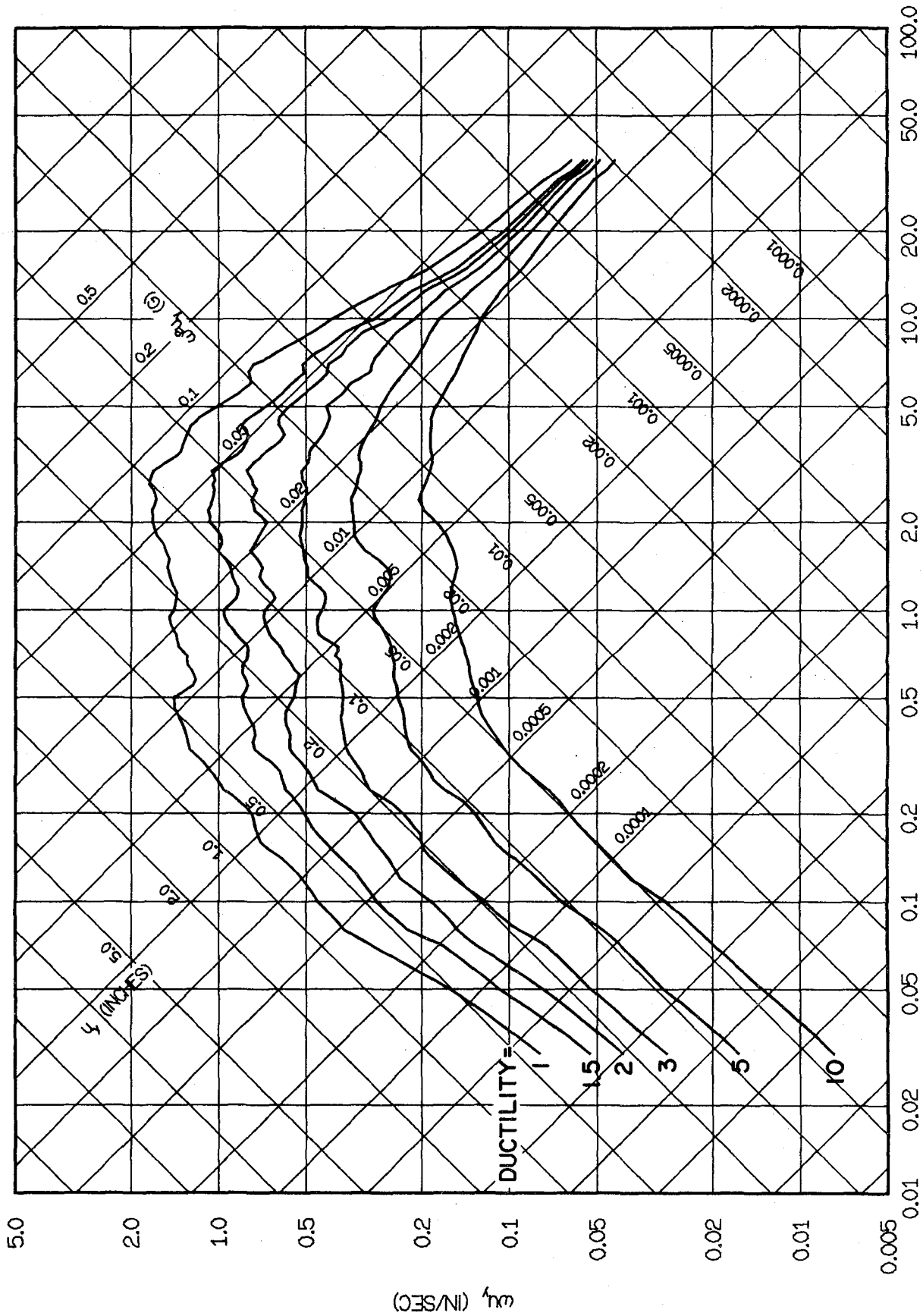
FIG. 4.13 MEAN OF YIELD SPECTRA NORMALIZED TO GROUND VELOCITY. BILINEAR SYSTEMS.
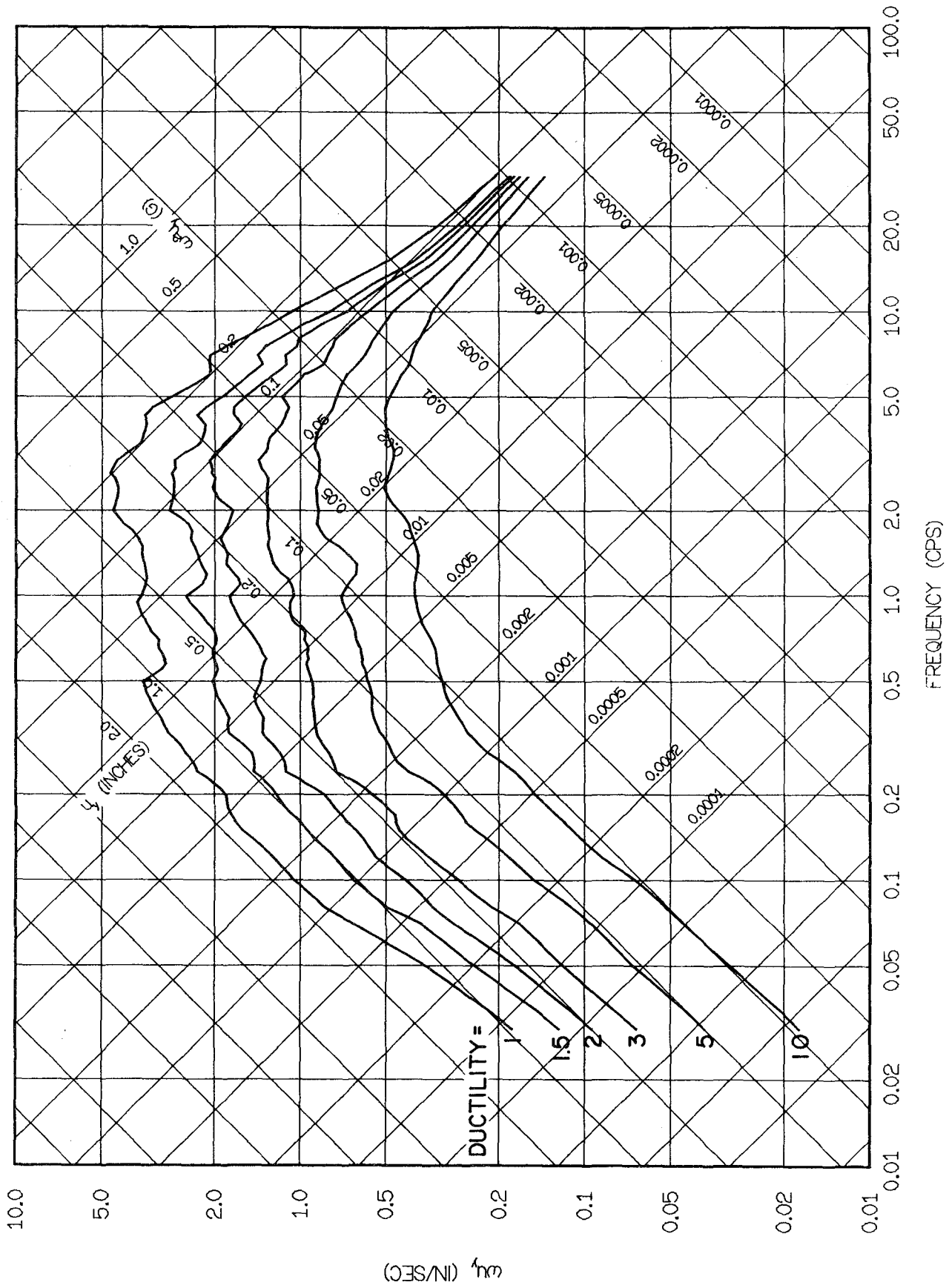
FIG. 4.14 MEAN OF YIELD SPECTRA NORMALIZED TO GROUND DISPLACEMENT. BILINEAR SYSTEMS.
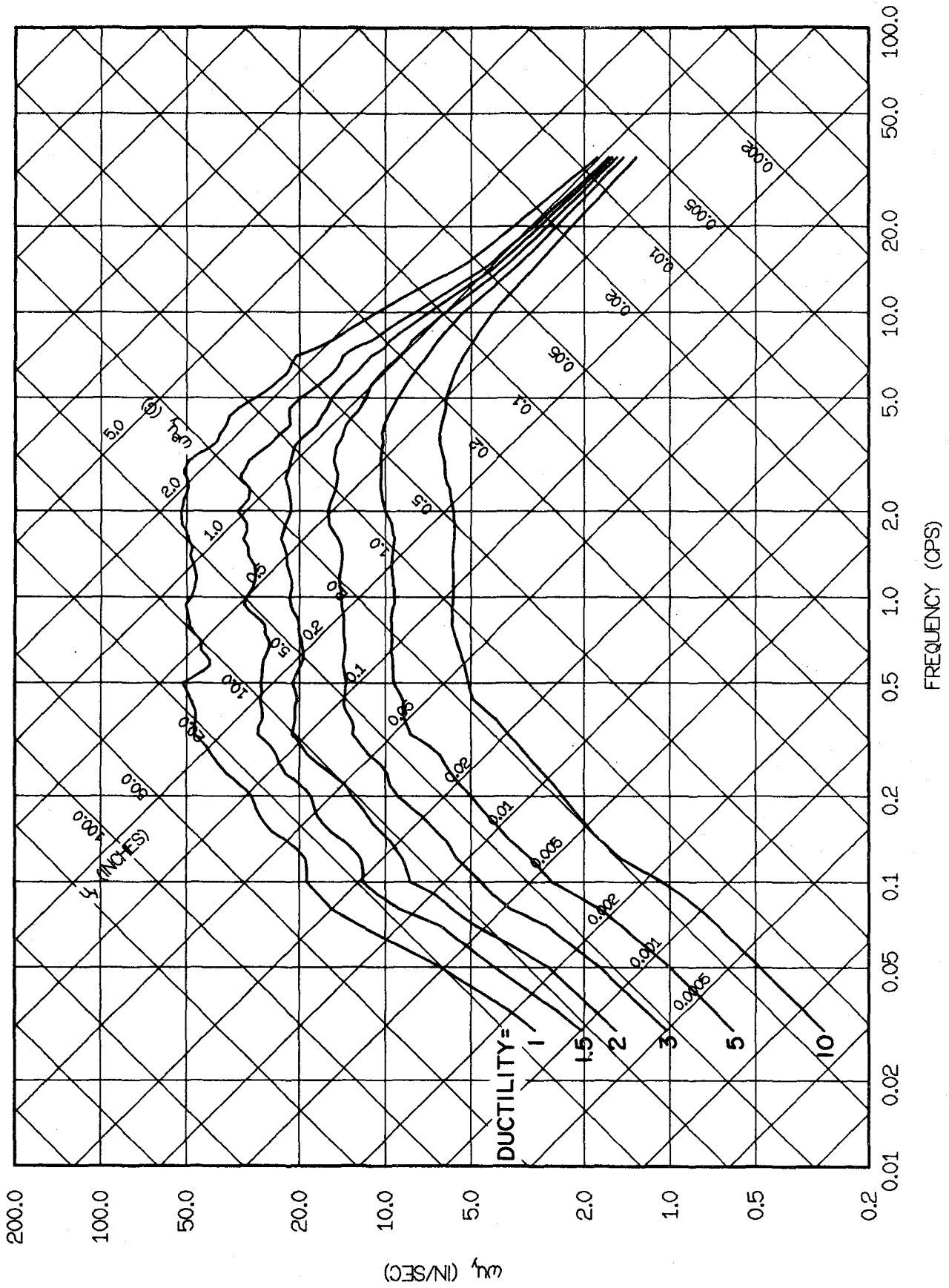
FIG. 4.15   MEAN OF YIELD SPECTRA NORMALIZED TO GROUND ACCELERATION.   DEGRADING SYSTEMS.
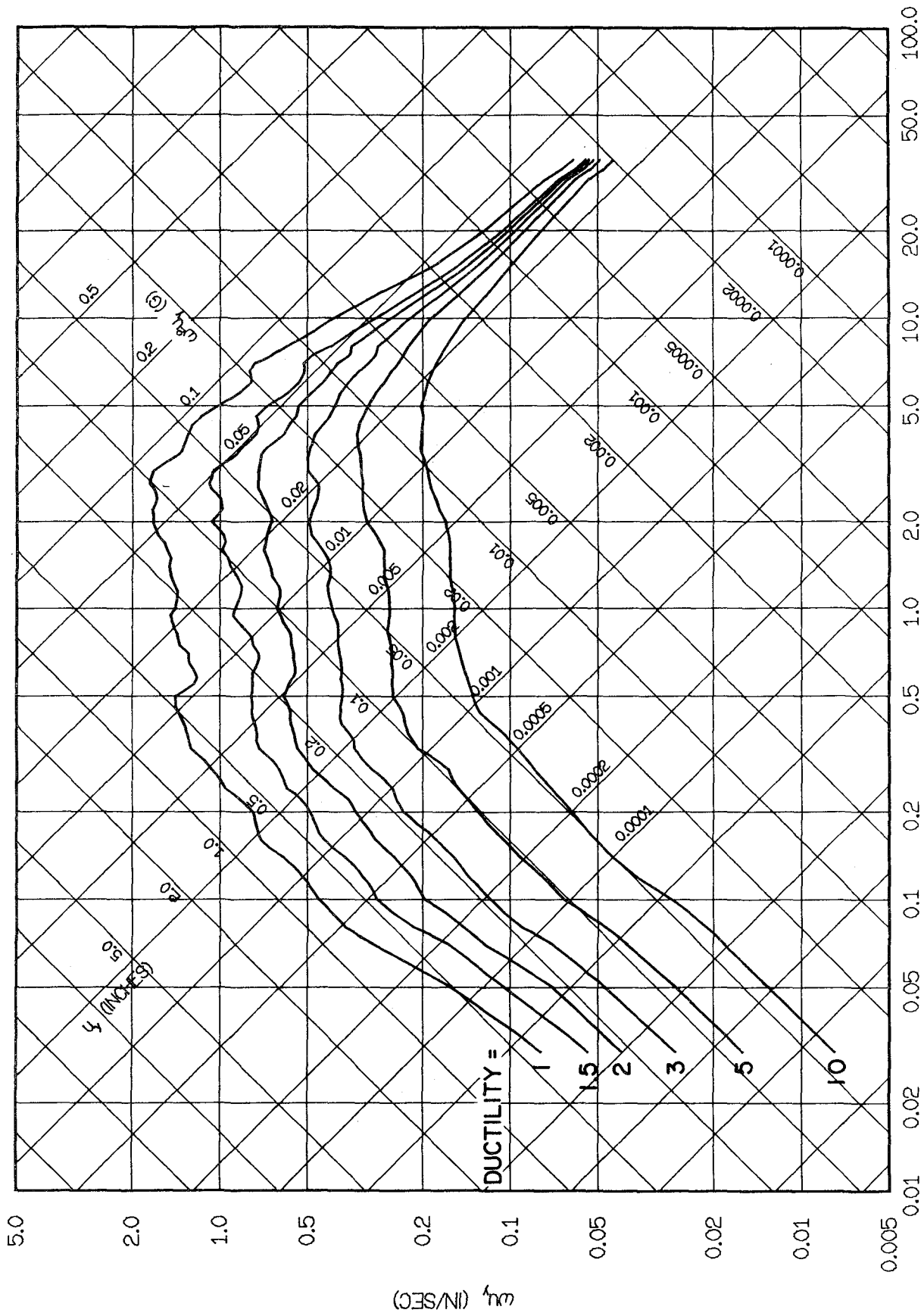
FIG. 4.16   MEAN OF YIELD SPECTRA NORMALIZED TO GROUND VELOCITY.   DEGRADING SYSTEMS.
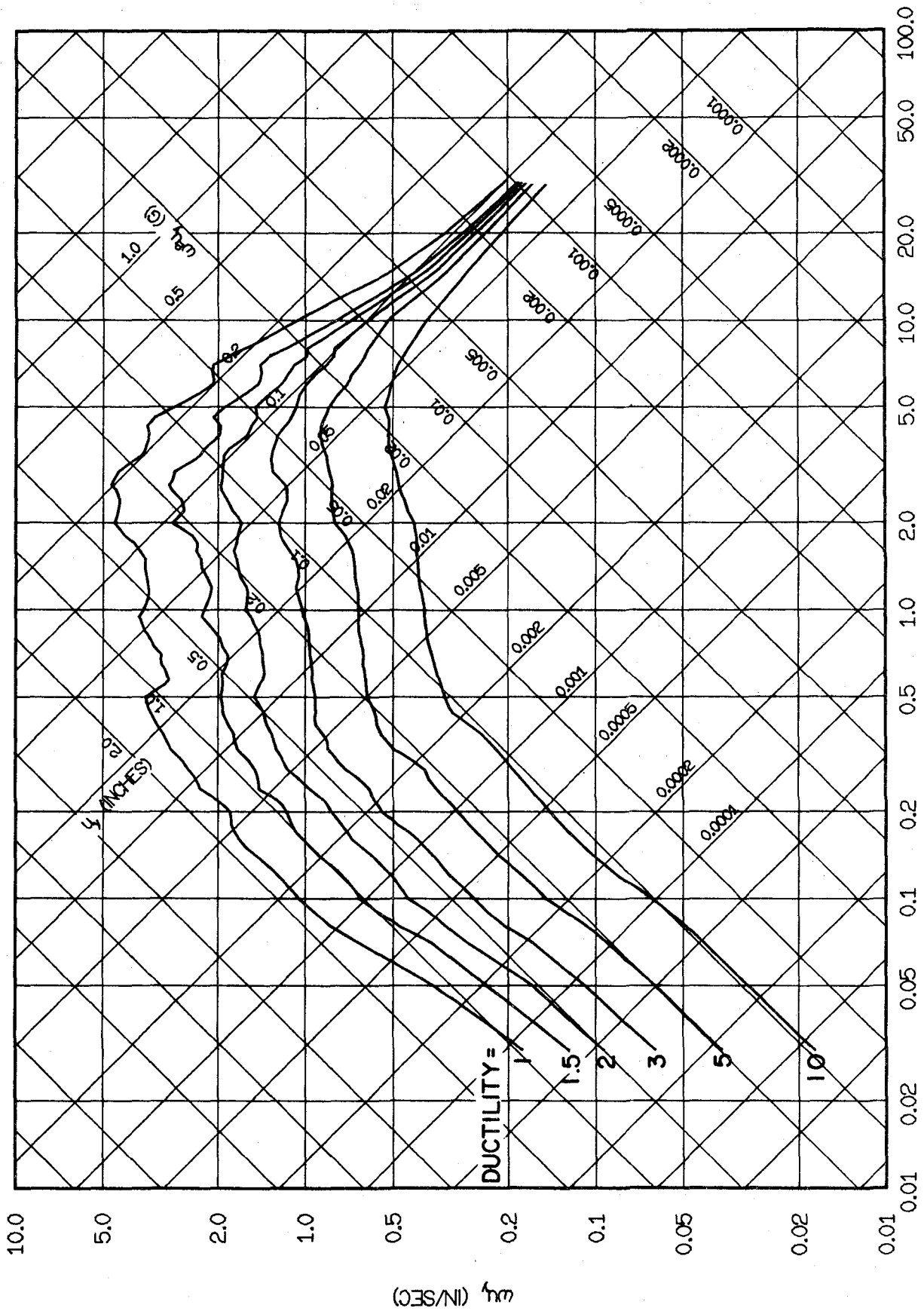
FIG. 4.17 MEAN OF YIELD SPECTRA NORMALIZED TO GROUND DISPLACEMENT. DEGRADING SYSTEMS.
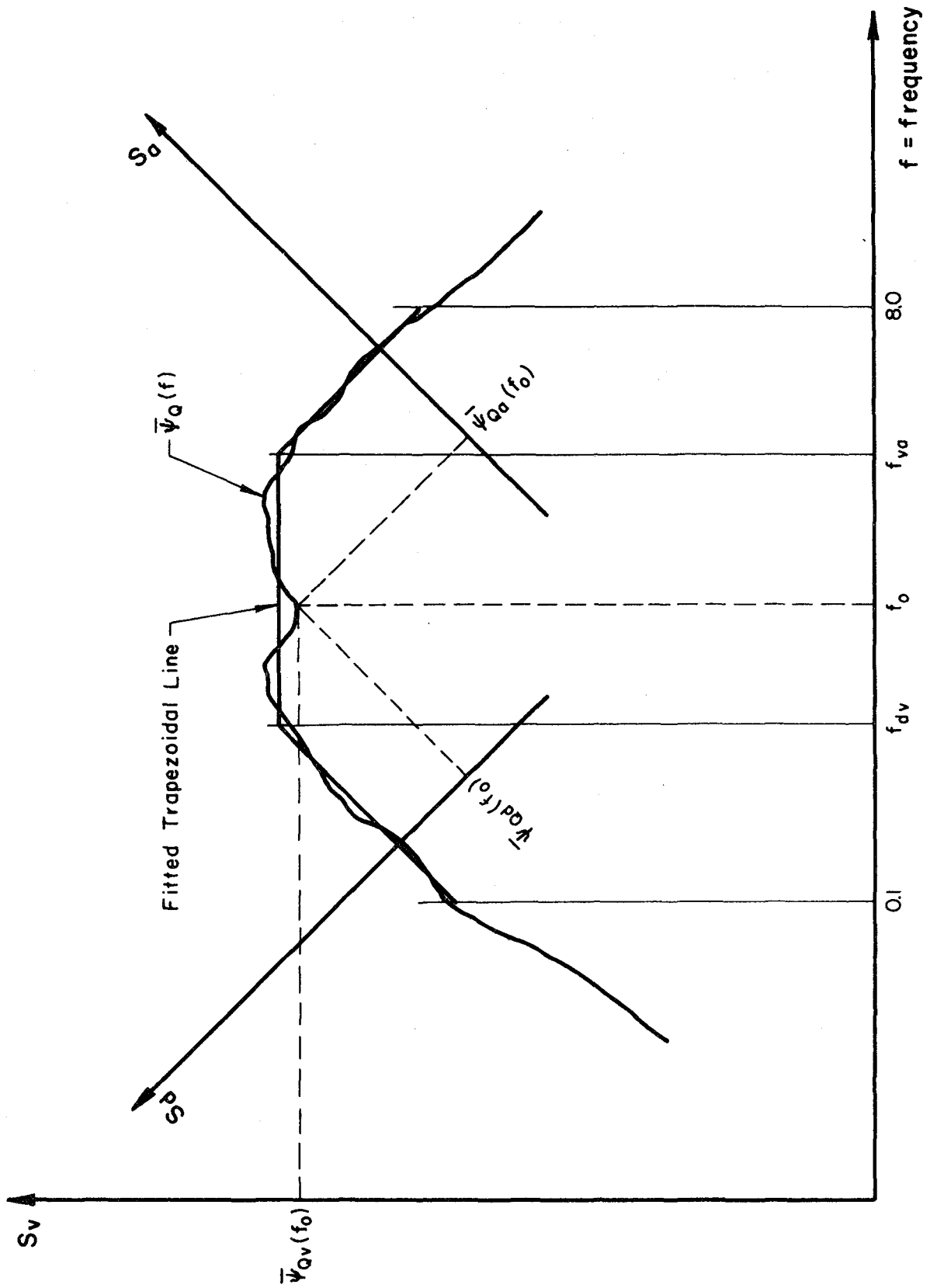
FIG. 4.18 TRAPEZOIDAL LINE FITTED TO AVERAGE SPECTRUM
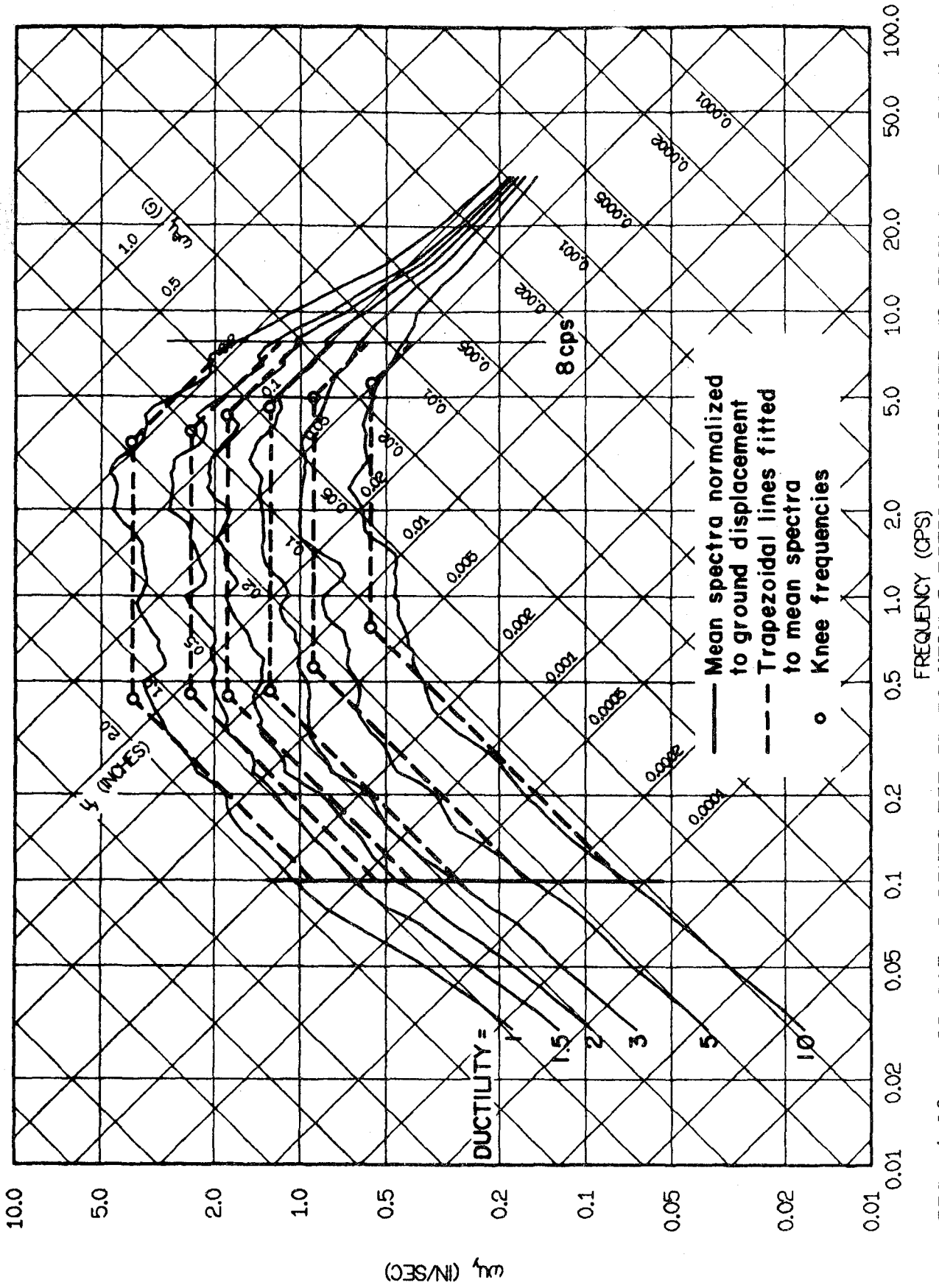
FIG. 4.19 TRAPEZOIDAL LINES FITTED TO MEAN SPECTRA NORMALIZED TO GROUND DISPLACEMENT
AND KNEE FREQUENCIES. ELASTOPLASTIC SYSTEMS WITH 5 PERCENT DAMPING
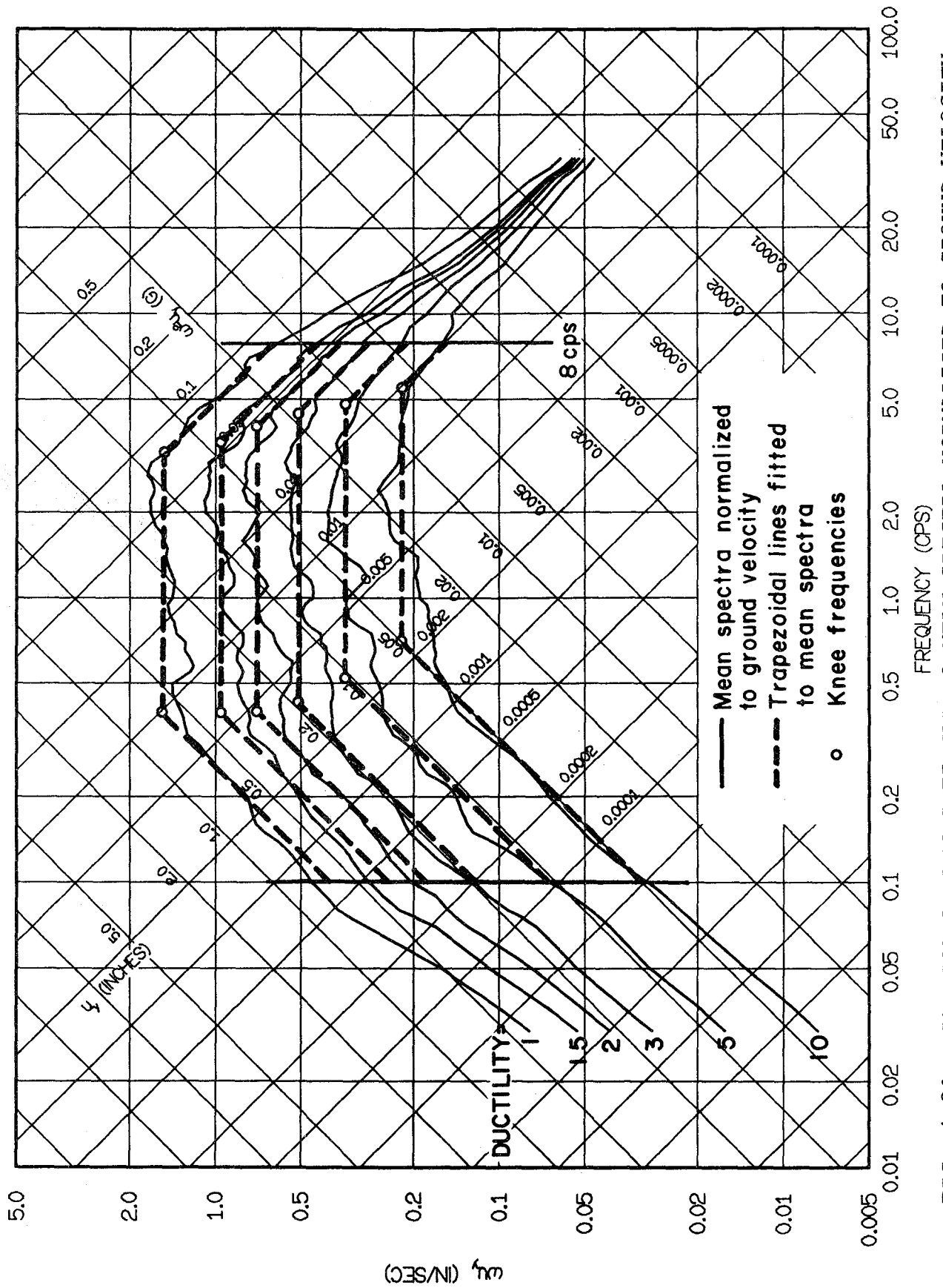
FIG. 4.20 TRAPEZOIDAL LINES FITTED TO MEAN SPECTRA NORMALIZED TO GROUND VELOCITY AND KNEE FREQUENCIES. ELASTOPLASTIC SYSTEMS WITH 5 PERCENT DAMPING.
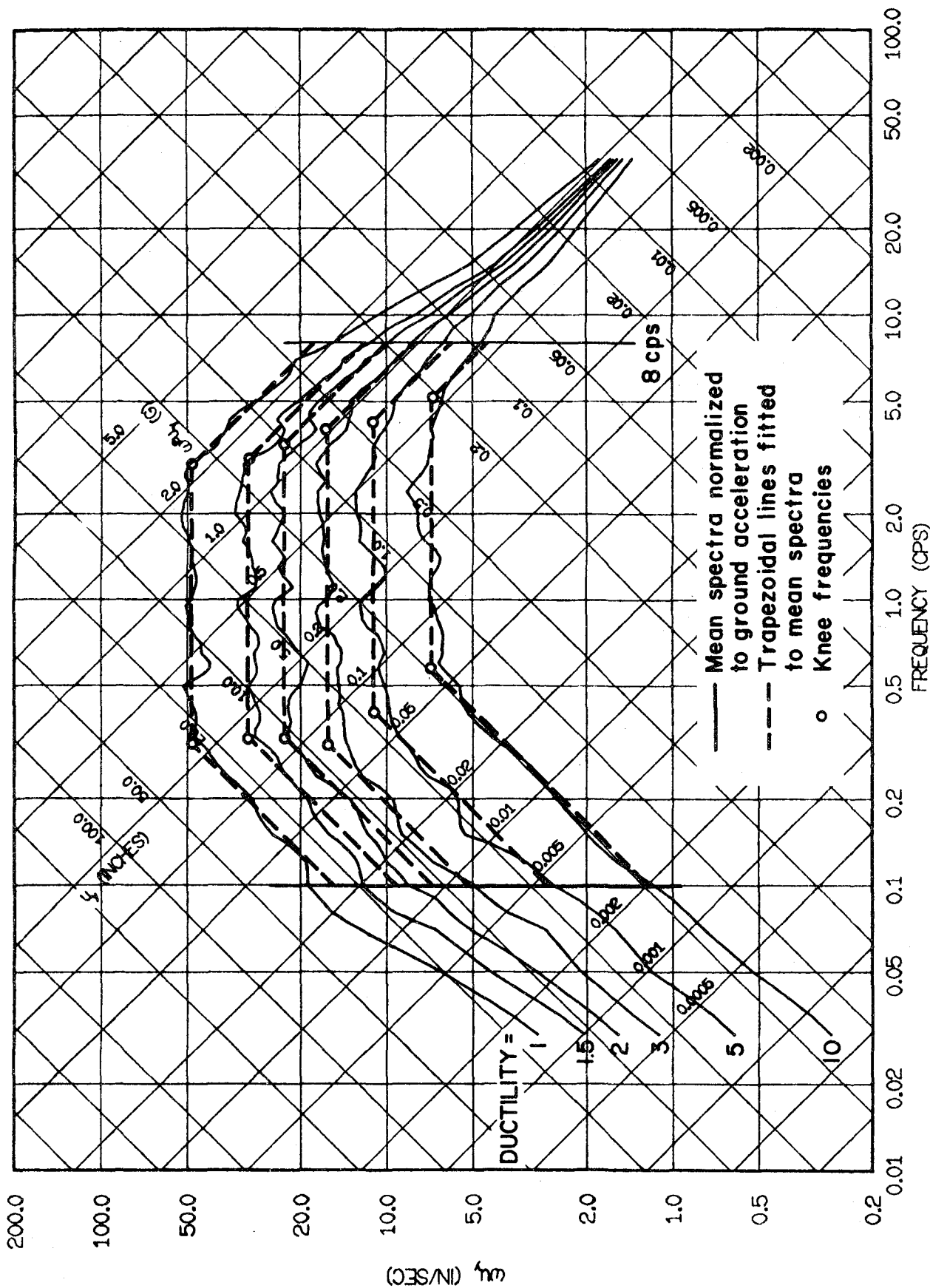
FIG. 4.21 TRAPEZOIDAL LINES FITTED TO MEAN SPECTRA NORMALIZED TO GROUND ACCELERATION AND KNEE FREQUENCIES. ELASTOPLASTIC SYSTEMS WITH 5 PERCENT DAMPING
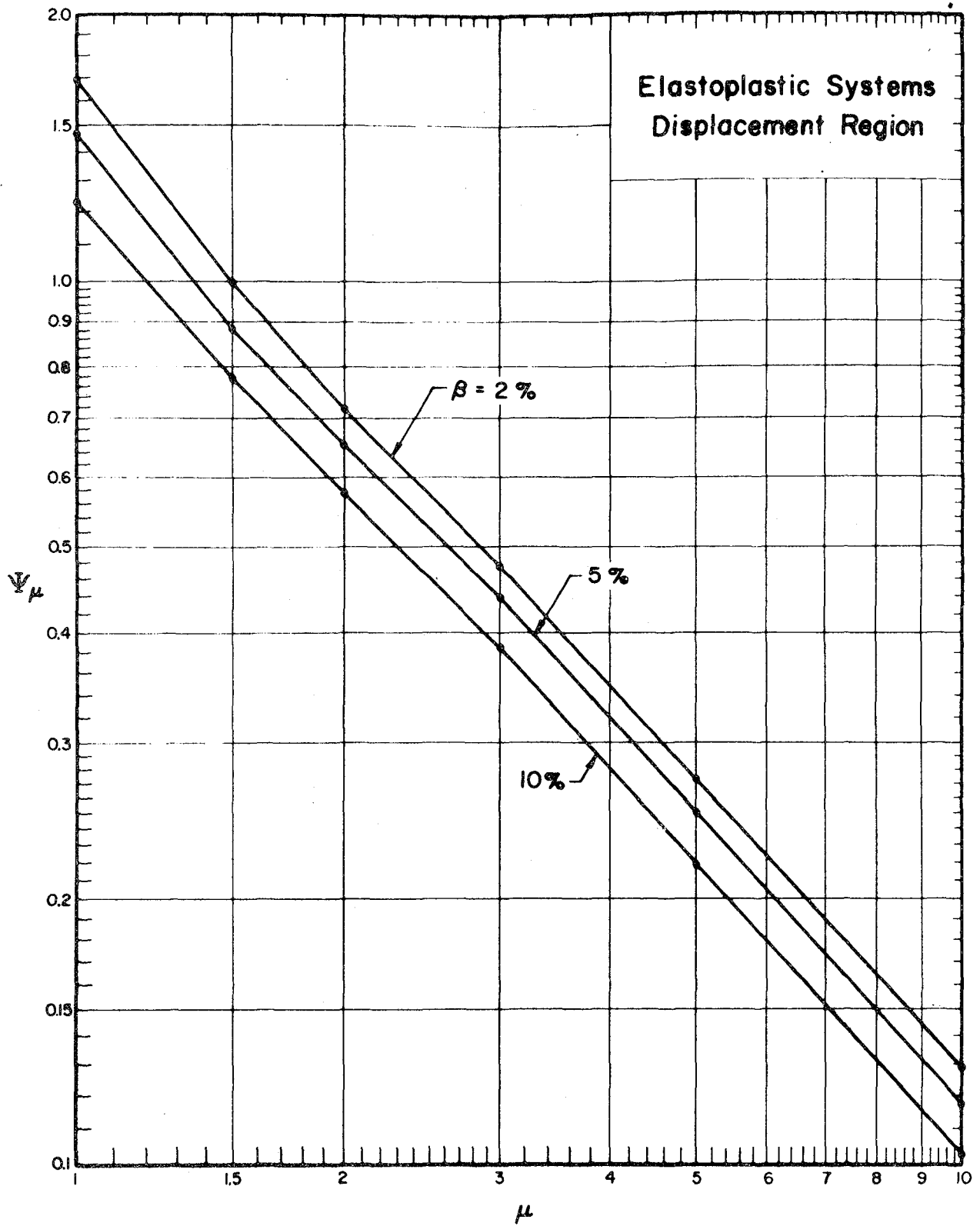
FIG. 4.22 ψ_μ FOR ELASTOPLASTIC SYSTEMS. DISPLACEMENT REGION.
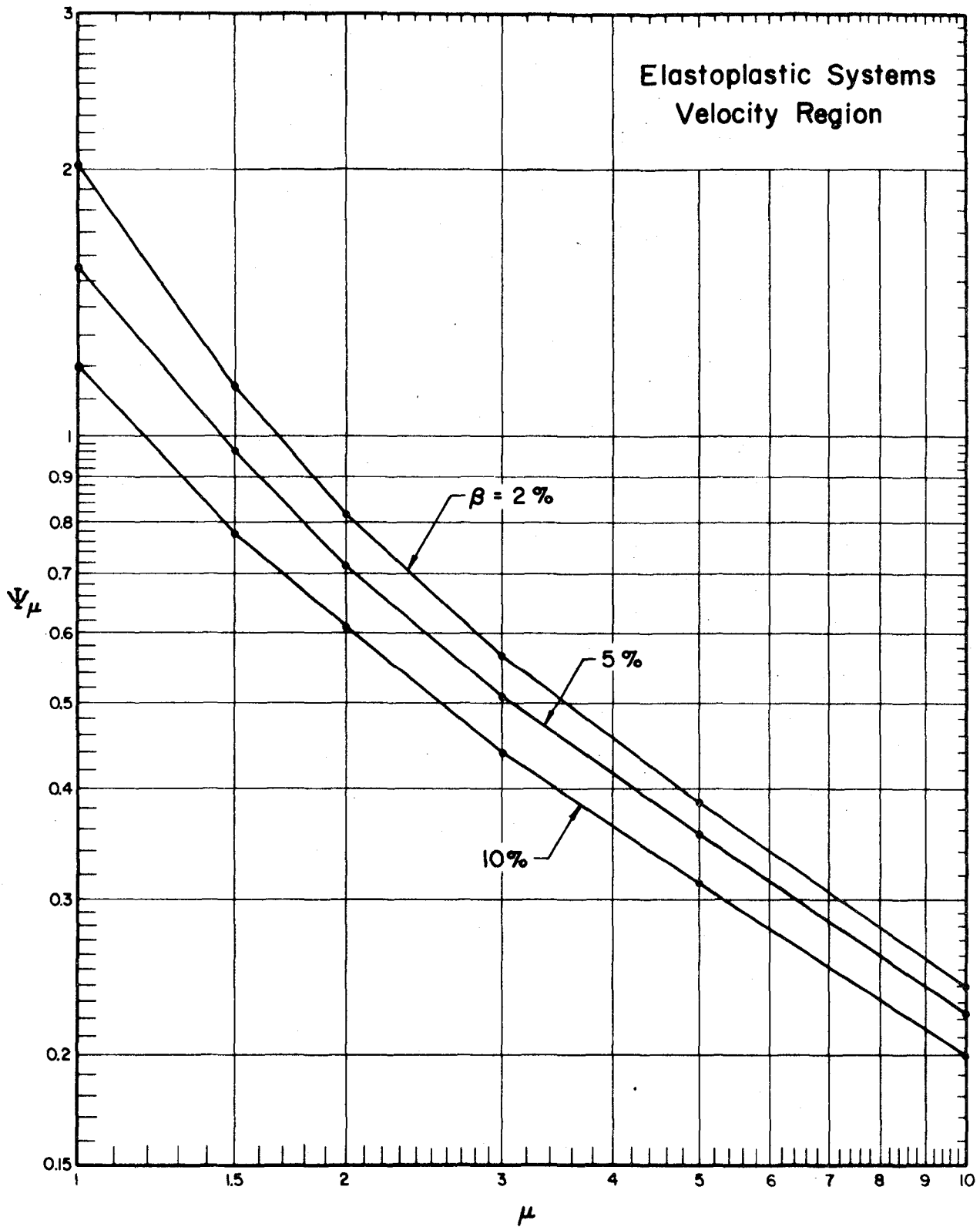
FIG. 4.23 ψ_μ FOR ELASTOPLASTIC SYSTEMS. VELOCITY REGION.
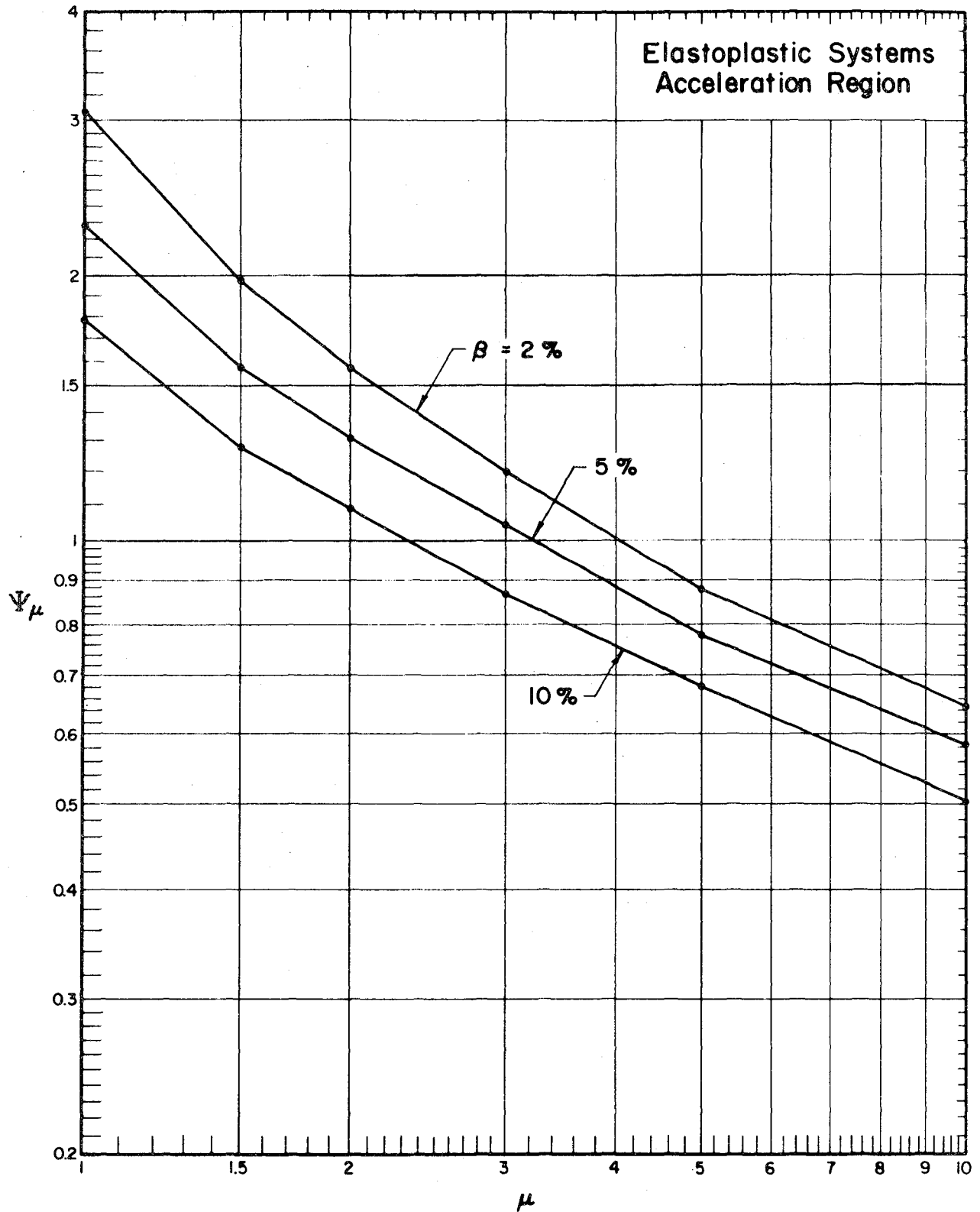
FIG. 4.24 ψ_μ FOR ELASTOPLASTIC SYSTEMS. ACCELERATION REGION.
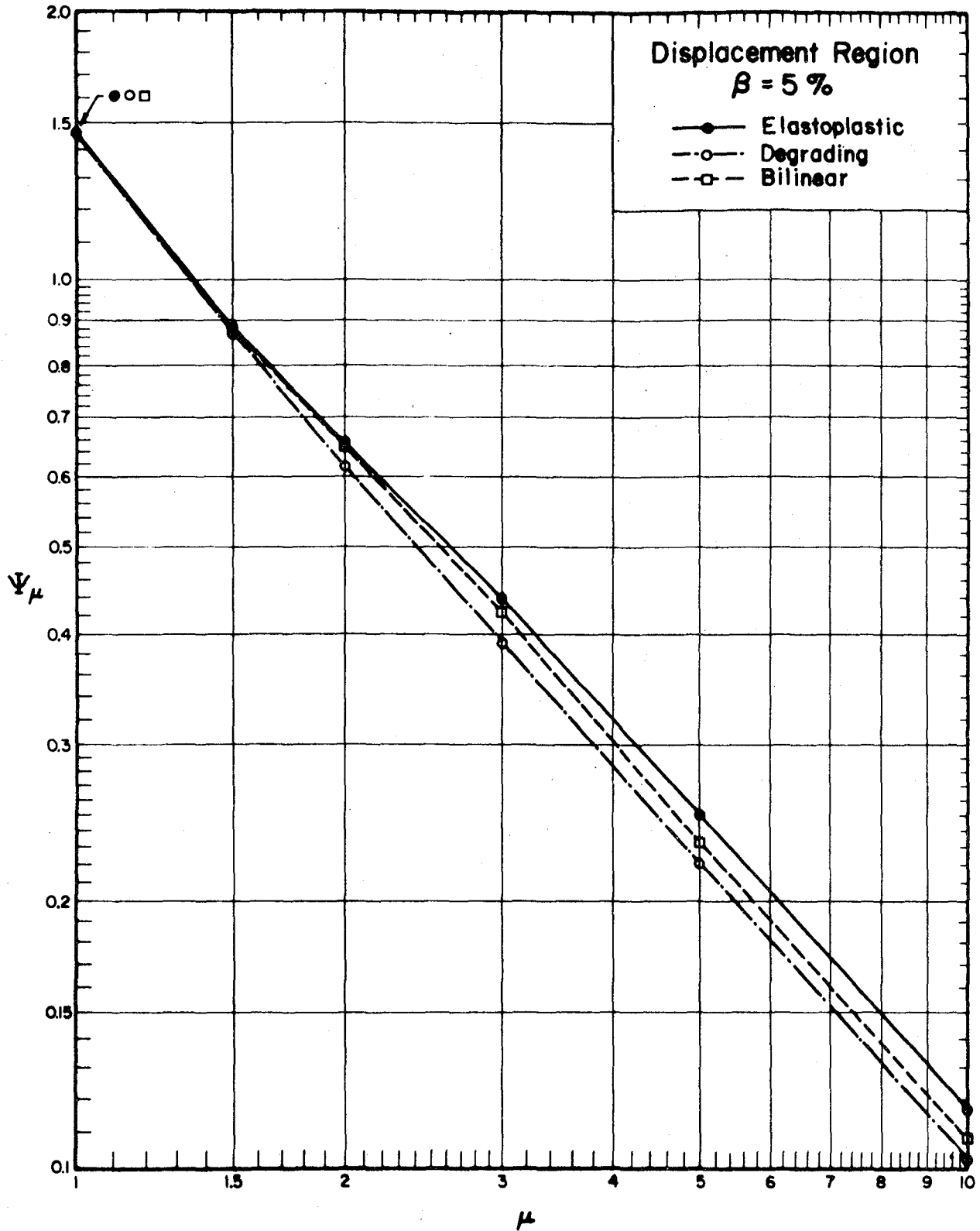
FIG. 4.25 Ψ_μ FOR ELASTOPLASTIC, DEGRADING, AND BILINEAR SYSTEMS. DISPLACEMENT REGION.
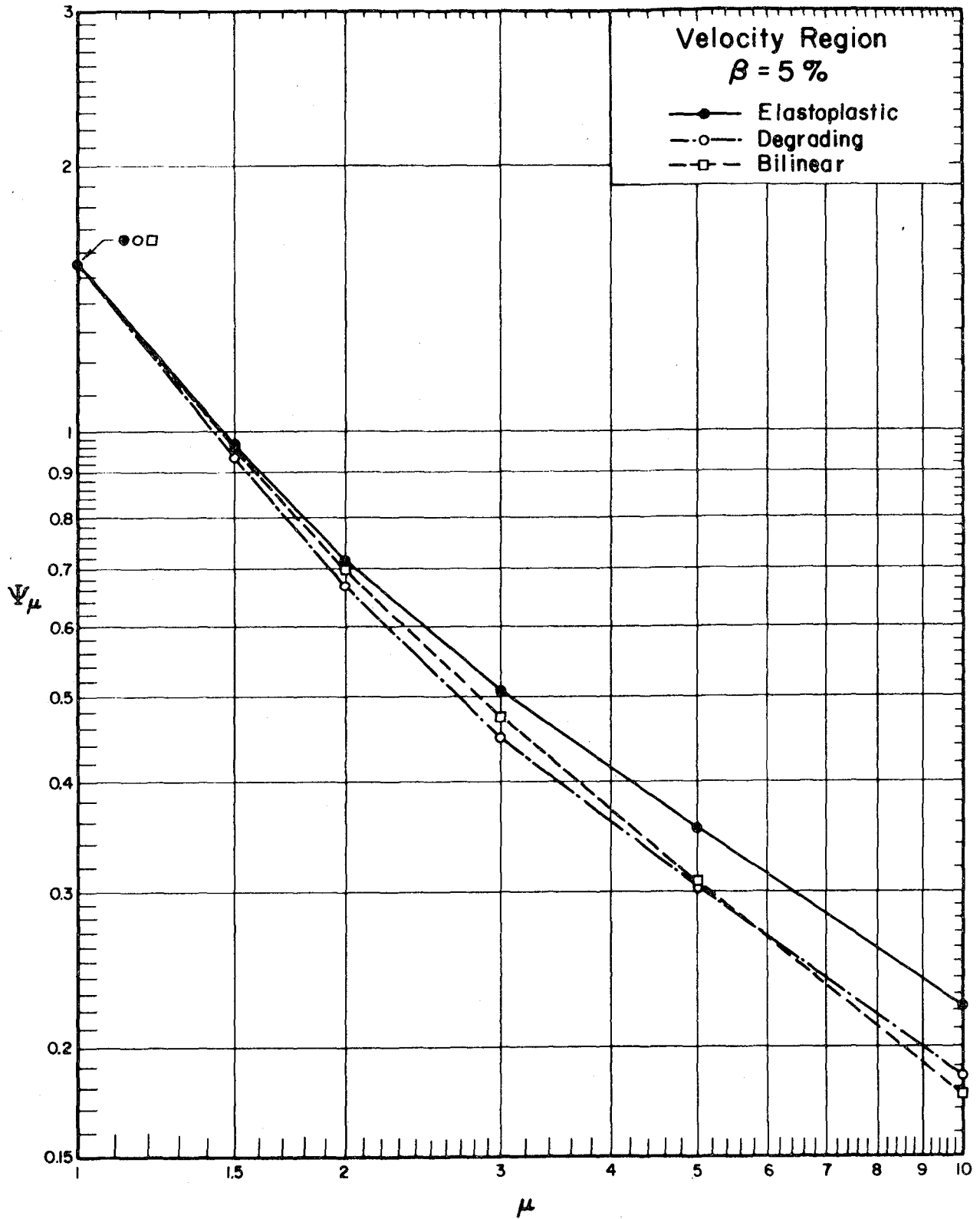
FIG. 4.26 Ψ_μ FOR ELASTOPLASTIC, DEGRADING, AND BILINEAR SYSTEMS VELOCITY REGION.
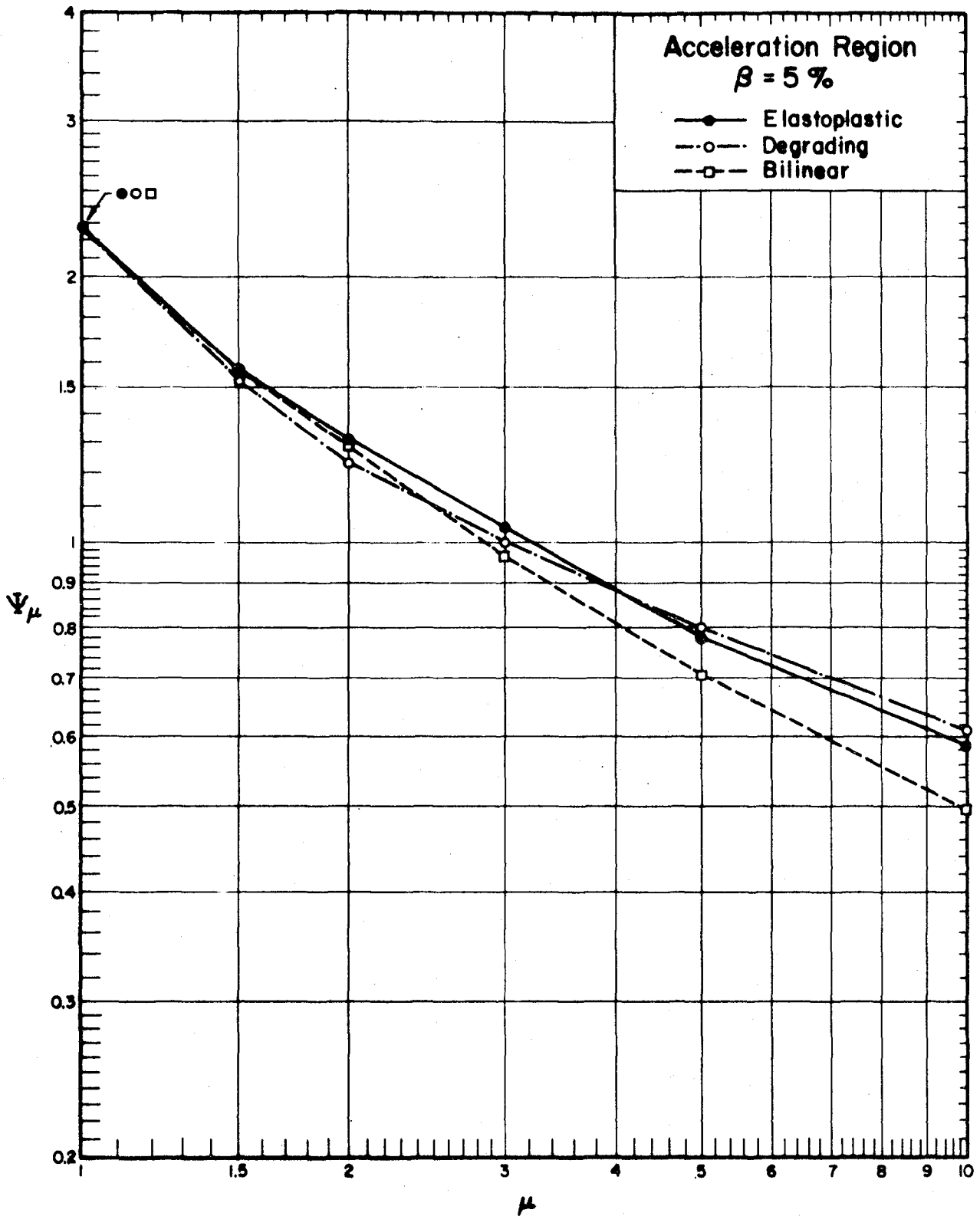
FIG. 4.27 Ψ_μ FOR ELASTOPLASTIC, DEGRADING, AND BILINEAR SYSTEMS. ACCELERATION REGION.
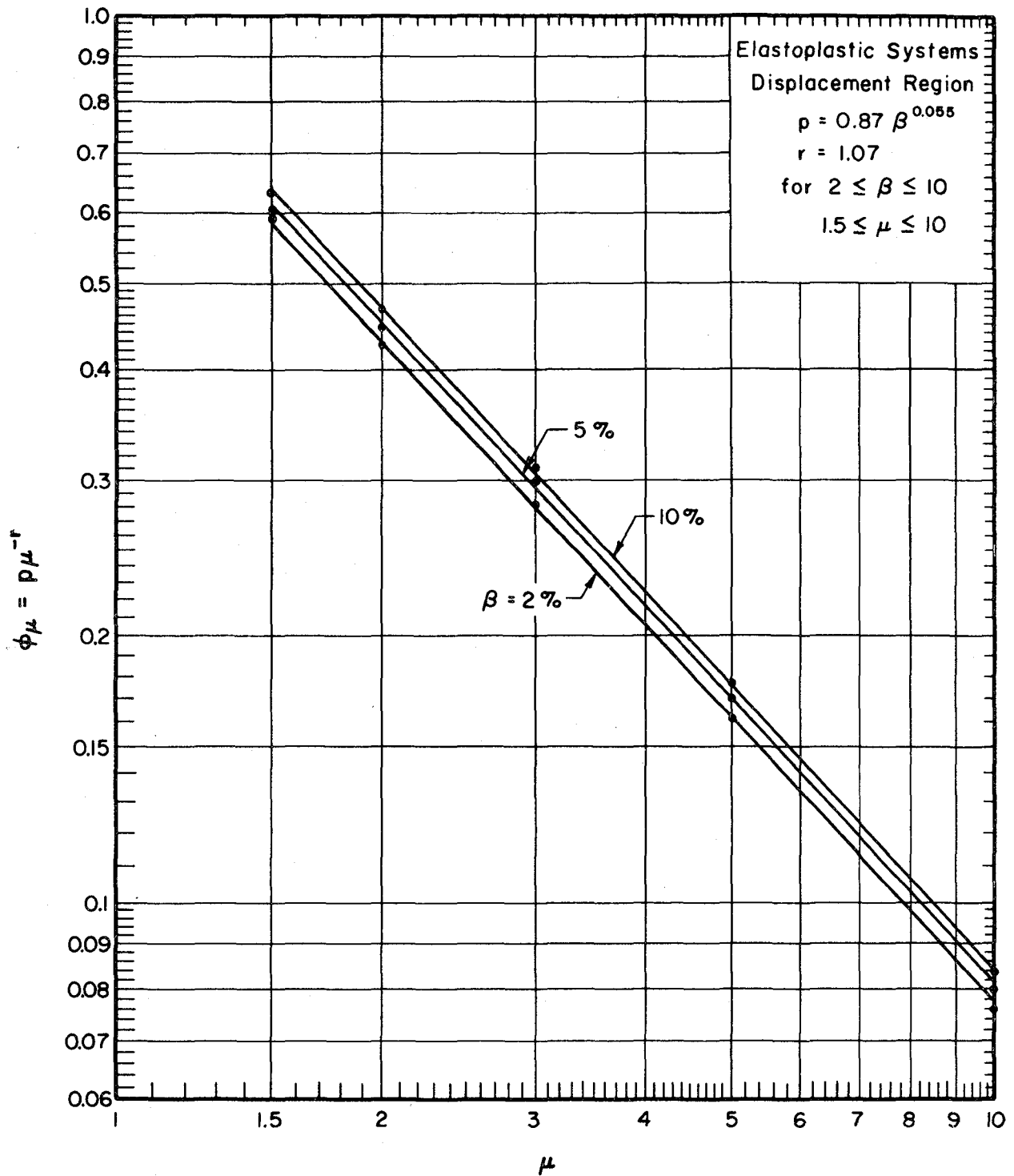
FIG. 4.28   DEAMPLIFICATION FACTOR FOR ELASTOPLASTIC SYSTEMS.
DISPLACEMENT REGION.
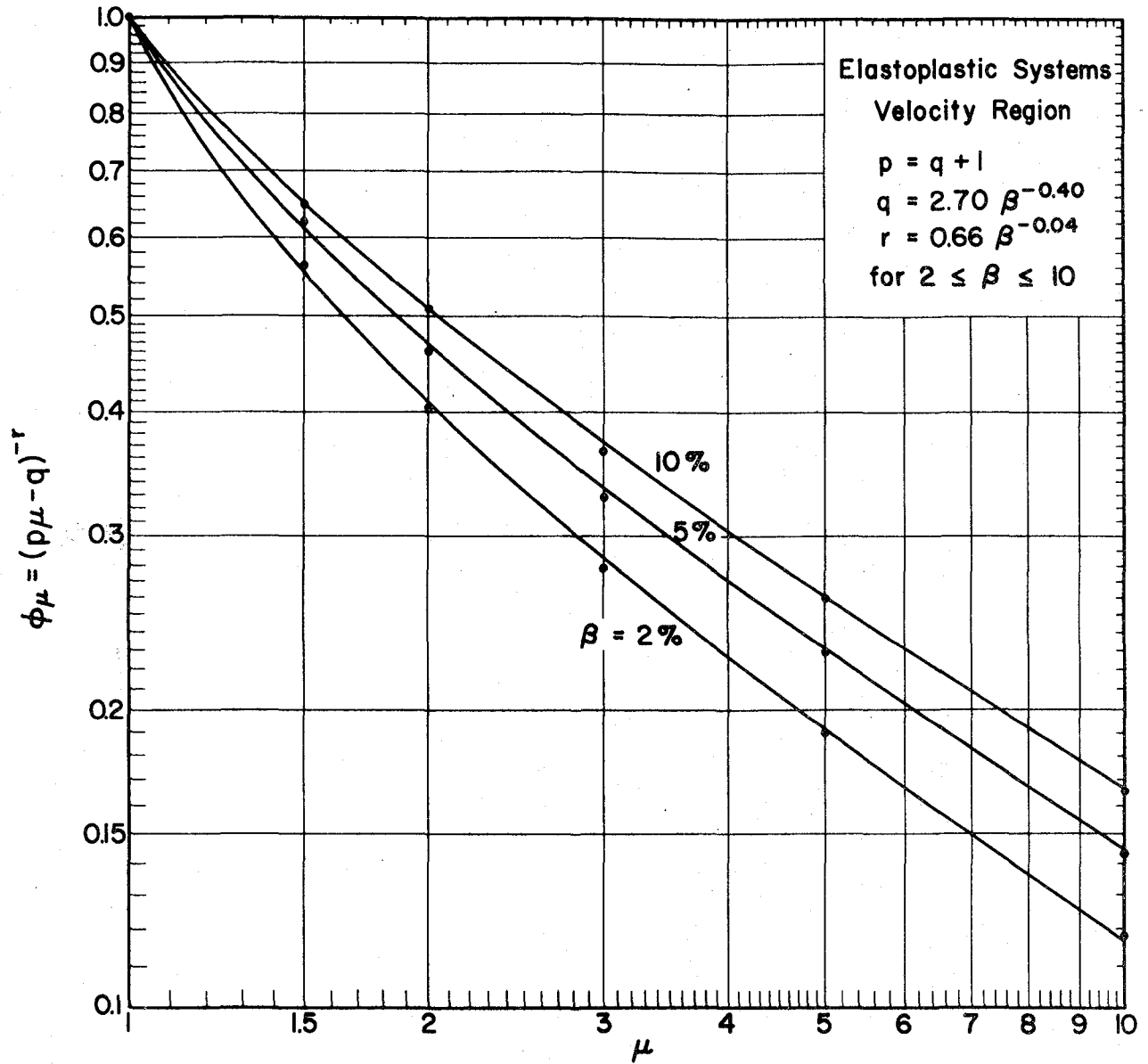
FIG. 4.29   DEAMPLIFICATION FACTOR FOR ELASTOPLASTIC SYSTEMS.
            VELOCITY REGION.
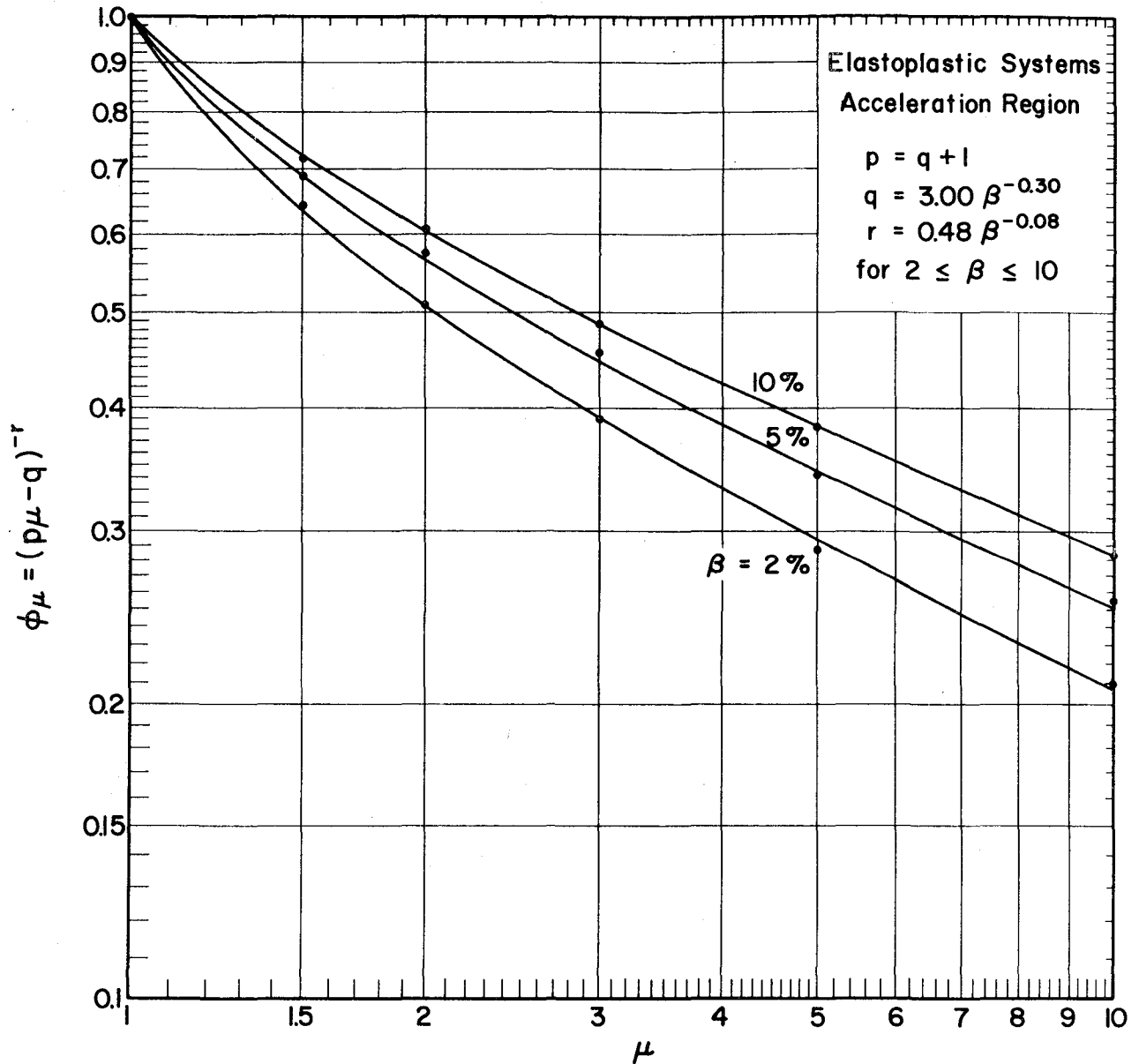
FIG. 4.30   DEAMPLIFICATION FACTOR FOR ELASTOPLASTIC SYSTEMS.
ACCELERATION REGION.
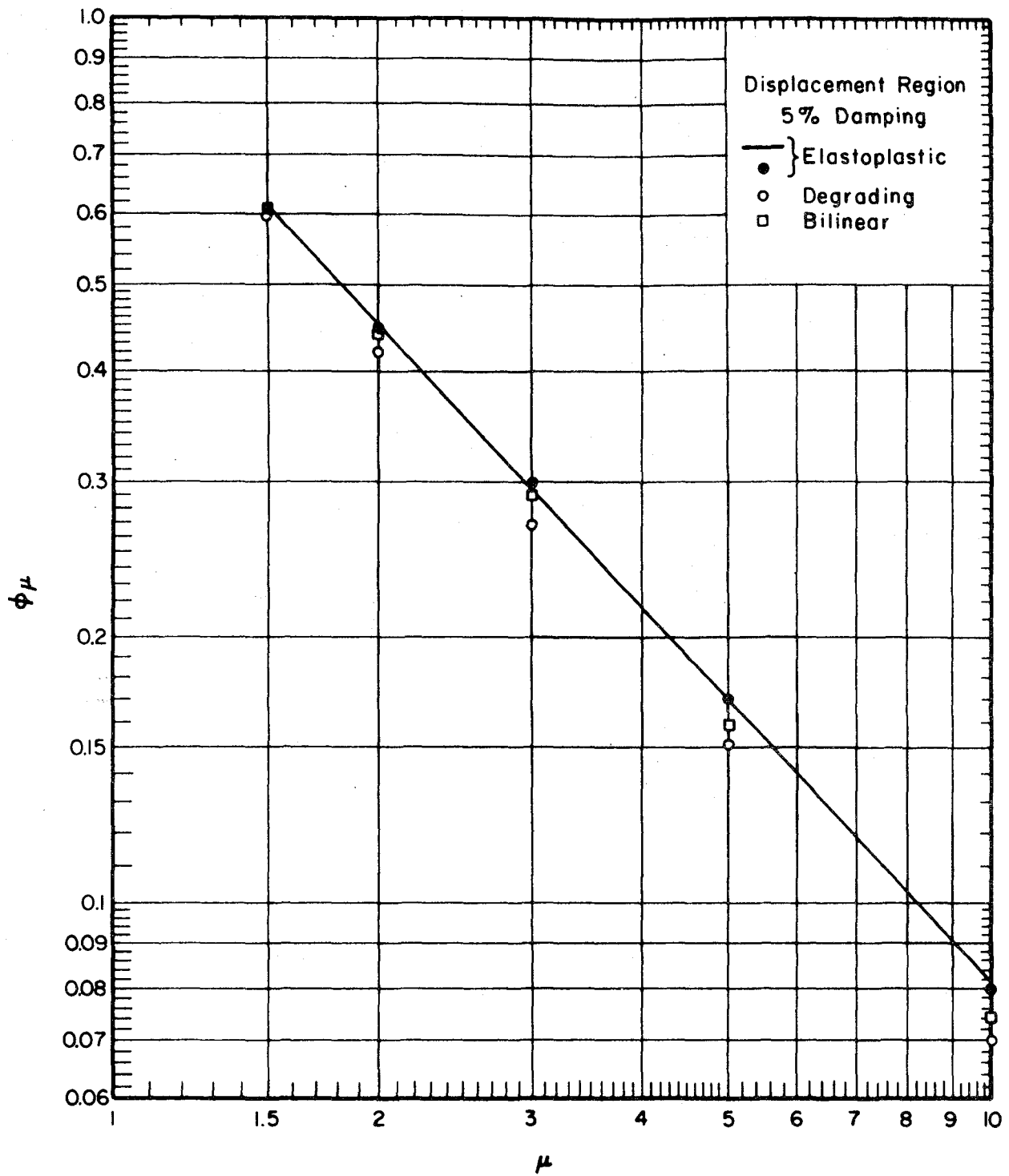
FIG. 4.31   DEAMPLIFICATION FACTOR FOR ELASTOPLASTIC, BILINEAR,
AND DEGRADING SYSTEMS.   DISPLACEMENT REGION.
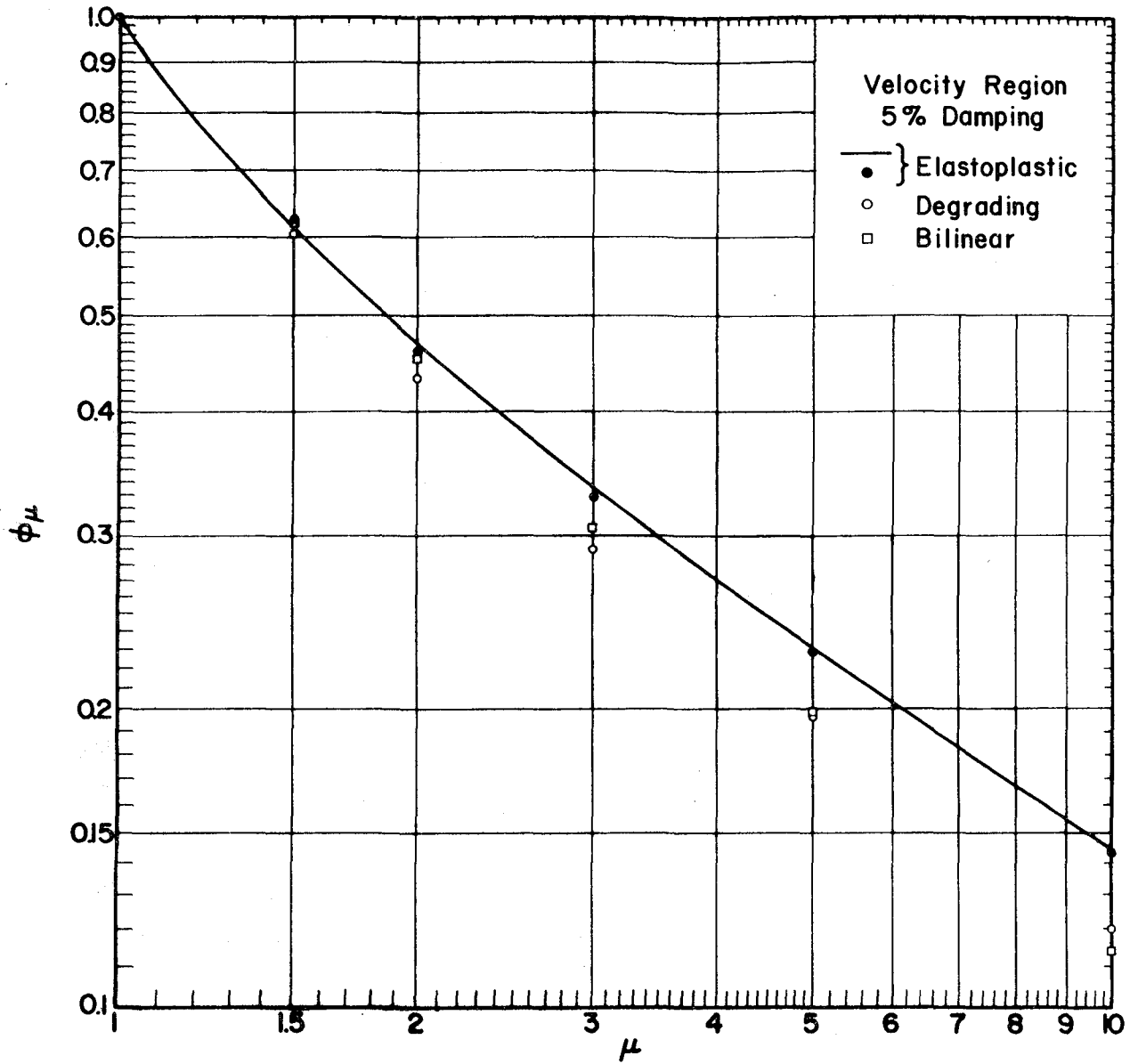
FIG. 4.32   DEAMPLIFICATION FACTOR FOR ELASTOPLASTIC, BILINEAR,
AND DEGRADING SYSTEMS.   VELOCITY REGION.
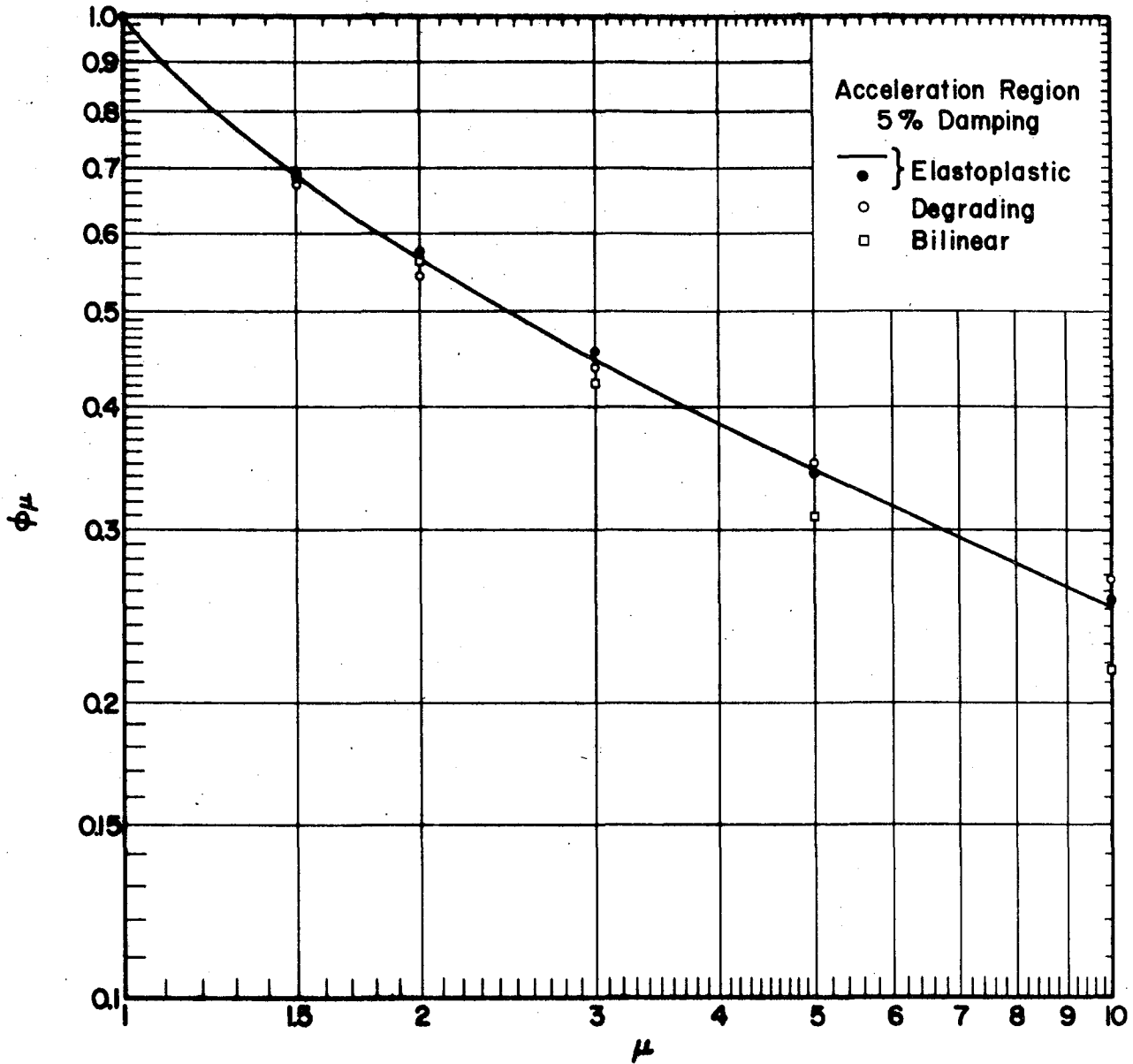
FIG. 4.33   DEAMPLIFICATION FACTOR FOR ELASTOPLASTIC, BILINEAR,
           AND DEGRADING SYSTEMS.   ACCELERATION REGION.

278
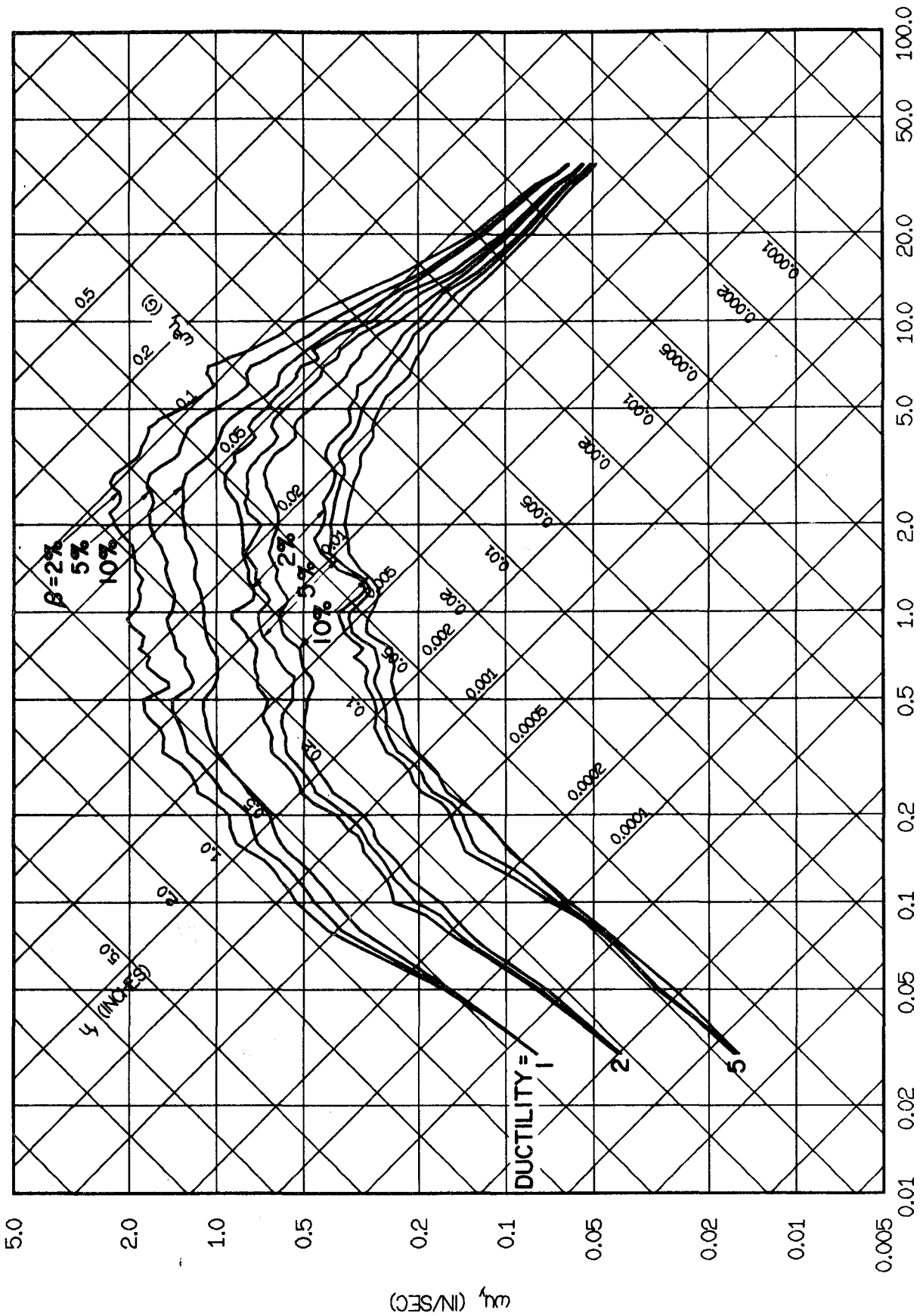
FIG. 4.34 COMPARISON OF MEAN SPECTRA NORMALIZED TO GROUND VELOCITY FOR ELASTOPLASTIC SYSTEMS WITH 2, 5, AND 10% DAMPING, AND DUCTILITY FACTORS OF 1, 2, AND 5.
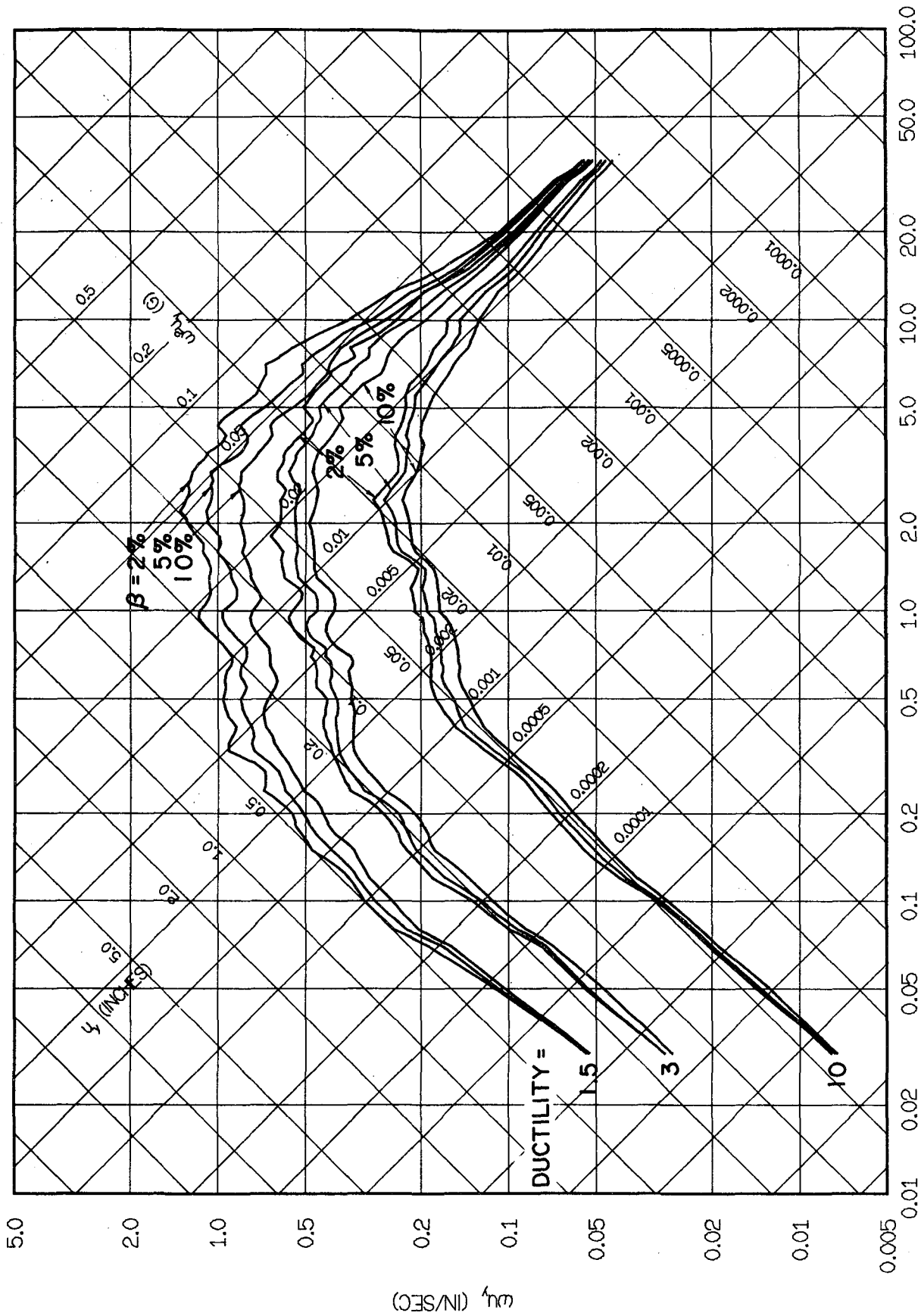
FIG. 4.35   COMPARISON OF MEAN SPECTRA NORMALIZED TO GROUND VELOCITY FOR ELASTOPLASTIC SYSTEMS WITH 2, 5, AND 10% DAMPING, AND DUCTILITIES OF 1.5, 3, AND 10.
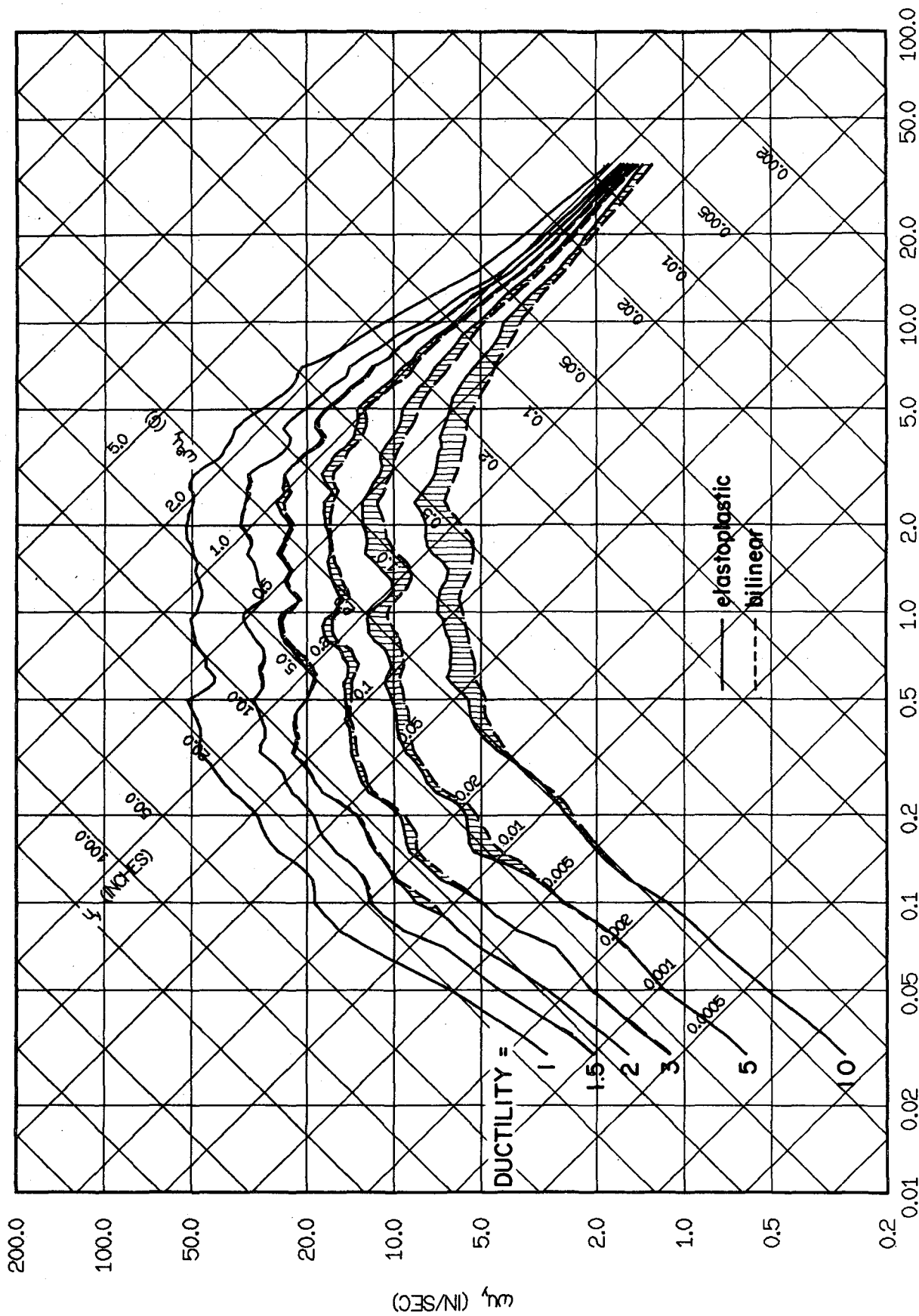
FIG. 4.36 COMPARISON OF MEAN SPECTRA NORMALIZED TO GROUND ACCELERATION FOR BILINEAR AND ELASTOPLASTIC SYSTEMS WITH 5% DAMPING.

FREQUENCY (CPS)
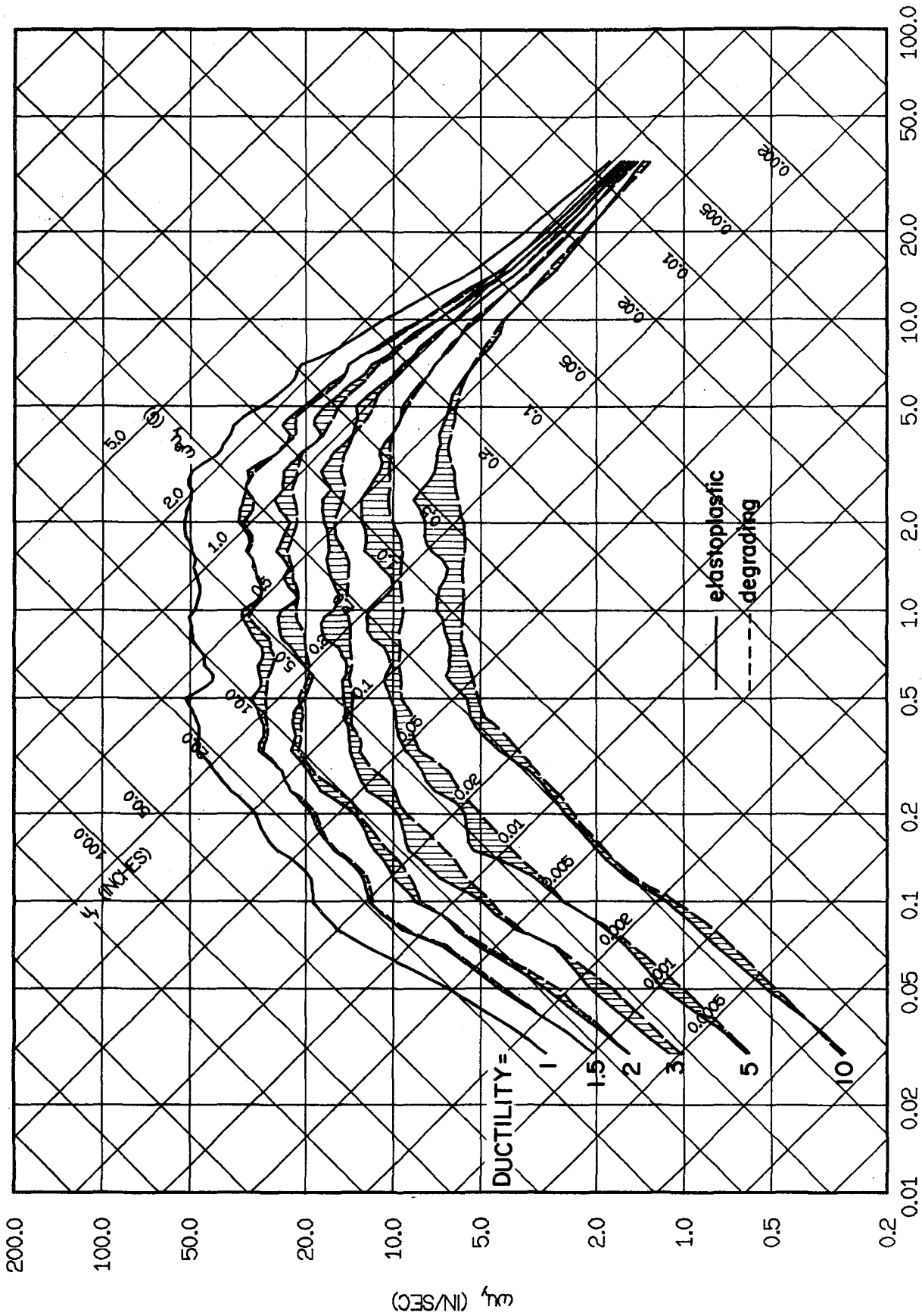
FIG. 4.37   COMPARISON OF MEAN SPECTRA NORMALIZED TO GROUND ACCELERATION FOR DEGRADING AND ELASTOPLASTIC SYSTEMS WITH 5% DAMPING.
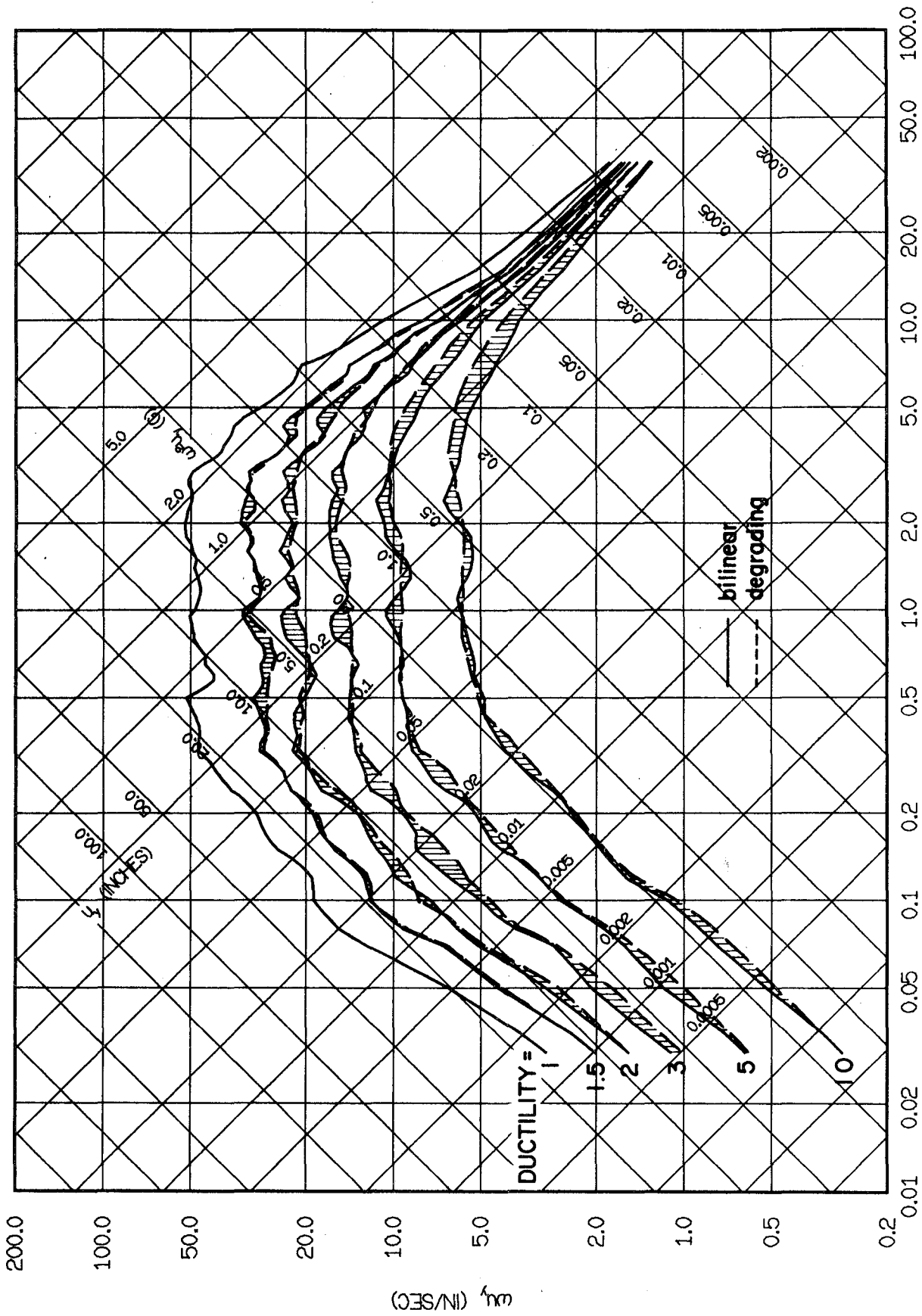
FIG. 4.38 COMPARISON OF MEAN SPECTRA NORMALIZED TO GROUND ACCELERATION FOR BILINEAR AND DEGRADING SYSTEMS WITH 5% DAMPING.
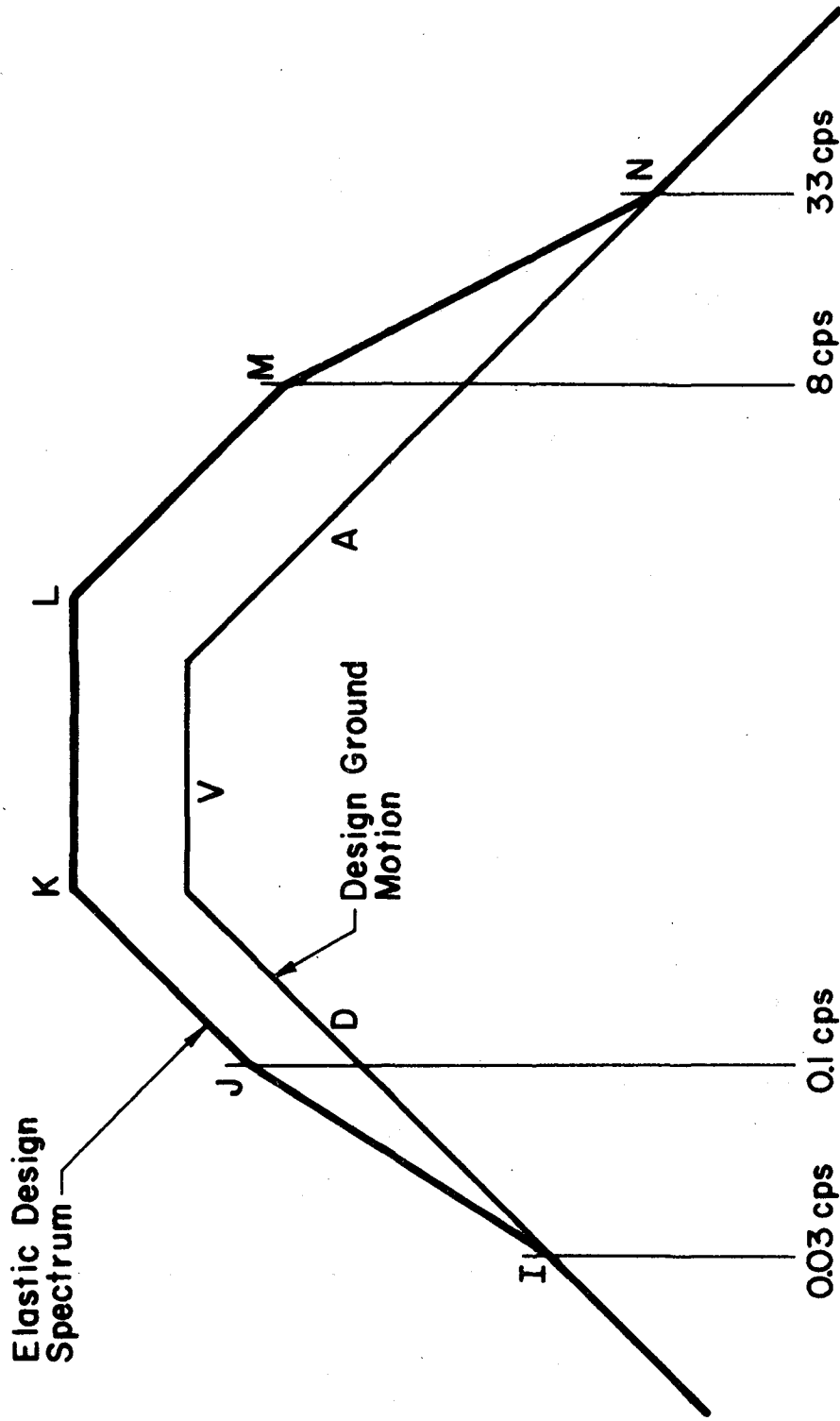
FIG. 5.1 CONSTRUCTION OF ELASTIC DESIGN SPECTRUM.
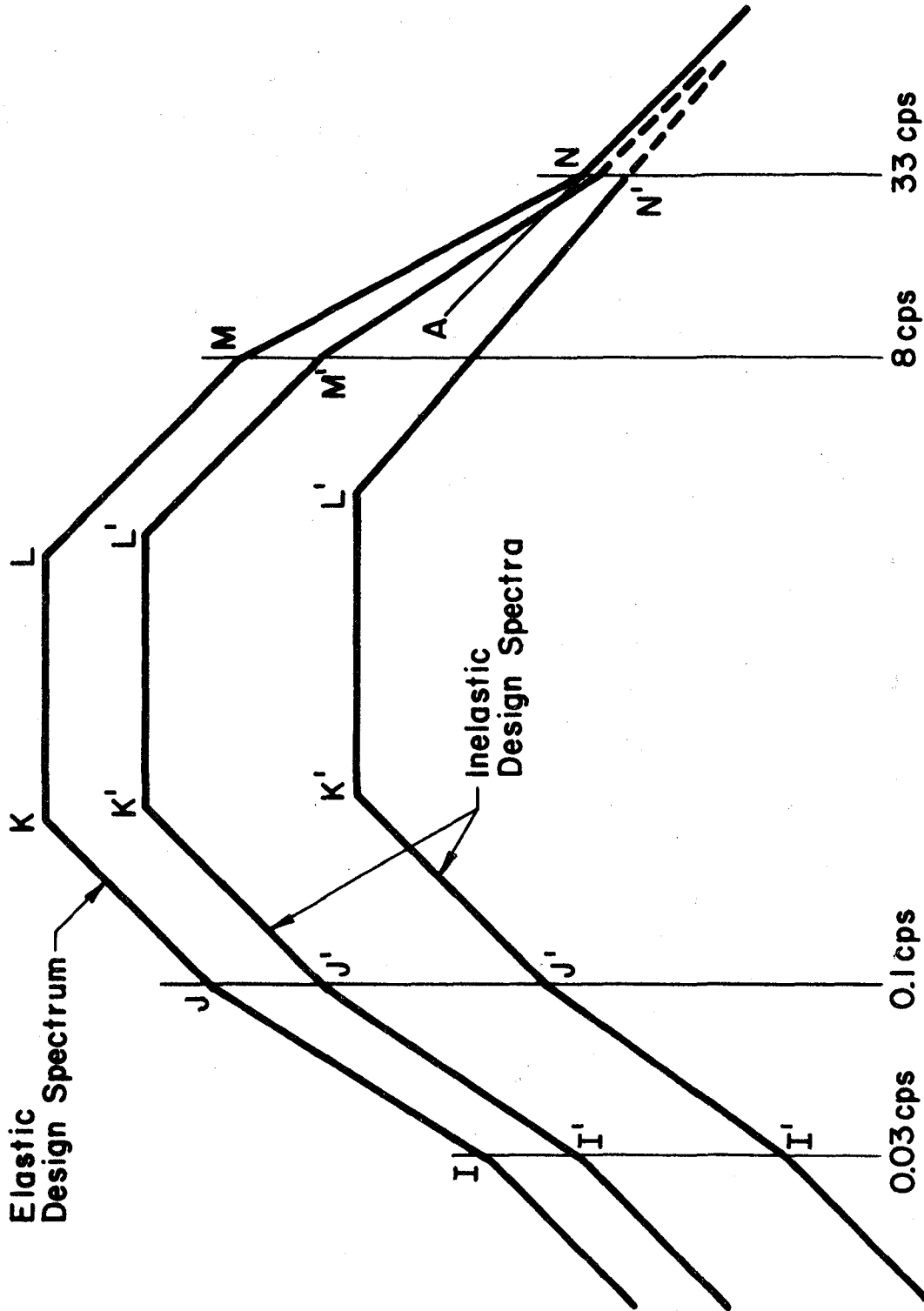
FIG. 5.2 CONSTRUCTION OF INELASTIC DESIGN SPECTRA.
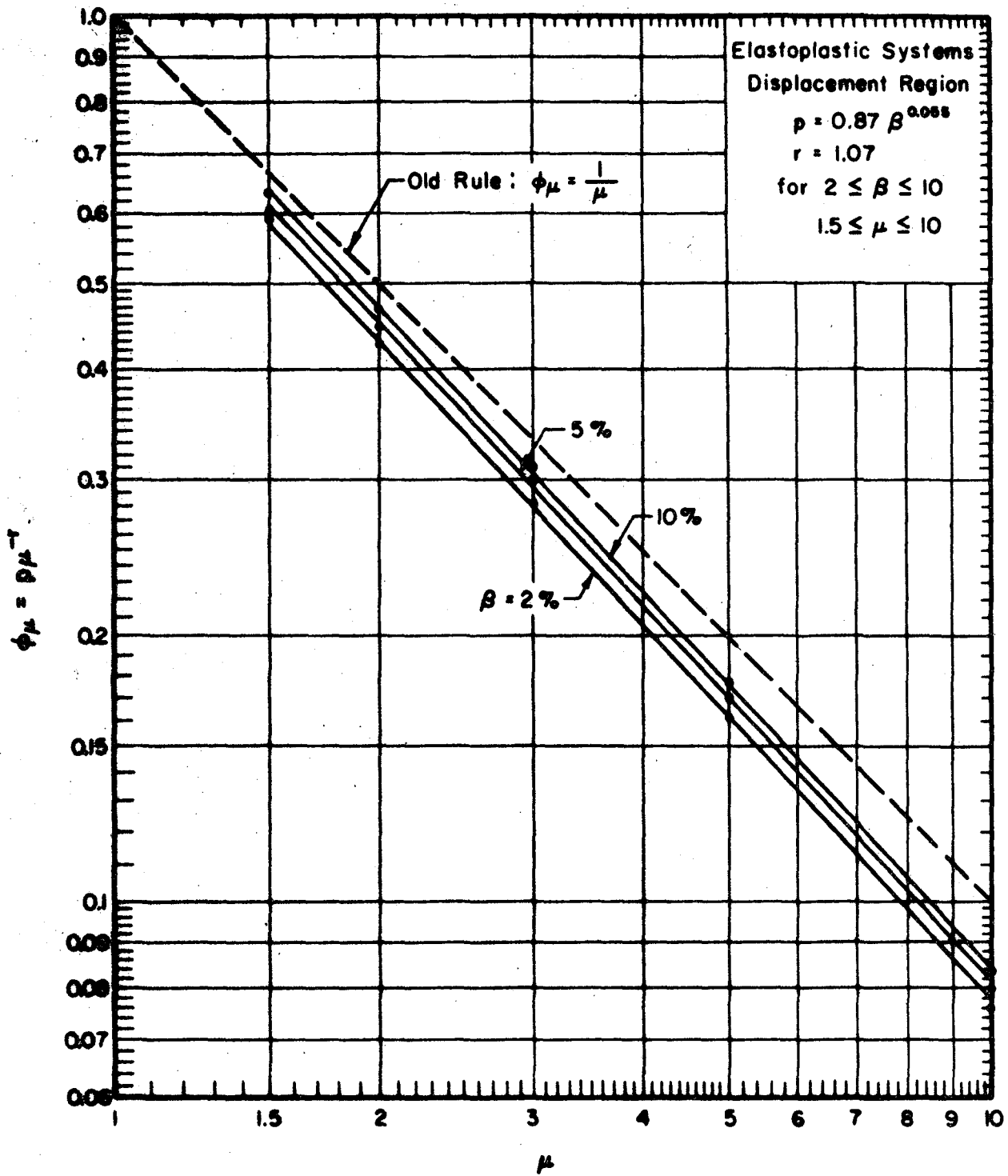
FIG. 5.3   COMPARISON OF DEAMPLIFICATION FACTORS DERIVED
IN THIS STUDY WITH PREVIOUSLY AVAILABLE RULES,
DISPLACEMENT REGION.
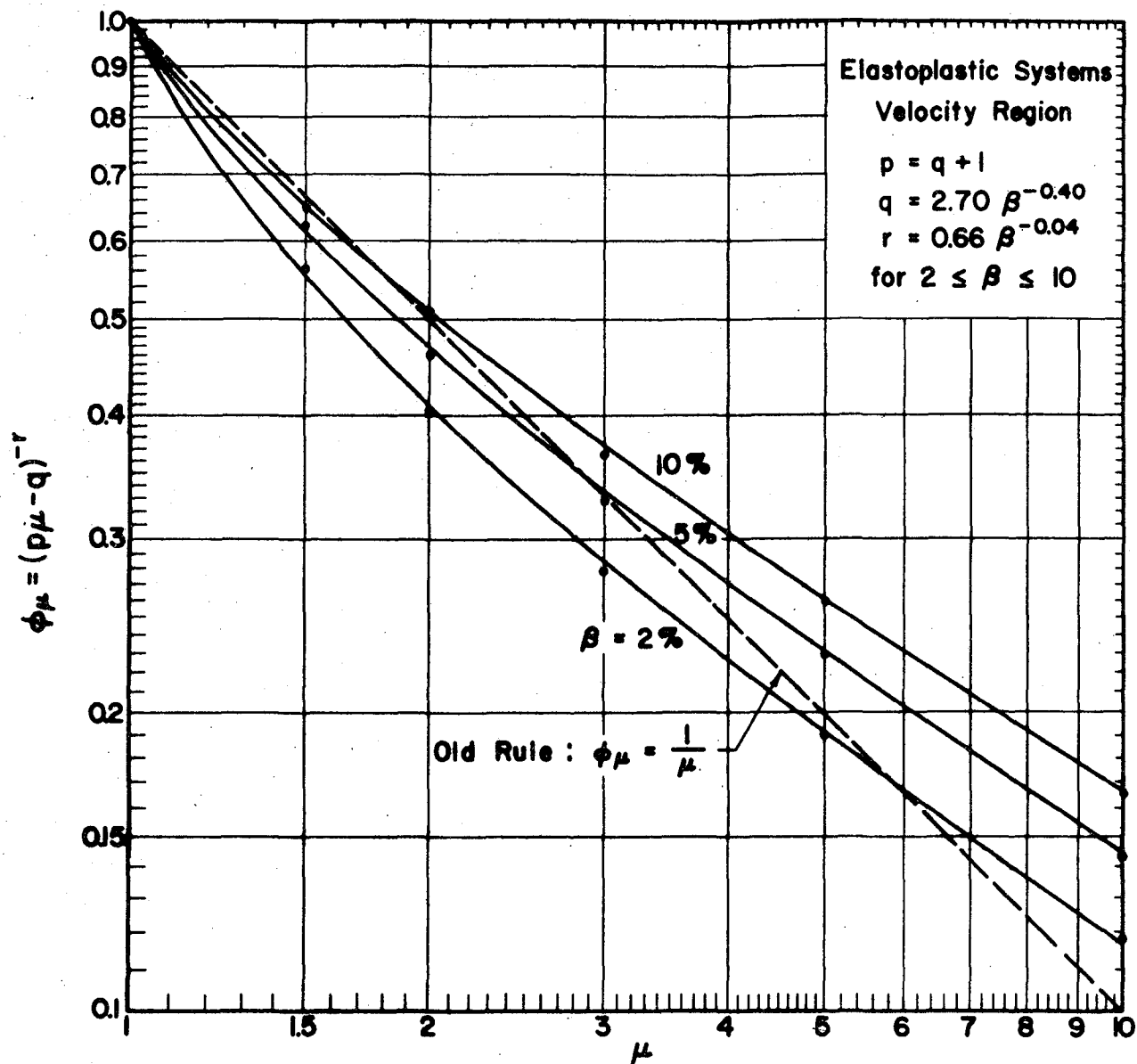
FIG. 5.4   COMPARISON OF DEAMPLIFICATION FACTORS DERIVED
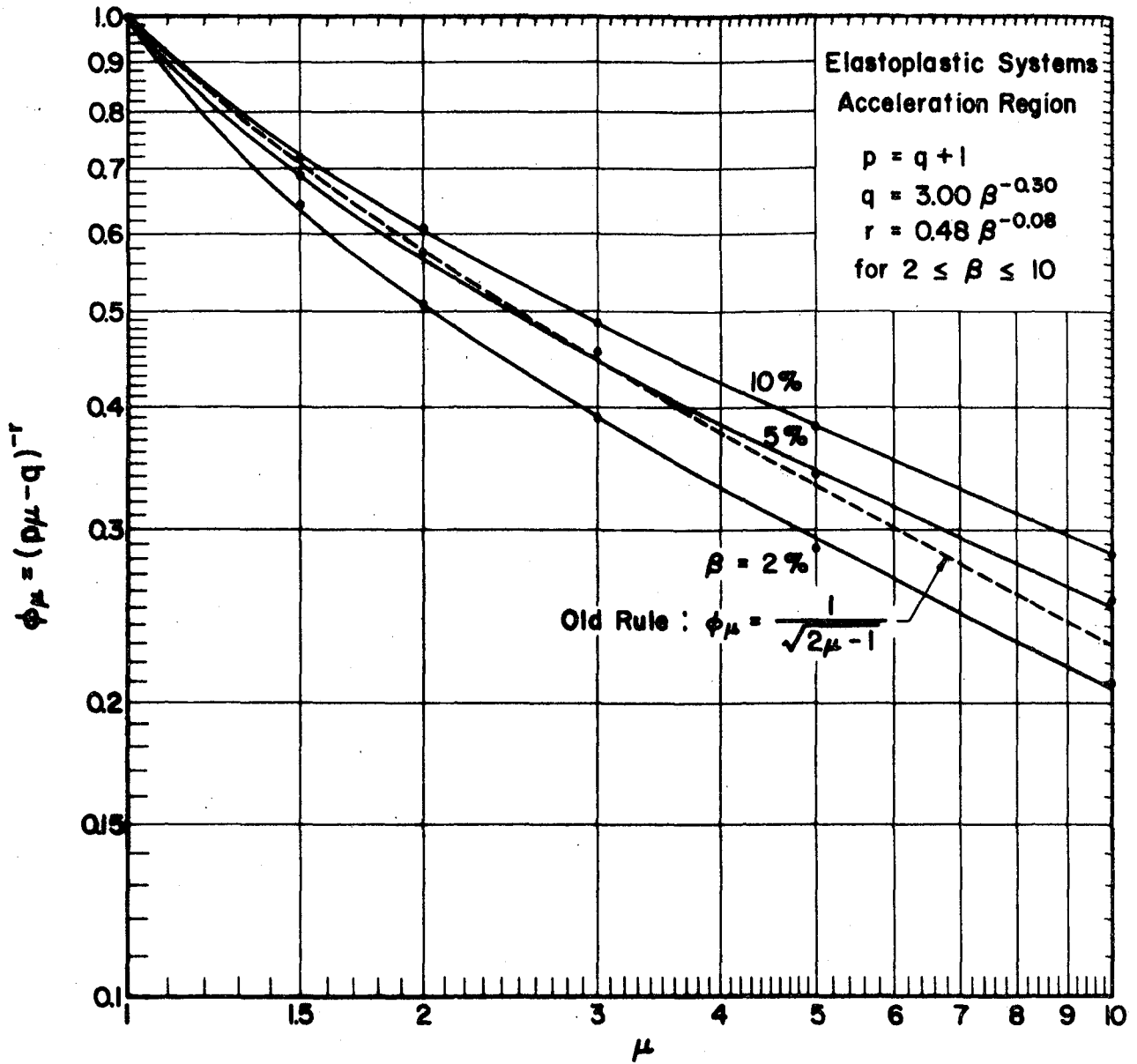IN THIS STUDY WITH PREVIOUSLY AVAILABLE RULES,
VELOCITY REGION.

FIG. 5.5   COMPARISON OF DEAMPLIFICATION FACTORS DERIVED
IN THIS STUDY WITH PREVIOUSLY AVAILABLE RULES,
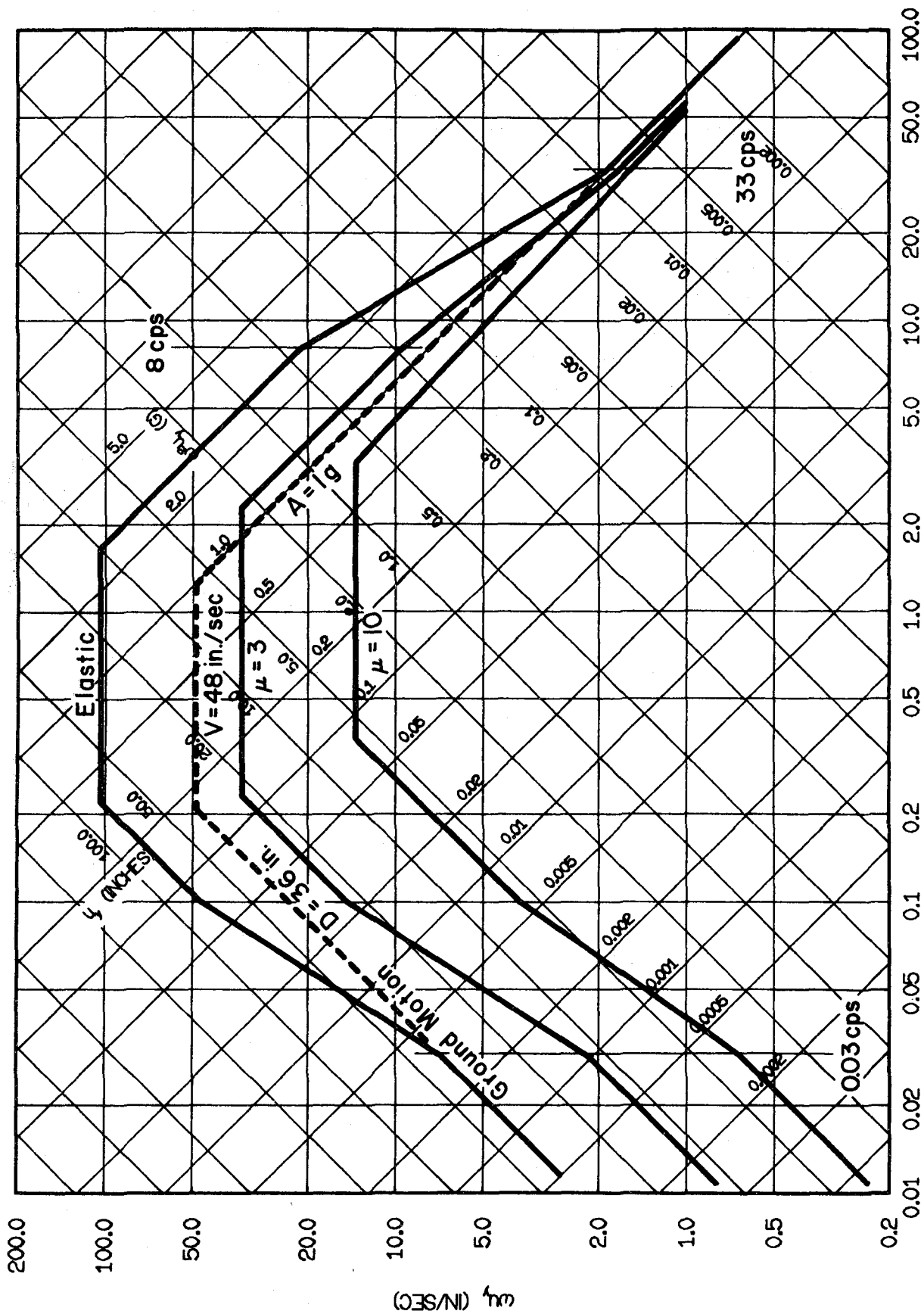ACCELERATION REGION.

FIG. 5.6   EXAMPLE OF DESIGN SPECTRA SCALED TO 1g GROUND ACCELERATION, FOR FIRM GROUND
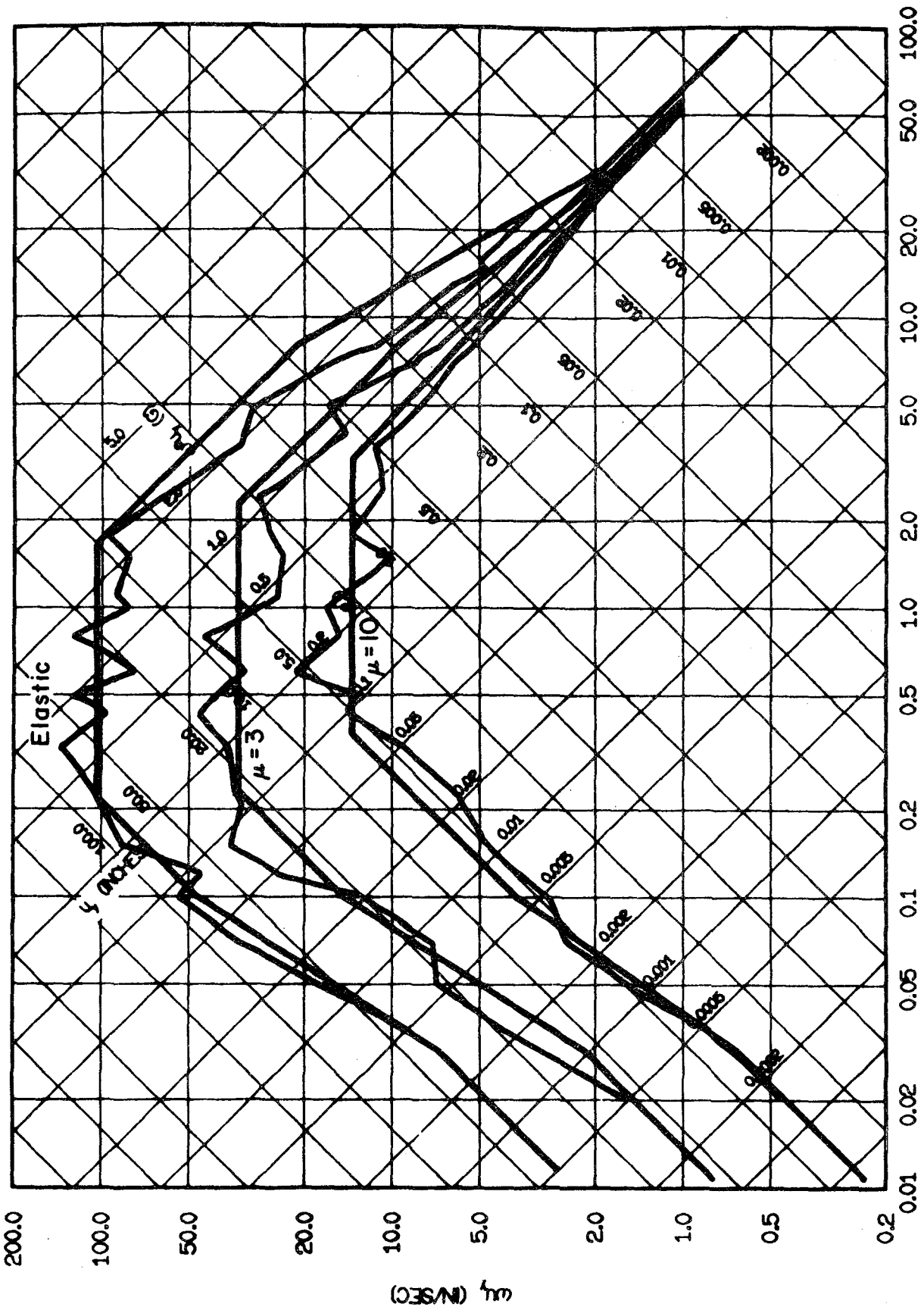AND 5% DAMPING, USING FACTORS CORRESPONDING TO THE MEAN + 1σ LEVEL.

289

FIG. 5.7 COMPARISON OF DESIGN SPECTRA WITH ACTUAL RESPONSE SPECTRA FOR EL CENTRO, MAY 18, 1940, E-W COMPONENT, NORMALIZED TO 1g GROUND ACCELERATION.
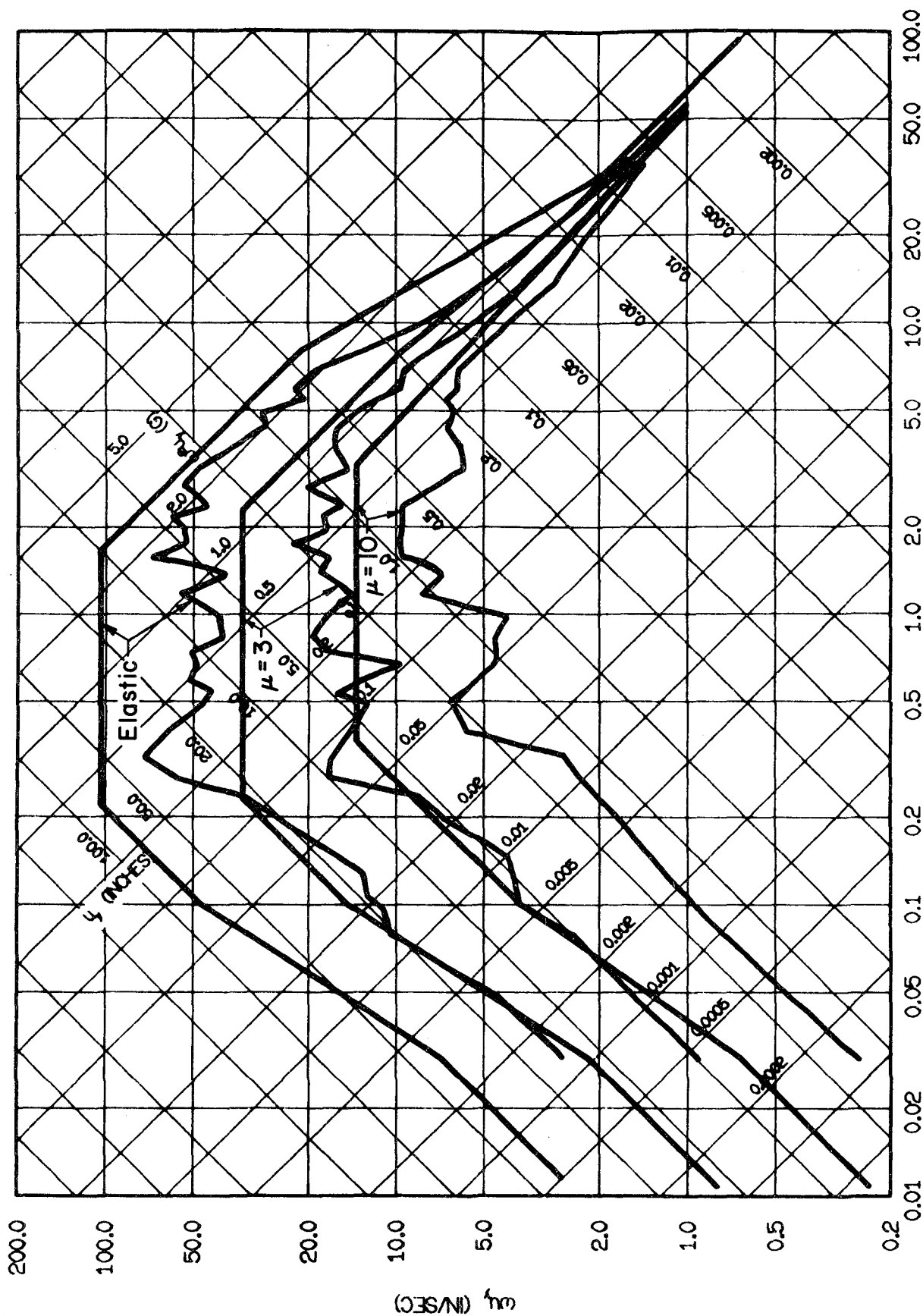
FIG. 5.8 COMPARISON OF DESIGN SPECTRA WITH ACTUAL RESPONSE SPECTRA FOR OLYMPIA,
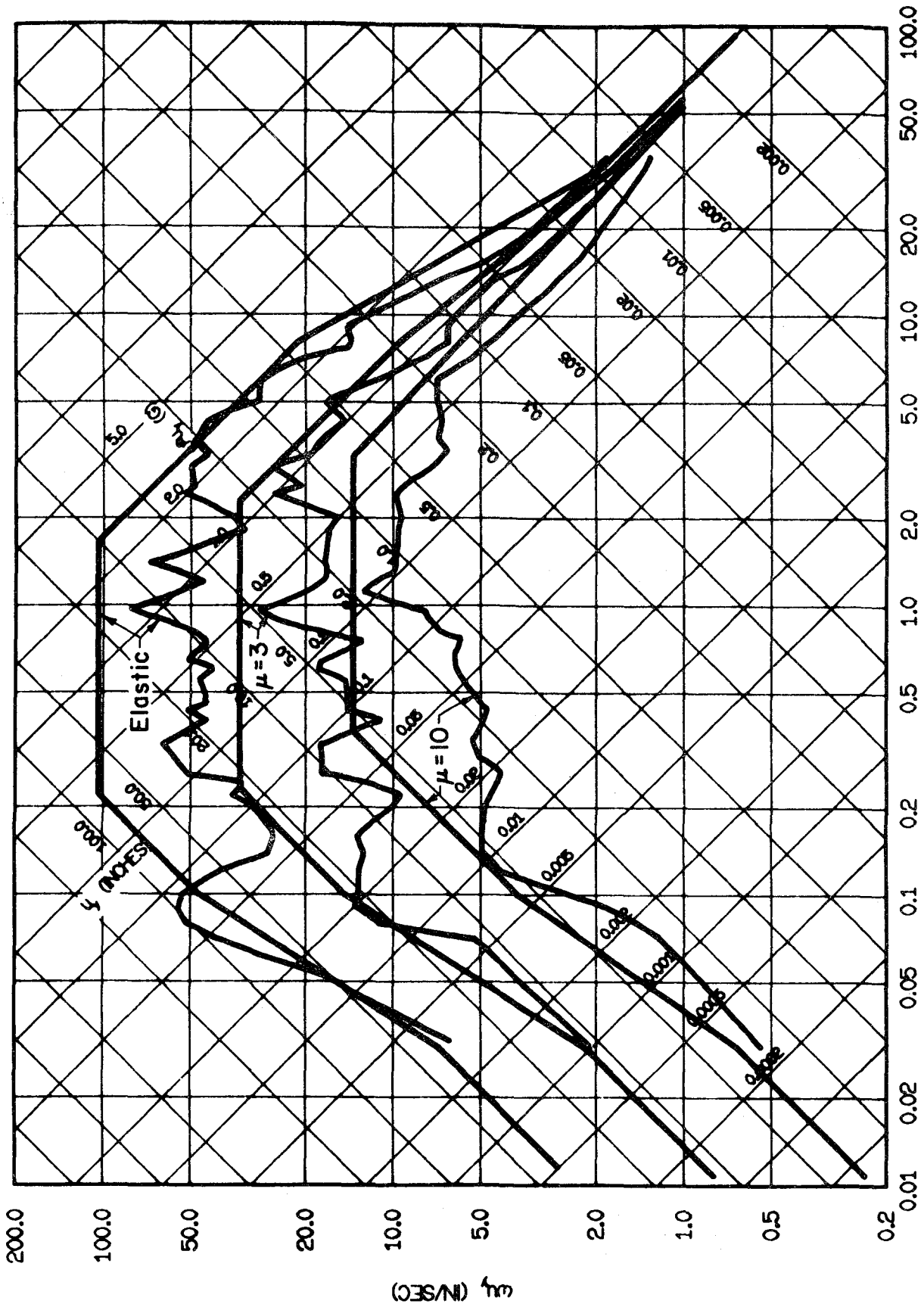APRIL 13, 1949, N86E COMPONENT, NORMALIZED TO 1g GROUND ACCELERATION.

FIG. 5.9   COMPARISON OF DESIGN SPECTRA WITH ACTUAL RESPONSE SPECTRA FOR SANTIAGO, JULY 8, 1971, N10W COMPONENT, NORMALIZED TO 1g GROUND ACCELERATION.